NON-GEMINATE CHARGE RECOMBINATION IN ORGANIC SOLAR CELLS

GEORGE F. A. DIBB

SUBMITTED FOR THE DEGREE OF DOCTOR OF PHILOSOPHY

DEPARTMENT OF PHYSICS
IMPERIAL COLLEGE LONDON

SEPT 2013

The work presented in this thesis was performed at Imperial College London, in the Departments of Physics and Chemistry, under the tutelage of Prof. Jenny Nelson and Prof. James Durrant between October 2009 and September 2013.

I declare that, except where otherwise cited or other contribution is referenced, the work presented herein is my own.

"To me the converging objects of the universe perpetually flow,

All are written to me, and I must get what the writing means."

Walt Whitman

Leaves of Grass

"Research is what I'm doing when I don't know what I'm doing."

Wernher von Braun

ABSTRACT

The efficiency of an organic photovoltaic (OPV) device is determined by the shape of its current-voltage (*J-V*) curve. Previous studies showed that the *J-V* curve for the best-studied OPV system, P3HT:PCBM, is determined mainly by non-geminate recombination where free electrons and holes recombine before being collected, thereby reducing output current. In this thesis we study non-geminate recombination experimentally, as well as charge collection efficiency and rates of geminate recombination, in several polymer:fullerene material systems. The aim is to determine limits to the performance of OPV devices and to quantify the recombination losses.

The first two experimental chapters investigate P3HT:PCBM devices. The first presents an analysis of non-geminate recombination, and the application of temperature dependent measurements and new transient techniques to probe the energetic distribution of trap states within the semiconductor. The second reconciles two apparently contradictory experimental results, namely, the highly non-linear dependence of non-geminate recombination rate upon charge density and the linear dependence of corrected photocurrent on light intensity.

In the third experimental chapter of this thesis both geminate and non-geminate recombination processes are studied and quantified in several material systems. Specifically we study the extent to which the two recombination mechanisms can impact upon the generation, collection and recombination of charges in the devices and we relate this directly to the fill-factor of the devices.

In the final experimental chapter, we study the effect of electronic doping space-charge accumulation upon the electrostatics of a device and hence on non-geminate recombination and charge collection. Through optical and electronic modelling we show that the doping of the photovoltaic active layer causes the accumulation of space-charge, which in turn alters the electric field within the solar cell, reducing the electric field driving collection of the minority carriers and consequently reducing charge collection.

ACKNOWLEDGEMENTS

There are so many people I want to thank, who have influenced and assisted me personally and academically throughout the course of my studies at Imperial College, that I should start with an apology if I've forgotten to mention you here! Being at Imperial has been not just a brilliant academic experience, but also a social one too, and I have made some wonderful friends over the past 4 years who have made the entire time a lot of fun.

The biggest thank you of all must go to my supervisors Jenny Nelson and James Durrant, who have given me so much help with my work and with my development as a scientist. People who are far more qualified to make such a statement than me have awarded you both for being accomplished scientists, but I'm in the privileged position to be able to say that you are also both excellent supervisors. The ability to know when to prod me in the right direction or leave me alone to work stuff out for myself has been invaluable to me and I wouldn't have achieved a fraction of the work contained here without your help and encouragement.

Almost none of the work I have done has been alone, and I must thank all the people who have helped me at any stage of my doctorate. A large part of my PhD has been spent in a dark room trying to convince bundles of wires, switches and lights to do what I want them to do and in the right order, and I have to thank Dan Credgington and Rick Hamilton for teaching me how to use the TPV rig and almost everything I know about transient measurements, which have formed the core of my thesis. Also I must thank Chris Shuttle for developing the techniques that I have used so extensively, and my partners in crime Florent Deledalle and Scot Wheeler who have endured hours of painstaking conversations. I received a huge amount of assistance with the computational side of my PhD from Rod MacKenzie and Thomas Kirchartz, who are due a big thank you. Thomas in particular is owed a huge amount of gratitude for inspiring large parts of the work in this thesis, and generally being an exceptionally helpful and intelligent friend. A large number of the devices I have studied during the course of my PhD have been made for me by Pabitra Shakya, who has tolerated my endless demands and always been extraordinarily helpful. One chapter of this thesis is the product of a large amount of work by Andrea Maurano, who I thank for being both helpful in the lab and great fun o spend time with. Also Fiona Jamieson has been a constant friend and talented collaborator throughout my PhD, who has helped me with TAS for years and generally cheered me up.

I also have to acknowledge the help of Merck Chemicals who generously funded part of my project and with whom a collaboration resulted in one of the chapters of this thesis. I owe a great deal of gratitude to Miguel Carrasco, for always being helpful and on my side, and Mathis Muth for the huge amount of help

he gave me in Chilworth and for the work that we did together. Additionally thank you to everyone else at Merck who helped me at any stage, particularly Priti Tiwana and Steve Tierney.

Now comes the long list of people in addition to those above who have made my PhD so much fun and accompanied me for many a celebratory (or commiseratory) pint after a particularly successful (or disastrous) day at work. Without the great people that I met at Imperial, this wouldn't have been anywhere near as much fun, so thank you! Sam, Mark, Clare and Anne, you made being in our office a brilliant experience as well as all being a great help to me, I will have many happy memories of our time together. Also, the rest of Jenny's group; Jarvist, Florian, Sheridan, Satchetan and Jizhong, who have always been so friendly and funny. Many thanks to James' group and other residents of the basement who made being in a windowless room so much fun; Safa, Stoichko, Chaz, Steve, Yvonne, Piers Adrian and Nurlan in particular. Additionally, thank you to the members of the Haque Shack, who have always been excellent drinking buddies as well as friendly rivals; Andy, Luke, Flannan, Simon D, Simon K and Ute. And whilst there are many more people who have helped me out and been great friends during this process, I have to name Alice, George B, Paul and Freddie in particular.

Without the constant support of my parents, who have always believed in me and supported me in anything I should wish to do, I wouldn't be here today. You have both been there for me through so much and always been a great inspiration and help to me. This is a tribute to all that you have done for me and I can't thank you enough. Thank you as well to my brothers, Lawrence and Patrick, and the rest of my family, for always being a source of relief and help, and for looking at me in a completely confused way whenever I talk about what I do at work. Finally, thank you to Sergio, who tolerated me whilst I wrote this thesis, and who I can't imagine being without.

CONTENTS

LIST OF FIGURES

LIST OF TABLES

CHAPTER I

CONTEXT

One of the greatest challenges to modern science is the search for new, clean and stable sources of energy which can provide the growing requirements of an increasingly populated planet, whilst simultaneously reducing damage to our natural environmental and halting man-made climate change. Finding ways to generate electricity securely, safely, reliably and non-destructively are key, as well as reducing the emissions of carbon dioxide.

The vast majority of climate scientists and those in surrounding fields have concluded that the recent changes in global climate, specifically rising temperatures, are caused by mankind. A recent survey of climatologists by Anderegg et. al. found a 97-98% agreement in the theory of anthropogenic climate change.[1] The consequences of rising global temperatures are potentially disastrous, ranging from reduced agricultural production and resulting food shortages to increased exposure to flooding and the destruction of fragile ecosystems. In addition these changes will be localised, mainly to already drought- and flood-prone areas.[2] The current route to mitigating global warming is to reduce the emission of carbon dioxide and other greenhouse gases, framing the challenge of new energy sources with additional goals and indicating the potential of renewable electricity generation.

Renewable energy sources include wind, tidal, solar, geothermal and hydroelectric power; the energy generation mix in the future will undoubtedly consist of a mix of these methods and the technologies for achieving them are all at different stages of development. Solar power is generally considered to be among the most promising technologies, mainly due to the huge amounts of energy the earth receives from the sun. In fact solar energy is by far the most abundant energy source available to humankind. The energy hitting the surface of the earth from the sun in one hour is approximately the same as the total energy used by mankind in a year. In 2006 the total world energy consumption was approximately 500EJ;[3] compare this figure to the total energy from the sun absorbed by earth's atmosphere, land and water of 3,850,000EJ.[4] In

comparison to other methods of energy generation, the annual solar energy that reaches earth is almost double that which will *ever* be gained from fossil fuels and uranium combined. Obviously collecting this energy is a practical challenge, yet a quick analysis of the magnitude of the figure involved shows that just a small amount of solar energy would be required to be harvested to provide a significant proportion of the world's energy needs. Additional advantages of solar power are the fact that once the solar energy harvesting infrastructure is implemented the fuel, sunlight itself, is entirely free and thus whilst a high up-front cost may be required the possibility of low cost generation is there. Energy usage in the developed world tends to peak around the middle of the day which coincides conveniently with the peak solar irradiance.[5]

Figure 1.1. A flexible OPV device fabricated using roll-to-roll printing powers a small motor. Photo reproduced courtesy of Satchetan Tuladhar.

Whilst photovoltaics appears initially to be exactly what is required to solve at least a proportion of our future energy needs, there are several significant barriers to implantation of the technologies required that must be removed. The first among these must be cost; the current market leading photovoltaic technologies use expensive semiconducting materials driving high costs. However the field of photovoltaics stands to benefit significantly from the wider development of organic or plastic electronics. The use of organic materials in semiconducting applications has benefitted from a huge amount of research effort in the past 20 years and is now beginning to be featured in commercial products, competing with conventional silicon and inorganic semiconductors. One of the main benefits of organic semiconductors is their potential for solution deposition, meaning that semiconducting devices could be fabricated using conventional printing and coating processes rather than the expensive crystal fabrication methods used in the silicon industry. The printing of organic semiconductors is seen as highly beneficial as it can also be a continuous rather than batch process, driving the cost of semiconducting devices down. Additionally whilst conventional semiconductors tend to be rigid when manufactured, if organic electronics can be printed onto substrates it opens up an entire new area of flexible electronic devices.

Organic semiconductors have been utilised with some success in solar power applications, and today the field of organic photovoltaics (OPV) is a rapidly growing research field. As shown in Figure 1.2 the record power conversion efficiencies, the test of how well a solar cell is performing, has grown extremely

quickly since the early 2000s, and now stands at 10.4% for tandem OPV devices.[6] Additionally the fabrication of flexible photovoltaics could mean easier integration into other devices and new applications of solar power that were not previously possible. Additionally flexible photovoltaics are far more rugged and robust when compared to traditional glass based solar cells, making them ideal for the sizeable off-grid solar applications.

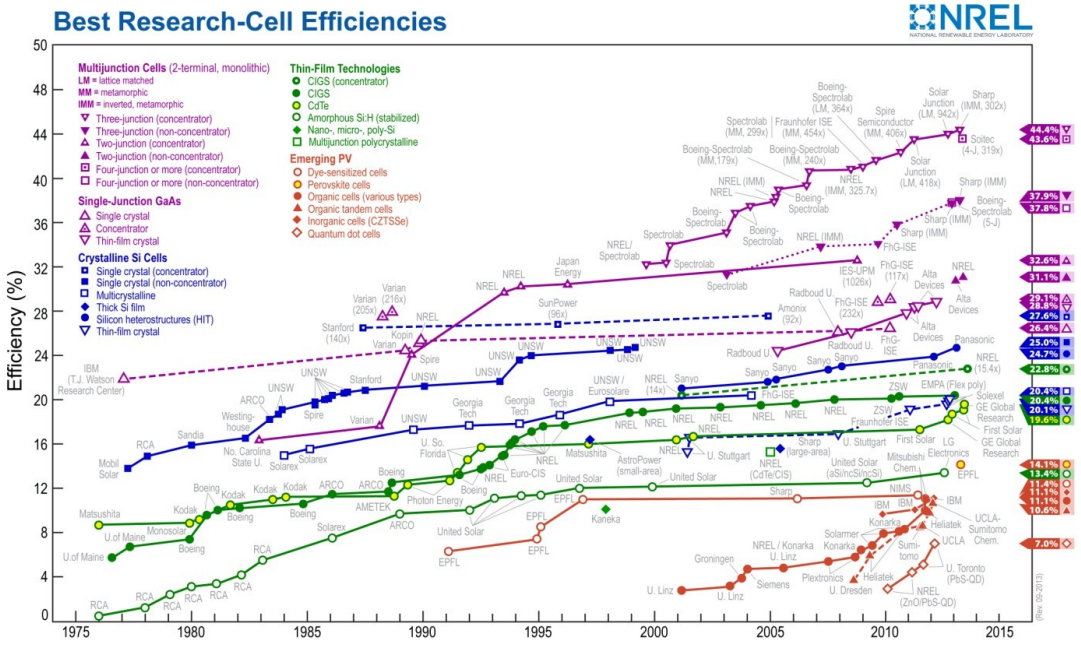

Figure 1.2. A figure showing the progression of record photovoltaic power conversion efficiencies for various PV technologies.[7]

As already described, the recent increases in device efficiency have been impressive, although they are not yet on the same level as competing technologies. The economics of renewable power is a large enough subject that an entire thesis could be written on that alone, however the most important metric in evaluating the economic viability of different technologies is the cost per unit power generated or the $/W or £/W. When photovoltaics are considered using this metric we can see how OPV, whose power generating performance may not yet be as good as other photovoltaics, can compete in the marketplace if the cost of manufacture can be brought low enough that the cost per watt is reduced. It is this that has spurred significant research in the large-scale printing of devices.

OPVs are a promising technology with the potential to constitute a large portion of the future energy generation capability, but only if gains are made in performance, lifetime and fabrication. To this end research into this technology is vital. In this thesis I shall describe the work I have performed, in collaboration with my colleagues, in understanding the fundamental device operation of OPVs, with the end aim of increasing device performance and furthering this promising technology.

CHAPTER II

PRINCIPLES OF ORGANIC PHOTOVOLTAICS

2.1 INTRODUCTION

Photovoltaic devices are electronic systems that can convert incident photons into electrical current; light energy into electrical energy. This is commonly achieved by the absorption of the incident photons in a semiconducting material of some kind, where the absorption of the photon leads to the excitation of an electron from the valence band to the conduction band of the semiconductor. In a photovoltaic device, to obtain an electric current, these charges must then be extracted from the semiconducting material and into an external circuit with a net electro-chemical potential. This is commonly achieved through the application of an electric field.

Several things are required for the photovoltaic process to occur; the first of these is the absorption of photons within the active semiconducting material within the device. To produce the highest electrical current possible, as many photons as possible must be absorbed.[8] In a semiconductor with an energetic bandgap between the conduction and valence band edges, E_G, only photons with an energy $E>E_G$ can be absorbed, thus the electronic structure of the semiconductor is linked to the photovoltaic performance.[9]

In a working photovoltaic device the semiconducting material is sandwiched between conducting electrodes. For a device to produce a current, one electrode must collect more electrons and the other more holes, commonly referred to as asymmetric collection. In conventional inorganic solar cells this asymmetry is provided by fabricating the semiconducting layer such that it acts as a diode; in silicon devices this is done by doping the two sides of the semiconductor differently such that a p-n junction is created. Other solar cell technologies utilise layers between the electrodes and the semiconductor that preferentially conduct one

carrier over the other. Whatever method is used, the diode property of solar cells is essential for the generation of current.

Finally for photovoltaics to work the generated charges must be collected from the semiconducting layer efficiently and thus generate current. For this to occur the material must allow the flow of charge with a high enough mobility that the charges are extracted before parasitic losses reduce the yield of charges.

2.1.1 *J-V* Curves

The main characterisation method for photovoltaic devices is the voltage dependence of current output, both under illumination and in the dark, this is commonly measured as the current density, *J*. Figure 2.1 shows typical *J-V* curves of a photovoltaic device in the dark and under simulated sunlight illumination. Consideration of the dark *J-V* curve allows the assessment of the devices diode characteristics, and the shape and magnitude of the light *J-V* curve allows calculation of the power conversion efficiency with which the device converts light to electrical energy. The power conversion efficiency is by definition the ratio of power incident upon the device in the form of light to the electrical power output by the device under optimal conditions. As power $P = VI$, this can be calculated from the *J-V* curve; Figure 2.1 shows a plot of power output and a *J-V* curve for the same device as a function of voltage. The voltage where power output is maximised is defined as the maximum power point (MPP) and therefore the efficiency is the ratio of the power output at the MPP to the radiant power from incident illumination. This is shown in equation *(2-1)*.

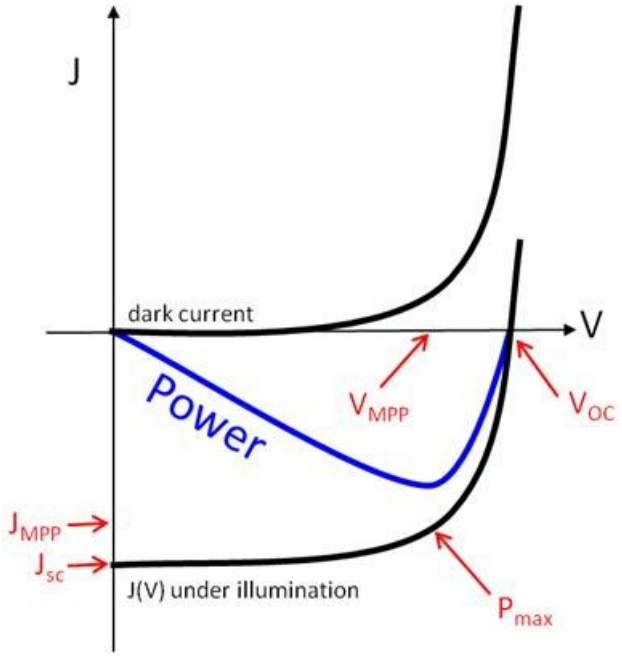

Figure 2.1. An example of light and dark J-V curves (black), as well as a plot of the power generated as a function of voltage (blue), with all the relevant points on the J-V curve indicated.

Several other points on the *J-V* curve of a device are particularly relevant to the study of photovoltaics devices. The voltage at which no current flows under illumination is defined as the open-circuit voltage (V_{OC}) as this is the state the illuminated device would be in were the electrodes of the device not connected to an external circuit. Similarly, were the electrodes of the illuminated device connected by an ideal wire creating a short circuit, there would be no applied bias between the electrodes and the device would be in the condition where current flows but no voltage is applied, this is defined as the short-circuit current (J_{SC} or I_{SC}). Both these points are marked on Figure 2.1. The maximum power point (MPP) is the voltage at which the device generates the maximum power $P = VI$. The voltage at the maximum power point,V_{MPP}, is always less than the V_{OC}, and corresponding current I_{MPP} is always less than the I_{SC}. The "square-ness" of the *J-V* curve, or how close the J_{MPP} and V_{MPP} get to the J_{SC} and V_{OC} respectively, is known as the fill factor (*FF*). This is calculated by the ratio of the actual maximum power output and the theoretical maximum power output, thus $FF = V_{MPP}J_{MPP}/V_{OC}J_{SC}$.

The power conversion efficiency (PCE) can now be calculated both by definition as the ratio of power input to power output, or it can be calculated as a function of the variables defined above. Thus

$$PCE = \frac{P_{OUT}}{P_{IN}} = \frac{V_{MPP}J_{MPP}}{P_{IN}} = \frac{V_{OC}J_{SC}FF}{P_{IN}} \qquad (2\text{-}1)$$

2.1.2 Diode Equation & Equivalent Circuits

Another way of understanding the behaviour of a solar cell is to characterise the dark current of the device using the Shockley diode equation.[10] This is commonly used to describe the current flowing through a p-n junction.

$$J = J_0(\exp\left(\frac{eV}{mk_BT}\right) - 1) \qquad (2\text{-}2)$$

where J_0 is the saturation current, e is the elementary charge, k_B is Boltzmann's constant, T is the temperature and m is the ideality factor. Furthermore the behaviour of a solar cell in operation can be understood and analysed by imagining that the diode above is in a circuit in parallel with a current generating component. This is known as the equivalent circuit approximation.

Figure 2.2a is the equivalent circuit of an ideal solar cell, consisting only of a solar generating component with light intensity dependence and a non-linear asymmetric resistor or a diode. The generator produces a current dependent upon light intensity which is divided between the backward-flowing diode and the load in the circuit, the diode creates the dependence of the cell voltage on the resistance of the load.

Thus the equation that represents this solar cell would be a generation term, J_{GEN}, with the dark diode term above subtracted.

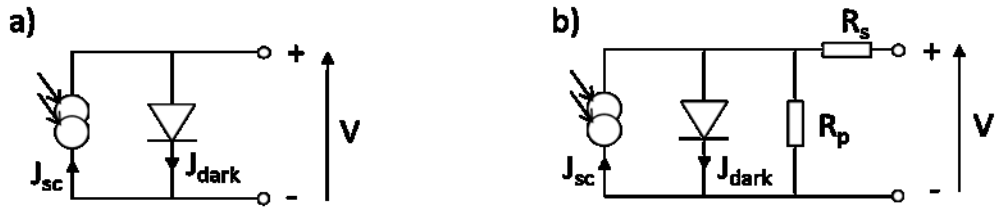

Figure 2.2. Equivalent circuit diagrams of a solar cell. a) shows the equivalent circuit of an ideal cell. b) shows the equivalent circuit of a real cell with parasitic resistances.

In non-ideal cells there are resistances associated with leakage currents, interface resistances and electrode effects. These can be represented by two resistors in the equivalent circuit, one in series (R_S) and one in parallel (R_P) as shown in Figure 2.2b). This circuit has a more complex equivalent equation,

$$J = J_{GEN} - J_0\left(\exp\left(\frac{e(V - JAR_S)}{mk_BT}\right) - 1\right) + \frac{V - JAR_S}{R_P} \qquad (2\text{-}3)$$

where *A* is cell area. By comparison to equation *(2-2)* it can be seen that all the voltages applied across the device are now reduced by series resistance.[10-11] This equation has been used to understand solar cells of various types with varying degrees of success.

The effects of these parasitic resistances can be observed in the current-voltage characteristics of the cell. An increasing series resistance produces a lower gradient in the *J-V* curve at open circuit and a decreasing parallel resistance produces a higher gradient at short circuit. Both these effects reduce the fill factor of a solar cell and therefore its efficiency.

2.2 ORGANIC SEMICONDUCTORS

Organic materials are formed from a structure of mostly carbon and hydrogen atoms, along with nitrogen, sulphur, oxygen and other elements. These molecules can take a huge range of different structures formed from many moieties or molecular building blocks that can be assembled into larger structures. With regards to their electronic properties, organic semiconductors can support the existence of delocalised electronic states and can thus function as conductors, however the molecules useful for photovoltaic applications are semiconductors. Additionally, organic materials can absorb and emit visible and near-visible wavelengths of light, therefore their ability to conduct and their responsiveness to the solar spectrum makes them ideal candidates for use in photovoltaics.

The early work on organic semiconductors found that the determining factor in the electronic properties of a molecule was the specific arrangement of the electrons within the carbon-carbon bonds that form the main structure of the molecule. The necessary structure for the existence of delocalised electronic states is a structure of conjugated carbon-carbon π-bonds. A π-bond is a bond in which the molecular orbitals of the two atoms are overlapping, otherwise known as an sp2 bond. In this bond the electron within the bond is slightly delocalised from the individual atoms. However for the material to exist as a semiconductor these delocalised electrons must additionally be able to flow. For this to occur the π-bonds must be conjugated, or alternating within the atomic structure. Figure 2.3 shows a very simple example of how a molecule consisting of alternating, or conjugated, double bond, or π-bonds, can allow the conduction of charge when excited.

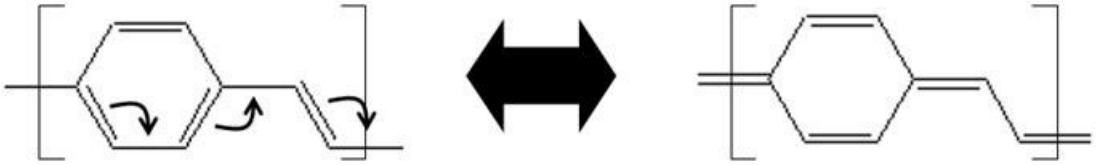

Figure 2.3. Molecular drawings showing how an alternating pattern of double bonds, or conjugation, can result in the transport of polarons along a polymer chain.

As described in full below organic semiconductors have now been utilised to fabricate reasonably efficient solar cells that function with high levels of internal quantum efficiency,[12] however there are two essential differences between organic and inorganic semiconductors that make this difficult. Firstly, organic materials, in general, have considerably lower dielectric permittivities than inorganics. Whilst in silicon PV devices the initially generated excited state on the absorption of a photon is a free electron, in organic materials the Coulombic attraction between the excited anion and cation is high enough that the electron cannot be described as free. Instead the initial excited state in organic semiconductors is an exciton, commonly described as a neutral bound electron-hole pair. This exciton can diffuse through the material but must be separated to allow the generation of current. In turn this implies an additional process that must occur within the photovoltaic device.

The second difference between inorganic and organic semiconductors is that free electrons cannot be described as fully delocalised in the same sense as electrons in band transport in inorganic semiconductors. Instead they are, to a degree, localised upon an atom within the semiconductor and charge transport cannot be described using the band approximation, but usually using a "hopping" model whereby the free charges tunnel from molecular site to molecular site. The result of this difference upon device performance is that charge transport is considerably slower in organic semiconductors than in inorganics, and therefore charge mobilities are reduced.

As the charge transport in organic semiconductors is not band-like, it is not possible to use the general terms of conduction and valence band as used elsewhere in semiconductor literature. Each molecular site that can be occupied by a charge has an unexcited ground state energy determined by the

energy of the electron in the highest occupied molecular orbital, or HOMO, and a first excited state defined by the lowest unoccupied molecular orbital, or LUMO. The molecules HOMO and LUMO energy levels are roughly analogous to the valence and conduction bands of a conventional semiconductor, respectively. Thus the band-gap of an organic semiconductor can additionally be defined as the energetic difference between the HOMO and LUMO levels. Similarly as only photons with energy greater than the bandgap of inorganic materials can be absorbed, in organics photons must have an energy exceeding the difference between the HOMO and LUMO.

A final characteristic of organic semiconductors that significantly affects the performance of devices fabricated with them is the disordered nature of the material. Organic semiconductors are known to be both physically and morphologically disordered on a range of length-scales, as well as energetically disordered in the distribution of the density of energetic states of the bulk material.[9, 13-16] The physical disorder of organic semiconductors, or the lack of long-range order, results in the many molecular sites within the semiconductor each being in a unique configuration with regards to its own position and its position with regards to other surrounding molecules, resulting in a unique energetic level. Taken as a bulk material this distribution of different energetic molecular environments naturally leads to a distribution of the HOMO and LUMO levels of the bulk material.[17] This is demonstrated in Figure 2.4. Thus the organic semiconductors can be treated similarly to amorphous silicon or other disordered inorganic materials whose valence and conduction bands are represented by a wide spread of energy levels rather than a defined level.

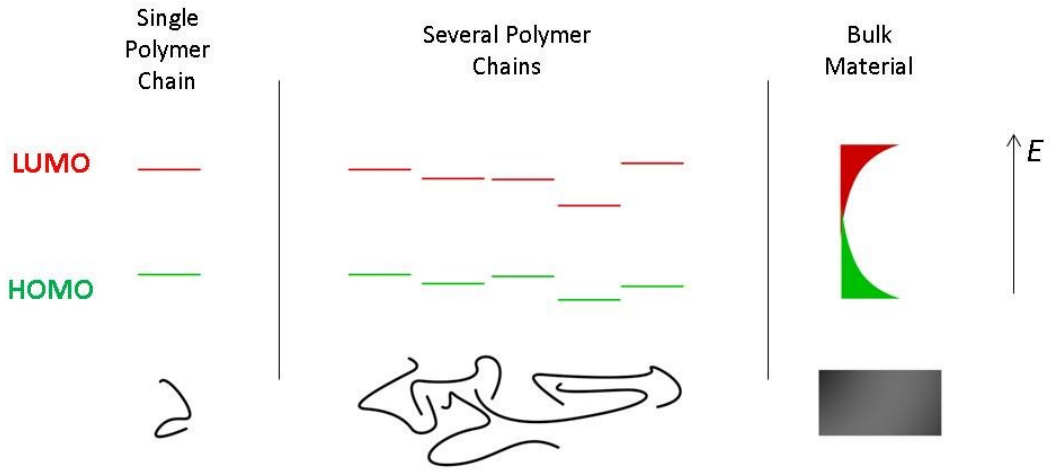

Figure 2.4. A demonstration of how the disordered HOMO and LUMO levels of a bulk organic semiconductor can originate from the define energy levels of many molecules in different conditions.

2.3ORGANIC SEMICONDUCTOR PHOTOVOLTAICS

2.3.1 Single Material Devices and Bilayers

Organic semiconductors were used in photovoltaic devices very soon after their initial discovery, however devices efficiencies were extremely low. These early devices were commonly in a metal-semiconductor-metal configuration where the driving force for the current generation was provided by the difference in work function between the two metal electrodes. In a single organic semiconductor layer the photons mainly generate excitons and only a tiny proportion (if any at all) separate to form free carriers, due to the increased coulombic binding between electrons and holes. Thus these devices suffered from extremely low photocurrents and the semiconductors used exhibited low charge mobilities and thus lossy transport.

The fabrication of the first OPV devices in a bilayer heterojunction structure, where two different organic semiconductors were sandwiched together was reported by Tang et. al. with copper phthalocyanine: perylene derivative (CuPc:PV) solar cells.[18] This step forward in device structure saw huge increases in device power conversion efficiencies, mainly by increasing the current generation resulting from an increase in bound electron-hole state separation. The bilayer structure increased this exciton separation as it was a heterojunction, and each of the materials had different energetic levels; in the case of the CuPc:PV device the majority of the photon absorption was in the CuPc layer, but the perylene derivative has a lower LUMO energy than phthalocyanine. When an exciton reaches the heterojunction it is energetically favourable for the electron component to transfer to the lower LUMO level of the other material and if the difference between the conduction band energies is high enough then the bound state will be separated into free charges. The discovery that a difference in energy between materials was enough to separate the bound electron-hole state revolutionised the field of OPV and allowed all further developments to occur. The material in which the photons are absorbed and excitons are generated is defined as the donor material, as on exciton separation a charge is donated to the other component, defined at the acceptor. In most cases the donor material transfers an electron to the acceptor and thus becomes the hole-transporting component, and this is shown in Figure 2.6, however this is not always the case.[19]

2.3.2 The Bulk Heterojunction

Whilst bilayer heterojunctions provided a huge increase in current output from photovoltaic devices, they were still limited. As exciton transport in the disordered materials is slow relative to the recombination of the bound electron-hole state, excitons have a limited diffusion length which they can travel before being lost to recombination.[20-22] In organic semiconductors the exciton diffusion length, L_{EX}, is of the order of 10nm. Thus if an exciton is not generated within L_{EX} of a heterojunction interface it will likely not be separated to form free charges. To maximise the exciton separation, or free charge generation, all excitons must be generated within L_{EX} of an interface.

The bulk heterojunction (BHJ) structure was first successfully demonstrated by Halls et. al.[23] and Yu et. al.[24] in 1995. Instead of simply a bilayer, this structure consists of a finely intermixed domain structure of donor and acceptor material throughout the entire active layer. The limitation of the bilayer structure was that the majority of photo-generated excitons were created too far from a heterojunction interface to be separated, this is shown in Figure 2.5. The BHJ therefore overcomes the limitations of the bilayer by allowing the heterojunction interface to bend and contort through the entire device consequently increasing the active volume within which excitons can be generated and successfully separated. If the domains of donor and acceptor material are on the length scale of the exciton diffusion length then it is possible to separate a high proportion of the excitons. This is evidenced by the fact that some BHJ OPV devices reach external quantum efficiencies (EQEs), or the ratio of incident photons to charge extracted as current, approaching 100%.[25]

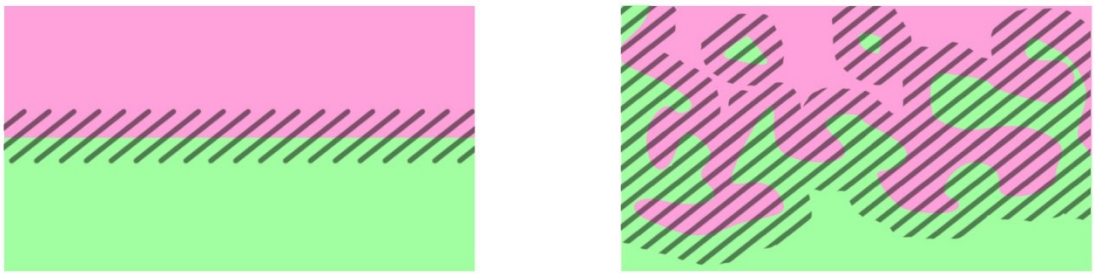

Figure 2.5. A depiction of bilayer (left) and bulk (right) heterojunctions, showing the different volumes within which excitons can be harvested as shaded.

The BHJ structure is commonly formed by mixing together the donor and acceptor materials in solution, then depositing this solution onto a suitable substrate and allowing the separate materials to spontaneously phase segregate.[26] The formation of the domain structure and the impact this has on charge species is still under active debate,[27-28] however we know that some material combinations are not perfectly miscible and when the solution is deposited form suitable domain structures. Another factor being studied is the morphology of the interface between these materials on the micro- and nano-scale and how this influences charge separation.[29-31] When relying on the materials themselves to spontaneously form domains, some amorphous or mixed phases will form in the BHJ structure.[32-33] Whilst some authors have concluded that these mixed and therefore inherently disordered regions hinder charge transport and therefore device performance, it has been shown by other groups that in fact in some material systems a mixed phase is required to separate the excitons and a large proportion of separation occurs in these regions.[32]

The structure of the bulk heterojunction, its crystallinity, the relative size of its domains and their relative purities, have a large influence upon the performance of any device fabricated from a blend material.[29, 34-35] As this blend is commonly deposited from a solution there are many factors that can affect the final morphology, such as the concentration of the solution, the particulars of the solvent used,[36] deposition temperature etc.. Furthermore, there are several post-deposition techniques that are commonly used to enhance device performance. The annealing of the deposited film by the application of heat is

widely used,[37] as is "solvent annealing".[38] Finally, as solution deposition is a dynamic process it should be noted that the resulting structure of the BHJ blend may not be in equilibrium and further post-deposition techniques can be used to further alter this structure by taking advantage of this fact.

Whilst the BHJ structure has been shown to optimise the likelihood of an exciton reaching a heterojunction, it is not immediately implicit that this will aid charge generation. When charge transfer from the donor to acceptor takes place, the two polarons are still Coulombically bound. Many authors supposed that in bilayer devices where the donor:acceptor interface is perpendicular to the electric field, that the separation of these charges was aided by the electric field.[39-40] However in a BHJ where the interface has no fixed orientation in respect to the electric field this is not necessarily the case.[40] However the evidence is that BHJ solar cells can obtain very high currents and EQEs at short circuit and therefore we assume that charge separation *can* be highly efficient in BHJs.[25]

Another consideration in the BHJ structure is how the charges will be extracted from the device and generate current once they have been separated. In the case of the bilayer structure charge extraction is simple, as once the charges have been separated they be driven by drift current to the electrodes to be collected provided that a sufficient electric field is present.[41] It is of course important that the charges can be extracted without meeting a charge of the opposite polarity as if this were to occur the charges would be lost by recombining either radiatively or non-radiatively. This recombination of two charges after they have been separated from the bound state is defined as non-geminate recombination. While enhancing exciton separation and charge generation, the BHJ structure also makes it more difficult for the free charges to escape from the device to the electrodes as the simple structure of the bilayer has been replaced with a contorted structure through which the charge must travel without encountering an opposite charge.[22, 40] Presumably the domain structure aids in this process as if the domains are large enough then the charges are spatially separated from opposite charges. Additionally it is possible that in the spontaneous formation of the BHJ structure some domains are formed that do not have a contiguous connection to an electrode but are large enough to allow charges to be separated into this domain. If this were to occur then charges would accumulate in the isolated domain and the domain would act as a recombination centre for opposite charges.

2.3.3 Processes in BHJ Devices: Photons to Electrons

We can now summarise how an OPV device with a BHJ structure operates, from photon absorption to current generation. Firstly photons with an energy greater than the bandgap of the donor material are absorbed, initially generating an excitonic bound electron-hole species due to the low dielectric of organic semiconductors. This exciton has a high enough binding energy that it is highly unlikely that it will be split spontaneously by the thermal energy present at room temperature. We assume that we have an ideal BHJ structure with domains on the same length scale as the exciton diffusion length so this exciton then travels via diffusion through the semiconducting medium until it reaches a heterojunction interface. If the exciton reaches an interface between the donor and acceptor materials, and the LUMO energy of the acceptor is

lower than the donor (and vice-versa for the HOMO energy) then charge transfer is favourable and the electron is encouraged to transfer to the acceptor material leaving the hole in the donor. Due to the low dielectric permittivity of organic materials these charges are still Coulombically bound and not yet free, but with the aid of either available thermal energy in the system, electric fields or crystalline disorder within the domains, the charges can separate. These free charges can then be extracted via drift transport through the respective domains, the hole through the donor domains and electron through acceptor domains. If this transport is efficient and the morphology of the domains doesn't inhibit charge transport then these charges will be collected at the electrodes and generate currents. Otherwise, if an electron meets a hole, presumably at a donor:acceptor interface, then they will recombine. Finally if these charges reach an electrode they can escape the device and flow as current. Despite the complexity of all these processes, and the reliance on material self-organisation and lack of consensus in how the charge separation process occurs, efficient single junction BHJ OPV devices have been fabricated with power conversion efficiencies now greater than 9%.[42]

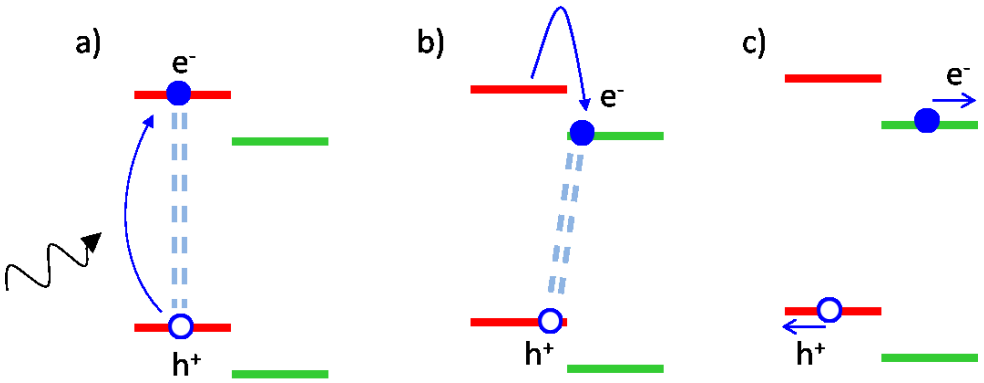

Figure 2.6. Depictions of the fundamental processes in an OPV device; (a) exciton generation, (b) charge transfer and generation and (c) charge transport and collection.

2.3.4 Loss Mechanisms In BHJ Devices

To truly understand the *J-V* behaviour of a complete OPV device it is necessary to possess a deeper understanding of the fundamental mechanisms operating within the device, and most importantly their voltage dependences. The disordered nature of organic semiconductors in comparison to their inorganic counterparts, and the fundamental differences in material structure and charge generation processes mean that in OPV devices charge loss processes must also be fully understood. Each process described in the operation of the BHJ solar cell has a corresponding loss mechanism that will reduce the extracted *J* at a particular *V*, and will consequently affect the device *J-V* curve and thus the PCE.

Once an exciton reaches an interface and undergoes charge transfer across the donor:acceptor interface it is still not free from recombination. As the electron and hole sitting on adjacent molecules on either side of the interface are still Coulombically bound and have a binding energy still higher than the

thermal energy present at room temperature this geminate charge pair will also recombine after a finite time unless induced to separate by some other process.[43-45] This will both waste the energy of the exciting photon and reduce the free charge generation and the resulting photocurrent. This loss mechanism is referred to as geminate recombination, as it involves the recombination of two opposite charges generated by the same photon. These processes are described as monomolecular or first order process (although these terminologies shall be discussed later) as the rate of recombination depends only upon the density of one species, the excitonic charge transfer state, not upon the concentrations of both electrons and holes.

If an exciton reaches an interface and the charge transfer state is separated via some non-specified mechanism then a free electron and free hole have been generated in respective donor and acceptor materials, thus the donor material has become the hole transporting medium and the acceptor correspondingly has become the electron transporting material. If one of these electrons meets a hole, presumably at an interface between the donor and acceptor, they will recombine in a process known as non-geminate recombination.[46-47] This process can occur in a variety of situations, either when both the carriers are free, or when one is trapped.[48] If this happens the electron and hole are lost, along with the energy of the absorbed photon and the current from the device is reduced. The non-geminate recombination process has been shown to be very important in determining the shape of the *J-V* curve of various OPV devices.[49-52] This process is clearly linked to the transport of the charges through the materials to the contacts. Starting with a simple example, in a bilayer device under high field the rate of non-geminate recombination would be very low as the transport of charge will be dominated by drift and therefore fast, the polarons will be rapidly separated by the field and it would be unlikely for them to meet again at the interface.[53-54] This obviously becomes more difficult to understand when the electric field within the device is reduced enough the diffusion transport competes with drift transport,[55] or when the morphology of a bilayer is switched to a BHJ in which even charges travelling away from a heterojunction towards an electrode via drift can still end up back at another interface where recombination can occur. In fact this process is sufficiently complex that it is still not fully understood, however various models have been developed and non-geminate recombination has been studied, this is described more fully below.

2.4 BASIC PROCESSES

2.4.1 Photon Absorption

As described above, when a photon is absorbed by an organic semiconductor a free charge is not generated as in inorganic semiconductors due to the low dielectric of organic materials. When the photon is absorbed it is excited from the HOMO to the LUMO and its energy is transformed into potential energy. This process is shown in Figure 2.6a. This electron is still Coulombically bound to the hole it left in the HOMO level, this bound pair is an exciton. The exciton is treated with a single wavefunction and therefore as a single particle rather than two bound carriers, and it has no dipole. Thus excitons are charge neutral and unaffected by electric fields and diffuse within the device.

The difference between the HOMO and LUMO energy levels of the donor material is referred to as the bandgap, and only photons with an energy greater than the bandgap, therefore photons with enough energy to excite an electron from its current level to the next, will be absorbed. The bandgaps of conjugated polymers tend to be somewhere between 1.5 - 2eV, which means these polymers only absorb the visible optical spectrum and not low energy photons, which constitute a significant proportion of the solar spectrum. Some inorganic semiconductors such as silicon absorb across the entire visible spectrum and to lower energies. This reduces the amount of current that can be generated by an OPV device, and significant research has gone into developing low bandgap polymers to increase the exciton generation.

Organic materials tend to have high optical absorption coefficients meaning they absorb photons strongly, thus 200-300nm films of organic material tend to absorb almost all of the photons with sufficient energy. This is better than some inorganic semiconductors such as crystalline silicon which require films with thicknesses of sometimes hundreds of micrometers to ensure adequate photon absorption.

2.4.2 Excitons

The electron and hole generated by the incident photon are tightly bound by electrostatic attraction and this binding energy is considerably larger than the thermal energy present at room temperature that could separate them. Excitons in organic semiconductors can be described as Frenkel excitons where the energetic balance means they are localised to one molecular site. In OPV polymer:fullerene systems the excitons are considered to be Frenkel type due to the low dielectric of the material, the exciton is therefore considered to be localised upon a single polymer monomer or occasionally extended along a single polymer.

Excitons have a finite lifetime and if not separated into constituent electrons and holes the exciton will recombine, this is classified as geminate recombination. This leads to the loss of energy from photons or alternatively the loss of charge carrier which could otherwise contribute towards the device current. The recombination of excitonic states is often radiative; a process known as photoluminescence (PL).

Observation of the PL from a film or device can be therefore used as a probe of the quantity of geminate recombination, thus a reduction in the PL with a change in blend morphology is indicative of an increase in the number of excitons separated and an enhanced morphology.[56-57]

2.4.3 Charge Separation In OPV

The process by which the bound excitonic state is separated into free polarons is still not fundamentally understood, and there are many suggested theories in the literature which try to understand this mechanism. However we do know that in some polymer:fullerene systems this apparently energetically unfavourable process can occur with remarkable efficiencies with EQE measurements greater than 90% at a certain wavelength.

The barrier to charge separation is the same as the barrier to initial photogeneration of separate electrons and holes; due to the typically low dielectric permittivity of organic semiconductors the coulomb binding force between charges of opposite polarities is very strong. Conventionally it is thought that when an exciton reaches an interface between two organic materials it undergoes charge transfer whereby either the electron or the hole transfers to a molecule across the interface, leaving a charge of the opposite polarity on the other side. Typically in a polymer:fullerene device the majority of the excitons are generated in the polymer and undergo charge separation where the electron transfers to the fullerene leaving the hole on the polymer. However, these two charges are still Coulombically bound and thus form a geminate bound pair. To generate free charges this bound pair must be separated, and how this occurs is still hotly contested, and quite possibly different in different OPV systems. It is clear from basic calculations that the coulomb attraction of an electron and hole (~0.5eV, if $\varepsilon=3$ and the charges are separated by 1nm) is far greater than the thermal energy present within the system (~25meV at 300K), thus some mechanism must overcome this binding energy to allow free charge generation.

The geminate bound pair is expected to have a finite lifetime, thus if it is not separated by some means recombination will occur and the energy of the exciting photon will be lost. This is a geminate recombination mechanism as the electron and hole recombining originated from the same absorbed photon, or they are a geminate pair. This recombination process is commonly referred to as first order as it scales with the density of just one species, the exciton or the bound polaron pair, rather than the densities of electrons and holes as in non-geminate recombination. Many authors have attempted to attribute all first order loss processes to geminate recombination of the exciton or bound pair,[48, 58] however this is unfounded as it is not the only loss process that can appear first order under certain circumstances.[59] This shall be discussed elsewhere in this thesis.

2.4.4 Charge Transport In OPV

Regardless of via which mechanism it occurs, we know that charge separation in some donor:acceptor systems can be very efficient. Once this charge separation/generation process has occurred the charges must travel to the electrodes to generate a current and power. This section shall describe the mechanism through which charges transport though the disordered semiconducting medium and methods used to understand this experimentally.

2.4.4.1 Drift and diffusion

The transport of charges in an OPV device can be approximated using the conventional equations used to understand charge transport in all semiconductors. Equations *(2-4)* and *(2-5)* show these equation for electrons and holes respectively.

$$J_n = eD_n\nabla n + en\mu_n E \qquad (2\text{-}4)$$

$$J_p = -eD_p\nabla p + ep\mu_p E \qquad (2\text{-}5)$$

where $J_{p(n)}$ is the current density of holes (electrons), $D_{p(n)}$ is the diffusion constant for holes (electrons), $\mu_{p(n)}$ the charge mobility for holes (electrons) and E is the electric field. These equations sum diffusion transport, the first term in the equation, which depends upon spatial gradients in charge carrier populations ($\nabla n(p)$) and drift transport, the second term, which is the charge transport driven by an electric field. The diffusion coefficient of electrons and holes are related to their respective mobilities via the Einstein equation $D = k_B T\mu/e$.

The equations above govern only transport of charges, these are then related to each other by the principle of conservation of charge, which takes into account charge transport as well as generation and recombination processes. Thus the continuity equations that govern electrons and holes (time dependent) relate charge transport to generation rate, G, and recombination rate, R. As the generation of charges in OPV devices is the separation of a bound electron-hole pair every generation event produces an electron and a hole, thus G is the same for both carriers. Additionally recombination of free charges, represents the non-geminate loss mechanism (discussed in detail below) which involves the recombination of both an electron and hole, so R is also the same for both carriers.

$$\frac{\partial n}{\partial t} - \frac{1}{e}\frac{\partial J_n}{\partial x} = G - R \qquad (2\text{-}6)$$

$$\frac{\partial p}{\partial t} + \frac{1}{e}\frac{\partial J_p}{\partial x} = G - R \qquad (2\text{-}7)$$

2.4.4.2 Charge Transport in Disordered Materials

Crystalline inorganic semiconductors are typically ordered and charge transport occurs via band transport, this is the efficient and fast movement of charge over distance and between individual molecules or atoms of semiconductor. Band transport occurs when there is sufficient overlap in the wavefunctions of

two charge sites that charges can move between those sites without impediment. It is known that as disordered semiconductors, organic materials have a highly complex and heterogeneous energetic landscape for the transport of charge. Additionally due to the disordered structure there is little or no long range order of molecules, resulting in little wavefunction overlap and consequently slow transport of charges. This is known as "hopping" transport as the charges effectively tunnel when moving from molecule to molecule and reside on a certain site for a finite amount of time, thus the charges appear to hop from site to site. Many models have been proposed for calculating the hopping of charges but the two most commonly used in organic systems are Marcus theory and Miller-Abrahams and both these approximations involve consideration of the difference in energy level of the two sites.[60] In particular the Marcus equation for rate of charge transfer from site i to j is

$$\nu_{ij} = \frac{\left|I_{ij}\right|^2}{\hbar}\sqrt{\frac{\pi}{\lambda kT}}\exp\left(-\frac{\left(\Delta G_{ij}+\lambda\right)^2}{4\lambda kT}\right) \qquad (2\text{-}8)$$

where I_{ij} is the overlap between the wavefunctions of sites *i* and *j*, k_B is Boltzmann's constant, T is temperature, ΔG is the difference in energy between the sites and λ is the reorganisation energy.

The energetic landscape that results from disorder in the semiconductor has been understood as a distribution of energetic states, as shown in Figure 2.4, where the random variation in energetic levels can be compressed into a density of states (DoS) below an energetic edge. This edge is referred to as a mobility edge; below the mobility edge the charges cannot move freely and are "trapped", for a charge in a trap state to move it must be excited out of the trap state to an energy above the mobility edge. This detrapping process requires energy input, however for a charge to be trapped requires only that a state of lower energy exists for the charge to transfer into. This mobility edge is thus defined by the distribution and density of energy states such that above the mobility edge there is a sufficient density of states of said energy that a charge with that energy can freely move, however a charge below the mobility edge is trapped as the density of states of that energy is not high enough for the charge to be transported without the input of energy. We can thus approximate the transport of charges above the mobility edge to be free and that of states below the edge to be trapped and require thermal or other excitation to move, thus charge mobilities above the mobility edge are constant and for states below the mobility edge they are zero. This therefore results in charge density dependent mobility dynamics as more of the trap states are filled at higher charge densities reducing the required energy for detrapping.[61] States above the mobility edge are analogous to the conduction band of a conventional semiconductor.

Several authors have shown that charge transport in organic semiconductors, at least in photovoltaic devices, is limited by the presence of trap states, thus this DoS of trap states is playing a part in the low mobilities of charges in organic semiconductors. There are several methods for measuring the bulk mobility of charges in devices, but one of the most common is to fabricate a transistor with said organic semiconductor and measure the current of charges across the gate. This method consistently measures higher charge mobilities by orders of magnitude compared to other device based measurements of charge

mobility such as time of flight (ToF) and space charge limited current (SCLC) measurements. It has been shown that this difference is due to variations in common charge densities between different types of devices fabricated and tested with organic semiconductors. Due to the large voltages and currents measured in transistors the typical charge densities within a transistor device are quite high, indeed compared to a typical OPV device under reasonable illumination there are many orders of magnitude more charges within the device. Thus in transistors there are enough charges that all the trap states are occupied and many charges can flow in the relatively more free states above the mobility edge. Whereas the lower charge mobilities within OPV devices results in charge transport being trap-limited, or the charge density within the device is below the density of trap states, thus almost all the charges within the device are trapped and require thermal excitation out of said trap states to move. This results in an overall lower bulk charge mobility in OPV devices as on a nano-scale the charges are repeatedly trapped, wait finite time on the trap site, and are then detrapped to continue to be transported.

Studies of the trap-limitations of OPV devices utilising transient absorption spectroscopy (TAS) on the common poly(3-hexylthiophene): [6,6]-phenyl-C71-butyric acid methyl ester (P3HT:PCBM) donor:acceptor blend found that charge transport and recombination stopped being charge density dependent at charge densities of ~1x10^18 cm^{-3}.[62] The transition from charge density dependent to charge density independent shows that the charges no longer require excitation out of trap states, thus places a value on the total density of trap states within this system.

In addition to the absolute magnitude of trap states, we need to know the shape of the density of states to truly understand the effect of trapping on charge transport. This is still a topic of contention within the literature, both in experimental measurements and in computational modelling studies. However most authors measure or assume either a Gaussian[63] or exponential[61] distribution of trap stated below the mobility edge. Additionally modelling studies have introduced various methods of including these trap states within the semiconducting material on the conventional semiconductor charge transport equations as shown by equations *(2-4)* and *(2-5)*. Most simply modify the equation such that the mobility and consequently the diffusion coefficient are charge density dependent. The effect of trapping upon recombination rates will be discussed below.

2.4.5 Charge Recombination

Non-geminate recombination is the process by which an electron and hole recombine, either radiatively or non-radiatively, and is an important energy loss process in photovoltaic devices. In an OPV device electrons and holes, produced by the separation of excitons, are usually considered to exist in separate material domains, thus non-geminate recombination presumably occurs at the donor:acceptor interface or in mixed regions. As this recombination process can only occur if an electron transfers to a molecular site occupied by a hole or vice-versa, at least one of the carriers must be free, i.e. a trapped carrier can recombine but only with an opposite charge that is free to move around the device. Non-

geminate recombination reduces the current obtained from the device, and thus if it occurs it can significantly affect the performance of an OPV device.

It is evident that as both electrons and holes are required for non-geminate recombination, if the amount of either within the device is increased then more non-geminate recombination will occur. We can represent this mathematically that the rate of non-geminate recombination is determined by the densities of both electrons *n* and holes *p* as well as some coefficient, *k*, which determines the magnitude of the relationship such that

$$R = knp \approx kn^2 \qquad (2\text{-}9)$$

If the densities of electrons and holes are similar then the rate of recombination scales with the density of electrons squared. This relationship distinguishes non-geminate recombination from geminate recombination, in that the rate of geminate recombination scales linearly with density of excitons whereas non-geminate recombination is a non-linear process with density of charge carriers. However it has been shown that this is only true when the densities of electrons and holes are similar, when one carrier is in excess then the rate of non-geminate recombination is dependent upon only the density of the minority carrier and the rate varies linearly with charge density.

2.5 ELECTRICAL OPERATION OF ORGANIC SOLAR CELLS

In a complete single junction photovoltaic device the active layer in which charge generation occurs is sandwiched between two conducting electrodes, an anode which collects holes and a cathode which collects electrons, and possibly some additional conducting layers to block carrier collection at the wrong electrode or ease the energetic transition from electrode to active layer. At least one of these electrodes must be transparent to allow light to enter the active layer. In OPV devices it is common to use indium tin oxide (ITO) as the transparent contact and a metal back contact to ensure that unabsorbed light is reflected back into the active layer. The metal contact is selected and the ITO electrode is coated with an interlayer, such that the work function of the anode approximately aligns with the HOMO level of the donor material and the cathode work function is aligned to the LUMO of the acceptor, thus each can efficiently collect the respective charge. The difference in work function between these two electrodes when in contact with the active layer provides the inherent electric field which drives charge from the device even under short circuit conditions when no external voltage is applied, this is the built in voltage of the system, or V_{BI}.

Figure 2.7a shows the band diagram for a BHJ donor:acceptor device under short circuit conditions. Charge has flowed from one electrode to the other due to their differing work functions so that their energies

are now equalised and such that the vacuum levels are now altered and an electric field is present through the device. Thus the voltage within the device is the built in voltage

$$eV_{BI} = \phi_{anode} - \phi_{cathode} \qquad (2\text{-}10)$$

where Φ_{anode} and $\Phi_{cathode}$ are the workfunctions of the anode and cathode respectively. As the Fermi levels in each material are identical there is no net potential difference between the electrodes in the device. Free charge carriers generated at the interface between donor and acceptor are driven to the contacts by the electric field, or difference in vacuum level.

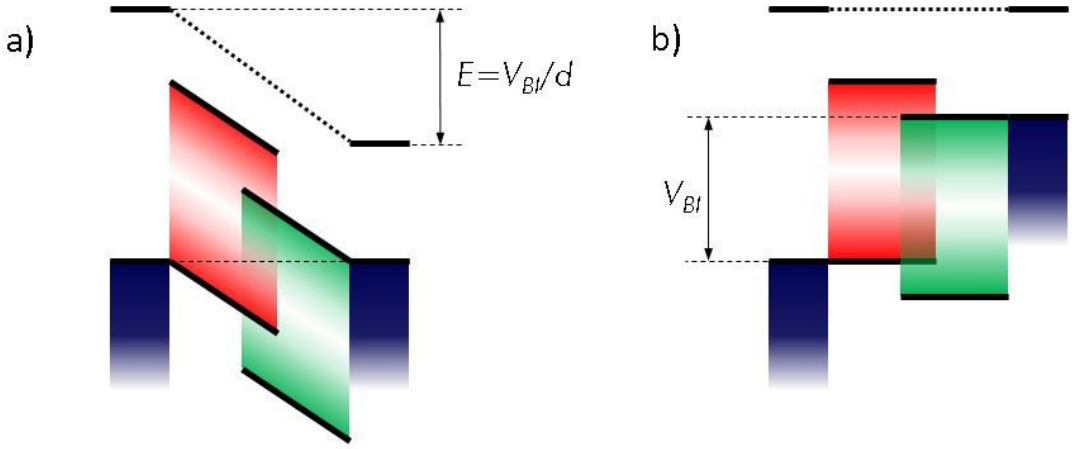

Figure 2.7. Schematic band diagrams of a donor:acceptor type solar cell under (a) short circuit and (b) open circuit conditions. The vacuum level is indicated by the black dotted line.

Figure 2.7b shows the same device now under open circuit conditions under illumination. The potential difference between the two electrodes is now approximately equal to the built in voltage, and the vacuum level is uniform such that there is no net electric field within the device. Thus the electron and hole populations within the device are much higher than under short circuit conditions. This increases their respective quasi-Fermi levels. As the Fermi levels in the respective phases are "pinned" to the electrode workfunctions at the electrode interfaces, the difference between the electron and hole Fermi levels roughly corresponds to the eV_{OC}. In the open circuit condition no net current flows, thus all charge generated recombines either geminately or more likely non-geminately.

Figure 2.8 shows a table, indicating the energy levels and alignments, as well as the net flow of electrons and holes in a BHJ device both in the dark and under illumination, and under five different bias conditions; (i) reverse bias, or $V<0V$, (ii) short circuit, or $V=0$, (iii) within the fourth quadrant, or power generating quadrant, so $0<V<V_{BI}$, (iv) at open circuit where $V\approx V_{BI}$ and (v) in far forward bias where $V>V_{BI}$. It can be seen in this diagram, by comparing the flow of electrons to the current extracted in the *J-V* curve, that the current obtained is relative to the electric field within the device. This is due to high rates of non-

geminate recombination that require charge to be swept from the device quickly to prevent recombination losses. Once the electric field is sufficiently reduced that diffusion transport competes with drift transport, then the charge density within the device begins to build and these higher quantities of accumulated charge lead to faster non-geminate recombination rates.

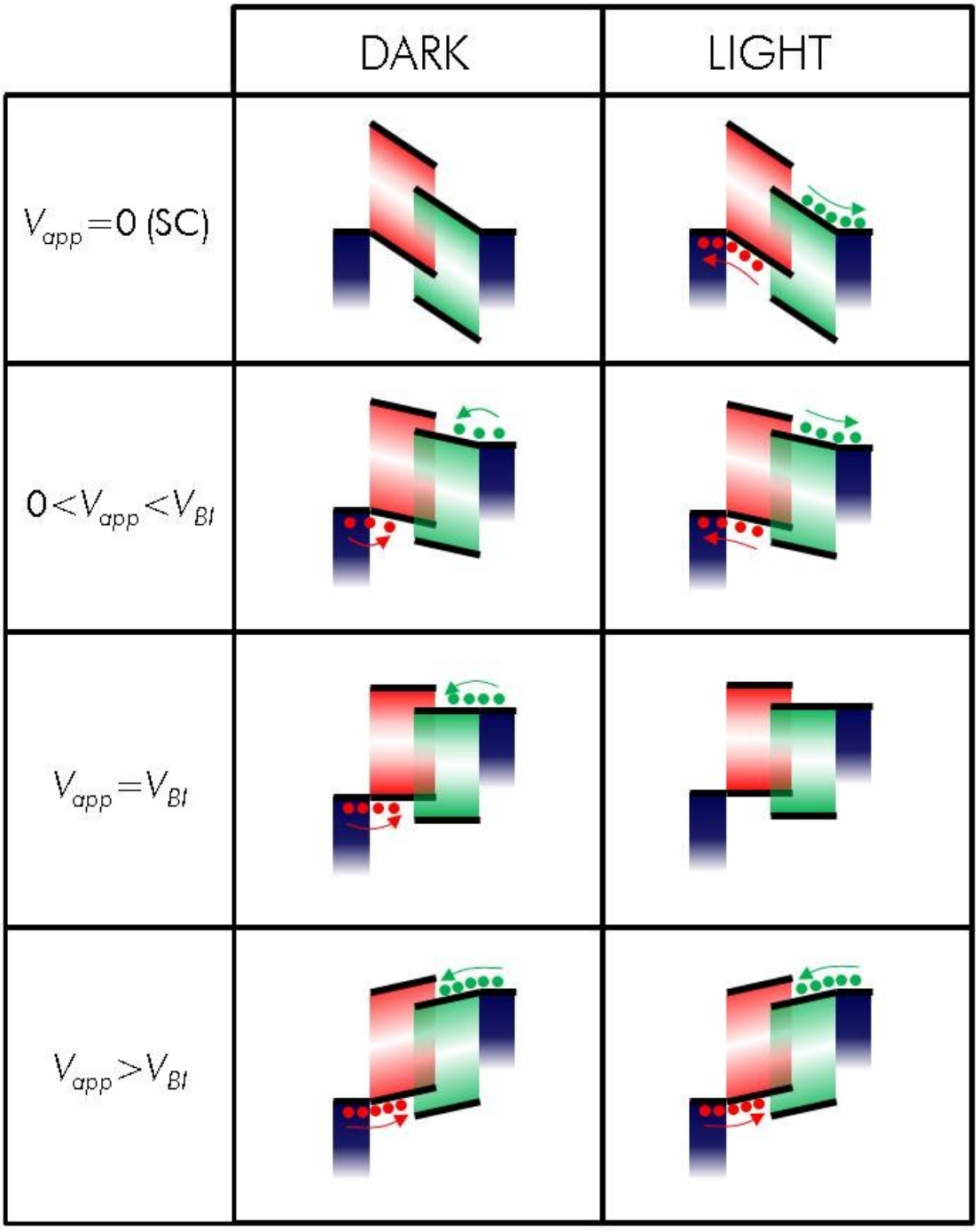

Figure 2.8. A table of schematic band diagrams showing the configurations of the conduction and valence bands, and indicating charge injection and extraction, in a donor:acceptor device under various applied biases and in the light and dark.

In this section we have assumed the effective medium approximation, or that the blend of two organic semiconductors in the BHJ structure can effectively be modelled by considering one semiconductor with the hole transporting properties of the donor and the electron transporting properties of the acceptor. This assumption is widespread in the modelling of OPV devices.

In Figure 2.7 and Figure 2.8 above the bands within the device are drawn as straight, indicating that the electric field distribution within the active layer of the device is uniform; in fact within a working device this is not always true. According to Gauss's law, any accumulation of charge within a semiconductor device produces a spatial variation in the electric field. Anything that generates an imbalance in the number of charges in the active layer of the device will cause the electric field to deviate from the constant value due to differences in work functions. In OPV devices, imbalances between the mobility of electrons and holes in the acceptor and donor materials respectively are known to cause some charge accumulation within the device. Additionally electronic doping, whilst not used intentionally in OPV as in inorganic devices, has been observed in some organic material systems, and this too can cause space-charge accumulation. Figure 2.9 shows a simulated band diagram for a polymer:fullerene OPV device showing the band bending observed when charge accumulation and depletion occurs, causing non-uniform electric fields within the device.

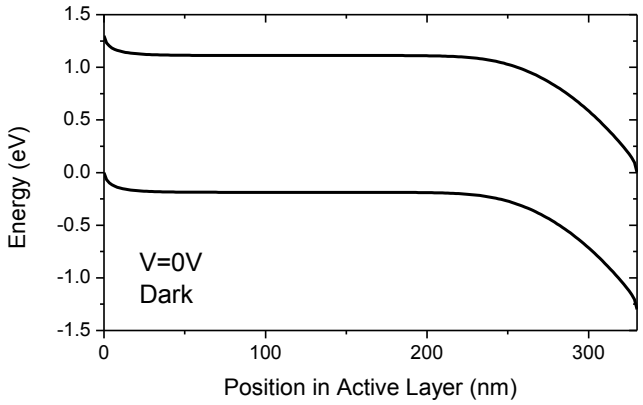

Figure 2.9. A simulated band diagram from drift-diffusion modelling of a thick and doped polymer:fullerene device, showing band bending and depletion region formation. This band diagram is identical to that in Figure 8.6, parameters used to simulate this device are detailed fully in Chapter 8 of this thesis.

As the diffusion of charges is slow in organic semiconductors and devices rely heavily upon the drift current to drive charges from the device and generate current, change in the electric field within the device are very important with regards to charge collection. The impact of mobility imbalances on charge collection has been extensively studied as in polymer:fullerene systems it is usually expected that electron transport through the fullerene is slower than hole transport through the polymer. Studies indicate that mobility imbalances can cause higher levels of non-geminate recombination in OPV devices obviously reducing charge collection and current generation.

Electronic doping of the active layer of solar cells is utilised in some inorganic devices and vacuum deposited small molecule devices to generate an electric field to drive charges to respective electrodes, and whilst this approach is not used in OPV devices unintentional doping has been observed in some devices. This doping is typically p-type (an excess of positive carriers), and this has been found to reduce charge collection in some organic solar cells. Electronic doping has some additional consequences which have not yet been fully understood in filling trap states. As charge transport is limited by trap states it has also been proposed that the presence of dopant charges could fill these traps and improve transport.

2.6 ISSUES TO BE UNDERSTOOD

2.6.1 Charge Separation in OPV

Currently the process by which the exciton is separated into free charges is not fully understood, as a comparison of the binding energy of the exciton and the available thermal energy would indicate a very low separation probability which is evidently not true. Below the various theoretical processes by which charge separation occur are summarised.

2.6.1.1 Onsager-Braun Theory

One possible explanation of the efficient separation of the bound pair is that it is aided by the electric field present within an OPV device under operating conditions. Whilst the exciton can be fully described as a single particle with neutral charge and unaffected by the electric field, the bound pair across the interface is can be represented by two separate charges and thus has a dipole. It is therefore expected that to some extent it should be affected by the electric field. The theory commonly used to model charge transfer state (CTS) separation was first devised theoretically by Onsager in 1938 and extended to donor:acceptor systems in 1984 by Braun.[39]

The Onsager-Braun theory (as it is commonly known) describes two charges of opposite polarity where one charge is in a potential well Coulombically bound to the other. The charge in the potential well has thermal energy at finite temperature and undergoes Brownian motion. The theory assigns a "capture radius" r_C at which the Coulombic potential energy is equal to the thermal energy, k_BT. According to the theory, if a charge carrier's thermalisation distance exceeds the coulomb capture radius then the charges can separate. The Onsager-Braun theory calculates the probability that by considering both the attraction and thermal diffusion the charges could separate spontaneously.

This model also implies that the efficiency of charge separation is a function of the local electric field. Whilst the Onsager-Braun theory has become one of the more common methods for modelling charge separation,[64-66] the literature is unclear upon whether this field-dependent bound pair separation has been observed. This is additionally confused by the structure of the BHJ; as the structure is contorted and

interlinked the interface is not always perpendicular to the electrodes and the electric field apparently necessary to separate the bound pairs. In fact if the interface is randomly oriented then there are likely to be as many sites there the electric field aids separation as there are where it is inhibited. This would suggest that possibly bilayer devices are ideal cases to study the expected electric-field dependent bound pair separation, however this has not conclusively been found, and the high *FF*s of some bilayer devices would suggest that there is little or no field dependence of charge generation.[41, 67]

Studies of charge populations using pump-probe experimental methods under bias produced contradictory results, with some authors observing differences with changes in electric field and some not. For example the work of Jamieson et. al. using TAS experiments shows no field dependence of charge generation in poly[2,6-(4,4-bis-(2-ethylhexyl)-4H-cyclopenta[2,1-b;3,4-b']dithiophene)-alt-4,7-(2,1,3-benzothiadiazole) (PCPDTBT):PCBM systems,[68] whilst the work of Albrecht et. al. on the same polymer:fullerene system with time delayed collection field (TDCF) methods come to the opposite conclusion.[69] Similarly TAS studies on the well-studied P3HT:PCBM system by Marsh et. al. observe significant changes in charge population, and presumably generation, with electric field, particularly in the power generating quadrant.[58] Whilst this directly contradicts many other TAS studies on P3HT which show the generation to be field-independent such as that by Shuttle et. al..[70]

Additionally the temperature dependence of charge generation predicted by Onsager-Braun has not been observed in experimental systems. In P3HT:PCBM systems the charge generation has been observed to be independent of temperature,[71] or at least not exponential as predicted by theory.[72] Regardless of the controversy surrounding experimental verifications of the Onsager-Braun theory, it has become one of the most commonly invoked theories of bound pair separation, and the concept of electric field assisted dissociation shall be studied in chapter 7 of this thesis.

2.6.1.2 Role of Excess Energy in Generation

Dimitrov et. al. have suggested that the binding energy of the geminate bound pair can be overcome by energy gained by the charge which undergoes charge transfer, as this charge is energetically driven from a higher energy state to a lower one, it must gain energy when charge transfer occurs.[73-74] This energy gained when undergoing charge transfer is normally referred to as "excess energy", and is the difference between the excitonic state and the separate polaron states. Whilst the energy gained by carriers during separation is difficult to calculate accurately, a large part of the energy comes from the difference between the LUMO levels of the donor and acceptor materials (in the case of electron transfer). It has been shown that as the difference in energy between the LUMO levels of the donor and acceptor increase, the corresponding polaron absorbance measured using TAS increased. This suggests that more free charges are generated, and presumably fewer recombine geminately, when the excess energy or driving energy was greater. It is suggested therefore that when free charges are generated by this mechanism, they are not generated in the ground state, but one carrier is energetically "hot".

2.6.1.3 Hot Carriers

It has also been suggested by several authors that excitons with energies greater than those in the ground state may use this excess energy to aid separation of the Coulombically bound state.[75-79] As excitons are generated by all photons that are absorbed, and some of these photons have energies far in excess of the bandgap of the organic semiconductors, some excitons must be generated with large energies. There are two important considerations and they are (i) do those excitons thermalise to the ground state and lose that excess energy before it can be used to separate the bound pair and (ii) if the exciton doesn't lose energy before reaching an interface, can that excess energy be used to overcome the binding energy of the bound pair.

As many of the thermalisation and charge transfer processes that occur within an OPV device are extremely quick, on the picosecond scale, they can only be measured using ultra-fast spectroscopy. Recent results from ultra-fast TAS experiments show that by measuring the decay of the exciton population and the generation of the polaron population, that a donor:acceptor blend pumped with higher energy photons generates free charges at a faster rate.[76] The authors therefore conclude that high energy photons access states in the donor material which allow more efficient transfer into free polaronic states with reduced loss mechanisms. Additionally these authors indicated from the internal quantum efficiency (IQE), or the ratio of absorbed photons to extracted charges, that even above the bandgap of the absorbing material higher energy photon is more likely to generate a free charge than a lower energy photon.

Furthermore, a relatively new experimental technique referred to as pump-push-probe spectroscopy has been used to study the thermally relaxed bound pair population.[79] By exciting the polymer:fullerene blend in the conventional manner used in TAS and other such methods (the pump) a population of relaxed bound pair is generated. By the applying a small additional excitation at sub-bandgap energy (the push) the authors claim to give additional energy to the bound pair, potentially enough to separate some more charges, this is measured by monitoring the device current (the probe). The results of this experiment upon various polymer:fullerene blends indicate that those with lower relaxed bound pair densities had higher photocurrents measured in steady-state. Thus the authors conclude that the lowest energy bound pair often or always recombines geminately, thus is a trap state, whereas only higher energy bound pair lead to free charge generation, supporting the "hot carrier" theory. However there is little information to suggest a cause for a certain polymer:fullerene blend to have a higher population of relaxed bound pair. Additionally, whilst it would appear that hot carriers aid charge separation at the interface, it is unclear whether there are thermally or energetically hot, and there is a need for further investigation in this area.

The theory that only hot carriers lead to separated charge states has also been countered by some other experimental measurements. By using extremely sensitive measurements of the optical absorption of a polymer:fullerene blend, such as photo-thermal deflection, Vanderwal et. al. claim to be able to observe the presence of bound pairs in that they observe a new absorption band that is not present in the absorption spectra of the neat donor or acceptor materials. It has been shown that the shape of the absorption spectra

and the IQE spectra at sub-bandgap energies is similar, thus leading to the conclusion that even the most thermally relaxed bound pair still give rise to separated charges. If the bound pair ground state were an energetic trap that always led to geminate recombination as suggested by proponents of the "hot carrier" theory, then this would be seen as a large difference in the absorption and IQE spectra at low energies. However, this conclusion relies on the accurate measurement of the absolute lowest bound pair energy through the optical absorption of the blend, and it is possible that perhaps this ground state bound pair is not optical accessible or is otherwise not observable in absorption measurements.

2.6.1.4 Charge Separation Not Via Charge Transfer States

Analysing both the energetic limits on charge separation from the bound pair and the high charge yields measured in some systems, some authors have concluded that charge separation from a bound pair is impossible or at least highly unlikely, and thus all charge generation must occur through a mechanism that doesn't involve the formation of a bound pair. One such mechanism would be the dissociation of the exciton by the long-range transfer of an electron to the acceptor material even when the exciton is not at an interface. This could occur if the electron component could effectively tunnel across long distances. This has been shown to be possible with the correct material properties through computational modelling studies,[80] however there is yet to be experimental validation of this theory, and the evidence obtained through comparison of the IQE and absorption spectra would seem to counteract this hypothesis.

Other groups have shown experimental evidence for the generation of free charges in a single material domain directly through photon absorption, without ever going through an excitonic state. The work of Burkhard et. al. indicate that photons with sufficient energy can excite free charges in many fullerene derivatives commonly used in OPV devices.[81] It is unclear whether these contribute significantly to the obtained photocurrent of the device or how long their lifetime will be as the free holes generated in the fullerene domains are probably likely to encounter an electron and recombine non-geminately. However it gives credence to theories that go against the conventional excitonic and bound pair separation theory of charge generation.

Finally, it has been hypothesised that other properties of the separated charges other than simply free energy and coulombic binding should be considered, such as the delocalisation of the charge and the energetic and structural landscape within which it resides. If charge transfer occurs and the electron is transferred into a localised state then it remains at the interface bound to its corresponding hole, however if the state it is transferred into is spatially delocalised, either within a molecule or within a crystalline domain, then it stands a higher chance of spontaneously dissociating. It has been proposed that the inherently disordered molecular structure of a polymer:fullerene interface may lead to a larger electronic bandgap in the molecules closest to the interface, leading to an energetic driving force for charges to separate spatially aiding separation.[82] Additionally experimental and modelling studies of energetic disorder and crystallinity have indicated that larger and purer crystalline phases may aid in the formation of more extended charge-transfer states that are consequently less bound and therefore do not require

an electric field for dissociation.[27, 35, 82-86] Problematically however it is very difficult to make any general conclusions upon charge generation due to morphology due to the lack of any microscopy technique that can probe the required morphologies on such a small scale. Additionally, whilst it is possible to study charge separation in different polymer:fullerene morphologies it is impossible to say which are actually present at the interface in a real device.[87]

2.6.2 Non-Geminate Recombination In OPV

2.6.2.1 Langevin recombination & the effect of transport

In a device under operation, when the device is not close to flat-band conditions, the electrons and holes are being driven by the electric field to move around within the active layer, this must be considered when analysing the recombination of electrons and holes. Considering a simple gas of electrons and holes moving in opposite directions in an electric field, the rate that the charges meet is dependent upon the speed with which the charges are moving. This was formalised into theory by Paul Langevin in 1903[88] and has since been applied to studies of non-geminate recombination by making the non-geminate recombination rate prefactor, k, dependent upon the mobility of the electrons and holes in the acceptor and donor materials respectively. This is expressed as

$$k = \frac{q}{\epsilon}(\mu_e + \mu_h) \qquad (2\text{-}11)$$

where q is the elementary charge and ε is the dielectric permittivity. However this formalism of the Langevin theory doesn't consider that in an OPV device charge recombination can only occur at an interface between separated electron and hole transporting domains, several authors have attempted to rewrite the equation to take account of this. In particular, Koster et. al. claim that once non-geminate recombination has depleted carriers from around the interface, the faster carrier will populate the interface whilst recombination cannot occur until the slower carrier has drifted to the interface.[47] Thus the recombination rate is dependent upon how quickly the slow carrier can reach the interface, or

$$k = \frac{q}{\epsilon}\langle\mu_e + \mu_h\rangle \approx \frac{q}{\epsilon}\min\{\mu_e, \mu_h\} \qquad (2\text{-}12)$$

Even with this modification of Langevin theory authors have found that their measurements of the non-geminate recombination rate were several orders of magnitude lower than the value predicted by mobilities obtained by time-of-flight measurements.[89] The authors therefore introduce a reduction parameter in the equation above such that

$$k = \zeta\frac{q}{\epsilon}\langle\mu_e + \mu_h\rangle \qquad (2\text{-}13)$$

where ζ is a parameter representing the reduction in Langevin recombination and $\zeta<1$. In a second paper of 2005, Pivrikas et. al. find that in P3HT:PCBM systems $\zeta\approx10^{-4}$.[90] The causes of reduced Langevin dynamics are unclear, yet it is most often attributed to the BHJ structure physically separating the two charge carriers and inhibiting recombination. This conclusion is corroborated by the modelling of experimental methods by Hamilton et. al..[91]

In addition to studies of the effect of mobility on charge carrier dynamics, there has been found to be an inverse relationship, in that the charge carriers can affect the mobility dynamics. Shuttle et. al. found in a P3HT:PCBM system that the charge carrier mobility measured using charge extraction measurements at short circuit was charge density dependent.[92] They concluded that as the charge density increased, the barrier to detrapping of charges reduced, thus the proportion of charges that are free increases, thus increasing the conductivity. This has since been strongly contested by Rauh et. al. who found that only under room temperature conditions were the dependence of mobility and recombination upon charge density the same.[52] They conclude that were recombination and mobility both determined by excitation from trap states the dependence should always be the same, thus an additional Langevin-limited process must act in OPV devices. As yet it is still uncertain how charge density and charge mobility are linked.

2.6.2.2 Effect of Disorder upon Recombination

Many experimental methods have been utilised to measure the rate of non-geminate recombination, and this is considerably easier to measure electronically as it affects free carriers, which in turn determine the voltage and current obtained by the device, as opposed to geminate recombination which is most commonly measured optically. The results mentioned above in which the non-geminate recombination rate was compared to that predicted by Langevin dynamics were measured using charge extraction with a linearly increasing voltage or photo-CELIV, which sweeps charges out of the device and measures the transient current which can then be modelled to determine the charge densities and recombination rates. Similarly transient photovoltage (TPV) has been used to measure the recombination rate by measuring the voltage response to a pulse of laser light, which corresponds to the recombination of a small number of excited charges.

One of the initially surprising results of these experimental probes of non-geminate recombination was that many studies found that in almost all the material systems studied, the non-geminate recombination rate did not scale with the charge density to the 2nd order but with a much higher order.[49, 93] If the order of the recombination process is defined as the power to which the rate scales with charge density, then the order of the recombination process, α, is determined by the relationship

$$R = kn^2 = k_0 n^{\alpha} \qquad (2\text{-}14)$$

Whilst non-geminate recombination with an order between 1 and 2 is easily interpreted by the equations described above, in experimental results show that the order of the non-geminate recombination process varies between 2-4 and even greater in extreme examples.

Super-second-order non-geminate recombination can only be understood when the energetic disorder within the semiconducting materials is taken into account. As described above, in photovoltaic devices the charge density within the device is always less than the density of trap states, thus the device is operating in a trap-limited regime where the majority of charges are trapped below a mobility edge. These trapped charges rely on thermal energy to excite them from the highest energy occupied trap state, to above the mobility edge where they can then move around within the blend and potentially recombine. As the steady-state charge density within the device increases, more and more trap states are filled, thus trap states of higher energy which are closer to the mobility edge are filled. This means that the energetic barrier preventing the charges from recombining is reduced. Thus as the charge density is increased, more charges can be excited above the mobility edge and can be transported within the device and recombine non-geminately. This is the cause of the charge density dependent non-geminate recombination prefactor.

This has been extensively measured using the charge extraction and transient photovoltage techniques by the Durrant group. These experimental methods together allow probing of both the charge density and recombination rate within the bulk of the device, thus allowing the study of the order of the recombination process etc..[70, 93-94] These techniques are particularly flexible in terms of the conditions in which the experiment can be performed, such that the recombination can be studied under various applied biases and light intensities. One interesting find in the work performed by Shuttle et. al. is that the recombination mechanism of photogenerated carriers in the light is the same as that of injected carriers in the light, thus the dark *J-V* curve is not simply determined by the diode characteristics of the solar cell, but additionally by the rates of non-geminate recombination.[49]

However the most important finding of these studies by the Durrant group was regarding the impact of non-geminate recombination upon device performance. For several polymer:fullerene systems, it was found that the non-geminate recombination measured under open-circuit conditions was equal to the charge generation, indicating that the voltage dependence of non-geminate recombination directly determined the open circuit voltage of these devices.[49, 95] It has been known that the V_{OC} is related to the difference in energy levels between the donor and acceptor material since this was shown by Scharber et. al.[96] however the relationship is not exact, only predicting the V_{OC} to within 100mV. The studies of non-geminate recombination using TPV predict the V_{OC} value to a much higher degree of accuracy indicating that whilst the maximum limit of the V_{OC} is set by the energetics of the materials used in the OPV device, the specific value and consequently the performance of the device, is heavily influenced by non-geminate recombination. This is because the voltage of the device is set by the difference in Fermi levels between the electrons and holes, if the populations of both are reduced by particularly strong non-geminate losses then this will reduce the Fermi level splitting and the device voltage.

Another important finding was that in the P3HT:PCBM system, not just the V_{OC} but the entire *J-V* curve appears to be determined by a non-geminate recombination process following a voltage-independent charge generation process.[49] By measuring the non-geminate recombination flux at applied voltages across the power-generating quadrant of the *J-V* curve and subtracting this from a generation flux roughly corresponding to the short circuit current density of the solar cell achieved a very close reconstruction of the experimentally measured *J-V* curve. This indicates that the non-geminate recombination process determines the fill-factor of at least the P3HT:PCBM system, and potentially others. Maurano et. al. extended the technique to P3HS:PCBM.[97] This work has further been repeated by various authors on a variety of different material systems,[41, 98-99] however a large range of recombination dynamics have been observed by different groups. This raises the question of what material properties and device properties effect the relationship between charge density and recombination rate, and more pertinently how can that relationship be manipulated to reduce recombination in devices.

2.6.2.3 Free or Trapped Charge Recombination

One current topic in the field of non-geminate recombination is what energetic states the two charges recombining are in when the recombination event occurs. In a disordered material where delocalisation from trapping is a limiting process there are three types of recombination; free-to-free in which both the electron and hole are delocalised when recombining, free-to-trapped where one charge is trapped and effectively stationary, and trapped-to-trapped which we assume to be negligible to impossible as both charges are localised.

The discussion of free or trapped charges recombining is important, firstly as demonstrated above the trapping process can have a large impact upon recombination lifetimes, but additionally as if the recombination is occurring via either trapped or free charges the dependence upon the density of states (DoS) is changed. If trapped charges play a large role in non-geminate recombination the shape of the DoS will play a large role in determining recombination rates, as well as the spatial location of these trap states. Furthermore, if recombination can only occur if both charges are free, the limiting process that determines the recombination rate will be the excitation of charges from the DoS. One way of probing whether free or trapped charges dominate recombination is via the ideality factor, determined either from the slope of the *J-V* curve in the dark, or from the light intensity dependence of the open circuit voltage. It is commonly claimed that if the ideality factor is approximately 1 then free-to-free recombination dominates, if it is close to 2 then the free-to-trapped process dominates, and anywhere between 1 and 2 indicates a more complex behaviour or mix of processes. Kirchartz et. al. have demonstrated using drift-diffusion simulations that this is valid, and additionally that the ideality factor is sensitive to surface recombination are the electrode.[100] Furthermore through studying the ideality factor they show that PCDTBT:$PC_{71}BM$ devices are limited by free-to-trap recombination at low voltages and surface recombination at higher voltages. This is similarly the conclusion of Street et. al. who show that free-to-trapped recombination is dominant in that material system, as well as demonstrating that the formation of new trap states significantly affects the amount of charge lost to recombination.[101] Furthermore Schafferhans et. al. showed that the increase in deep trap states can

reduce the *FF* and V_{OC} of P3HT:PCBM devices,[102] as well as altering the charge carrier mobilities, as would be consistent with Shuttle et. al. discussed above.[92]

Another common method of determining the mechanism of charge recombination is to analyse the dependence of the non-geminate rate upon charge density, or α, as described above. The conventions on referring to recombination processes are not always the same for all authors. Many authors describe recombination with α=1 as monomolecular even if it is a non-geminate process involving two particles,[48] this is because they only count free charges and conclude that if the recombination process if first order then it must be a free-to-trapped process. This was shown by Deibel and Wagenpfahl to be incorrect, both in the method used to determine the order of the recombination process (corrected photocurrent), and in the conclusion that this specifically refers to free-to-trap type recombination.[59] This is a contentious issue in the study of non-geminate recombination, and a certain method for determining the recombination order is yet to be universally accepted. Furthermore the relationship between recombination order and recombination process is yet to be fully understood.

2.6.2.4 Role of Electric Field in Non-Geminate Recombination

Whilst few authors counter the statement that non-geminate recombination dominates within an OPV device under open circuit conditions, there is not yet a consensus upon whether the same process occurs at higher applied biases. Under short circuit conditions a strong electric field is present in the active layer of an OPV device driving charges to the electrodes. Whilst some devices exhibit flat *J-V* curves through short circuit conditions, indicating that charge generation and collection is efficient under these conditions, various authors have attributed poor J_{SC}s to low rates of charge collection.[27, 103-106] Additionally, as has already been shown by Shuttle et. al. non-geminate recombination reduces the current of a P3HT:PCBM device around the maximum power point.[49] Evidently different material systems exhibit different charge collection probabilities. It is thus important to characterise how the rates of non-geminate recombination change in various devices with applied bias. In a simple device model, if charge generation is voltage-independent, then the voltage-dependence of the non-geminate recombination process determines the fill-factor of devices.

2.7 MOTIVATION FOR THESIS

Whilst OPVs have achieved relatively high power conversion efficiencies and large gains have been made in the understanding of device operation, there are still significant barriers to large-scale implementation and thorough understanding of all the processes occurring in a device. As highlighted in this chapter there are large gaps in the current understanding of the fundamental processes that charges undergo during the operation of an OPV device, particularly the charge separation/generation process and the detailed nature of the non-geminate recombination process. Additionally relating these fundamental

processes directly to the performance of a complete device has proved difficult, and if we are to improve OPV performance to a level at which commercialisation is possible, this must be achieved.

In this thesis I will aim to address the issues raised above through the use of new and established techniques, notably the use of transient opto-electronic measurements. These techniques have proven to be among the most useful in the analysis of fundamental charge behaviour as they allow the study of processes in actual devices under operating conditions. Additionally they are versatile tools that have already successfully elucidated charge transport and recombination processes in several material systems. I will extend these techniques to study these charge processes in new ways and in efficient and novel material systems with a desire to address the issues and gaps in our current understanding of device operation.

In addition to the use of transient opto-electronic measurement techniques, I will utilise various computational models of OPV device behaviour to attempt to truly relate bulk device measurements to fundamental, single-charge processes.

CHAPTER III

SUMMARY OF THESIS

In the first experimental chapter we study a P3HT:PCBM device and show how several transient opto-electronic experimental techniques can be used to measure various aspects of non-geminate recombination. Namely, we use charge extraction (CE) experiments to determine the charge density within the solar cell (*n*) and transient photovoltage (TPV) the rates of non-geminate recombination (*R*). We utilise these two techniques to show how the open circuit voltage (V_{OC}) and fill factor (*FF*) of the P3HT:PCBM device, and consequently the power conversion efficiency, are impacted by non-geminate recombination. Furthermore, we study the temperature dependence of this loss process to further study this loss mechanism and the energetic structure of the material system. Additionally we demonstrate how transient photocurrent (TPC) experiments can be used to study the distribution of energetic states within a P3HT:PCBM device. This distribution of "trap" states has been shown to have a significant effect upon the charge transport within organic semiconductors, and therefore upon device performance. Using TPC experiments we study the distributions of trap states in a P3HT:PCBM device with various structural morphologies by studying devices that have been thermally annealed to various degrees.

In the second experimental chapter we further study non-geminate recombination in P3HT:PCBM devices, particularly with respect to the linearity of the loss processes within the device with regard to the light intensity with which the device is illuminated. We study the device's corrected photocurrent, or the *J-V* curve of the device in the dark subtracted from the *J-V* curve of the device under illumination. In this chapter we reconcile two apparently contradictory experimental results which show that the limiting non-geminate recombination rate depends highly non-linearly upon charge density, whilst the corrected photocurrent of the device appears to be linear of a large range of operating light intensities and voltages. We show how a 3rd order process can still give rise to apparently linear performance under various conditions.

In the third experimental chapter of this thesis we study recombination processes in a selection of material systems; P3HT:PCBM, poly(2,7-(9,9-dioctylfluorene)-alt-5,5-(4,7-di-2-thienyl-2',1',3'-benzothiadiazole)) (APFO-3):$PC_{71}BM$ and PCPDTBT:$PC_{71}BM$+ODT. Specifically we study the extent to which geminate and non-geminate recombination mechanisms can impact upon the generation, collection and

recombination of charges in the devices and we relate this directly to the *FF* of the devices, and therefore the power conversion efficiency. Whilst the limitations on a devices short circuit current density (J_{SC}) and open circuit voltage (V_{OC}) are well established, the fill factor is less well understood and a comprehensive discussion of different limitations is required. We study the OPV devices using charge extraction and transient photovoltage experiments, as well as transient absorption spectroscopy. The findings of the chapter show that whilst the APFO-3 and PCPDTBT devices (as well as the P3HT device under high light intensity) have very similar shaped *J-V* curves and *FF*s, they are in fact limited by different recombination mechanisms. Whilst P3HT and PCPDTBT devices are limited by non-geminate recombination, we show that in APFO-3:$PC_{71}BM$ devices a voltage-dependent charge generation (or a voltage-dependent geminate recombination) process limits the achievable *FF* of OPVs.

In the fourth and final experimental chapter, we study the effect of electronic doping and the electrostatics of a device with space-charge accumulation upon non-geminate recombination and charge collection. We study devices fabricated from a blend of PBDTTBTZT:$PC_{71}BM$ in both standard and inverted device architecture and with a wide range of active layer thicknesses. Through studies of *J-V* curves and external quantum efficiency, and capacitance-voltage experiments to study the electronic doping of the organic semiconductors, we show that in different configurations these devices are significantly limited by charge collection. Through optical and electronic modelling we show that the doping of the photovoltaic active layer causes the accumulation of space-charge, which in turn alters the electric field within the solar cell, causing some charges to not feel any electric field driving them from the device and consequently reducing charge collection.

CHAPTER IV

EXPERIMENTAL AND COMPUTATIONAL METHODS

4.1 MATERIALS AND DEVICE FABRICATION

All the devices studied in this thesis are solution processed polymer:fullerene solar cells. The most widely studied material system in OPV research by far is the P3HT:PCBM blend (with molecular structures shown in Figure 4.1) and this system is the basis of the measurements in chapters 5 and 6 of this thesis. In addition these P3HT:PCBM devices, as they are characterised so thoroughly and their operation is well understood, are used as a comparison for other materials when studying device FFs in chapter 7. The P3HT used in these devices was purchased from Reike Materials. The other polymers used in chapter 7, PCPDTBT and APFO-3, were obtained from Konarka and Plextronic respectively. The polymer PBDTTBTZT studied in chapter 8 was synthesised by, and provided through a collaboration with, Merck Chemicals Ltd.. $PC_{60}BM$ and $PC_{70}BM$ were purchased from either Solenne or Nano-C.

All the devices in this thesis, except those in chapter 8, were fabricated in standard architecture by spin coating. Substrates were prepared by first spin-coating a solution of PEDOT:PSS upon a pre-patterned indium tin oxide (ITO) electrode on glass. The PEDOT:PSS layer was dried by annealing at 100°C for 15 minutes. Active layer deposition was achieved by spin-coating a solution of polymer and fullerene. The solvent used was specific to the polymer, however typically ortho-dichlorobenzene (oDCB) was used. The polymer and fullerene were dissolved in a ratio of 1:1.5 for P3HT:PCBM, 1:4 for APFO-3:PCBM and 1:3 for PCPDTBT, with a typical solution concentration of 20-30mg/ml. These solution were always left stirring for several hours under heat to aid dispersion and solution. The solution was then spin-coated onto the prepared substrates with a spin speed of typically 1,000-2,000 rpm. Finally the top electrode of aluminium

was evaporated onto the film, additionally some polymers require an interlayer to be evaporated between the active layer and aluminium of either calcium or lithium fluoride. Devices were stored and tested under a low-oxygen and low-water nitrogen environment. Device fabrication at Imperial College was assisted by Dr. Pabitra Shakya.

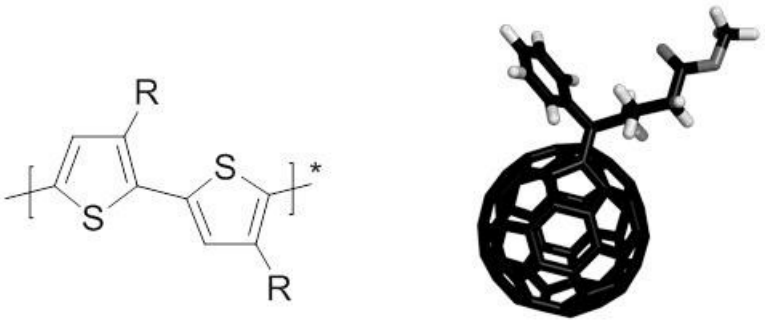

Figure 4.1. A molecular drawing of poly-3-hexylthiophene and a rendering of the structure of [6,6]-phenyl-C_{61} butyric acid methyl ester (PCBM).

The devices studied in chapter 8 were all blade-coated at Merck Chemicals facilities in Chilworth, Southampton. Solutions, and PEDOT:PSS and ITO coated substrates, were prepared as above. Polymer:fullerene blend solutions in oDCB were then coated using an Erichsen Coatmaster 509MC. The blade coating process provided the flexibility to fabricate devices with a wide range of active layer thicknesses. Aluminium electrodes were the evaporated onto the films with calcium. Inverted devices were also fabricated in the same manner, however ITO substrates were coated with a zinc oxide layer, and the polymer:fullerene blends were additionally topped with a spin-coated PEDOT:PSS layer before being evaporated with gold electrodes. Device fabrication at Merck Chemicals was assisted by Mathis Muth.

J-V measurements of complete devices was performed using a Keithley 2400-series source-measure unit. Illumination was provided by a xenon arc lamp solar simulator, calibrated with a Newport silicon photodiode with known performance under 1 sun illumination.

4.1.1 Device Selection

In general throughout this thesis devices were prepared in batches of 16 due to space constraints in the evaporation stage. In some of these batches changes to the solution formulation or device fabrication conditions were made during the device making, and in some batches, particularly those of blends with well established, optimised recipes, 16 nominally identical devices were fabricated. Experiments utilising charge extraction, TPV or TAS techniques require long experimental times, sometimes greater than 24 hours, making it impractical to test a whole batch of devices, thus one or two devices must be selected for extensive

experimental analysis. Devices were selected by measuring current-voltage curves in a solar simulator for all of the devices in a batch and selecting the most efficient device or devices.[107]

Whilst there has been discussion in the field of the best way to measure device efficiencies using statistics,[108] the policy of performing in-depth testing on the most efficient devices available rather than those that best represent the average performance of a batch is widespread (and used here).[109] This is for many reasons; firstly, there are many sources of poor device performance apart from the efficiency of the active layer at converting light to electricity. Interlayers in the device and interfaces with electric contacts can provide barriers for efficient charge transport and, in addition, degradation of devices has been shown to occur in these layers just as strongly as in the BHJ blend. In the case of the experiments in this thesis, the aim is to study the processes of the charges within the active layer and not on the scale of the entire device. Thus selection of the device with the highest efficiency is a way of selecting the device in which the active layer processes are least impeded by additional losses in the other layers. Additionally as there are many sources of reduced efficiency, comparison of two devices with only the average efficiency of the batch may not be representative as they may exhibit reduced efficiencies for different reasons.

In addition to the practical reasons detailed above, there is the more general problem that the best device to measure is the device that best "represents" the properties of the material system in question. As has been shown in various studies in the literature, small changes in device fabrication conditions can greatly affect the final performance, making it almost impossible to select a device which is truly representative of the material system when another optimisation to the fabrication procedure could result in an additional increase in efficiency. Thus it is just as valid to suggest that the average device from a small batch is "representative", as it is to say the most efficient device is "representative" of the performance of the blend.

To summarise, the devices subjected to extensive study of generation and recombination processes in this these are selected as he highest performing of the batch in which they are fabricated. This is done to ensure that the processes being measured are as unimpeded by other losses as possible, and that the device represents the best possible performance of the material system under study.

4.2 CHARGE EXTRACTION

Charge extraction is a transient experimental technique to measure the equilibrium charge density, *n*, within an organic solar cell under various operating conditions; its simplicity and the variety of conditions in which it can be applied make it one of the most versatile transient techniques used to measure dynamics within a solar cell.

Charge extraction is performed by electronically switching the device from the conditions in which the charge density is to be measured (e.g. open circuit under illumination) into a state where the charge carriers

are quickly swept out of the active layer and the measurement of the resulting current transient. By integrating the current transient with time, thus literally counting the charges that are swept out of the device, a measurement of charge density can be made. Thus the measurement of charge density, n, is made such that

$$n = \frac{\int Idt}{eV} \qquad (4\text{-}1)$$

where I is the measured current, t is time, e is the elementary charge and V is the device volume.

The technique consists of three phases; before, during and after the transient. Before the transient the device being measured is held under the appropriate conditions in which the charge density is to be measured, specifically the cell voltage and applied light intensity. The device must be held in these conditions long enough to allow the device to reach steady state. The device is then switched to short circuit conditions and the applied light is simultaneously switched off. This switching is performed by simultaneous electronically controlled switches. In the dark there are no new photogenerated charge carriers and at short circuit it is assumed there is sufficient electric field to efficiently extract carriers, the limits of these assumptions are described below. During the transient the cell equilibrates to the new conditions with charge rapidly flowing out of the device. This is measured as a current transient across a resistor, using an oscilloscope. After the transient, the device is now in steady state conditions in the dark at short circuit and no charge is flowing, the transient is over and can now be integrated against time to obtain a measurement of the total number of charges that were in the device before the transient.

Figure 4.2a shows typical current transients under varying applied light intensities, of devices held under open circuit conditions; these are integrated to produce the charge transients shown in Figure 4.2b. The plateau levels of these transients provide a measure of the total charge within the device which can then be divided by the volume of the device and the elementary charge to obtain a measurement of charge density within the device.

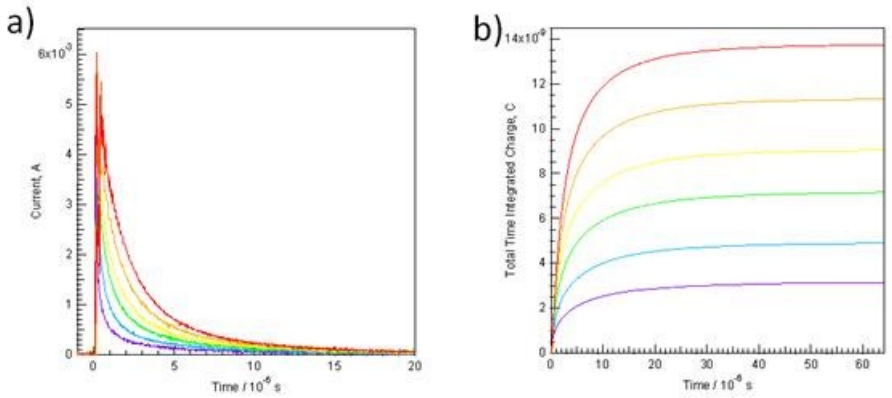

Figure 4.2. (a) Raw charge extraction transients as a function of illumination intensity and (b) the same transients integrated to give a measure of total charge.

These measurements are performed with a white light bias provided by a ring of 12 white Lumiled LEDs focussed upon the device and thus with a variable power up to ~5 suns and with a fast MOSFET switch between open and short circuit conditions.

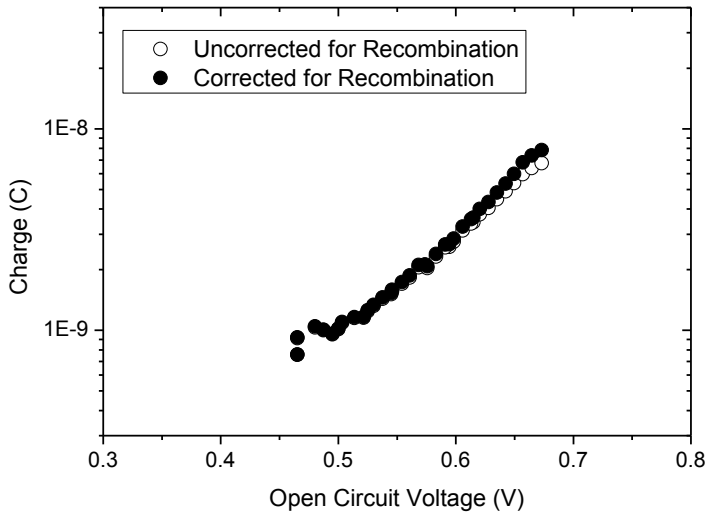

Figure 4.3. A plot showing typical charge measurements resulting from a charge extraction experiment under open circuit conditions, both uncorrected and corrected for recombination during the transient.

4.2.1 Experimental Details

The charge extraction experiments in this thesis are performed with white light illumination provided by a ring of 12 white lumiled LED's, focussed upon the device under test, powered by a programmable power supply. These are capable of providing illumination as high as approximately 5 suns, and the brightness is calibrated such that under nominal 1 sun illumination the JSC of the device is the same as that measured in a solar simulator. The device under test is switched between open circuit and short circuit conditions, this is achieved by connecting the device to a MOSFET transistor; when the transistor is open the large resistance of the transistor (~3MΩ) holds the device at open circuit, when the transistor is closed the device is connected to an oscilloscope to measure the current flowing from the device across a 50Ω resistor. This is shown in the circuit diagram in Figure 4.4. When switching from open circuit to short circuit, the open circuit voltage at which the device is held is determined by the illumination intensity of the LEDs. When switching from applied bias the open terminals of the MOSFET are replaced with the terminals of a Keithley 2404B source-measure unit, applying the required voltage.

Using a PC to control both the MOSFET and the programmable power supply makes it possible to simultaneously switch off the illumination source whilst sweeping the device to short circuit. When the device

is switched to short circuit and the illumination turned off the current transient is recorded by the oscilloscope across the 50Ω resistor. This transient is then passed to the PC for integration and other data processing.

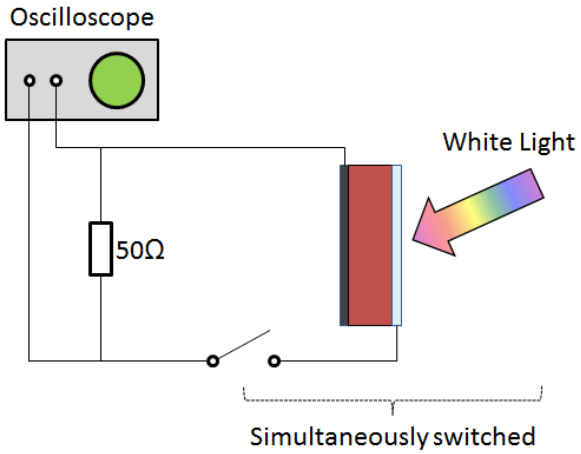

Figure 4.4. A circuit diagram indicating the experimental setup for charge extraction experiments.

4.2.2 Recombination During The Transient

To gain an accurate measurement of the charge density the technique assumes that all the charges present within the device before the transient are extracted from the device and are measured as current, however this is not necessarily true as some charges may be lost to non-geminate recombination during the transient and are thus not measured. To correct the final measured values of charge density for this an iterative algorithm, taking the n vs. t charge recombination dynamics as an input (where t is measured using TPV), allow an accurate initial charge density to be estimated from the final measured values. Figure 4.3 shows charge extraction data before and after this correction showing that higher charge densities result in a larger change on correction.

An appropriate alternative to this correction would be to switch into negative biases where there is a higher electric field, charge transport is thus quicker and therefore less non-geminate recombination is occurring. However this complicates the experiment and induces difficulties in switching and measuring the device conditions, thus all charge extraction measurements in this thesis are measured by switching the short circuit conditions and correction the measurement.

4.2.3 Electrode Charge

In addition to the charges within the bulk of the solar cell, there are charges present on the electrodes, referred to as capacitative charges as they correspond to the charge on the electrode were the active layer not photoactive but simply a dielectric and thus the device was a capacitor. Thus

$$n_{extracted} = n_{active\ layer} + n_{capacitative} \approx n_{active\ layer} + \frac{\epsilon_R \epsilon_0 V}{ed^2} \qquad (4\text{-}2)$$

where ϵ_0 and ϵ_R are the relative dielectric permittivities of the vacuum and material respectively, e is the elementary charge and d is the thickness of the active layer. Thus by calculating the geometrical capacitance of the device from literature values of the active layers dielectric it is possible to subtract from the final measured charge density the component that corresponds to charge on the electrodes, leaving only the charge density relevant to device behaviour, that within the active layer.

4.2.4 Distinguishing Electrons and Holes

Finally, as the charge extraction technique simply measures a current it cannot distinguish between electrons and holes when extracting the charge carriers, thus the technique cannot measure imbalances in charge carriers. Additionally as the technique switches to short circuit conditions in the dark it only measures charge in excess to those present there. Although that is sufficient to observe charge carrier dynamics under active conditions, it means the technique is not sensitive to charged dopants and fundamental charge imbalances which would be present under those conditions.

4.3 TRANSIENT PHOTOVOLTAGE

Transient photovoltage (TPV) is an experimental technique used to electronically measure the overall recombination rate of free electrons and holes in an organic solar cell in response to optical stimuli.

4.3.1 Technique

Transient photovoltage is an electro-optical technique in that it measures the electrical response to an optical pulse. TPV is performed by holding the device under open circuit conditions by connecting the device to an oscilloscope with high impedance; the device is then photo-excited using a laser pulse in addition to a standard white light background illumination. This laser pulse excites a small number of additional charges

within the device. The wavelength of the pump laser is selected such that the blend material does not absorb too strongly, thus on the shoulder of the absorption spectrum, so photons are absorbed throughout the device rather than just at the transparent contact. Under open circuit conditions the difference between the Fermi levels corresponds to the device voltage, this is directly probed using the oscilloscope to measure the decay of populations of electrons and holes as they recombine to return to equilibrium conditions after the small perturbation. The rate of decay of these charge carrier populations corresponds to the non-geminate recombination rate of the device under these conditions. As the non-geminate recombination rate changes with charge density, by varying the background white light illumination and therefore the charge density within the device, the way this process depends upon charge density can be studied.

It is essential to the analysis of TPV results that the device remains under open circuit conditions, thus the laser pulse that provides the excitation must be very small, such that the additional charge carriers excited do not substantially move the device away from open circuit conditions. This is done by monitoring the change in voltage upon laser excitation and maintaining a change below 1mV.

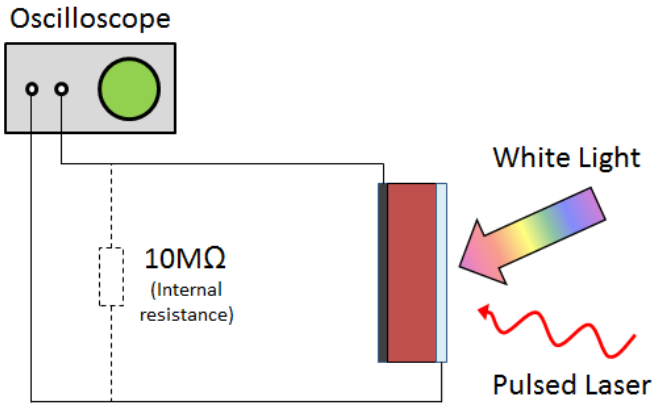

Figure 4.5. A circuit diagram indicating the experimental setup of TPV experiments.

4.3.2 Experimental Details

In transient photovoltage experiments the device is held at open circuit conditions for the entire experiment and thus no switch is required. The device is held at open circuit simply by connecting its outputs to the input of an oscilloscope (Tektronix TDS3032B) with a large input resistance, this oscilloscope is then used to monitor the voltage of the device throughout. The V_{OC} can then be varied by changing with illumination intensity of the white LEDs, this setup is shown in the circuit diagram of Figure 4.5. The small perturbation measured in the experiment is provided by a monochromatic illumination from a wavelength adjustable nitrogen laser fitted with a dye module. The wavelength of this pulse is chosen such that the light is absorbed only weakly by the blend, thus generating charges throughout the device. Additionally the power of this pulse is kept intentionally low such that the smallest number of charges are generated as is possible

and still be measured, this is important to utilise the small perturbation approximation in the analysis of the results. The power of the laser is kept low enough that the measured change in V_{OC} is <1mV.

4.3.3 Results

Figure 4.6a shows typical transient photovoltage decays under various white light illumination levels. The exponential nature of the decays can be observed. In addition, the smallest and fastest decay corresponds to the highest light intensity, this is due to the high charge carrier densities under these conditions creating conditions with high non-geminate recombination. Figure 4.6b shows the lifetimes obtained from exponential fits to the data plotted against the open circuit voltage of the device, showing the reduction with recombination lifetime with light intensity and voltage.

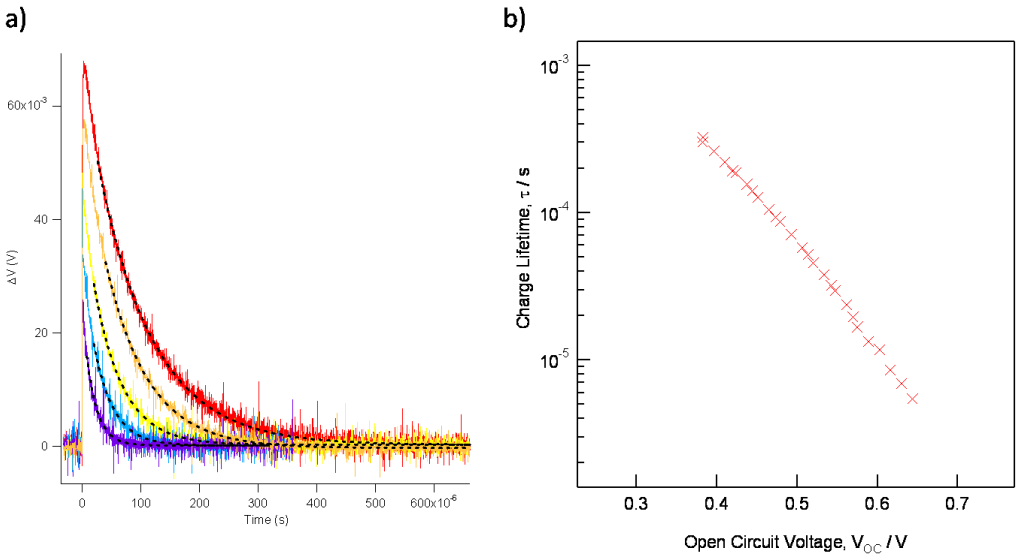

Figure 4.6. (a) Raw TPV transients under various illumination intensities with exponential fits (dashed) and (b) the exponential fits of the same transients as a function of open circuit voltage.

4.3.4 Mathematics

TPV measures the recombination of a small number of excited charges, whilst the most important quantity to the operation of the solar cell is how quickly *all* the charges within the device recombine. Thus measurements of recombination rate using TPV are corrected to probe this quantity. In other words what is measured in a TPV experiment is $\frac{d\Delta V}{dt}$ which is proportional to $\frac{d\Delta n}{dt}$ which is the relationship that is fit to determine the recombination rate, however the most relevant quantity for device performance is $\frac{dn}{dt}$. As

$$\frac{dn}{dt} = -k(n)n \text{ and } k(n) = k_0 n^{\lambda} \qquad (4\text{-}3)$$

Thus

$$\frac{dn}{dt} = -k_0 n^{\lambda+1} \tag{4-4}$$

$$\frac{d(n+\Delta n)}{d} = -k_0 (n+\Delta n)^{\lambda+1} \tag{4-5}$$

Therefore

$$\frac{d\Delta n}{dt} = -k_0 (n+\Delta n)^{\lambda+1} - \frac{dn}{dt} = -k_0 (n+\Delta n)^{\lambda+1} + k_0 n^{\lambda+1} \tag{4-6}$$

$$\frac{d\Delta n}{dt} = k_0 n^{\lambda+1} \left[1 - \left(1 + \frac{\Delta n}{n}\right)^{\lambda+1}\right] \tag{4-7}$$

As the number of excited charges is small $\frac{\Delta n}{n} \ll 1$, thus

$$\frac{d\Delta n}{dt} = k_0 n^{\lambda+1} \left[1 - (1 + (\lambda+1)\frac{\Delta n}{n})\right] \tag{4-8}$$

$$\frac{d\Delta n}{dt} = k_0 n^{\lambda} (\lambda+1)\Delta n \tag{4-9}$$

As we already know the rate law for the decay is $\frac{d\Delta n}{dt} = -k_{\Delta n}\Delta n$, we can say that

$$k_{\Delta n} = k(\lambda+1)n^{\lambda} = (\lambda+1)k_n \tag{4-10}$$

Or alternatively

$$\tau_n = (\lambda+1)\tau_{\Delta n} \tag{4-11}$$

Using this method we can calculate the bulk recombination charge lifetime from that measured using a small number of excited charges in a small perturbation method.

4.3.5 Limitations

One limitation of the TPV technique is that, whilst there are almost certainly spatial variations in recombination rate throughout the device due to changes in charge carrier populations, the experiment only probes a "bulk" recombination rate. It is not entirely clear how the decay of the Fermi levels corresponds to the different recombination rates in the device but the response is certainly complex. However the experiment does give consistent recombination rates. Another limitation is the fact that as the technique only measures the device voltage it only measures the recombination rate of charge carriers that effectively "communicate" with the electrodes and affect the Fermi levels. Thus the recombination rates of charge carriers which may degrade device performance such as those upon isolated fullerenes or in small domains are not measured.

4.4 TRANSIENT PHOTOCURRENT

Transient photocurrent (TPC) is a wide term that can be used to refer to several different measurements with different uses. In general it refers to the time-resolved measurement of the current response of a device to some optical stimulus. Various uses of this technique have been published and various techniques exist, such as probing the response of the current to a switch white light or laser source. In general the technique measures a convolution of transport and recombination characteristics.

4.4.1 TPC under Short Circuit Conditions

Transient photocurrent can be used to analyse the collection losses under short circuit conditions due to non-geminate recombination. This is performed by holding a device very close to short circuit conditions (across a small resistor), then whilst exposing the device to background white light illumination, applying a small perturbation using a laser. An oscilloscope can then be used to measure the current that flows from the device in response to the charges generated by the laser pulse.

As the charge density under short circuit conditions is typically low it is usually assumed that non-geminate recombination is similarly low, however under increasing background light intensity the charge density can become high enough such that non-geminate recombination impacts the current extracted by the device. Assuming that the charge density under short circuit conditions in the dark is small enough that non-geminate recombination is not playing a part, these conditions can be used to count exactly how many additional charges are being generated by the small perturbation pulse. This can then be compared to the number of charges extracted under various light intensities. As the generation of charges by a constant laser pulse is not expected to alter with background light intensity, any reduction in the number of charges extracted can be assigned to reduction by non-geminate recombination.

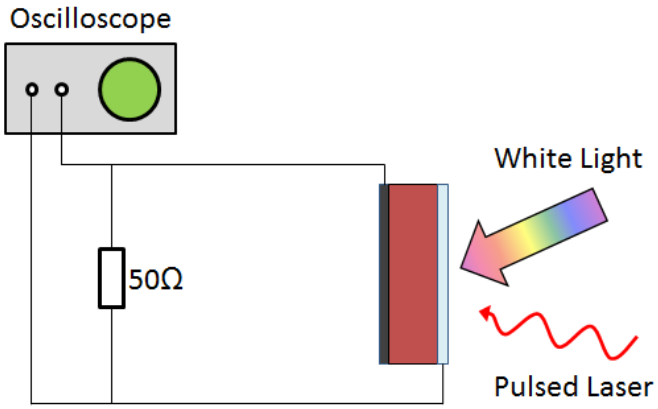

Figure 4.7. A circuit diagram indicating the experimental setup of a TPC experiment.

4.4.2 Experimental Details

Transient photocurrent experiments are performed using a similar experimental set-up to TPV experiments, however instead of using the oscilloscope (Tektronix TDS3032B) to measure the voltage of the device as it is held at open circuit, the device is shorted across a 50Ω resistor thus holding it at short circuit and the oscilloscope is used to measure the current flowing from the device. The illumination conditions, both with respect to the LEDs and the laser pulses are the same. The circuit diagram of the TPC setup is shown in figure 4.7.

4.4.3 TPC under Applied Bias

As the charge carriers excited by the small perturbation applied to a device in TPC experiments are assumed to be generated throughout the energetic density of states of the semiconducting material, and we know that charge transport in organic solar cells is trap-limited, all the carriers exiting the device must be being excited out of a distribution of trap states. As this transport is statistical and dependent upon the thermal energy available by measuring the time dependence of the current it is possible to gain an understanding of the shape of the density of states in the device through TPC measurements. To probe the DoS these measurements must be much more sensitive than the TPC used to measure recombination at short circuit as the actual shape of the transient is important, not just the area under it. Additionally as some of the transient may result from free carriers initially, it is only the low current "tail" that is of interest. Thus the current transient must be measured over a large range of both time and current.

To perform this measurement several transients are measured over different ranges and then stitched together to create one large transient. Each transient is measured of a different resistor, between 50Ω and 500kΩ. This means that the TPC can accurately measure smaller and smaller current transients.

4.4.3.1 Results

Figure 4.8a shows a collection of transients measured on a P3HT:PCBM device using various load resistors. For the high load resistances you can see three phases in the transient; (i) an initial discharge over the resistor followed by (ii) the actual current transient and then (iii) a descent into noise. Only the middle section of the transient is relevant. Thus the initial discharge in the transients can be discarded, as can the very noisy section at long timescales, and then the different transients averaged together at their overlaps resulting in the complete transient shown in Figure 4.8b. When viewed over a large time and current scale various features can now be seen in the transient rather than the simple exponential shape observed in normal transients; these features correspond to the features of the DoS.

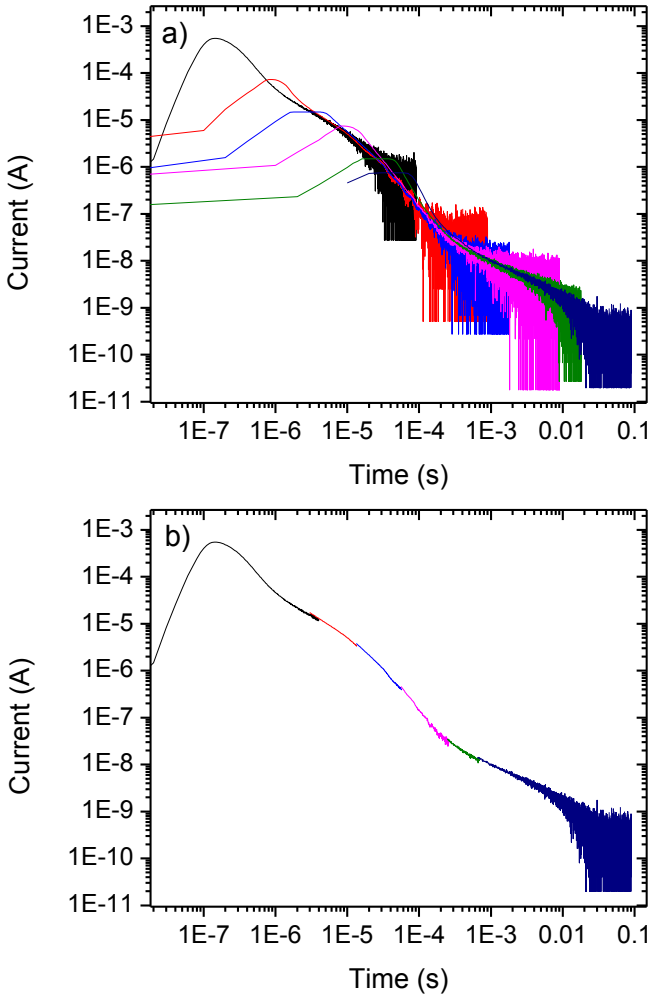

Figure 4.8. Two plots demonstrating how one large TPC transient can be stitched together, (a) before processing and (b) post-processing.

4.4.3.2 Limitations

As this measurement is recording small numbers of charges non-geminate losses can make a large difference to the shape of the transient causing inaccurate results. Therefore it is key that the transient is measured under sufficiently high bias that charge transport is efficient and non-geminate losses are negligible. The transients shown above were measured under short circuit conditions, it was verified that losses here were negligible by additionally measuring transients under reverse bias and observing they were of the same shape. Thus measurements at short circuit, which is technically easier to perform, were acceptable. If this condition is not met then the transient must be measured under applied negative bias.

As with charge extraction measurements, as all that is measured is a current transient it is impossible to distinguish between current coming from the transport of holes and the current from electrons. Clearly the DoS for each will be different and impact the transport differently but these cannot be seen using this TPC method. What can be measured is the "representative" DoS, which shows peaks and slopes that are useful

to computational modelling of devices, and additionally will show changes with device composition or annealing etc.

4.5 TRANSIENT ABSORPTION SPECTROSCOPY

Transient absorption spectroscopy (TAS) is an optical technique used to probe excited state dynamics within films or multi-layer devices by the measurement of changes in the absorption, or optical density, of the sample. In this thesis this experimental technique is used to measure the evolution in time of the polaron populations within device active layers, and thus the generation and recombination processes that change these populations. As excited species (such as holes in the donor and electrons in the acceptor) can absorb incident photons, the presence of these species absorb light, and thus the concentration of these species correlates to the change in overall absorption of the film at the set wavelength where they absorb. TAS is a pump-probe laser technique, meaning that a pulsed laser source illuminates the device and generates a population of excited species (in this thesis namely charges) whilst a second, continuous laser probes the optical absorption of the film or device. In this thesis, as the TAS experiments were performed on complete devices rather than thin films, the experiment was performed in "reflection mode". This means that the probe laser is incident upon the device through the transparent electrode, passes through the active layer, reflects from the metal back electrode, passes through the active layer a second time, and is then directed to a detector. Additionally as the experiments presented in this thesis are performed upon a device under bias a Keithey 2402B SMU was used to hold the solar cell under a constant bias of variable magnitude whilst each TAS trace was obtained.

To allow the measurement of small changes in the optical density of the film with high resolution, an optical detector with a nanosecond response is utilised in combination with a high-pass filter and amplification system. This is then connected to an oscilloscope which allows the electronic averaging of hundreds of signals to obtain a clear signal-to-noise ratio. This measured signal is then passed to a PC where further averaging and data analysis can be performed.

The wavelengths of the pump and probe lasers used in TAS experiments b=must be carefully chosen for each type of excited state being measured and for each material system being studied; the pump must excite charges in this case in the device and the probe must be at a wavelength such that it is absorbed by the charged species under investigation. In the experiments presented here a pump laser used was a Nd-YAG laser with a variable wavelength OPO system (OPO LD 355 from Quantel) and then probe laser was a continuous laser diode (Thorlabs TCLDM9) controlled by temperature and current controllers.

4.6 DRIFT-DIFFUSION MODELLING

Drift-diffusion modelling is the computational technique used to model the performance of semiconductor devices, particularly charge carrier dynamics, by solving a series of coupled differential equations which describe the transport, recombination and collection of charges. In the case of photovoltaics these equations are those included in the previous chapter, namely the equations governing the flow of charges from drift and diffusion components (equations *(2-4)* and *(2-5)* and those that describe the generation, collection and recombination processes (equations *(2-6)* and *(2-7)*).

In addition the electric field is related to the charge densities of electrons and holes using Gauss's law and the total current density of the device is the sum of the electron and hole current densities such that $J = J_n + J_p$. Using a computer program to simultaneously solve these equations results in a solution that includes a complete description of charge dynamics within the device, including variables that are not experimentally accessible such as the spatial changes in charge density or the relative importance of drift and diffusion under various voltages.

Drift-diffusion modelling is a one-dimensional model, meaning that it models charge transport in one dimension, through the active layer of the device. Additionally the model assumes that the semiconducting medium is isotropic and homogeneous. This is problematic for OPV as the active layer of devices is formed from a BHJ blend of two materials, this can be overcome by generalising the two semiconducting materials into one "effective semiconductor" which takes its hole transporting energy levels, trap distributions and charge transport rates from the hole-transporting materials and vice-versa for the electron transporting material. This has been shown to effectively represent that charge transport properties of an OPV blend and is widely used.

In addition to the equations above, it is also required that the generation and recombination of charges, G and R, are adequately described. In the model used in this thesis, the generation of charges is calculated using a transfer matrix model (TMM) to describe the spatial variations in photon absorption. It is then assumed that, due to the fine donor:acceptor structure of many BHJs, the exciton is split very close to where it is generated by the absorption of a photon, thus the charge generation profile is set equal to the photon absorption profile. Additionally, as organic solar cells rarely achieve 100% internal quantum efficiencies, an exciton dissociation probability is used to calculate how many absorbed photons will be separated into free charges. Thus, the free charge generation is determined by the photon absorption profiles of the TMM reduced by a dissociation probability which represents the geminate loss of excitons.

As described in chapter 2, there are various competing theories used to understand non-geminate recombination in organic solar cells, and in disordered materials in general. The drift-diffusion modelling utilised in this thesis calculates charge transport and recombination via a density of trap states, the occupation of which is determined not by Boltzmann statistics but by Shockley-Reed-Hall statistics. These calculations involve consideration of four different processes with different rates that can be balanced to

calculate the probability of occupation of a localised energetic state. These processes are shown in Figure 4.9 and are the recombination of a free electron with a trapped hole, the trapping of a free hole, the recombination of a free hole with a trapped electron and the trapping of a free electron. These rates are set within the model and are then balanced for every energetic state to determine the occupancy of said states. The application of Shockley-Reed-Hall statistics in organic photovoltaics is fully described by Kirchartz et. al. and the approach used here follows this formalism.[110]

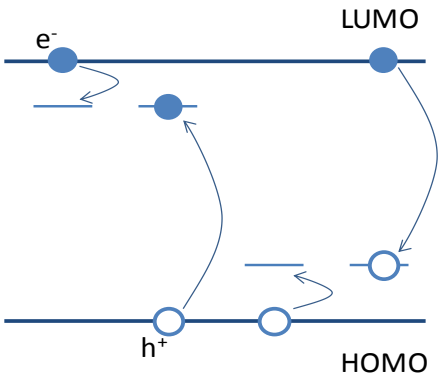

Figure 4.9. A schematic showing the four different capture and recombination mechanisms described by Shockley-Read-Hall statistics.

4.6.1 Application of Drift-diffusion Modelling

To use a drift-diffusion simulation to model a particular solar cell, all the parameters used to describe the charge carrier behaviour must be determined, either from experiment, or for those that are not experimentally accessible, by fitting them to the performance of the device in question. Thus to perform such a simulation, the known parameters are input and then the model is allowed to vary the remaining parameters to fit them to the actual device. This is usually done by fitting both light and dark *J-V* curves, and sometimes an additional experimental measurement such as the device external quantum efficiency, or the results of a charge extraction experiment. A fitting routine is used to then compare the modelled results with the actual results and determine the unknown parameters. Once the parameter space is fixed, it is then possible to model the performance of the device under a multitude of different conditions, including those not possible in the laboratory. Additionally the model allows the probing of processes that are not experimentally accessible.

In all cases in this thesis, drift-diffusion simulations were performed using commercially available software developed at the Technical University of Delft called Advanced Semiconductor Analysis (ASA), this has previously been used in the literature to model many thin film solar technologies, including amorphous silicon and organic BHJs.[111-113] This software is a one-dimensional drift-diffusion solver, which solves all the equations governing charge transport, recombination and generation detailed in section 2.4.4 of this thesis. ASA also utilises a Transfer Matrix Model to calculate photon absorption and thus charge generation, and

also uses the equations described previously that detail Shockley-Reed-Hall statistics to calculate charge recombination rates. ASA is used in conjunction with a parameter fitting routine which inputs a model parameters into the software, and can be used to determine unknown parameters required to accurately fit experimental data. The list of parameters input into the ASA simulation are listed in table 1.

Table 1. A list of device parameters input into ASA device drift-diffusion simulations.

Electron mobility	Hole mobility
Doping density	Effective density of states of the conduction and valence bands
Total density of tail states in the conduction and valence bands	Tail slop of the conduction and valence bands
Neutral hole capture coefficient	Negative hole capture coefficient
Positive electron capture coefficient	Neutral electron capture coefficient
Band gap	Series resistance
Parallel resistance (light and dark)	Surface recombination velocities

CHAPTER V

TRANSIENT MEASUREMENTS OF NON-GEMINATE RECOMBINATION IN P3HT:PCBM SOLAR CELLS

5.1 DISORDER AND THE DENSITY OF STATES IN ORGANIC SOLAR CELLS

Organic semiconductors typically exhibit low charge carrier mobilities and high rates of non-geminate charge recombination.[114] Related to these characteristics, charge transport in organic photovoltaics and other devices fabricated from organic semiconductors has been shown to be substantially limited by the presence of a large distribution of energetic states.[115-117] This distribution of energetic states is often described as a distribution of trap states energetically deeper than a conduction band edge..[17, 61] In this approximation charge transport occurs with a constant mobility when charge carriers occupy states above the conduction edge, and charge carriers below this value are temporarily "trapped" where conduction can only occur via excitation to a conduction band state.[61, 118] The ease with which a charge carrier can be excited into conduction band states through which it can travel through the device is determined by the energetic depth of the trap state in which it lies. Therefore the bulk charge transport properties of the semiconductor are substantially determined by the magnitude and shape of the distribution of these trap states. Thus knowledge of the distribution of energetic states is important in comprehensively understanding charge transport and recombination.

The shape of the density of states in disordered semiconductors, including organic semiconductors, is often approximated by an exponential or Gaussian distribution with respect to energy below the "band-

edge".[61, 63, 118] Additionally charges occupying these tarp states within this distribution are usually assumed to be localised. At zero temperature all photogenerated charges will fill these trap states until they are all filled and thus no charge transport will occur. At finite temperature, the exchange of thermal energy with these trapped charge carriers leads to excitation from this density of states, charge transport can occur and an equilibrium exists between the total density of charges, n, and the density of free charges, n_{free}. In this approximation, it is this quantity of free charges, rather than the total number of charges that determines the electrical properties of the semiconductor as they are the only mobile charges, thus understanding this trapping and detrapping behaviour is vital. Whilst many models have been proposed to understand this equilibrium such as Boltzmann statistics and Shockley-Reed-Hall statistics, it is understood that the ratio of free to total charge density is closely related to temperature via the amount of thermal energy available to excited charges out of trap states.

Non-geminate recombination, a process which has been shown to significantly affect the performance of OPV devices,[47, 50, 119] is highly dependent upon the presence of trap states and thus studies of this process are relevant to studies of the energetic density of states described above. Free electrons and holes are spatially separated and in the conventional view of an organic bulk heterojunction (BHJ) located in separate material domains, thus presumably the recombination process must occur at an interface or mixed domain within the BHJ and at least one of the polaron species must be untrapped and free to transport about the device.[120] If one carrier must be untrapped, this means all recombination processes are dependent upon at least one excitation from the distribution of trap states, and therefore the number of free carriers present to recombine and the recombination rate must be linked in some way to the size and shape of the DoS. As charge carriers in shallow trap states are easier to detrap than deeper states the non-geminate recombination rate coefficient is charge density dependent, this is because if all charges are thermalised to the lowest trap states then adding more charges places them in shallower trap states from which they are more easily excited. Thus the size and shape of the DoS also affects the charge density dependence of the non-geminate recombination rate.[70, 92]

The generation and collection of charges in organic solar cells is a complex process that is not entirely understood, involving several processes and competing energy loss mechanisms. These processes are interlinked, operate on an ultra-fast timescale and are still being studied. In addition to this, the conventional methods of analysing the efficiency and performance of OPVs, such as current-voltage (*J-V*) and external quantum efficiency (EQE) measurements, probe the steady state behaviour of devices. Although some analysis of the *J-V* curve allows some conclusions to be drawn upon the underlying mechanisms of charge generation, *J-V* curves are actually relatively featureless and do not allow the evaluation of different charge processes. Therefore, analysis of steady-state experiments is insufficient to completely understand the fundamental charge processes, both generation, transport and recombination, that determine the performance of OPV devices.

Experimental methods that utilise small amplitude changes or small perturbations to a photovoltaic device have the potential to study the fundamental excited state processes in devices.[46, 93, 106, 121-122]

Techniques of this kind typically use a small "pump", either electronic or optical in nature, to perturb the system under examination. The advantage of these methods is that the small perturbation can be applied under a multitude of different operating conditions such as voltage and illumination to probe device behaviour in various states. These methods can thus be used to reveal the fundamental physical processes in terms of charge densities within the device rather than the more external quantities of illumination and voltage.

Additionally, experimental methods that probe the excited states within photovoltaic devices with a time resolution, and on fast time-scales, have the potential to elucidate these underlying processes. These experimental methods can be either purely optical spectroscopic methods such as transient absorption spectroscopy,[21, 35, 46] or opto-electronic which study the electrical response of devices to optical stimuli,[49, 123-124] and vice-versa. As these are not steady-state methods an excitation or change of state of the device is used to study the device response, this is the "pump" and whatever technique is being used to study it is the "probe", be it another optical probe or and electrical one. These methods give a wealth of information, particularly those on a time-scale that is relevant to the excited state processes being studied. By combining these transient experimental probes with broad measurements of the device performance truly allow the limiting processes of OPVs to be determined.

In this thesis chapter we shall utilise small-and large-perturbation time-resolved opto-electronic probes of the kind described in chapter 4 to study the underlying charge processes that determine device behaviour. Additionally these techniques will also be used not just to probe the behaviour of charges but to measure the density of trap states in the semiconducting medium and its effect on device performance.

5.2 NON-GEMINATE RECOMBINATION & UNDERSTANDING THE *J-V* CURVE

Transient analyses of charge processes can be related back to the steady state performance of OPV devices, this is particularly true of quantifications of the loss mechanisms of photo-excited states. For example if a process is observed using spectroscopic or opto-electronic methods that involves the loss of free charges prior to excitation this has to correspond to a loss of extracted current seen by an observer analysing a *J-V* curve under the same conditions. The results of these transient experimental methods are fully described in this section, reproducing results previously shown in the literature by Shuttle et. al. for P3HT:PCBM devices.[49, 70] These results are provided for completeness, to provide quantitative data for comparison to following sections and chapters, and to provide an introduction to experimental methods and the "*J-V* reconstruction" technique before the experimental methods are expanded.

As described in chapter 2 of this thesis, the recombination of free electrons and holes in OPV devices, or non-geminate recombination, depends on the density of charges within the device; the higher the density

the more likely opposite charges are to meet and recombine, resulting in a faster recombination rate. The rate of non-geminate recombination, *R*, is related to the densities of electrons and holes, *n* and *p*, by the recombination rate prefactor, *k*, as shown in equation *(2-14)*. The limits of this assumption are discussed in chapter 9 where the recombination behaviour of doped devices with imbalanced charge densities is studied. Both *R* and *n* are experimentally accessible; charge density can be directly measured using charge extraction (CE) and the non-geminate recombination rate can be measured using transient photovoltage (TPV), both transient optical and electronic techniques. Together these measurements can quantify the non-geminate recombination process in an organic solar cell and allow the specific rate prefactor for that device to be determined. This rate prefactor is dependent upon many things, including the physical morphology of the blend structure and the energetic landscape seen by polarons, among others.

Figure 5.1 shows the steady-state *J-V* curve of a P3HT:PCBM device in the dark and under 1 sun illumination, that we have studied here using these transient techniques. Figure 5.2a shows the measured charge density within the device under varying light intensity at open circuit conditions, plotted against the open circuit voltage at which it was measured. As can be seen there is a clear exponential relationship, thus we can describe the relationship with the equation $n = n_0 \exp(\gamma V_{OC})$ where n_0 and γ are fitting variables. Similarly Figure 5.2b shows the link between the recombination lifetime measured using TPV under open circuit conditions and varying light intensity against V_{OC}, similarly there is a strong exponential relationship between τ and V_{OC}, thus we can describe the relationship using $\tau = \tau_0 \exp(-\beta V_{OC})$ where τ_0 and β are fitting variables.

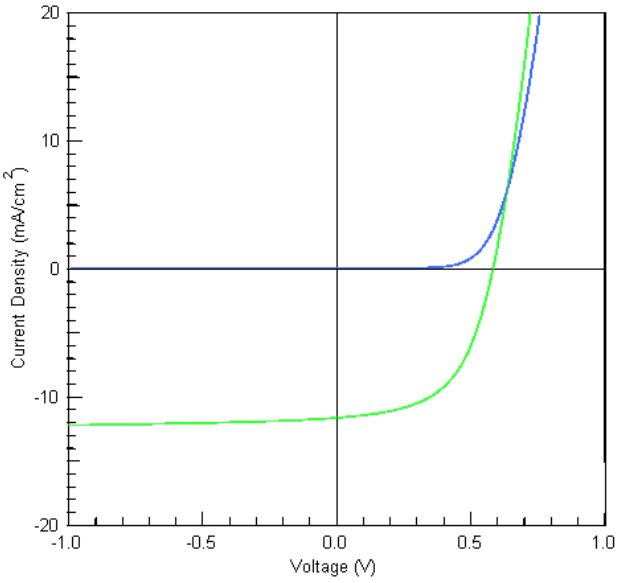

Figure 5.1. Light (1 sun) and dark J-V curves of a P3HT:PCBM solar cell.

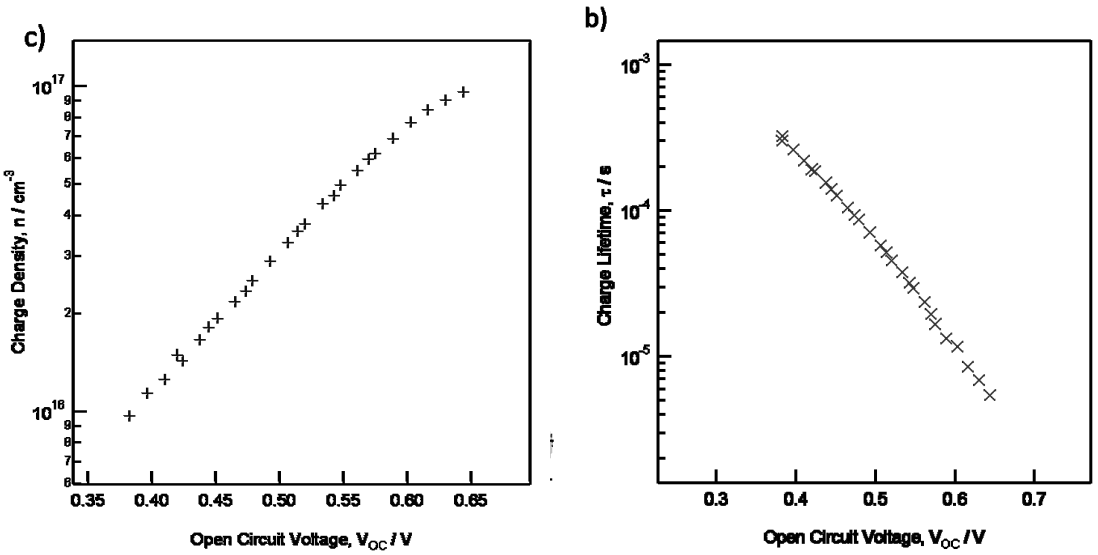

Figure 5.2. Plots showing the dependence of (a) charge density measured via charge extraction and (b) non-geminate recombination lifetime measured with TPV upon open-circuit voltage of a P3HT:PCBM solar cell.

Using separate experimental techniques we have now quantified the non-geminate recombination rate and the charge density within the device, under open circuit conditions and at various light intensities. Importantly the measurement of charge density by the charge extraction technique is corrected for both the loss of charges to recombination during the extraction, and for capacitative charges present on the electrodes of the device which do not contribute towards non-geminate recombination, these corrections are more fully described in chapter 4. Due to charge trapping, the non-geminate recombination prefactor *k* will also be dependent upon charge density, as shown in equation *(2-14)* i.e. the power law dependence of the recombination rate. Additionally we can express the recombination rate as $R = {}^{n}/_{\tau}$. Using the exponential relationships described above for n and \tau we can rewrite that as

$$R = \frac{n}{\tau} = \frac{n_0 \exp(\gamma V_{OC})}{\tau_0 \exp(-\beta V_{OC})} \qquad (5\text{-}1)$$

Figure 5.3 shows the relationship between the recombination lifetime and the charge density, along with a power law fit of the behaviour. It can be seen that the recombination lifetime clearly reduces with increasing charge density with a strong power law relationship. The order of this process, for this device, is 2.55. Importantly as this relationship is super-second order, this indicates that the non-geminate recombination prefactor is strongly charge density dependent and this is shown in Figure 5.3b.

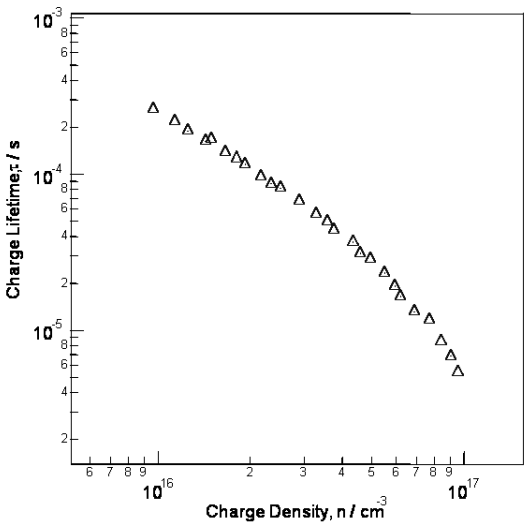

Figure 5.3. Plot showing the relationship between non-geminate recombination lifetime and charge density within the P3HT:PCBM solar cell.

Once this recombination relationship has been quantified, we can attempt to relate it to the behaviour of the device, particularly the *J-V* curve under 1 sun illumination. The charge extraction technique can be used to probe the charge density not just under open circuit conditions but under different applied biases at constant illumination, effectively across the *J-V* curve in the departing region, between short and open circuit. This is shown in Figure 5.4, it can be seen that the charge density is low under short circuit conditions where the field in the device is strong and charge collection is efficient, and increases towards open circuit. As the TPV technique can only be used under open circuit, for each charge density a non-geminate recombination lifetime must be calculate from the relationship shown in Figure 5.4. To do this we assume that recombination rate depends only on the total charge density and not on its distribution within the device determined by external voltage, thus at a constant charge density the recombination rate is voltage independent. It has been shown that this assumption becomes invalid in devices with very thin active layers, as there is a greater change is spatial distributions of charges in these devices, this consequently creates a more voltage dependent recombination rate.[125]

By assuming that the charge recombination lifetime is independent of device voltage, implicitly it is assumed that the charge recombination and the charge density are independent of position within the device and both are bulk properties of devices. This is a considerable assumption as firstly, as described above, applied voltage is known to alter spatial charge distributions, but also because the electrostatics of at the junction between the metallic electrode materials and the semiconductor active layers can also cause depletion regions in the bulk. Whilst it is known that using electrode materials with Fermi levels unaligned with the HOMO or LUMO energy levels of the BHJ can cause significant reduction in device efficiency, typically all the devices studied in this chapter, and in fact in this thesis, are structurally optimised such that the electrode:BHJ junction does not generate a significant ohmic barrier to charge transport. Even in the most optimised devices however small depletion regions exist, yet for this analysis to function we must assume that these are small when compared to the thickness of the entire active layer. As described above

for the assumptions relating to voltage-dependence, this assumption may break down for devices fabricated with thinner active layers, or for those with ohmic contacts. Finally, it has been demonstrated by Credgington et. al. that analyses of non-geminate recombination can still accurately determine open circuit voltage in devices fabricated with the same donor:acceptor blends, but differing electrode materials, interlayers and exposed to different aging conditions.[50] In addition extensive drift-diffusion modelling of charge extraction and TPV experimental data with P3HT:PCBM devices showed no significant deviation from the experimental results even with the depletion regions of the electrodes taken into account.[61]

The current density of charges lost to non-geminate recombination, J_{loss}, at various voltages can now be calculated using the relation

$$J_{loss}(V) = \frac{n(V)ed}{\tau(n)} = ed\frac{n_0}{\tau_0}n(V)^{\frac{\beta}{\gamma}+1} \qquad (5\text{-}2)$$

where e is the elementary charge and d is the thickness of the device. Calculating this from the data in Figure 5.4 allows the calculation of the loss to non-geminate recombination across the *J-V* curve. It has previously been shown that in several polymer:fullerene systems free charge generation is efficient and voltage independent.[49, 68-69, 84] If the photocurrent generation is treated as a free charge generation current density, J_{GEN}, we can subtract from that the voltage-dependent loss current density to non-geminate recombination to determine the net current density. Thus

$$J(V) = J_{GEN} - J_{LOSS} \qquad (5\text{-}3)$$

As the *J-V* curve in this case appears to be saturated at J_{SC} and the current density doesn't change much in reverse bias, we can assume that this figure corresponds to the generation current of free charges, thus $J_{GEN} = J_{SC}$. For the system studied here this is shown in Figure 5.5 by the points, compared to the actual experimental *J-V* curve under 1 sun illumination which is shown by the line.

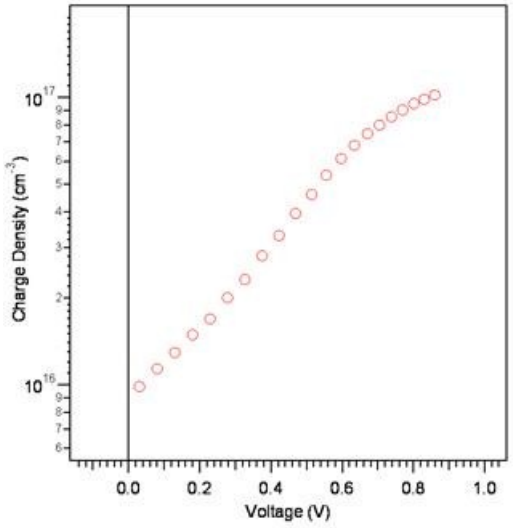

Figure 5.4. A plot of charge density under 1 sun illumination under various applied biases between short circuit and open circuit conditions.

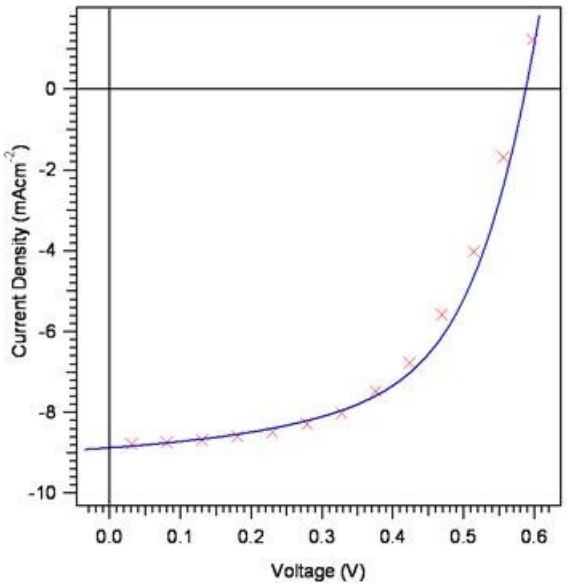

Figure 5.5. A plot showing the results of J-V curve reconstruction from calculations of non-geminate recombination (points) compared against actual J-V performance (line) of a P3HT:PCBM solar cell under 1 sun.

Evidently the experimental and "reconstructed" *J-V* curves match closely, with the reconstruction slightly overestimating the fill-factor of the device. Importantly the reconstruction also closely matches the V_{OC} of this device. These results indicate that for the P3HT:PCBM device shown here, the device *J-V* behaviour, particularly the V_{OC} and the *FF* can be closely related to the non-geminate recombination process. In fact we have shown that non-geminate recombination loss current actually determines the *FF* and V_{OC} of these devices, as it does with other polymer:fullerene devices.

This *J-V* reconstruction process is an important calculation in understanding the performance and OPV devices, and also important as it fundamentally relates fast charge processes to absolute steady-state device performance. Additionally as the method directly measures the quantity and behaviour of charges it is equally important in testing the assumptions made in the analysis such as the assumption that charge generation is voltage independent. The next section of his chapter will elaborate upon this analysis by utilising temperature dependent measurements to study the device recombination dynamics as well as the density of states. The following chapters of this thesis will expand this concept to understand other fundamental charge processes and other polymer:fullerene solar cell devices, particularly in chapter 7 where the *J-V* reconstruction technique is used to analyse and compare different recombination mechanisms in P3HT, APFO-3 and PCPDTBT devices.

5.3 TEMPERATURE DEPENDENT TRANSIENT STUDIES OF OPV DEVICES

5.3.1 Introduction

The detrapping and excitation of charges from a distribution of trap states is a thermal process dependent upon the temperature of the system. At 0K all the charges will be thermalised into the DoS, however at finite temperature there is a quasi-equilibrium. At higher temperatures more charge carriers will be excited into the transport band and it is expected that the non-geminate recombination rate will increase. By experimentally probing the non-geminate recombination using charge extraction (CE) and transient photovoltage (TPV) methods we can measure the charge density dependence of non-geminate recombination, by additionally altering the temperature of the experimental system we can additionally hope to probe the DoS.

The effect of temperature upon non-geminate recombination has previously been investigated by Deibel et. al. who studied this mechanism using the photo-CELIV technique,[120, 126] additionally other authors have studied the temperature-dependence of simple device parameters to attempt to draw conclusion upon the charge carrier dynamics within the device.[127] Deibel et. al. conclude that recombination in P3HT devices occurs via a reduced Langevin mechanism and that charges are resident in a Gaussian DoS, contrasting with other authors work particularly those who conclude the DoS is of an exponential shape.[61, 110] Two papers by Montanari and Nogueira et. al. particularly, have utilised TAS experiments measuring non-geminate dynamics as a function of temperature to study the dynamics of charges excited from a DoS, concluding the DoS is of an exponential shape.[46, 128] Furthermore transient absorption spectroscopy has been performed under varying temperature to study the charge generation mechanism by Grzegorczyk et. al. who concluded that in P3HT:PCBM devices the charge generation is temperature independent.[71]

In an exponential density of states the charge density will increase as the voltage, or Fermi level splitting, increases, filling more and more trap states. The charge density thus depends upon the voltage, V, in an exponential equation such that

$$n \propto \exp\left(\frac{qV}{kT_0}\right) \qquad (5\text{-}4)$$

where q is the elementary charge, k is Boltzmann's constant and T_0 is the characteristic temperature, a measure of the exponential gradient of the density of states within the bandgap. Additionally Boltzmann statistics state that the free charge density depends upon both temperature and voltage such that

$$n_{free} \propto \exp\left(\frac{qV}{kT}\right) \propto n^{T_0/T} \qquad (5\text{-}5)$$

Thus as the temperature of a system with fixed charge density increases, the free charge density will also increase, leading to temperature dependent charge mobilities and non-geminate recombination rates.

Here we study the temperature dependence of the non-geminate recombination process in a P3HT:PCBM organic solar cell. As non-geminate recombination is dominant in this system and it is well understood it is a good test-case for this experiment.[49] Temperature dependent measurements were made using an Oxford Instruments cryostat, detailed in the experimental methods at the end of this chapter.

5.3.2 *J-V* Behaviour

The current-voltage (*J-V*) response under 1 sun illumination at various temperatures between 90K and 350K, can be seen in Figure 5.6. Additionally the temperature dependence of each *J-V* parameter is plotted below in Figure 5.7. These changes in *J-V* behaviour were reversible and repeatable with the same and similar devices. Under room temperature the device had the following characteristics: V_{OC}=628mV, J_{SC}=10mAcm^{-2}, *FF*=49%, η=3.1%. The open circuit voltage (V_{OC}) decreases with increasing temperature by the reasonably large amount of approximately 150mV, whereas the J_{SC} and the *FF* both increase considerably. The change is open circuit voltage can be attributed to the increase in free charges with increasing temperature causing a consequent increase in non-geminate recombination losses, as described above.

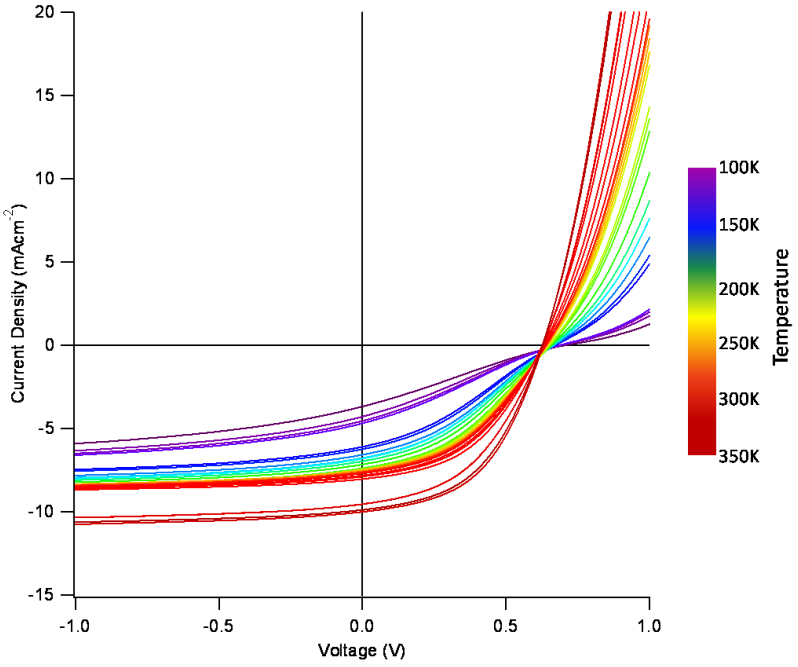

Figure 5.6. A plot showing the temperature dependence of the J-V curve of a P3HT:PCBM solar cell under 1 sun illumination.

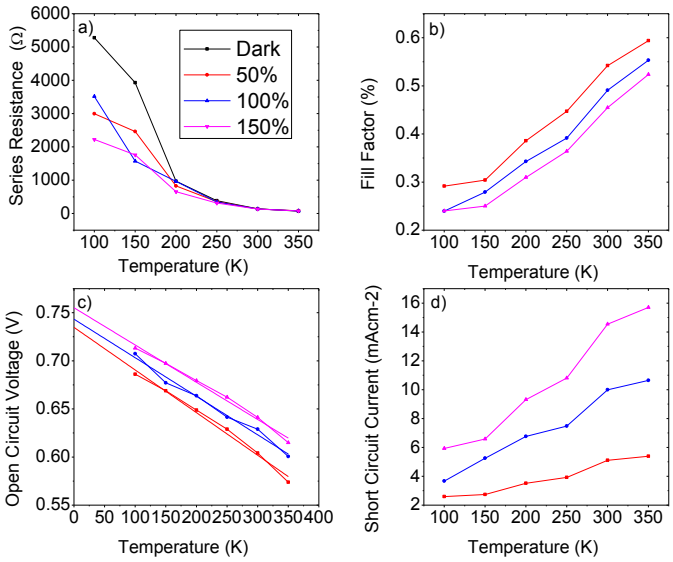

Figure 5.7. Plots of a) series resistance, b) fill factor, c) open circuit voltage and d) short circuit current density of the J-V curves in Figure 5.6 against temperature.

One of the largest changes in device behaviour, impacting particularly the fill factor of the device, is the change in series resistance, as seen by analysing the gradient of the *J-V* in forward bias, past the open circuit voltage. This series resistance is plotted against temperature in Figure 5.7d. It is clear by looking at the behaviour around in V_{OC} in Figure 5.7a that this change is significantly reducing the *FF* of the device studied here; at low temperatures an S-shaped kink appears in the *J-V* curve close to V_{OC}, this has previously been shown to be caused by series resistance limitations or by problems with the active layer:electrode interface. The series resistance of a device is usually ascribed to the electrodes or contacts, however low mobilities and consequent poor transport in the active layer can also cause series resistance losses in the device. We can tentatively ascribe the changes in series resistance here to reductions in mobility at low temperatures, caused by reduced thermally stimulated detrapping.

5.3.3 Charge Extraction

Charge extraction experiments probe the steady-state charge density within the device. Figure 5.8 shows the charge density present within the device under open circuit conditions at different light intensities with changing device temperature. This data is shown plotted against the open circuit voltage (a) and the white light intensity (b), as the V_{OC} additionally changes with temperature, whilst the generation rate is assumed to only depend upon light intensity. Figure 5.8b indicates that the steady-state charge density at open circuit is largely dependent only upon the generation rate and there are only very small temperature dependences. However Figure 5.8 indicates that at a constant V_{OC}, the charge density increases with increasing temperature by almost an order of magnitude over the temperature range measured here.

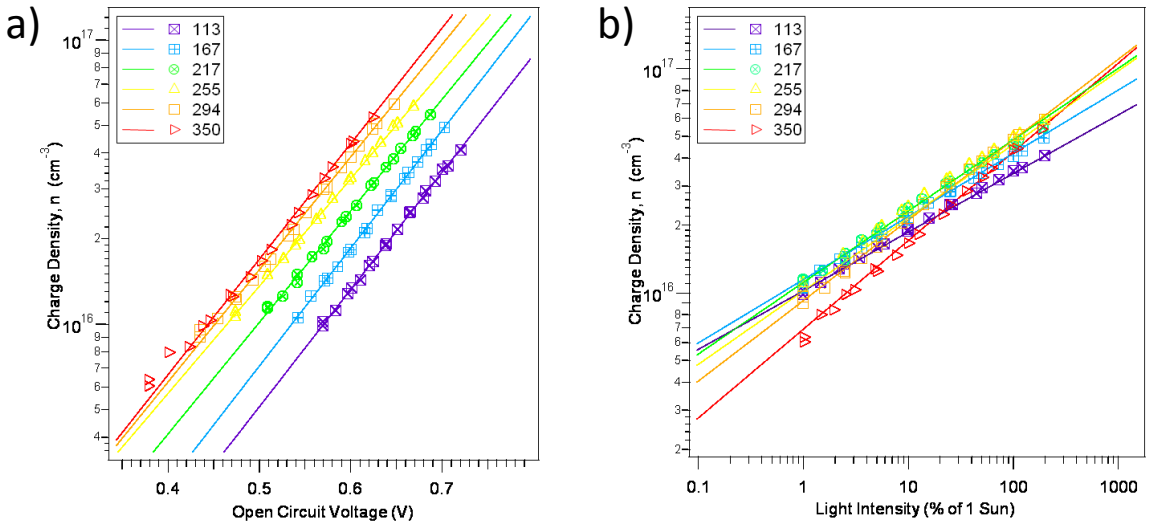

Figure 5.8. Plots of charge density against under open circuit conditions against (a) open circuit voltage and (b) illumination intensity.

The steady state charge density within the device is determined by a balance between generation, extraction and recombination. As the light intensity increases and more charges are generated in the system the charge density increases as more charges accumulate within the device. As the device studied here is believed to be in the trap-limited regime under all light intensities measured here, we can assume that the majority of charge in the device is in trap states, thus the shape of the charge density curve with light intensity (or generation) shown in Figure 5.8b gives us an approximation of the convolution of the densities of states for the electron and hole. It can be seen in the figure that the charge density follows an approximately exponential relationship with V_{OC}, whilst there is some temperature dependence of the gradient of this exponential, the values are quite similar.

As the charge within the system can be calculated using the equation $n \propto \exp(qV/kT_0)$ we can use the fits to the charge extraction data to estimate T0, or the slope of the representative density of states of the P3HT:PCBM device. The values for different temperatures vary between 1214K and 1334K, however due to the similarities of the slopes in Figure 5.8 we can take the average of 1262K as the value of T0 for this device.

5.3.4 Transient Photovoltage

Transient photovoltage measures the rate of non-geminate recombination under open circuit conditions, Figure 5.9 shows the non-geminate recombination lifetime under varying illumination intensity and temperature. As above the lifetime values are plotted against both open circuit voltage and against light intensity, in this case the two graphs also show quite different behaviour. Figure 5.9b shows that between 113K and 350K at a fixed illumination intensity the recombination rates change enough that the lifetime of a charge reduces by over an order of magnitude. The increase in recombination lifetime with temperature is

entirely consistent with more charges being excited out of trap states and residing in states in the conduction band, thus free to recombine.

Figure 5.9a shows the recombination lifetime plotted against the open circuit voltage. This shows similarly that the recombination lifetime decreases considerably with increasing temperature, but also that when the change in V_{OC} with temperature are taken into consideration, the gradient of the lifetimes dependence also changes.

The faster non-geminate recombination at higher temperatures also allows us to understand why the open-circuit voltage of the device is strongly temperature dependent. It has previously been shown that the V_{OC} of P3HT:PCBM devices is determined solely by the non-geminate recombination. The V_{OC} value is defined as the difference between the electron and hole Fermi levels, as under the low operating charge densities these lie in the distribution of trap states within the "band-gap" of the material system these are pushed further apart and closer to the conduction energies by the generation process, and reduced by the non-geminate recombination process which reduces the charge populations. The V_{OC} is thus a balance between generation and recombination. TAS studies have shown the charge generation process to be temperature independent and Figure 5.9a shows that at a fixed voltage the recombination increases considerably, therefore the voltage at which recombination completely balances generation reduces with temperature. This is consistent with the reduced V_{OC} and we conclude that this is due to increased non-geminate recombination at high temperature.

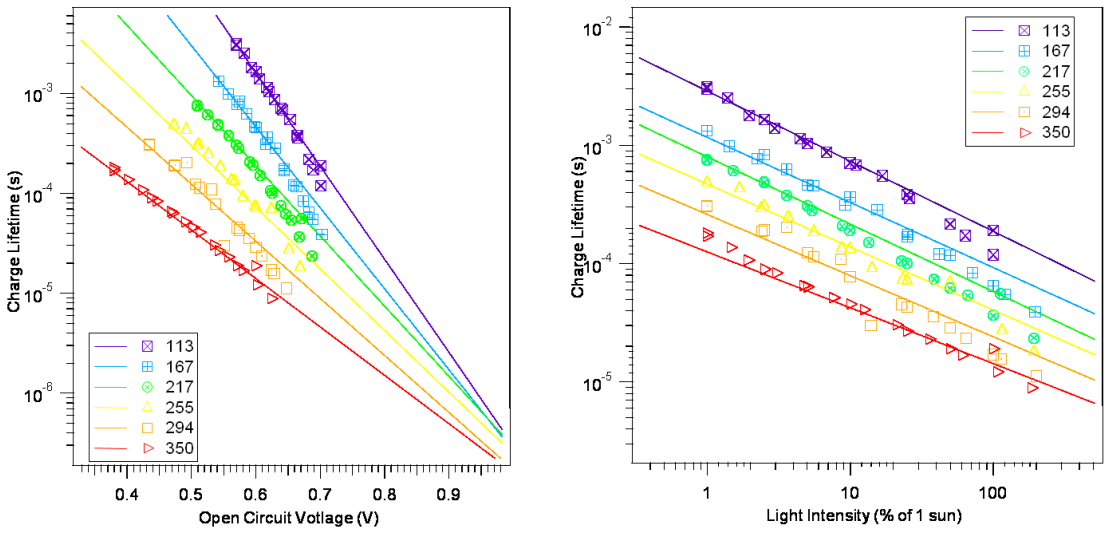

Figure 5.9. Plots of the non-geminate recombination lifetime of a P3HT:PCBM solar cell measured using TPV plotted against (a) open circuit voltage and (b) illumination intensity.

5.3.5 Analysis & Discussion

Now we have analysed separately the charge extraction and TPV results under open circuit conditions we may combine the results to analyse the order of the recombination process, or the dependence of the recombination rate upon the charge density present in the device.

Figure 5.10 shows plots of the non-geminate recombination rate and lifetime against charge density. Firstly these show quite clearly the effect of temperature on the non-geminate recombination process, mainly that as the temperature decreases the recombination rate slows by orders of magnitude for a set charge carrier density.

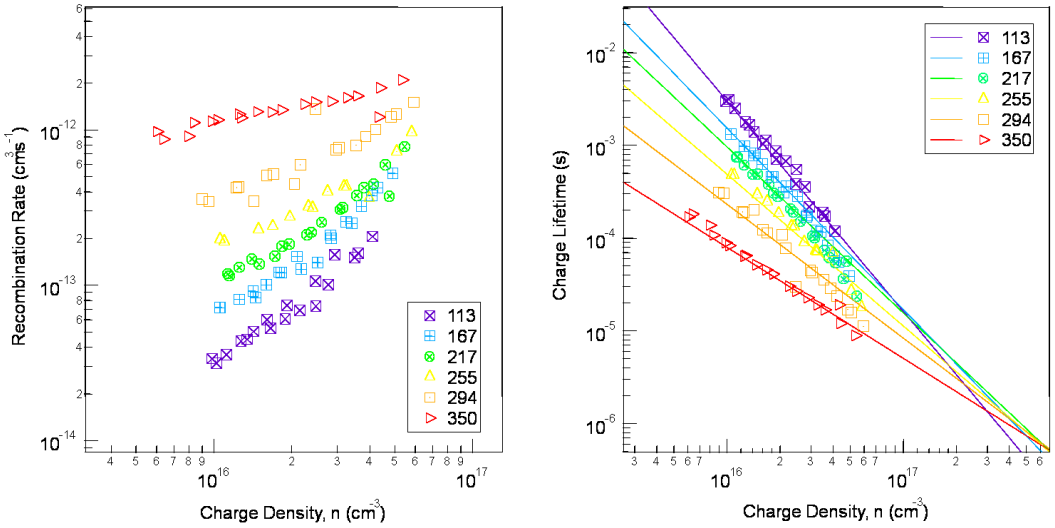

Figure 5.10. Graphs showing the charge density dependence of the recombination rate prefactor and the non-geminate recombination lifetime at various temperatures.

It is evident that the order of the recombination process, or the power law dependence of the recombination rate upon charge density, is changing considerably. Whilst it may be expected that a higher number of charges in the conduction band would result in higher rates of free-to-free bimolecular recombination thus increasing the order of the reaction, in fact the order of the non-geminate recombination mechanism is reduced. This is because at low temperatures the recombination pre-factor k_0 is highly dependent upon charge density, this in turn is because at low temperature a higher proportion of charges are trapped thus a small increase in the charge density will affect the number of charges in the conduction band more. This can be understood using the equations linking free and trapped charge density shown above. The density of free charges scales with the total charge density to the power of T_0/T, and this reduces in magnitude as the temperature increases, as T0 is constant for all these datasets. Thus the power law dependence of tau upon n can be predicted by the T0 value determined earlier. We can show that

$$\tau = \frac{n}{R} = \frac{n^{1-\alpha}}{k_0} \qquad (5\text{-}6)$$

thus the power law fits in Figure 5.10 should correspond to $1-\alpha$ where $\alpha = T_0/T$. The values of the actual power law fits and the predicted fits are show in Figure 5.11. Evidently the actual power law fits follow

the same temperature dependence but with a considerably reduced magnitude. This has previously been demonstrated and explained for device studies at room temperature using drift-diffusion simulations.[110] These simulations show that in a regime in which the large majority of charges are trapped the resulting tau vs. n power law can be significantly reduced compared to calculations considering T0.

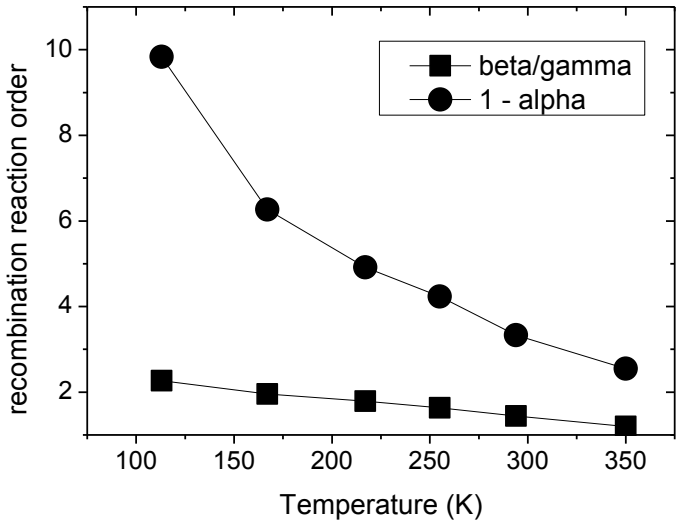

Figure 5.11. A plot comparing the calculated values of the reaction order of the recombination process. One calculated from the experimental dependence of recombination lifetime upon charge density and the other from the dependence of charge density upon temperature.

In addition to analysis of slope of the DoS, we can attempt to estimate the total number of trap states in the system from his data. Power law fits are shown in Figure 5.10b of the recombination lifetime plotted against charge density. These evidently converge at high charge densities. If we assume that these fits are representative of the recombination behaviour and can be extended far beyond the range measured here, then the point where the fits converge is important. This point indicates the point at which the charge density is high enough that the recombination process is no longer temperature dependent. As the temperature dependence comes from the thermal detrapping from the distribution of trap states, the point where recombination is no longer temperature dependent corresponds to the situation where all the trap states are filled and thus the charges no longer require thermal detrapping to undergo recombination. Since the fits converge between 4-6x10^{17} cm^{-3}, this is approximately the total number of trap states in the system. This figure matches a similar figure measured using transient absorption spectroscopy of P3HT:PCBM devices where the transition from the trap-limited limited domain occurred at 1x$10^{18}$$cm^{-3}$.

5.3.6 Conclusions

To conclude, we have performed charge extraction and TPV experiments under varying temperature and observed the order of the recombination process. As expected, in a device that is trap limited and is known to have a distribution of trap states, such as P3HT:PCBM, the rates of recombination scales with

temperature as when the device is hot more charges detrap and are free to recombine. We have compared the observed variation in recombination order with a theoretical expectation with an exponential DoS, this reproduced the general trend in order but not the magnitude, confirming that detrapping from a DoS is affecting the recombination but implying a more sophisticated model is required. In addition, from the temperature dependence of the recombination process we were able to extrapolate our results to determine the charge density at which detrapping will cease to limit the recombination/transport of charges. This figure represents the total number of charge traps in the system and was found to be 4-6x10^{17} closely matching other experimental probes of the same system.

5.4 TRANSIENT STUDIES OF THE ENERGETIC DENSITY OF STATES

Transient photocurrent (TPC) is used to refer to various techniques that measure the current response of a photovoltaic device through time in response to some stimuli, normally some form of pulsed illumination. TPC can be used under certain circumstances to analyse the energetic distribution of the density of states in semiconducting materials.[129-130] If a short laser pulse is assumed to generate free charges throughout the active layer of a solar cell instantly then transient photocurrent can measure the response of the device to this sudden excitation of charges. With time, the charges will thermalise and relax into the trap states and reach quasi-equilibrium, however initially it can be assumed that these charges are generated proportionately throughout the density of states. Experimentally TPC can be performed at any applied bias; under short circuit conditions, the initial majority of the flow of current will be of free charges in the transport band being extracted from the device. Once these free charges have been largely removed from the device the majority of the current will be of charges excited from the "trap" states below the conduction edge and subsequently being transported. The charges most likely to be detrapped by the thermal energy present in the system and extracted are those in the shallowest states, i.e. those closest to the conduction edge, and as time proceeds charges occupying increasingly deep trap states will flow from the device. Thus as long as the charges are extracted prior to thermal relaxation, the transient current as a function of time directly corresponds to the magnitude of the density of states as a function of energy. Clearly this approximation neglects the differences in times taken to extract charges from different parts of the device which are likely to be negligible with respect to the detrapping time. Additionally in this description the term trapped applies to charges that are temporarily in an electronic state where transport is not possible, however excitation out of that state is possible, as opposed to some authors who use the term to refer to charges that are permanently trapped in a state, thus resulting in eventual recombination.

The analysis of TPC data collected to analyse the density of states is complicated by the presence and extraction of two charge carriers. The device current resulting from the laser excitation results from the

extraction of both electrons and holes thus the density of states obtained is a convolution of both densities of states relevant to charge transport in a polymer:fullerene device; the distribution of trap states below the electron conduction band of the fullerene and the distribution of trap states above the hole transport band in the polymer. As has been shown by other authors,[118, 131-132] the density of states g as a function of energy can be defined as a product of time t and the current $i(t)$,

$$g\big(E(t)\big) = i(t)t\left(\frac{N_T}{N'e\mu \mathrm{EA\tau kT}}\right) \qquad (5\text{-}7)$$

where N_T is the total number of states, N' is the fraction of charges in traps, τ is the transit time a charge must undertake to be collected, A is the area of the device, μ is the charge mobility, E is the electric field, e is the elementary charge, k_B is Boltzmann's constant and T is the temperature. Additionally the equation that results from Boltzmann statistics that links the energy of a given state to the time taken to be collected is

$$E(t) = -kTln(\upsilon_0 t) \qquad (5\text{-}8)$$

where υ_0 is the frequency with which the charges attempt to detrap.

Figure 5.12 shows a TPC transient for a P3HT:PCBM device with a thickness of approximately 150nm the exhibited power conversion efficiency of ~3%, thus representative of other devices in the literature. These transients are measured over several decades of time and many orders of magnitude of current, to achieve this with a constant laser pulse intensity the photocurrent is measured over resistors of various sizes. This results in transients which consist of two phases, firstly a large RC discharge followed by a transient that results from detrapping of charge carriers. The RC discharge transient is not relevant, thus this can be discarded and the sequential transients stitched together at the overlaps, additionally where the transients overlap and one clearly has much higher noise that the other the noisier transient can be replaced for that time period. This produces one large transient shown in Figure 5.12.

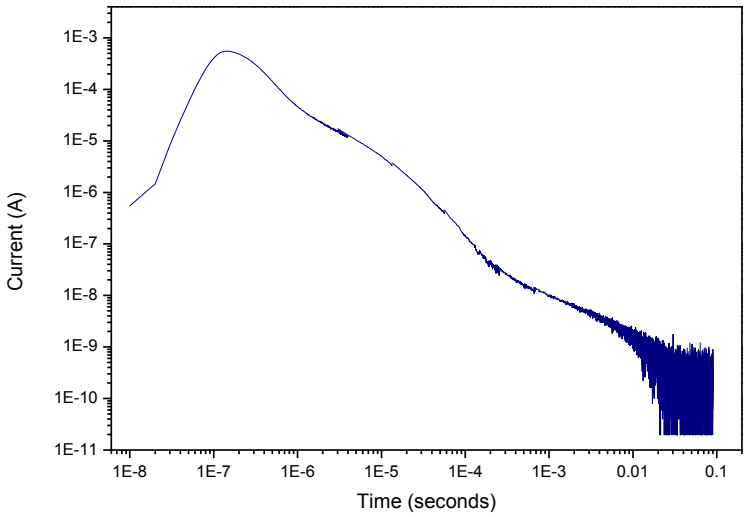

Figure 5.12. A photocurrent transient of an annealed P3HT:PCBM device under short circuit conditions.

This transient was measured at short circuit conditions where it is known that there is little non-geminate recombination in P3HT:PCBM devices, thus we assume that this recombination process is not affecting the shape of the TPC transient. This current transient can be seen to include several features, yet discerning what this can tell us about the density of states requires the mathematical transformation described in equation *(5-8)*.

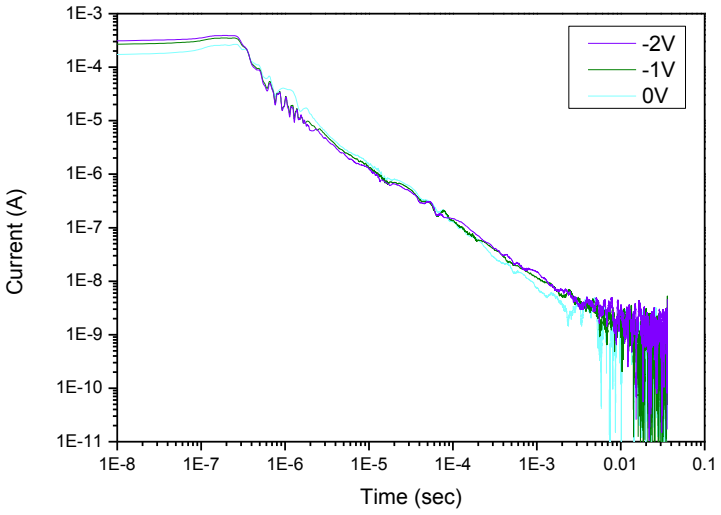

Figure 5.13. Photocurrent transients of a P3HT:PCBM device measured under -2V, -1V and 0V showing the transients are unchanged in shape.

One way of checking to see if the non-geminate recombination is affecting a TPC transient is by performing the experiment at biases away from short circuit; further into forward bias toward open circuit will result in higher rates of non-geminate recombination whilst further into reverse bias results in the opposite. Such transients are shown for another P3HT:PCBM device in Figure 5.13. It can be seen that whilst the charges are extracted faster in reverse bias than at short circuit, thus the transient peaks earlier and the population is lower at fixed time, the actual slope of the transient with time representing the DoS remains the same. However in forward bias the charges are extracted slower but more importantly the slope changes. This can be assigned to the increased rates of non-geminate recombination in forward bias.

5.4.1 Study Of Annealing

It is known that to achieve the highest possible efficiency device using the material combination of P3HT and PCBM the active layer of the device must be thermally annealed, and several authors have shown that this results in a different and presumably better microstructure.[37, 133] It is additionally possible that if at least some of the distribution of the DoS in these devices results from structural and morphological disorder, then the DoS may change as a function of the thermal annealing. The resulting changes in device performance on annealing may be due to differences in charge mobilities due to the devices having different DoS.

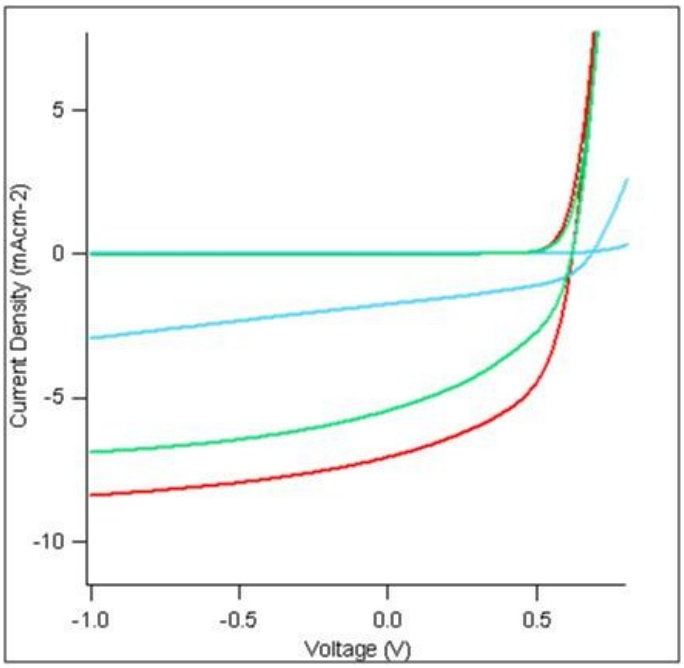

Figure 5.14. Current-voltage curves of a three P3HT:PCBM devices processed with different annealing conditions; no annealing (blue), annealed at 80°C (green) and annealed at the optimum 140°C (red).

To investigate this three P3HT:PCBM devices were fabricated and whilst one of these was left unannealed the other two were annealed separately at 80°C and 140°C, both for 20 minutes. It has previously been found that the optimal annealing temperature for these devices was 140°C. This is shown in the *J-V* curves for these three devices shown in Figure 5.14 which clearly show that whilst the open circuit voltage is reduced with annealing, the short circuit current and the fill-factor massively improve.

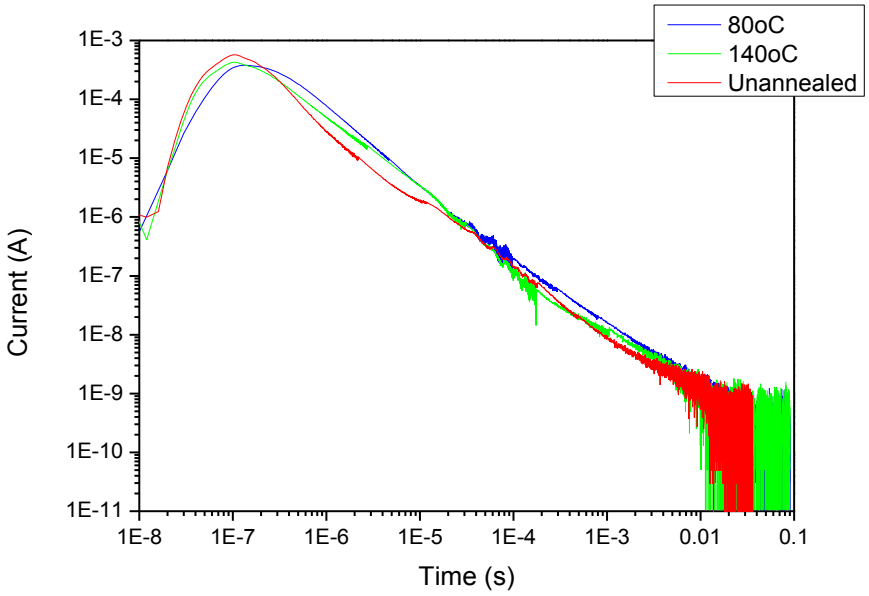

Figure 5.15. TPC transients for three P3HT:PCBM devices processed using different annealing conditions.

The transients for these three devices measured under short circuit conditions are shown above in Figure 5.15. Additionally the transforms into DoS/energy using equation *(5-7)*, which have been heavily filtered to reduce the noise in the low current region of the transient, are shown in Figure 5.16.

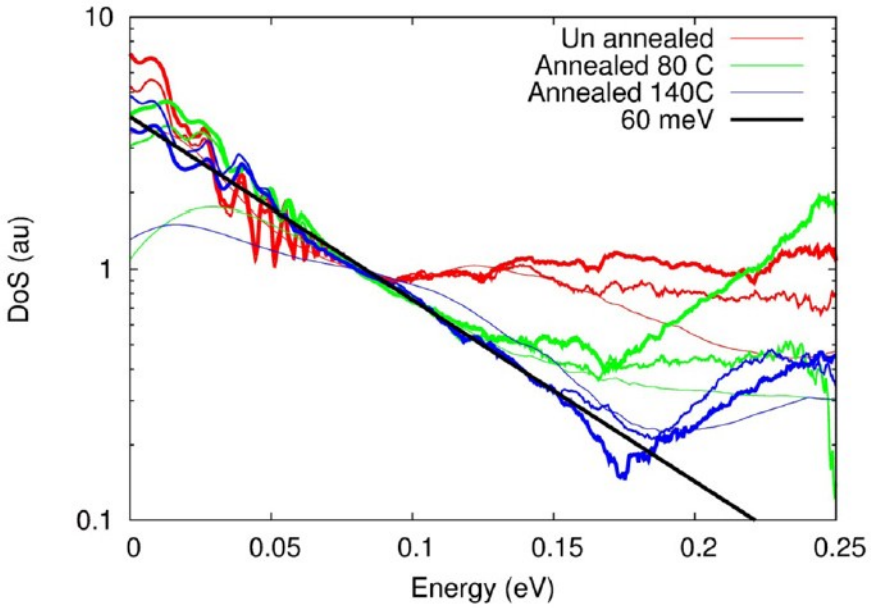

Figure 5.16. A plot of the DoS extracted from TPC measurements obtained from series of P3HT:PCBM solar cells which were unannealed (red), annealed at 80 °C (green) and annealed at 140 °C (blue). The TPC measurements were performed at short circuit (thin lines), −1 V (thick lines), and −2 V (thickest lines). This figure is reproduced from MacKenzie et. al. copyright of the American Chemical Society.[129]

The first thing that can be seen by comparison of the transients is that the initial slope of the density of states is very much the same. On the DoS plot is superimposed a line corresponds to an exponential distribution of traps with a slope of 60meV, and this closely matches the shallowest trap distribution in all three devices. This implies that there is a distribution of traps with such an exponential distribution in all these devices that is unchanged by morphological changes on the scale of tens of nanometres and possibly smaller. The second perhaps more relevant point is the differences between the densities of states for the different devices. Whilst the deepest parts of the DoS are often the noisiest, likely due to the long detrapping time and probable recombination of some charges, there is a clear difference between the deep traps of the devices. The unannealed device has a large number of trap states that lie deep in the distribution, a similar feature is seen in the data for the device annealed at 80°C. Finally the device annealed at 140°C, or the optimised device, has the lowest concentration of trap states at these deep energies by almost an order of magnitude. Deep traps are obviously the most difficult to detrap from due to the high energy between them and the conduction band, and as trapped charges may recombine with free carrier of the opposite polarity, being trapped for long periods likely results in high charge recombination losses. Other authors have shown using transient techniques that recombination rates are higher in unannealed devices. This is consistent with our results that show a higher concentration of deep limiting trap states in unannealed devices that gradually reduce with annealing.

This reduction in trap state concentration on top of an unchanging DoS distribution suggests that several factors contribute to the distribution of trap states in devices. Firstly some deep traps can be linked to morphological disorder that can be reduced using thermal annealing to change the P3HT:PCBM morphology into a more thermodynamically favourable state. Additionally there is some portion of the DoS, at least in these devices with an exponential distribution of slope 60meV, which is unrelated to the morphology altered by thermal annealing, but to some other energetic disorder mechanism.

5.4.2 Conclusions

To conclude, we have studied the energetic density of states distribution in P3HT:PCBM devices, particularly as a function of morphological change, enabled by thermal annealing. Transient photocurrent measurements over several decades of time and several orders of magnitude of current allow us to discern features and sizes of the density of states in these devices. When observed for devices that were either unannealed or annealed at different temperatures the TPC measurements show significant changes in the concentration of deep trap states consistent with reductions in deep traps and therefore more efficient charge transport in the most efficient devices. Furthermore we have observed an underlying density of states that remains unchanged in all the device studied herein and is therefore unrelated to the structural changes that the devices undergo with thermal annealing.

5.5 CONCLUSIONS

In this chapter we have introduced the analysis of charge extraction and transient photovoltage data and the method of *J-V* reconstruction used to relate measurements of non-geminate recombination to device performance. To do this we initially reproduced the analysis of Shuttle et. al.[49] with measurements of a P3HT:PCBM device to successfully recreate the *J-V* cure under 1 sun illumination. We then extended these charge extraction and TPV experiments to probe both non-geminate recombination, but also the energetic DoS within the device by performing the measurements under varying temperature. These results showed that as expected, as temperature is decreased the non-geminate recombination rate and charge densities reduce as the available thermal energy to excite charges out of trap states is reduced. By plotting the recombination lifetime against charge density and analysing the recombination order as a function of temperature we were able to estimate both the exponential slope of the distribution of trap states from which charges must be excited, as well as the magnitude of the total number of trap states available to fill. These measurements were compared to previous measurements using transient absorption spectroscopy by Clarke et. al. on the same material system which yielded a similar figure.[62]

In the third section of this chapter we utilised transient photocurrent measurements on the same material system as above, not to measure the non-geminate recombination but to measure the detrapping of charges as a means of probing the DoS. This was done by using a range of measurement resistances to measure a current transient over 5 decades of both time and current. This TPC transient essentially represents the excitation out of traps, as a charge is less likely to be detrapped from a deeper trap thus it will statistically take a longer time. Using a mathematical transformation we convert the results of the TPC experiments into a representative DoS for both electrons and holes.

To conclude, in this chapter we introduced the use of transient techniques to probe non-geminate recombination and charge density dynamics and related them to P3H:PCBM device performance. Furthermore we analysed the effect of an exponential distribution of energetic trap states upon the recombination and charge transport properties of the P3HT:PCBM devices.

5.6 EXPERIMENTAL METHODS

P3HT:PCBM devices were fabricated by spin coating a blend solution of the donor and acceptor in a 1:1 ratio, onto an ITO substrate coated with a thin layer of PEDOT:PSS. These were then capped with an aluminium electrode and annealed for 30 minutes at 140°C.

Charge extraction, transient photovoltage and transient photocurrent measurements were made as summarised in chapter 2.

In the temperature dependent measurements the device temperature was changed using an Oxford Instruments Optistat DN-V liquid-nitrogen cryostat which was thermally coupled to the device using a copper mask contacting the glass substrate which also allowed light to pass through to the device. The temperature of the cryostat was measured by two thermocouples within the vacuum chamber, as the illumination of the solar cell heated the device slightly the device temperature was additionally measured directly by a thermocouple sandwiched between the metal heat transfer contact and the glass substrate of the solar cell.

CHAPTER VI

THE RELATIONSHIP BETWEEN LINEARITY OF CORRECTED PHOTOCURRENT AND THE ORDER OF RECOMBINATION IN ORGANIC SOLAR CELLS

6.1 INTRODUCTION

Charge transport in organic semiconductors has been shown to be limited by the excitation of charges from distributions of energetic trap states within the electronic band-gap of the donor and acceptor materials.[62, 134-135] These trap states, and excitation out of them into transport bands, therefore play a significant part in determining the performance of devices fabricated from these materials. The energetic landscape as seen by an electron or a hole, particularly whether it is trapped or free to move, determines the rate of charge transport and consequently the rate of the non-geminate recombination. Both of these processes are very important in determining photocurrent generation and collection and thus the characteristics of devices such as short-circuit current density (J_{SC}), open-circuit voltage (V_{OC}) and fill factor (*FF*) in organic solar cells.

The non-geminate recombination process, which has been shown to be the dominant loss mechanism in some devices,[49, 97-98, 123, 136] is fully described in chapter 2 and 5 of this thesis. This recombination process depends upon the density of electrons[70, 120] and in the presence of energetic disorder in organic solar cells is highly non-linear as the recombination rate will change when more trap states are

filled and the charges can be more easily excited into the transport/recombination bands. Thus, the recombination rate varies as $R \approx k(n)n^2 = k_0 n^\alpha$, where α is the order of the recombination rate with regard to charge density. Non-geminate recombination has been experimentally measured in various systems and the charge density dependence of this process, or α, has always been observed to greater than 2. [50, 70, 137] In some systems far greater apparent reaction orders have been observed, even as high as 5, this has been shown to be due to changes in the distribution of charge carriers within devices when the thickness of the active layer is very low.[125] This non-linear behaviour is characterised in chapter 5 of this thesis, in which transient opto-electronic measurements of the behaviour of a P3HT:PCBM device show that the *J-V* curve of the device under illumination is shaped by non-geminate recombination, but also that this non-geminate recombination rate depends upon charge density with a power law of $\alpha>2$.

Contrasting the observations above with actual device performance observed in measurement of various parts of the *J-V* curve, it is striking that OPV device behaviour with light intensity is typically very linear and well-behaved. Many authors have observed the J_{SC} of devices to be approximately linear with the light illumination levels, as well as the saturation current under illumination in reverse bias.[48, 127, 138-139] Additionally the open-circuit voltage of OPV devices which has previously been shown to depend upon the rates of non-geminate recombination,[50, 97, 137] typically varies logarithmically with light intensity,[127] consistent with the behaviour of an ideal diode. Finally several authors have observed the corrected photocurrent of devices, or the additional current observed in the light compared to the dark, to vary linearly with light intensity at all voltages.[48, 59, 138, 140] This is significant as when recombination is non-linear, *J* can only be linear with light intensity when $J_{GEN}>>J_{REC}$, when this is not the case *J* should be non-linear. Thus measurements of linear corrected photocurrents appear to directly contradict measurements detailed in chapter 5 and in the literature[49] that show that at voltages close to the maximum power point and V_{OC} the current is determined primarily by a non-linear process. Some authors who measure a linear corrected photocurrent have concluded that the recombination process limiting the current at such voltages must be first order, or linear, with the charge density, directly contradicting transient measurements.[48, 138]

This chapter will aim to reconcile these two apparently contradictory observations; of devices whose performance is determined by excitation out of an approximately exponential density of states into a transport band where loss processes vary non-linearly with charge density, yet the device characteristics when measured in the steady-state still change linearly with illumination level. We will utilise both transient and steady-state measurements to quantify device behaviour as well as analyse device physics to understand these effects.

6.2 LINEARITY OF CORRECTED PHOTOCURRENT

Two types of energy loss mechanisms are particularly important in OPV, geminate and non-geminate charge recombination, understanding these loss mechanisms is essential in the development of more efficient solar cells. As discussed earlier in this thesis the order of the dependence of the recombination rate upon the density of charges within a solar cell is often used to analyse the type of recombination process occurring, where the recombination rate, R, is related to the total charge density, n, by the reaction order of the process, α,[99] by

$$R \propto n^{\alpha} \qquad (6\text{-}1)$$

For example, geminate recombination of singlet excitons is a first order process depending linearly only upon the population of excitons. However non-geminate recombination depends upon the density of dissociated charges, *n*, and whilst commonly assumed to be a second-order process with *n*, can appear to have orders from first-order[59] to values far greater than 2 under certain conditions. Determining which recombination process is limiting the performance of organic solar cells is difficult and has previously been studied using transient analyses of charge populations such as charge extraction and photo-CELIV, however some authors have attempted to analyse this by studying the corrected photocurrent of a device.[48, 103, 141]

The current density generated by a solar cell, *J*, is determined by the balance of the volume generation rate of free charge carriers, *G*, and the volume non-geminate recombination rate of those carriers, *R*,

$$-\frac{1}{e}\nabla.J = G - R. \qquad (6\text{-}2)$$

Measurement of the corrected photocurrent has been used to gain an understanding of the device performance and recombination processes. Corrected photocurrent is defined as the current density at a certain voltage under illumination with the current density at the same voltage in the dark subtracted,

$$\mathrm{J_{corr}}(\mathrm{V},\phi) = \mathrm{J_{light}}(\mathrm{V},\phi) - \mathrm{J_{dark}}(\mathrm{V}) \qquad (6\text{-}3)$$

where J_{corr} is the corrected photocurrent density, J_{light} and J_{dark} are the current density in the light and dark, and Φ is the illumination intensity. The aim of this measurement is to isolate the component of the device performance related to charge photogeneration in isolation from the fundamental device diode properties present in the dark *J-V* curve. It is important here to measure the light and dark *J-V* curves under identical conditions, particularly temperature which can be influenced by illumination, as device performance has been shown to vary considerably with temperature.[126, 140] Additionally, this is problematic as it has been shown that the dark *J-V* curve is determined by non-geminate recombination rates,[94] just the same as *J-V* curves in the light. Since non-geminate recombination is a non-linear process (in general), simply subtracting J_{dark} from the light curve may not be mathematically sound.

Several authors have observed J_{corr} to be linear with the illumination light intensity across a wide range of applied voltages and light intensities in various polymer:fullerene systems.[48, 138, 140] It has been suggested that the linearity of the corrected photocurrent implies the linearity of the loss processes that determine the *J-V* performance, and thus that the recombination processes themselves must be linear with charge generation. Several authors have thus ascribed this linear loss process to either a voltage dependent geminate process limiting *G* or a non-geminate process *R* that scales linearly with charge density. However both these conclusions contradict transient opto-electronic measurements of generation and recombination processes in devices; transient absorption spectroscopy studies have indicated that charge generation in OPV devices is not always dependent upon the voltage applied across the cell and that in some efficient polymer:fullerene systems external electric field is not required to separate the bound charge state.[68] It has been shown that in P3HT:PCBM devices the generation of free charges is efficient and insensitive to the voltage applied to the device.[70] Additionally extensive transient opto-electronic experiments using many techniques have shown that non-geminate recombination varies highly nonlinearly with charge density within the device, and that these super-linear processes dominate device behaviour around open circuit.[50, 137]

Combining equations *(6-2)* and *(6-3)* the corrected photocurrent can be expressed in terms of the recombination in the dark and light and generation rates,

$$J(V,\phi) = -edG(\phi) + edR(V,\phi) \qquad (6\text{-}4)$$

$$J_{corr}(V,\phi) = ed\left(\left(-G(\phi) + R_{light}(V,\phi)\right) - R_{dark}(V)\right) \qquad (6\text{-}5)$$

$$= -ed(G(\phi) - \Delta R(V,\phi)) \qquad (6\text{-}6)$$

where $\Delta R = R_{light} - R_{dark}$, the difference between the recombination rates in the light and dark. From equation *(6-6)* it is clear that measurements of J_{corr} don't actually probe the recombination rate directly, but the generation rate and the difference between the recombination rates in the light and dark. Thus the linearity of J_{corr} with light intensity doesn't *necessarily* mean that the loss processes themselves are linear. When corrected photocurrent is used to draw conclusions upon the generation and recombination processes in devices two main assumptions must be made:

(i) it must be assumed that $R \approx \Delta R$, thus that the quantity being measured J_{corr} is related to the quantity of interest, *R*.

(ii) it must be assumed that charge density scales with light intensity Φ such that $n \propto \Phi$. This is not necessarily the case because the order of the recombination process is the dependence of recombination rate upon charge density, not upon light intensity or generation.

Here we shall analyse these assumptions and the performance of an organic photovoltaic device by analysing the behaviour of the corrected photocurrent across the *J-V* curve, as well as utilising transient opto-electronic experimental techniques to probe the generation and non-geminate recombination rates. We study a P3HT:PCBM device, as this is a well studied material system and the recombination dynamics in this system have been analysed by many groups. In this case the P3HT:PCBM device comprised of a layer

structure of ITO/PEDOT:PSS/P3HT:PCBM/Al, where the P3HT:PCBM layer was a 1:1.5 polymer:fullerene weight ratio and was 200nm thick.

6.3 RESULTS & ANALYSIS

6.3.1 Device Behaviour

Figure 6.1 shows the *J-V* curves in the dark and under 1 sun illumination, as well as the corrected photocurrent curve under 1 sun illumination. The curves were all measured using pulsed illumination, this allows the light and dark *J-V* curves to be measured almost simultaneously meaning that changes to the *J-V* behaviour in time or with changing device temperature on exposure to bright light will be minimised. The pulses of light are short compared to the time the device spends in the dark (2ms in the light followed by 420ms in the dark) thus minimising any heating of the device.

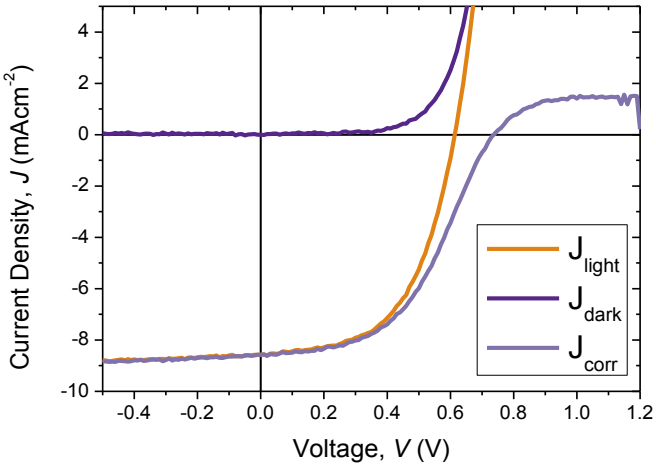

Figure 6.1. J-V curves for a P3HT:PCBM device measured under 1 sun illumination and in the dark, and the corrected photocurrent under 1 sun illumination measured using pulsed 1 sun illumination.

Figure 6.2a shows the corrected photocurrent curves against voltage at various illumination intensities between dark and 200% of 1 sun illumination. All presented corrected photocurrents show the characteristic S-shape, flattening out at voltages >1V. Figure 6.2b shows the same data but plotted against light intensity with each trace representing a cut at constant voltage of the data in Figure 6.2a. Each of these data sets shows the light intensity dependence of the corrected photocurrent at a fixed voltage; additionally a linear fit is shown for all the voltages indicating that the corrected photocurrent is effectively linear over the light intensities measured.

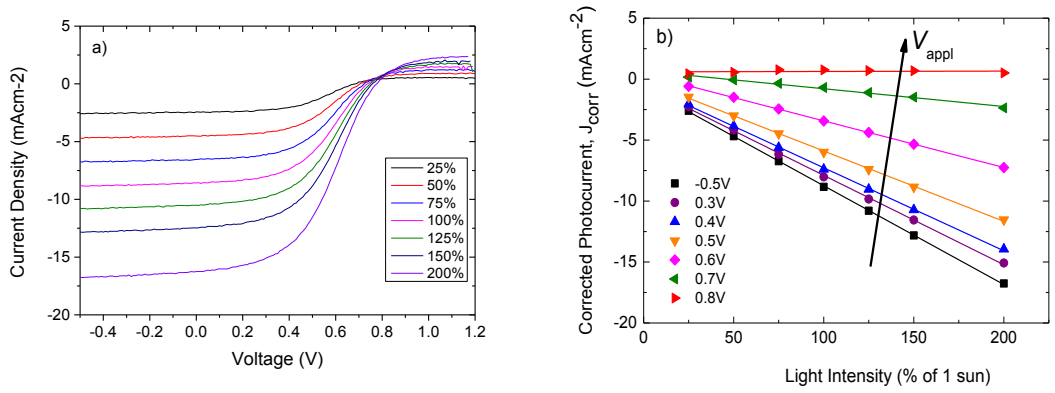

Figure 6.2. (a) Corrected photocurrent curves of a P3HT:PCBM device under various light intensities between 25% and 200% of 1 sun illumination plotted as a function of voltage and (b) the same data but plotted as a function of illumination intensity such that the linearity of the corrected photocurrent can be observed. Linear fits to the data are shown.

6.3.2 Transient Experiments

Charge extraction (CE) and transient photovoltage (TPV) experiments were performed to measure the charge density within the device and the bulk non-geminate recombination rate respectively. These transient measurements allow the apparent dependence, or order, of the recombination rate upon charge density to be determined. Figure 6.3a & b show the lifetime and charge density extracted against the open-circuit voltage at which they were measured. The exponential dependence upon voltage can be seen in each case. Figure 6.3c shows the non-geminate recombination lifetime plotted against the charge density with a power law fit. The fit corresponds to an order of recombination, or α, upon charge density of 2.9. This indicates that the linearity of the corrected photocurrent can still be consistent with a highly non-linear non-geminate recombination rate.

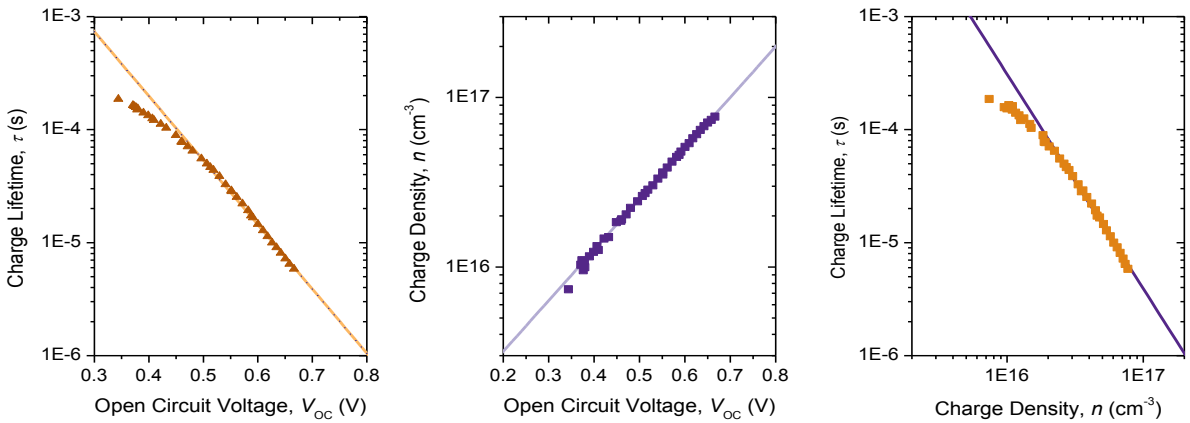

Figure 6.3. (a) Non-geminate recombination lifetimes at open circuit conditions as a function of VOC for the P3HT:PCBM device and measured by TPV, (b) the average steady-state charge density within the same device in the same conditions and (c) the charge recombination lifetime plotted against the charge density. Exponential (a, b) and power law (c) fits are shown.

6.3.3 *J-V* Reconstruction

It has previously been demonstrated that the *J-V* curves of P3HT:PCBM solar cells are dominated by non-geminate recombination, particularly around open circuit conditions where the voltage dependence of the rate of non-geminate recombination determines the open circuit voltage.[49] By using the recombination-charge density relationship shown in Figure 6.3 along with CE measurements at various applied biases through the operating quadrant of a solar cells *J-V* curve, it is possible to calculate the magnitude of the non-geminate recombination losses in the device. Shuttle et. al. showed that by subtracting this measured non-geminate recombination from a constant voltage-independent charge generation flux it is possible to approximate the *J-V* curve of a P3HT:PCBM device, showing that the *J-V* curve, particularly the fill factor, is determined by non-geminate recombination losses.[49] Additionally the dark *J-V* curve can be closely approximated simply by considering a recombination current density with no generation current.[94] As both dark and light *J-V* curves can be "reconstructed" using the transient quantities measured, it is possible to calculate a reconstructed corrected photocurrent. It must be stressed that this *J-V* reconstruction technique neglects all loss mechanisms except the measured, highly non-linear, non-geminate recombination process.

Figure 6.4a shows the measured charge density at various light intensities under applied bias and Figure 6.4b shows the resulting reconstruction of the *J-V* curves for all light intensities. This shows that a close approximation of the *J-V* curve can be made at all voltages, particularly the non-geminate losses accurately match the open circuit voltages of the devices. Note the dark *J-V* curve is well reconstructed by the calculations as well.

Figure 6.5a shows the reconstructions of the corrected photocurrents made by subtracting reconstructed dark curves from reconstructed light curves. Due to the fact that calculations of non-geminate recombination consistently overestimate the fill factor of these devices, the reconstructed corrected photocurrent curves all underestimate the voltage at which the corrected photocurrent is zero, however they match the experimental data well over most of the voltages measured.

When the reconstructed corrected photocurrents are plotted against light intensity for each voltage, shown in Figure 6.5b, it can be seen that they are still almost completely linear within the error of the measurements. These reconstructed J_{CORR} values take only the charge extraction and TPV results as inputs as well as the device, thus are calculated using only a highly non-linear relationship, and yet they still appear to be linear. Even at voltages greater than 0.4V where in Figure 6.4b it can be seen that almost all charge is recombining, the corrected photocurrent still appears linear. This proves that a non-linear recombination process shaping the *J-V* curve can still give rise to a linear corrected photocurrent at all voltages.

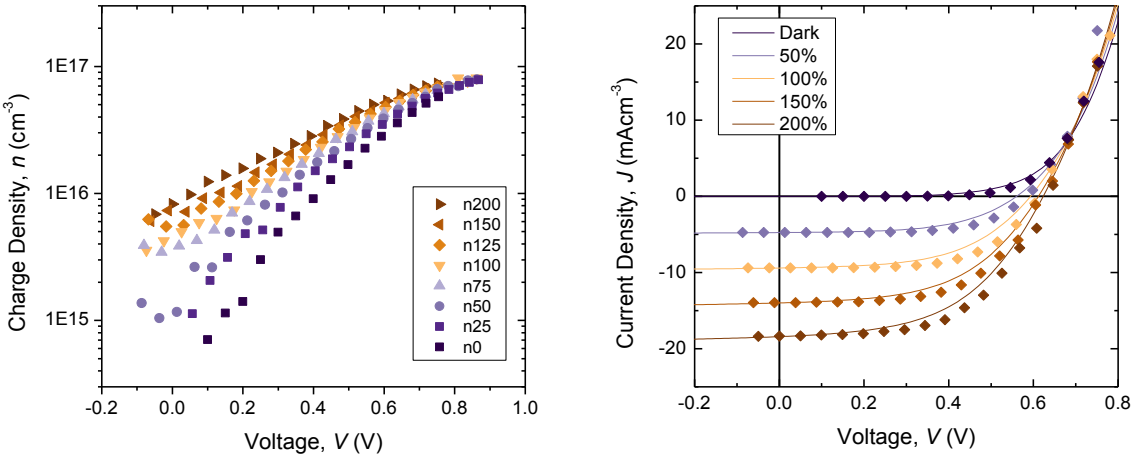

Figure 6.4. (a) average charge density within the P3HT:PCBM device under applied biases in the power generating quadrant and under various light intensities including in the dark. (b) J-V reconstructions from data for charge density under applied bias (points) compared to experimental J-V curves under the same light intensities (lines), showing the close similarities between the experimental and reconstructed curves.

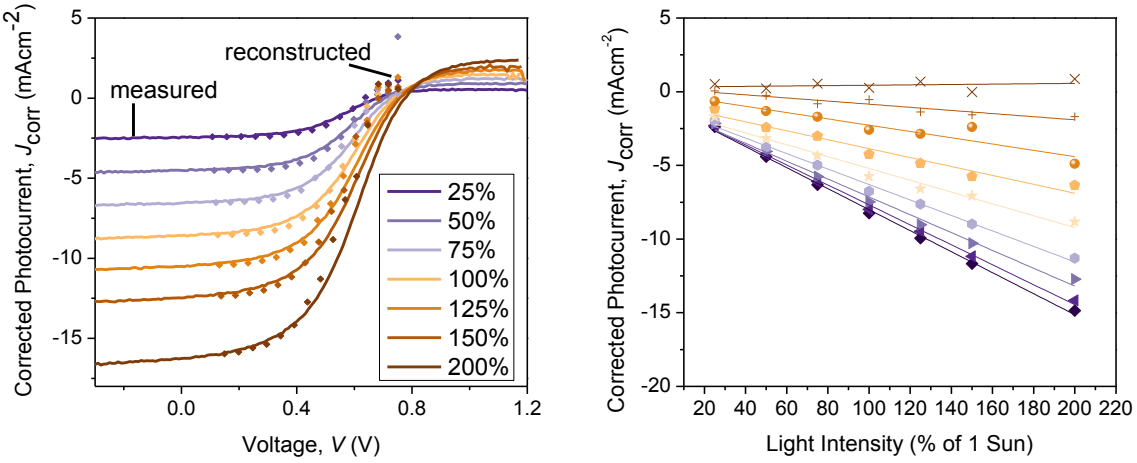

Figure 6.5. (a) reconstructed corrected photocurrent curves under various illumination levels (points) as calculated from the data shown in figure 4b based upon the transient analyses, plotted with measured corrected photocurrents under the same conditions (lines). (b) Corrected photocurrents plotted against applied biases, along with linear fits, indicating the linearity of the reconstructed corrected photocurrent curves.

6.4 ANALYSIS

Now we have shown that linear corrected photocurrent doesn't necessarily indicate a linear loss mechanism, we can discuss and counter the assumptions that would give rise to such a conclusion; namely that $R \propto \Delta R$ and that $n \propto \Phi$.

6.4.1 Relationship Between Charge Density And Light Intensity

Showing that the charge density is not proportional to the light illumination intensity is relatively trivial; it is first taken that the generation is proportional to the light intensity $G \propto \Phi$ as the generation of charges is generally observed to depend only on the number of photons absorbed. The definition of V_{OC} is the voltage at which no current flows, thus all generated charge recombines, so $G = R$. Therefore if recombination rate varies as $R = kn^{\alpha}$, then under open circuit conditions $n = (G/k)^{1/\alpha}$. It follows that $n \propto G$ only when $\alpha = 1$, or when the recombination is first order. Thus when the recombination is second order with charge density and $\alpha \approx 2$ this assumption can no longer be assumed to be valid at open circuit. Charge extraction experiments allow direct measurement of the charge density, particularly at open circuit. Figure 6.6 shows the open circuit charge density n_{OC} against light intensity, showing that the behaviour is highly non-linear.

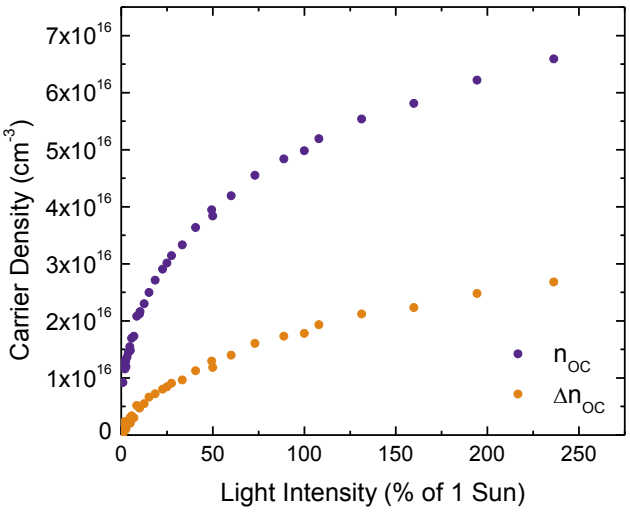

Figure 6.6. Plot showing the average charge density under open circuit conditions from charge extraction experiments as a function of light intensity (purple) and the difference in charge density between light and dark at the same voltage (orange). This shown the non-linearity of n and Δn with light intensity.

6.4.2 Differences Between Recombination In The Light And Dark

Secondly we analyse the assumption that $\Delta R \propto R$ where ΔR is the difference in recombination rates between a particular light intensity and the dark. To do this we must look at the charge density within the device, which is known to directly determine the non-geminate recombination rate, thus we define

$$\Delta R(\phi) = R_{light}(\phi) - R_{dark} \quad (6\text{-}7)$$

$$= k_0(n_{light}^{\alpha}(\phi) - n_{dark}^{\alpha}) \quad (6\text{-}8)$$

$$= k_0((n_{dark} + \Delta n(\phi))^{\alpha} - n_{dark}^{\alpha}) \quad (6\text{-}9)$$

where $\Delta n = n_{light} - n_{dark}$, the difference in charge carrier density between light and dark conditions at a set voltage. The TPV and CE results shown above demonstrate that in this particular device α is 2.9 and greater than 1, therefore we can use the binomial expansion to express

$$\Delta R = n_{dark}^{\alpha}\left[\left(1 + \frac{\Delta n(\phi)}{n_{dark}}\right)^{\alpha} - 1\right] \quad (6\text{-}10)$$

$$= n_{dark}^{\alpha}\left[\frac{\alpha \Delta n(\phi)}{n_{dark}} + O\left(\frac{\Delta n(\phi)}{n_{dark}}\right)^{2}\right] \quad (6\text{-}11)$$

when $\Delta n / n_{dark} \rightarrow 0$, where $O(x)^2$ indicates all the terms of x with indices of 2 or more. Note that at a set voltage n_{dark} is a constant, and the only component here that is light intensity dependent is Δn. This shows that ΔR will scale with Δn quite differently in two different regimes. When $\Delta n \gg n_{dark}$ then all the higher orders of Δn will dominate the equation and ΔR will scale super-linearly with Δn, and therefore it is likely that J_{corr} will scale non-linearly with charge density. The only way in which ΔR could still appear linear was if Δn varied sublinearly with ϕ to the exact opposite that ΔR varies super-linearly thus cancelling out. Whilst Δn_{OC} can been seen in Figure 6.6 to be sub-linear with light intensity it is unlikely that it will cancel the dependence of ΔR exactly. In the opposite regime where $\Delta n \ll n_{dark}$, the second order terms and higher will be negligible and ΔR will scale linearly with Δn regardless of the order of recombination. As both Δn and n_{dark} are accessible by CE experiments we can analyse our results and determine in which regime the P3HT:PCBM device studied here operates. Figure 6.4 shows the results of CE experiments under applied bias at various levels of illumination, including in the dark. There is a large variation between charge densities at biases close to short circuit conditions. However as the voltage approaches V_{OC} the charge densities all converge with dark. Figure 6.7 shows the same charge density data with n_{dark} subtracted, thus the figure shows Δn against applied bias, along with n_{dark}.

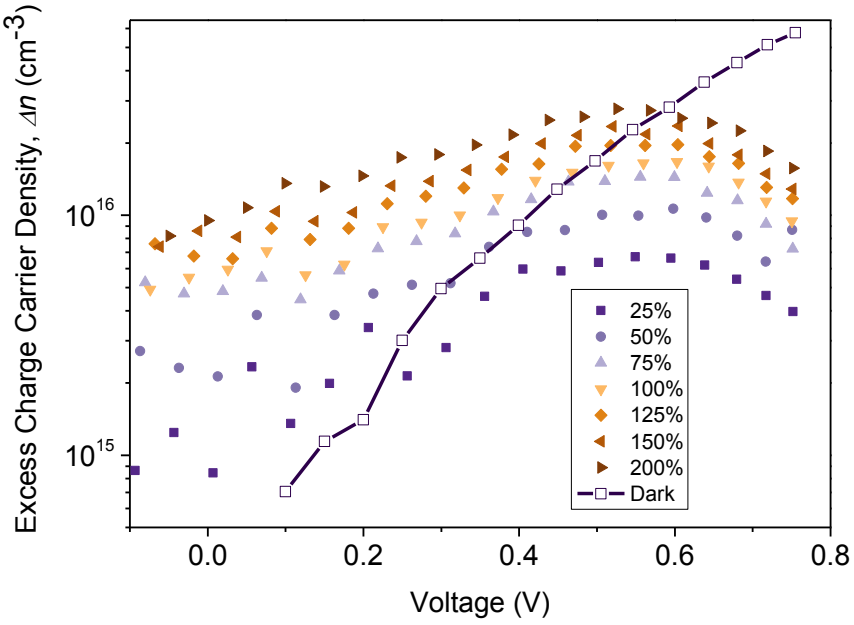

Figure 6.7. Excess charge densities Δn obtained from the difference between the charge density in the light and dark, against applied voltage under various light intensities. The dark charge density is shown for comparison (line & points).

What this shows is that essentially one of the main causes of misinterpretation of the corrected photocurrent, is that the dark *J-V* curve has also been shown to be determined by the non-geminate recombination of injected carriers, with the same super-second-order dynamics as recombination in the light. Thus the calculation of the corrected photocurrent by the subtraction of the dark current from that measured in the light, is the subtraction of one highly non-linear process from another. Thus the resulting quantity does not necessarily have the same order or behaviour as either of the initial measurements and conclusions based on the calculation on the behaviour of the device is invalid.

6.4.3 Linearity Of ΔR

It is clear from Figure 6.7 that for voltages where non-geminate recombination dominates the *J-V* curve (close to the maximum power point and V_{OC}) $\Delta n < n_{dark}$, holds. Thus, ΔR is in the regime where it scales linearly. Conversely it is evident from the figure that for a certain voltage range (around short circuit and low voltages) $\Delta n > n_{dark}$ so here ΔR is in the non-linear regime. However, this is the region where measurements of non-geminate recombination show that recombination flux is low. Thus, looking at equation *(6-6)*, the component of J_{corr} that corresponds to ΔR is nonlinear, however that is small and is dwarfed by the generation term which is linear with light intensity, thus J_{corr} still apparently linear with ϕ. This can be seen in Figure 6.8 which compares Δn and n_{dark} with the non-geminate recombination current density in the light and dark as a function of voltage all measured under 1 sun illumination. It is evident that for the region where $\Delta n > n_{dark}$ the recombination currents are low, only rising to levels where it significantly affects the *J-V* curve in the linear region where $n_{dark} > \Delta n$.

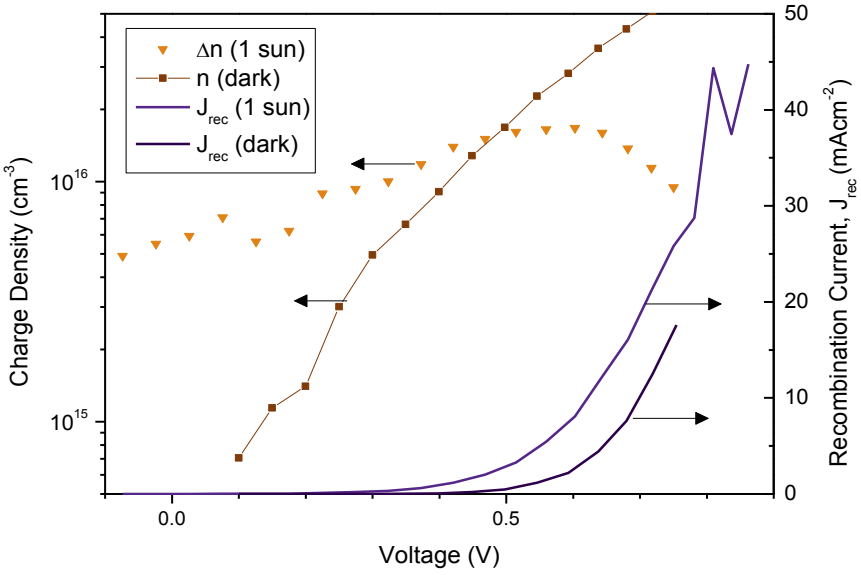

Figure 6.8. A plot comparing the excess charge density under 1 sun illumination (orange triangles) and the charge density in the dark (brown squares/line), as well as the non-geminate recombination currents in the dark (dark purple line) and under 1 sun illumination (purple line). This shows that the non-geminate recombination current becomes large and limiting, when Δn *is lower than ndark.*

As we can calculate the recombination rate *R* from the CE and TPV data at all relevant voltages and light intensities we can analyse its voltage dependence, and in particularly its linearity to test the conclusions related to equation *(6-11)*. Figure 6.9 shows the change in recombination rate between light and dark as a function of voltage for various light intensities. When this subtracted from the generation rate this is the actual quantity being probed by the corrected photocurrent measurement.

Figure 6.10a shows the normalised values of ΔR plotted against light intensity for a select few voltages. Additionally each has been fit with a $y = ax^b$ power law to measure its "linearity" with light intensity. These fit values along with the values for other voltages are plotted in Figure 6.10b. This data shows, as predicted by equation 6 in conjunction with Figure 6.7 and Figure 6.8, that as the voltage increases and the device transitions from a state in which $\Delta n > n_{dark}$ (non-linear regime) to a situation where the values are equal and then where $n_{dark} > \Delta n$ (linear regime), the values of ΔR become more linear with light intensity. It can be seen that close to short circuit the behaviour scales to the 4th power, then as the voltage reaches ~0.4V the data becomes linear. This corresponds very well to the experimental Δn and n_{dark} data. Again, we note that as $J_{corr} \propto G - \Delta R$, J_{corr} still appears linear around short circuit even when $\Delta R \propto \Phi^4$ as $G \propto \Phi$ and *G* is approximately 2-3 orders of magnitude greater than ΔR at those voltages.

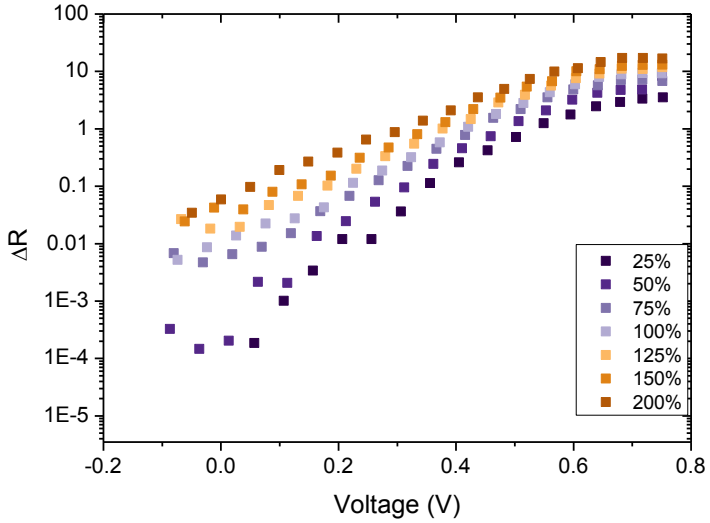

Figure 6.9. The difference between recombination rates in the light and dark, ΔR, as a function of voltage under various light intensities.

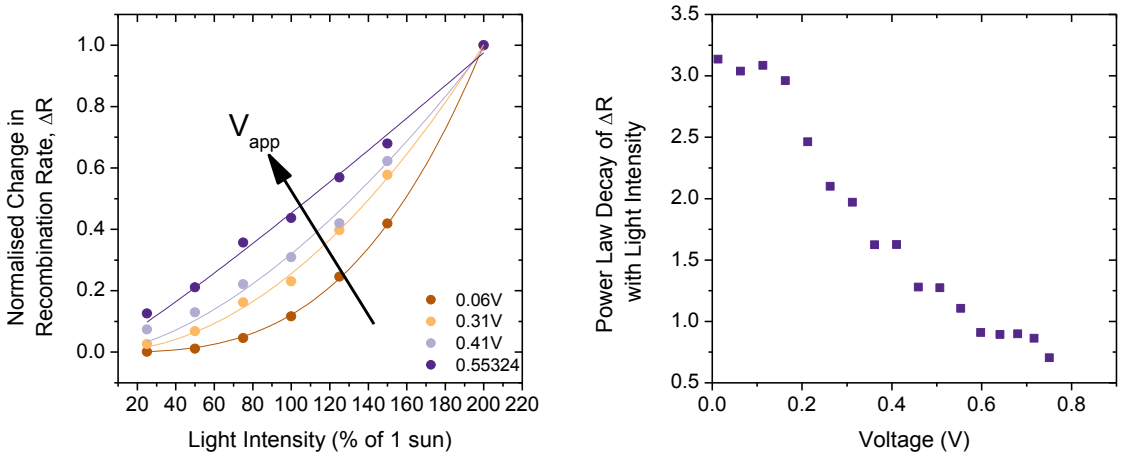

Figure 6.10. (a) a plot indicating the non-linearity of ΔR as a function of illumination intensity at various applied voltages and (b) the power law fit of these datasets as a function of voltage. This indicates that ΔR becomes increasingly linear with regard to light intensity at higher voltages.

The behaviour of Δn with both voltage and light intensity can be explained as follows. The charge density n present within a device under steady state conditions is the result of a delicate balance between charge generation, non-geminate recombination and the flow of charges as current out of the device, thus the dependence on charge density, voltage and light intensity of each of these processes contributes to the final n value, which is therefore difficult to compute. However, some general trends of Δn can be made: From Figure 6.6 it is clear that both Δn and n vary sub-linearly with light intensity, at least under open circuit conditions. Additionally, from Figure 6.7 it can be seen that the difference between light and dark charge densities peaks at approximately 0.5V. This is due to the differences at low voltage being small because the

absolute values of charge density are low as high field efficiently extracts the majority of charges from the device. At high voltage the absolute magnitude of charge density in the device, $n = n_{dark} + \Delta n$, is high as the field extracting charges is low. At high charge densities high recombination rates make it increasingly difficult for more charge to be introduced into the device via photogeneration. Consequently Δn is limited at high voltages and the charge densities under different light intensities begin to converge. This explains the peaking and subsequent reduction of Δn.

It can also be seen in Figure 6.7 that the voltage where $\Delta n = n_{dark}$, and therefore the system transitions from the non-linear to linear regime, moves to higher voltages at greater illumination intensities. The results shown here are for light intensities up to 200% of 1 sun illumination; were this trend to continue up to higher light intensities eventually $\Delta n > n_{dark}$ for all the voltages shown here. This would result in the ΔR being non-linear and it would be expected that the measurement of the corrected photocurrent would cease to be linear with light intensity.

This work conclusively shows that at least in the case of P3HT:PCBM devices, the fill-factor and V_{OC} of the solar cell are determined by a nonlinear recombination loss process whilst the corrected photocurrent is still linear with illumination intensity. This should lead to the re-evaluation of the conclusions of previous works in the literature that measured linear corrected photocurrents. For example Street et. al. conclude from a measured linear corrected photocurrent that the recombination mechanism must be first order, whereas here we have shown that that is not necessarily true.[48] Alternatively other authors such as Marsh et. al. and Liu et. al. conclude from a linear corrected photocurrent that the recombination process itself is geminate in nature not non-geminate.[138, 141] By showing that the assumptions that led to these conclusions were incorrect, and by examining the root causes of the incorrect assumptions this work has reconciled two apparently opposing measurements of device operation by showing they are complimentary.

6.5 CONCLUSIONS

In this section it has been shown that whilst corrected photocurrent may be linear with illumination intensity, this is not necessarily because the individual measurements that are used to calculate J_{corr} are themselves linear or determined by linear relationships. We demonstrate using steady-state and transient measurements on a P3HT:PCBM device, that whilst the non-geminate recombination rate is dependent upon charge density to the power of ~3, a linear corrected photocurrent is still observed up to 2 suns illumination intensity. This is shown to be true because (i) close to open circuit conditions where non-geminate recombination determines *J-V* behaviour the change in charge density between light and dark is smaller than the charge density in the dark and this small perturbation appears linear. Additionally because (ii) over a large range of operating voltages of the solar cell the change in recombination rates between light

and dark is significantly smaller than the generation rate of charges, this quantity is linear with light intensity and dominates the device behaviour.

6.6 EXPERIMENTAL DETAILS

P3HT:PCBM solar cells were made using similar procedures to those studied in previous publications, with the structure ITO/PEDOT:PSS/P3HT:PCBM/Al. Under a calibrated solar simulator, the characteristics of the cell were measured to be η = 3.15%, V_{OC} = 612 mV, J_{SC} = 9.51 mAcm^{-2}, and FF = 54%. Pulsed J(V) measurements were made to minimize the influence of temperature changes between the light and dark measurements. Illumination was provided by 12 white LEDs which could be pulsed by interrupting their power supply using a fast MOSFET switch; in these measurements, the light remained on for 2 ms and off for 420 ms. The cell was held at applied bias using a Keithley 2400 source-measure unit, and the current was measured across a 50Ω resistor using a Tektronix TDS3032B oscilloscope. By measuring the current flowing during the light and dark periods it was possible to alternately measure the light and dark J(V) response.

Charge extraction and transient photovoltage experiments on P3HT:PCBM devices were performed as in chapter 5.

I thank Thomas Kirchartz for the considerable part he played in the theoretical background for this work, and Dan Credgington for experimental advice and useful conversations. Additionally I thank Pabitra Shakya for the fabrication of the P3HT:PCBM solar cells.

CHAPTER VII

LIMITS ON FILL FACTOR IN ORGANIC PHOTOVOLTAICS: DISTINGUISHING GEMINATE AND NON-GEMINATE RECOMBINATION MECHANISMS

7.1 INTRODUCTION

Many polymers, that were designed to offer higher J_{SC}s and V_{OC}s according to the accepted understanding of interface energetics,[96, 142-144] resulted in disappointing PCEs. This was due to either poor collection of photogenerated charges at short circuit, or they exhibited disappointingly low fill factors.[145-147] Indeed, with few exceptions, even the best organic solar cells exhibit fill factors of 60-70% compared to the best inorganic devices whose fill factors can be as high as 85%.[148] The reasons for the low values are not presently well understood, and there is some disagreement on the mechanisms that limit fill factor. Therefore understanding the many processes that limit the *FF*s of photovoltaic devices is essential to attaining high efficiency organic solar cells.

Several processes can reduce the *FF* of devices and these are more thoroughly examined in chapter 2 of this thesis. These processes include:

i. Non-geminate recombination - the recombination of two dissociated charge carriers of opposite polarity. Non-geminate recombination is non-linearly dependent upon the density of

charge carriers present to recombine, and in turn the charge density is dependent upon the voltage within the device driving charges from the device via drift. The non-geminate loss process is thus highly dependent upon voltage, and thus can significantly reduce fill factor, and upon the transport properties of the material system.

ii. **Geminate recombination** - the recombination process of an electron and hole, or bound state. The Onsager-Braun theory of charge separation includes a voltage-dependent term and if this process is voltage dependent in the power generating quadrant then it will reduce current generation and importantly the device *FF*.[39, 66, 69]

iii. **Shunt and series resistance** - a shunt corresponds to a charge carrier bypassing the active layer of a photovoltaic device and a series resistance corresponds to any parasitic resistance that results in a drop of voltage, thus reducing the voltage applied across the active layer of a device. Low shunt resistances manifest as an apparent ohmic reduction in photocurrent around short circuit conditions, as the bias across the device causes current to flow through any shunt bypasses routes in the device. Shunts clearly reduce the *FF* of devices when they are present. Series resistances impact the gradient of the *J-V* curve around open circuit conditions and also reduce the *FF*.

iv. **Leakage** – leakage refers to the recombination of charge carriers at the "wrong" electrode, or the electrode which normally collects charges of the opposite polarity. Leakage is what happens if an electron reaches the cathode or when a hole reaches the anode.

Some distinction must be made between points (iii) and (iv), which largely correspond to inherent physical characteristics of the device, and points (i) and (ii) which are photo-activated processes, dependent upon the photogeneration of charges or excited states within the device.

As described in detail in chapter 2, non-geminate and geminate charge recombination mechanisms are yet to be fully understood, yet have been thoroughly studied in many experimental systems with various techniques. In devices where the *J-V* curve is very flat through short circuit it can be assumed that there is little non-geminate recombination in this voltage range. Devices with obvious slopes at short circuit obviously exhibit low *FF*s however the difficulty is determining which process is creating this slope.

In some devices high levels of non-geminate recombination under short circuit conditions has been found to be reducing the fill factor, this is particularly true in devices that exhibit space-charge accumulation as demonstrated by Kirchartz et. al. in Si-PCPDTBT and by Koster et. al. in OC_1C_{10}-PPV.[149-150] Other mechanisms suggested include new loss pathways such as photo-shunts or contact selectivity.[151-153] Finally both TAS experiments and transient opto-electronic measurements have shown that in P3HT:PCBM and P3HS:PCBM devices can be limited in *FF* by non-geminate recombination under short circuit conditions simply if the charge transport is not efficient enough to maintain low charge densities within the device.[97, 106]

In the case of P3HT the charge transport was altered by reducing the device temperature and observing a consequential reduction in *FF*.[106]

Geminate recombination and energy loss before and during exciton dissociation has been observed to determine the fill-factor of some polymer:fullerene solar cells,[58, 66, 69, 83-84, 154-155] however not all as some systems have been shown to not be affected by this loss process.[49, 68] Previously transient absorption and photoluminescence studies on APFO-3:PCBM devices under applied bias have shown a variation in the yield of free charges on early timescales, interpreted to indicate a field-dependence of the charge separation process.[66] Additionally computation studies of APFO-3's mobility properties have additionally indicated that a voltage dependent geminate process is impacting *FF*s.[155] There is however controversy about the use of voltage dependent TAS as this technique was used by Marsh et. al. to observe voltage-dependent geminate losses in the P3HT:PCBM system,[58] whilst Shuttle et. al. used the same technique and observed no such dependence.[70] Additionally the discovery of voltage dependent charge generation in P3HT:PCBM devices contradicts transient opto-electronic measurements which show that the fill factor is limited by non-geminate recombination.[49, 70, 156]

While many experimental and computational studies in the literature have attempted to address the issue of low fill factors in OPV, there is considerable disagreement, detailed above, over different mechanisms and the correct experimental procedures to measure them.

In this chapter we will use transient opto-electronic experimental techniques to probe the charge generation and recombination kinetics of three OPV systems comprising three different polymers blended with [6,6]-phenyl-C61-butyric acid methyl ester (PCBM); poly(2,7-(9,9-dioctylfluorene)-alt-5,5-(4',7'-di-2-thienyl-2,1,3-benzothiadiazole)) (APFO-3), poly[2,6-(4,4-bis-(2-ethylhexyl)-4H-cyclopenta[2,1-b;3,4-b]dithiophene)-alt-4,7-(2,1,3-benzothiadiazole) (PCPDTBT) and poly(3-hexylthiophene) (P3HT). The structures of these polymers are shown in Figure 7.1. It has been shown that charge generation in P3HT:PCBM devices is voltage-independent[70] and that the fill-factor of the device is determined by non-geminate recombination losses around the maximum power point but which is negligible around short circuit.[49] The P3HT system serves mainly as a comparison to the other OPV systems as it performs well, however we additionally study the performance of the P3HT:PCBM system under higher light intensity where non-geminate recombination losses begin to impact upon short circuit performance. APFO-3 is a polymer that gives a high open-circuit voltage but whose PCE is limited by low *FF* and J_{SC}, some authors have shown that the behaviour of APFO-3:$PC_{71}BM$ devices is consistent with a voltage-dependent geminate recombination loss,[155, 157] this is investigated here. Finally these systems are additionally compared and contrasted with PCPDTBT:PCBM+ODT devices, which Jamieson et. al. show can generates charges independent of the voltage applied,[68] yet still are limited by low fill-factors.

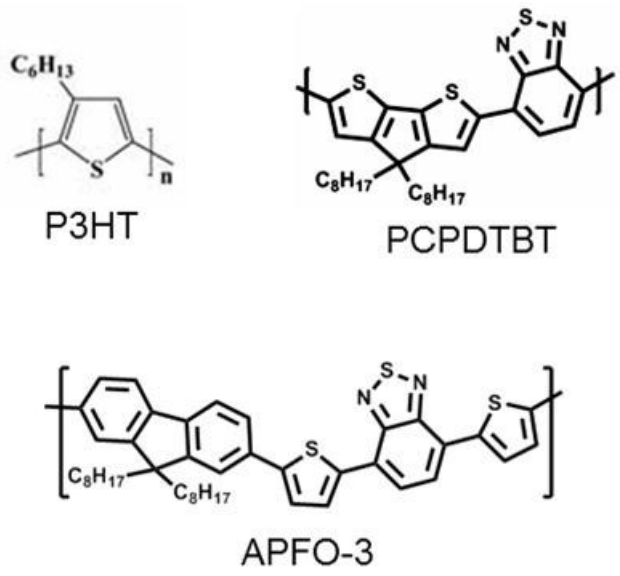

Figure 7.1. Molecular structures of P3HT, PCPDTBT and APFO-3, the three polymers studied in this chapter.

7.2 FILL FACTOR IN P3HT:PCBM SOLAR CELLS

It has been shown in chapter 5 of this thesis that the *J-V* curve of an efficient P3HT:PCBM device under 1 sun illumination is determined by a voltage-independent (or weakly dependent) generation of free charges, which is then reduced around the maximum power point (MPP) and open circuit conditions by a non-geminate loss process. Additionally in chapter 6 we have demonstrated that this non-geminate loss process is non-linearly dependent upon the charge density within the device which is itself dependent upon the voltage applied across the solar cell. The non-geminate recombination flux is thus determined by the relationship between the non-geminate recombination lifetime and the charge density, and the relationship between the charge density and the cell bias. These relationships can be determined using charge extraction and transient photovoltage (TPV) measurements. However under higher light intensities the fill factor of a P3HT:PCBM device reduces significantly, as we understand the processes that reduce the fill-factor under 1 sun we can extend these to higher light intensities to analyse the loss processes, and thus generalise these findings to other devices that suffer similar low *FF* under 1 sun. Here we extend the transient analyses of P3HT:PCBM devices to specifically investigate how the changing recombination dynamics under increased light intensity correspond to the reduced fill-factors measured in *J-V* curves under the same conditions. This is generalised to understand how non-geminate recombination can limit both the *FF* and J_{SC} of different systems.

7.2.1 Device Performance

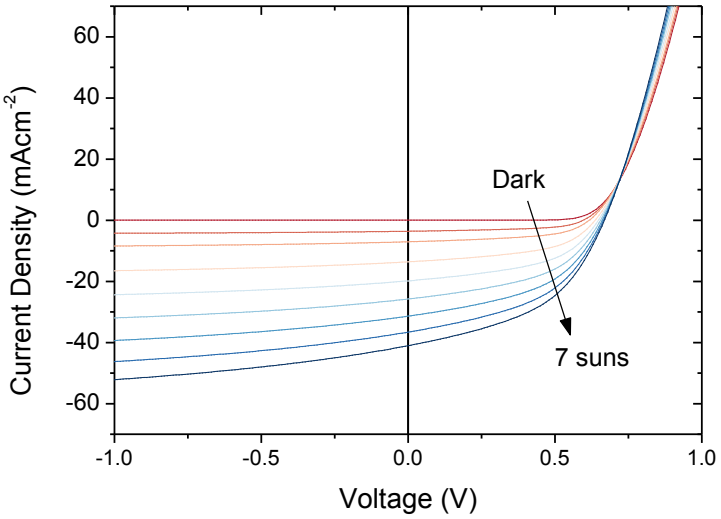

Figure 7.2. J-V curves of a P3HT:PCBM device under white light illumination up to the equivalent of 7 suns.

Here we study a P3HT:PCBM device with a power conversion efficiency of 2.5% whose *J-V* curves under various light intensities (up to 7 suns) and in the dark are shown in Figure 7.2. The *J-V* curve under 1 sun illumination shows that the device behaves characteristically, in that the *J-V* curve is relatively flat though short circuit conditions (this is not true at higher intensities), additionally the V_{OC} is very typical for annealed P3HT:PCBM devices.

Figure 7.3 shows plots of the device characteristics as a function of light intensity and the same *J-V* curves as shown in Figure 7.2 normalised to the current density at -1V for evaluation of device behaviour as function of light intensity. These plots indicate that whilst the V_{OC} increases with light intensity, the fill-factor shows a clear reduction.

7.2.2 Non-Geminate Losses In P3HT

Figure 7.4 shows the J_{SC} of this P3HT device, normalised by dividing the value by the illumination intensity, as a function of light intensity. Evidently the J_{SC} varies linearly with light intensity up to intensities ~80% of 1 sun and then sub-linearly at high light intensities. As charge generation is linear with light intensity whilst charge density increases with light intensity, we can conclude that this non-linearity is likely caused by non-geminate loss processes.

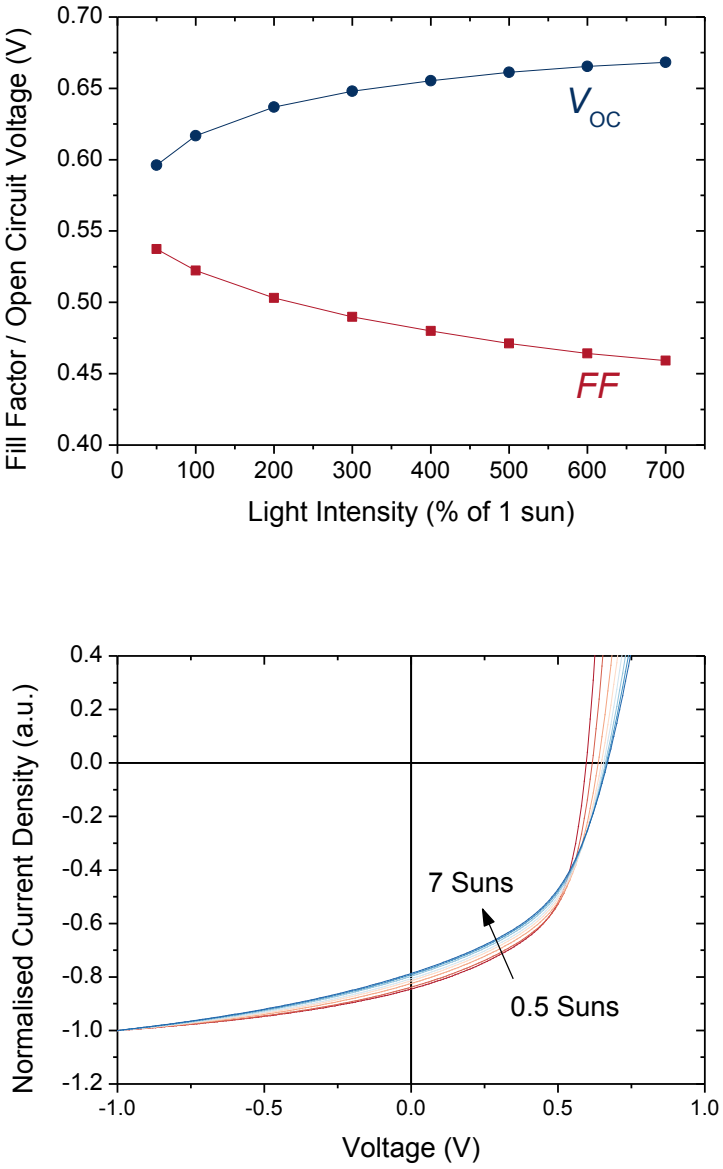

Figure 7.3. (a) open circuit voltage and fill-factor values for the P3HT:PCBM device as a function of light intensity and (b) J-V curves under various light intensities normalised.

In addition to the linearity of the J_{SC}, another experimental technique that can be used to determine if the device's extraction of charge is limited by non-geminate processes under short circuit conditions is transient photocurrent (TPC). As described in chapter 4, TPC experiments use a laser pulse of fixed intensity to photoexcite a small number of charge carriers, Δn, within the device. By performing this under varying light bias, and thus varying charge density, and keeping Δn constant, it is possible to probe non-geminate recombination by observing what proportion of Δn are extracted from the device. For example, a reduction in extracted current at 1 sun compared to 0.5 suns would indicate an increase in non-geminate recombination.

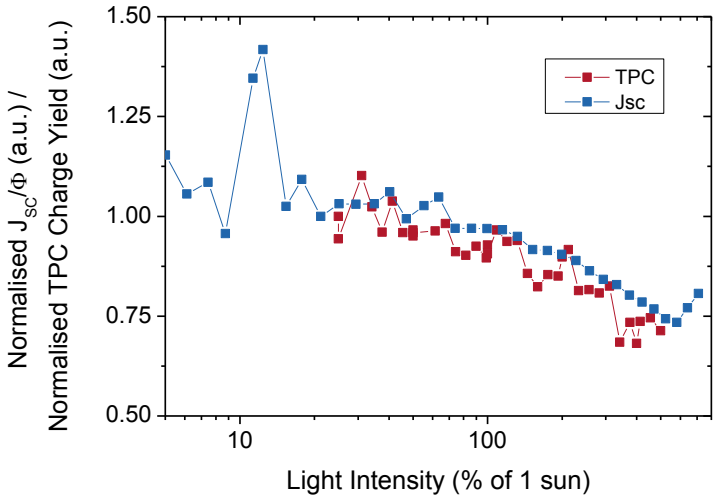

Figure 7.4. A comparison of the charge yield from transient photocurrent measurements under short circuit conditions (red) and the short circuit current density normalised to the incident light intensity (blue) of a P3HT:PCBM device both as a function of light intensity.

Figure 7.4 shows the number of charges extracted in these TPC experiments as a function of the background white light intensity. A clear reduction in the number of charges extracted can be seen, starting at light intensities around 70% of 1 sun. This data is plotted with the normalised J_{SC} data and it can be seen that the J_{SC} and TPC extracted charge are linked. We can thus conclude that these results qualitatively indicate that non-geminate recombination is limiting the J_{SC} of the P3HT:PCBM devices under high illumination intensities greater than 0.7-0.8 of 1 sun illumination. Alternatively, we assign the sub-linear dependence of J_{SC} upon light intensity to an increasing non-geminate recombination process.

7.2.3 Transient Measurements Of Non-Geminate Recombination

We can now analyse these non-geminate losses using transient techniques such as TPV and charge extraction which have successfully been used to evaluate non-geminate recombination processes under 1 sun illumination in chapters 5 and 6. Figure 7.5 shows the results of charge extraction experiments under applied bias at various illuminations. Note that the relationship between charge density and non-geminate recombination lifetime under open circuit conditions is similar to that shown in previous chapters.

From Figure 7.5a it is clear that the charge density under short circuit conditions is increasing with light intensity. As previously discussed non-geminate recombination varies non-linearly with charge density with a power >2, thus a relatively modest change in charge density, such as shown here between 1 sun and 3 suns, can results in a large increase in the magnitude of non-geminate losses. As performed in previous chapters we can now analyse this charge density data, along with the results of TPV experiments (not shown here) to calculate the magnitude of the non-geminate losses. Crucially this allows us to calculate the losses at all voltages and light intensities.

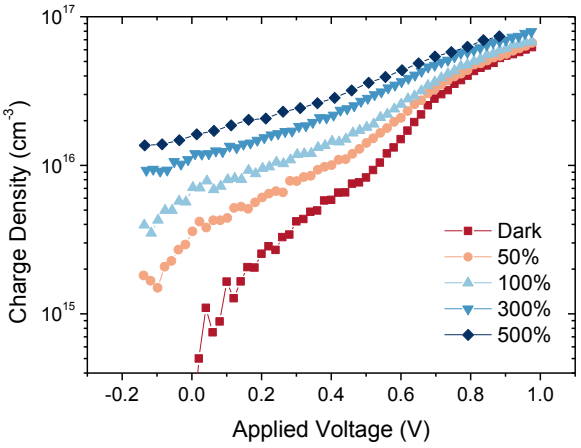

Figure 7.5. Extracted charge density as a function of applied bias for a P3HT:PCBM device under various illumination levels.

To perform the *J-V* reconstruction analysis we must have a value assigned to the generation current, J_{GEN}, from which the non-geminate loss currents are subtracted. In the case of a device where non-geminate recombination only occurs around the MPP we can use the assumption that $J_{SC} \approx J_{GEN}$. However in the device studied here, under higher light intensities, we have seen that this is no longer true due to non-geminate losses. One way to measure the J_{GEN} is assume that there are no voltage dependent geminate recombination effects, as shown by TAS studies on P3HT:PCBM blends,[70] thus as at open circuit all charge that is generated must recombine non-geminately, the generation current is equal to the non-geminate recombination current under open circuit conditions. The non-geminate loss current under open circuit, $J_{REC,OC}$, inferred from transient measurements, is plotted in Figure 7.6 along with the actual short circuit current density. This shows that the recombination current, our approximation for J_{GEN}, is linear with light intensity as expected, even where the J_{SC} becomes sub-linear. This validates the use of $J_{REC,OC}$ as J_{GEN} in our *J-V* reconstruction.

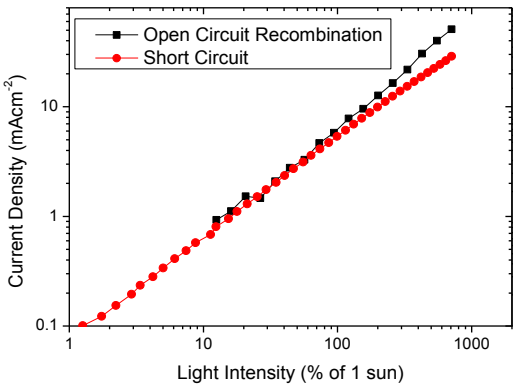

Figure 7.6. A comparison of the measured short circuit current density and calculated non-geminate recombination current density under open circuit as a function of light intensity of a P3HT:PCBM device.

Figure 7.7a shows the non-geminate recombination currents and Figure 7.7b shows the reconstructed normalised *J-V* curves inferred from the charge densities in Figure 7.5, and the generation currents in Figure 7.6. The reconstructed *J-V* curves are normalised to the most negative voltage available aiding comparison with Figure 7.3b. It is clear from these data that the reduction in fill-factor of the *J-V* curve of P3HT:PCBM devices at high light intensity is due to increased non-geminate recombination at low applied voltages and around short circuit.

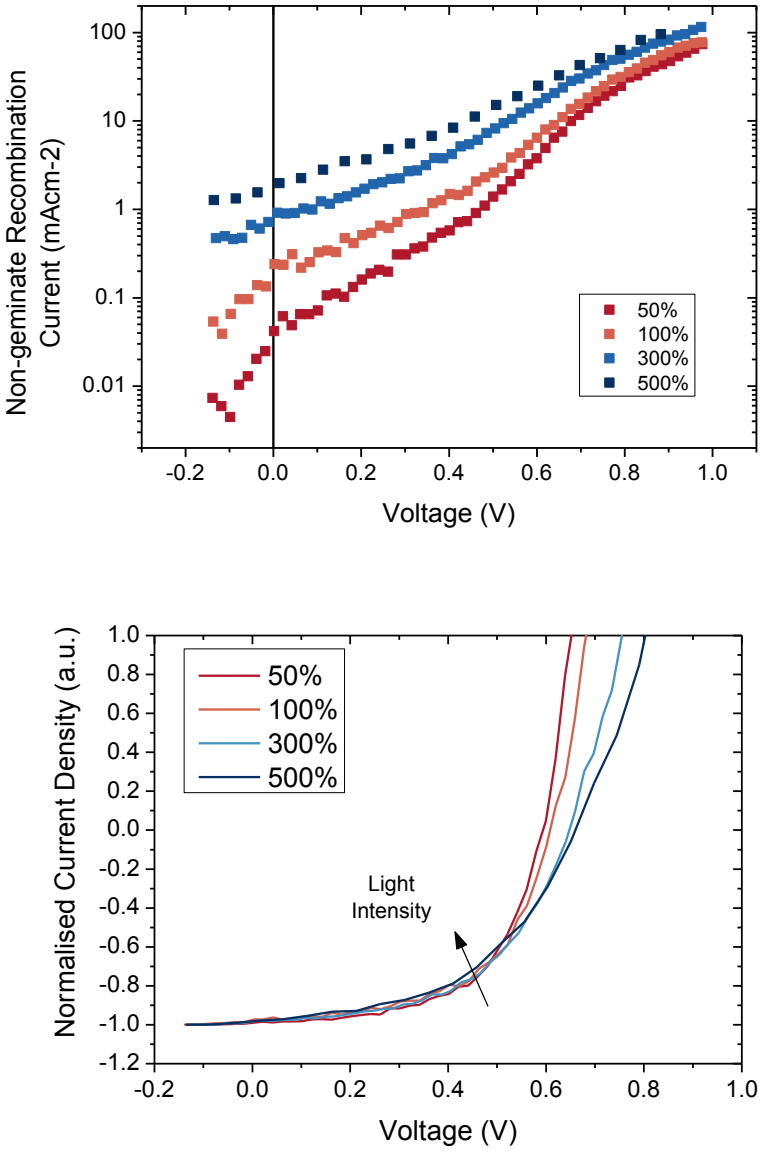

Figure 7.7. (a) Non-geminate recombination currents and (b) J-V curves reconstructed from measurements of charge density and recombination under various illumination levels, normalised values in reverse bias.

7.2.4 Fill-Factor Losses Under High Light Intensity

Another way of comparing the behaviour of the same device under different light intensities, is to analyse the ratio of charge generated and charge lost to non-geminate recombination. Figure 7.8 shows the ratio of recombination rate to generation rate as a function of voltage for various light intensities. It is clear from this figure that at increasing light intensities, whilst the ratio of recombination to generation at high voltages actually reduces, at lower voltages around short circuit it increases. The reduction at approximately open circuit voltages is consistent with the logarithmic increase in open-circuit voltage with light intensity, consistent with the diode equation. This behaviour additionally explains why the device *FF* reduces at high illumination intensity, and that is that non-geminate recombination affects the extracted current at increasingly low voltages. For example, at the voltage under which the recombination rate is 10% of the generation rate reduces from ~0.4V under 0.5 suns illumination, right down to ~0.2V under 5 suns. Essentially, whilst at low light intensity non-geminate recombination only dominates around the maximum power point, as the light intensity increases the recombination dominates lower and lower voltages, eventually significantly limiting the J_{SC}.

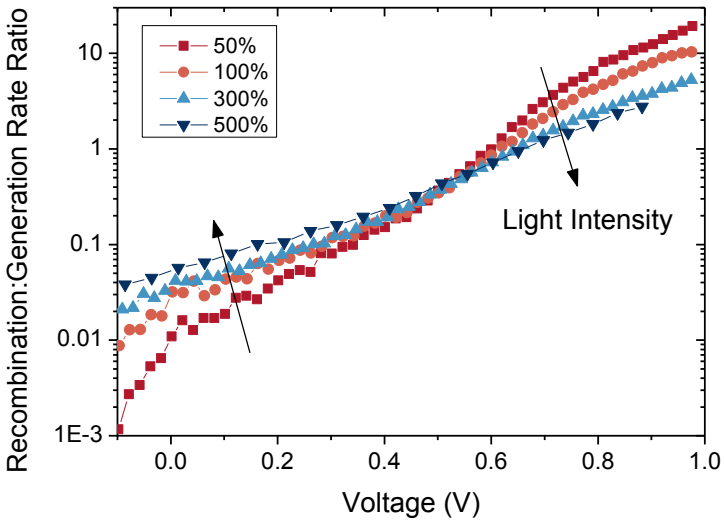

Figure 7.8. A plot of the ratio of generation and non-geminate recombination rates as a function of voltage for a P3HT:PCBM device under different illumination intensities.

This work corroborates that of Shuttle et. al. who used the same techniques to reconstruct the *J-V* curve of the P3HT:PCBM device up to light intensities of 1.4 suns,[49] although here we have specifically addressed the changing magnitude of non-geminate recombination under short circuit conditions and related that to the sub-linear behaviour of J_{SC}, and TPC currents, under high light intensities. Shuttle et. al. additionally reconstructed the *J-V* curves of P3HT devices up to 4 suns and found their *FF*s consistently underestimated the experimental *FF*. The data presented here also quantitatively underestimate the *FF* of the *J-V* curves, however the data qualitatively represent the trends in recombination current with light intensity allowing the processes that reduce the *FF* under high light intensities to be studied. It is believe that this

underestimation of the magnitude of non-geminate recombination current away from open circuit conditions is due to a spatial reorganisation of the charge density within the active layer of the device causing the recombination-charge density relationship to additionally be voltage dependent.[125]

In conclusion we have demonstrated that whilst under 1 sun conditions, a P3HT:PCBM device exhibits negligible non-geminate recombination under short circuit conditions, as the illumination intensity is increased the non-geminate recombination begins to limits the *FF* at increasingly lower voltages. The cell efficiency eventually undergoes a further limiting when, under sufficient illumination to generate enough free charge carriers, even at short circuit some charge undergo non-geminate recombination and the J_{SC} of the device is limited. Furthermore we find no evidence to suggest that voltage-dependent geminate recombination is significant in these devices, and even at high light intensities all aspects of the *J-V* behaviour in particular the *FF* can be accounted for entirely by non-geminate recombination.

7.2.5 Conclusions

To conclude we have shown that the behaviour of the *FF* of a P3HT:PCBM device under high light intensity is dominated by increasing non-geminate recombination. It was previously known that under 1 sun illumination the P3HT:PCBM *J-V* curve was relatively flat through short circuit where there was a very low non-geminate recombination flux, and began to be limited around the MPP. Additionally it was well known that the J_{SC} of such device became sub-linear at high light intensities. We have confirmed that this reduction in short circuit current density is due to increased non-geminate recombination at increasingly low voltages, closer to short circuit, as the illumination intensity is increased. We have also demonstrated that the yield of charges in a TPC experiment as a function of light bias is directly correlated to the J_{SC} and the non-geminate recombination losses. Finally we demonstrated that the *J-V* reconstruction method accurately reproduces the trends of the *FF* under high light intensity. We conclude that whilst the transport properties of P3HT:PCBM devices are sufficient to keep charge density low at 0V, and consequently non-geminate recombination low as well, under 1 sun illumination this is not true at higher light intensities. This leads to an increase in charge density at high illumination and a non-linear increase in the non-geminate recombination loss process.

7.3 RECOMBINATION IN APFO-3:PCBM DEVICES

7.3.1 Background

APFO-3 is a donor-acceptor polymer which was designed to have a high V_{OC} by designing a molecular structure with a deep LUMO energy relative to the commonly used acceptor $PC_{71}BM$.[147, 158-159] APFO-3 has been extensively studied in the literature as it exhibits good photovoltaic performance and relatively good hole mobilities.[158] However transient absorption studies of APFO-3:$PC_{71}BM$ blends indicate

that the yield of free charges is relatively low, concluding that the geminate recombination decay pathway is particularly strong in this material system.[21, 44] Additionally, the recombination dynamics, and the ratio of geminate to non-geminate recombination has been shown to be heavily dependent upon the morphological composition of the system.[54, 147]. Finally, and particularly relevant to these studies of device fill factor, some authors have concluded that device behaviour of APFO-3:$PC_{71}BM$ devices is dominated by a voltage-dependent geminate recombination process, using both transient optical techniques[66] and computational modelling techniques.[155]

As the device studied below shows, whilst the V_{OC} of APFO-3 devices is very high at almost 1V, the device efficiencies are only modest, limited primarily by J_{SC} and *FF*. Here we study an APFO-3:$PC_{71}BM$ device with an active layer 100nm thick. The structure of the device is Glass/ITO/PEDOT:PSS/APFO-3:$PC_{71}BM$/Ca/Al, fabricated by spin-coating the solution coated layers onto an ITO coated substrate and evaporating the metal contact.

7.3.2 Device Performance

Shown below in Figure 7.9 are light (50% and 100% of 1 sun illumination) and dark *J-V* curves for an APFO-3:$PC_{71}BM$ device with power conversion efficiency η=3.34%, J_{SC}=7.19mAcm^{-2}, V_{OC}=978mV and *FF*=47.6% under 1 sun illumination. Whilst the device does show a high V_{OC}, the *J-V* curve is sloped through short circuit. This indicates that firstly the J_{SC} is not as high as it possibly could be, as when a higher reverse bias is applied to the device a higher current density is measured, but also that this slope through short circuit is limiting the *FF* of the device. In the *J-V* curve in the dark at 0V, the curve has a very low gradient, thus we assume that under illumination shunts through the device can be neglected as a cause of the low *FF*. Similarly the devices exhibit a high gradient past V_{OC}, thus the series resistance would appear to be low in these devices. We can therefore conclude that the device is not limited by parasitic resistances but by the fundamental excited state processes. Were the device able to both generate and extract charges efficiently at short circuit, the device efficiency should be higher as both the J_{SC} and *FF* would be enhanced. It is therefore important that the loss processes causing this slope through short circuit are identified. Several authors have studied APFO-3:$PC_{71}BM$ devices and found their *J-V* curves to be dominated not by non-geminate recombination as in other polymer:fullerene devices described in this thesis and elsewhere, but by voltage-dependent charge generation.[66, 157]

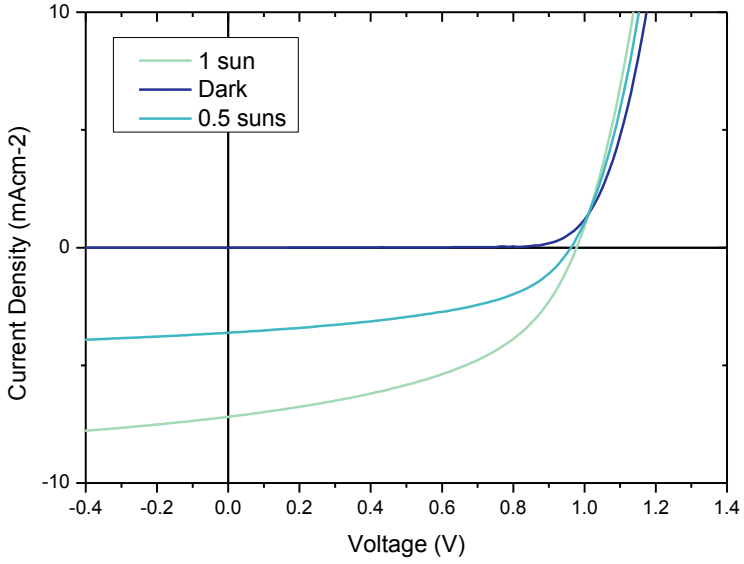

Figure 7.9. J-V curves of an APFO-3:$PC_{71}BM$ device in the dark and under 50% and 100% of 1 sun illumination.

Analysing first the light intensity dependence of the *J-V* parameters to determine if their behaviour is consistent with either loss mechanism; these are plotted in Figure 7.10. The J_{SC} varies linearly with light intensity over a large range of light intensities measured here, while this isn't a quantitative method for analysing non-geminate losses, a linear J_{SC} would tend to indicate that there are no light intensity, or charge density, dependent loss mechanisms limiting the J_{SC} that are conventionally assigned to non-geminate recombination. Additionally it can be seen that the V_{OC} varies logarithmically with light intensity, with an ideality factor in the light of 0.97. As discussed previously in chapter 2, an ideality factor close to 1 indicates a device operating with little recombination through trap states.[101]

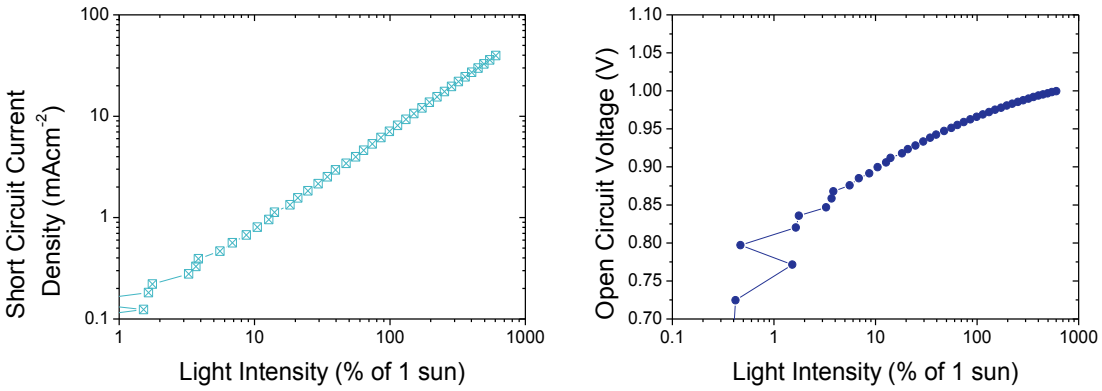

Figure 7.10. Plots of short circuit current density (a) and open circuit voltage (b) of an APFO-3:$PC_{71}BM$ device against white light illumination intensity, as a percentage of 1 sun illumination.

7.3.3 Transient Measurements

Figure 7.11 shows the non-geminate recombination lifetime (τ) plotted against the average charge density within the device under open circuit conditions. The magnitude of the results of the charge extraction experiments indicates that there is very low charge density within the APFO-3 device, among the lowest measured using this technique. This can be seen when compared to other τ vs. n plotted for various material systems by Credgington et. al.[50] which shows every system in the study exhibits higher charge densities than APFO-3:$PC_{71}BM$. These results of charge extraction measurements have been corrected to remove charge accumulated on the electrodes and for charges lost to recombination during the extraction experiment. In addition, when plotting the non-geminate recombination rate against the charge density, it is observed that there is a very strong dependence of the recombination rate upon the charge present within the device, so steep in fact that a doubling of the charge density can result in an order of magnitude reduction in the charge recombination lifetime. This shows the device cannot support high densities of charges and is therefore very sensitive to the accumulation of charge density within the device.

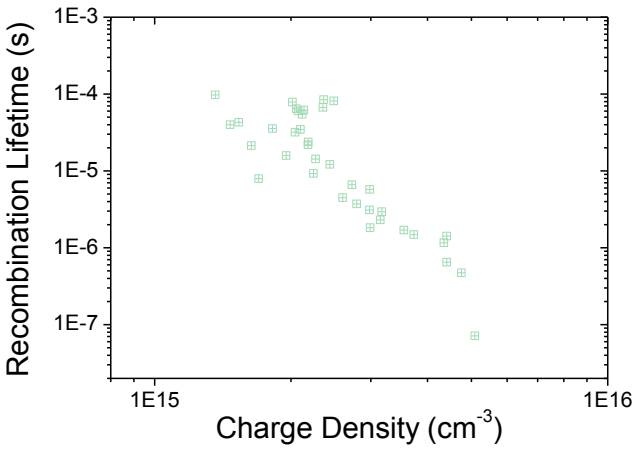

Figure 7.11. A plot of the non-geminate recombination lifetime against the average charge density within an APFO-3:$PC_{71}BM$ device, under open circuit conditions and various light intensities.

Whilst charge extraction experiments under open circuit measure an equilibrium charge density that results in an exactly balanced charge generation and recombination, and can be affected by many processes, what is essentially measured is how the density of disordered energy states fills with increasing charge density.[61] This is because OPV devices operate in the trap-limited regime in which the majority of charges are thermalised into low energy trap states below a mobility edge.[62, 160-161] The charge density as a function of light intensity measures the sum of both the electron and hole distributions of trap states. Thus as Figure 7.11 shows a charge density that depends very steeply upon the light intensity, this could be interpreted such that the density of trap states is very steep away from the band-edge.

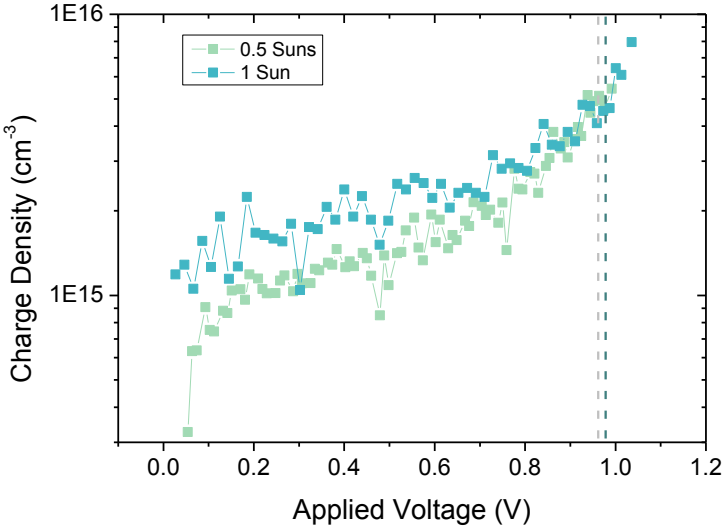

Figure 7.12. Average charge density under applied bias under 0.5 and 1 sun illumination.

7.3.4 Non-Geminate Recombination And *J-V* Behaviour

Figure 7.12 shows the charge density measured using charge extraction under applied bias, under 1 sun illumination at voltages across the power generating quadrant of the device. The charge density under applied bias is very low in comparison to other systems measured in the past and in the literature (see later sections of this chapter).[50, 94, 97] These charge densities have been corrected for both loss of charges due to recombination during the extraction and capacitative charges on the electrodes which do not contribute to recombination, and the voltages under which they have been measured have been corrected for the drop in voltage due to series resistance. These low charge densities suggest that the morphology and mobility of the blend make collection of charge from the active layer very efficient. From the charge extraction data under applied bias and the relationship between τ and n it is possible to calculate a non-geminate recombination current density at all voltages. The non-geminate recombination current within the APFO-3:$PC_{71}BM$ device is shown in Figure 7.13. Analysing the data here, it can be seen that the non-geminate recombination flux is very low, particularly at low applied voltages up to ~0.6V. At approximately 0.6V the non-geminate recombination current density increases rapidly to equal the approximate generation flux around open circuit (indicated by a dash vertical line). This is due to the very steep dependence of recombination rate upon charge density, as soon as any charge builds up in the active layer of the device a very rapid increase in the non-geminate recombination flux results.

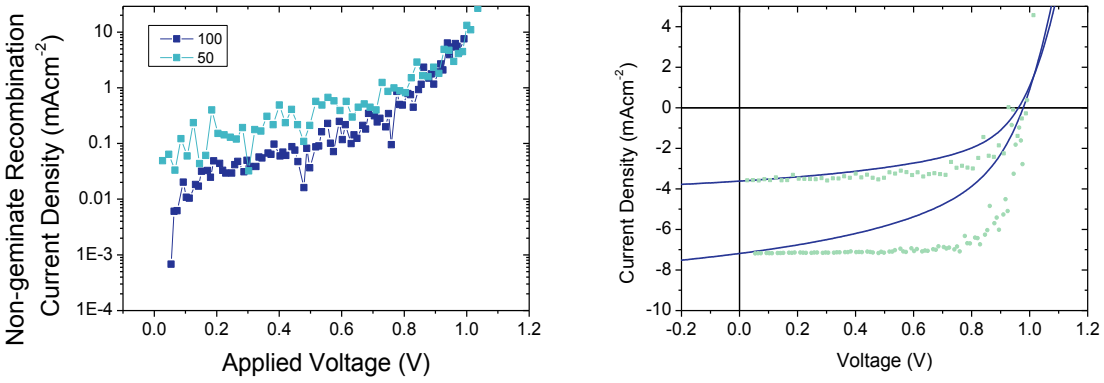

Figure 7.13. (a) a plot of the non-geminate recombination current density across the power generation quadrant and under 0.5 and 1 suns illuminations, and (b) J-V curve reconstructions under the same light intensities compared to the experimental J-V curves.

If we approximate the charge generation current density to be voltage independent and equal to the short circuit current density we can "reconstruct" the *J-V* curve. This is shown in Figure 7.13. Evidently the non-geminate recombination flux does not accurately approximate the device *J-V* behaviour, and the fill factor is greatly over-estimated. This is because the slope in the *J-V* curve through short circuit is evidently not due to non-geminate recombination, and this accounts for the loss in *FF*.

7.3.5 Field Dependent Charge Generation

Another explanation for the low *FF* of the device must be found, and the possibility of field-dependent charge generation, assigned to field-dependent geminate recombination, must be considered. As all the transient electrical experimental methods rely on free charges communicating with the electrodes or being collected it is not possible to probe the excitonic state directly and difficult to measure any mechanism prior to exciton or charge transfer separation. However if Figure 7.13 implies that a voltage dependent generation term must be included we can approximate J_{GEN} as $J_{GEN}(V) = J(V) - J_{NGR}(n, V)$, subtracting the inferred non-geminate recombination loss current density from the experimentally measured *J-V* curve. This quantity measures the generation current density required for the reconstruction to match perfectly, or alternatively the "missing" recombination from the non-geminate analysis. This is plotted in Figure 7.14 against bias voltage and shows an approximately 50% drop in the number of charges generated between short circuit and 1V.

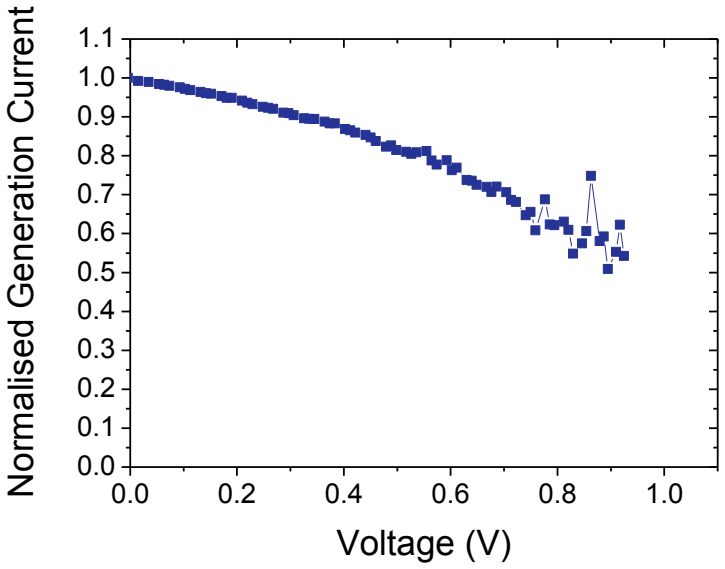

Figure 7.14. A plot of the generation current calculated by subtracting the non-geminate loss current from the experimentally obtained current density.

Another technique that can be used to study charge recombination processes is transient absorption spectroscopy (TAS). This is an optical pump-probe technique in which the behaviour of various excited states can be studied optically in response to a pulse of light, in this context it is particularly useful for studying the populations of charge carriers generated immediately after optical generation.[83] In addition to the optical probes, the device being studied can be electronically biased allowing investigation of charge processes under various operating conditions.

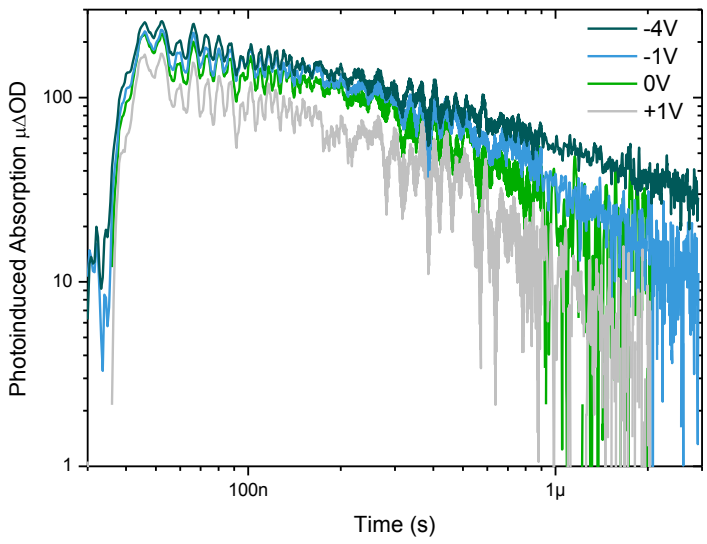

Figure 7.15. TAS decay kinetics of an APFO-3:$PC_{71}BM$ device as a function of four different applied biases (+1 V, 0 V, -1 V and -4 V). This data was collected in collaboration with Dr. Fiona Jamieson.

Figure 7.15 shows TAS traces for the APFO-3:$PC_{71}BM$ device under different biases between -4V and +1V. These transients were measured by exciting the device at 520nm and probing the polymer positive polaron absorption band at 980nm. These traces indicate both changes the amplitude of the TAS signal, corresponding to a change in charge population, as well as differences in the kinetics, which would be consistent with a changing rate of decay. Similar TAS studies on other polymer:fullerene material systems such as P3HT: and PCPDTBT:$PC_{71}BM$ show that externally applied voltage has no impact upon either the amplitude of the signal or the rate at which it decays.[68, 70]

These results indicate significant changes in device behaviour, particularly the yield of free charges, under bias. This has previously been observed directly with TAS in small molecule:fullerene solar cells,[83] and using similar transient techniques in polymer:polymer blend solar cells. Several authors have studied the charge generation mechanism in APFO-3:$PC_{71}BM$ devices and concluded that the process is field dependent, and this result is consistent with this work.

If we examine the magnitude of the signal as function of voltage as shown in Figure 7.16 we can quantify this change in the yield of free charges. As the decays of charges correspond to the recombination of non-geminate recombination we can assume that some of the changes in signal magnitude are due to non-geminate recombination reducing the polaron population, however on early time scales (<100ns) the transients in Figure 7.15 can be seen to plateau. Thus we can take the voltage dependence of the signal on the earliest possible reliable timescale to be approximate to the voltage dependence of free charge generation. This signal analysis is complicated slightly by the presence of triplets present in the APFO-3 with a similar absorption band to the polaron, thus some spectral overlap is likely, however as triplet excitons are neutral their decay is not expected to be altered by electric fields and to come extent we can remove this component from the calculations. Finally as the reduction in signal magnitude changes with time, we must normalise out the signals and average the reduction in charge population over a range of early timescales. When this averaging is performed between times of 30ns and 100ns we obtain a reliable measure of the voltage dependence of charge generation in the APFO-3:$PC_{71}BM$ device, this is shown in Figure 7.16. Looking at the same voltage range as for the J_{GEN} data shown above, we observe a reduction of ~45% in charge generation between 0V and 1V; this corresponds well to the "missing" charge reduction from the non-geminate recombination analysis.

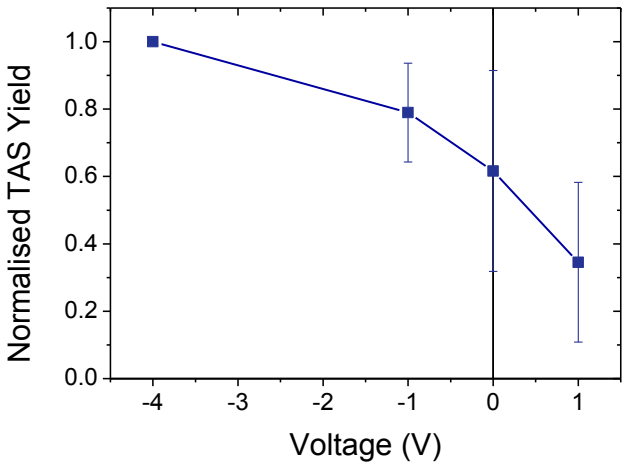

Figure 7.16. A plot of normalised TAS yield on early timescales under applied bias, indicating a significant voltage-dependence of charge generation.

7.3.6 *J-V* Reconstruction with Geminate And Non-Geminate Recombination

If for the simplicity of analysis we assume that between 0 and 1V the charge generation is linearly dependent upon voltage, and we can incorporate this measure of geminate recombination into our non-geminate analyses by simply replacing the voltage-independent charge generation current density with a linear decreasing function with the corresponding gradient to approximate the voltage dependence of charge generation measured by TAS. This is shown on Figure 7.17 where the dashed line is the new charge generation current density. The combination of voltage dependent geminate and non-geminate recombination now approximate the *J-V* considerably better than the non-geminate alone. Notably the reconstructed *J-V* curve at short circuit now closely approximates the slope through 0V and the corresponding loss in fill factor. The actual *FF* of the APFO-3 device measured here was 48%; this can be compared to the predicted value without voltage-dependent generation of 79% and the value of the reconstruction in Figure 7.17 taking in account the voltage dependence of charge generation of 58%.

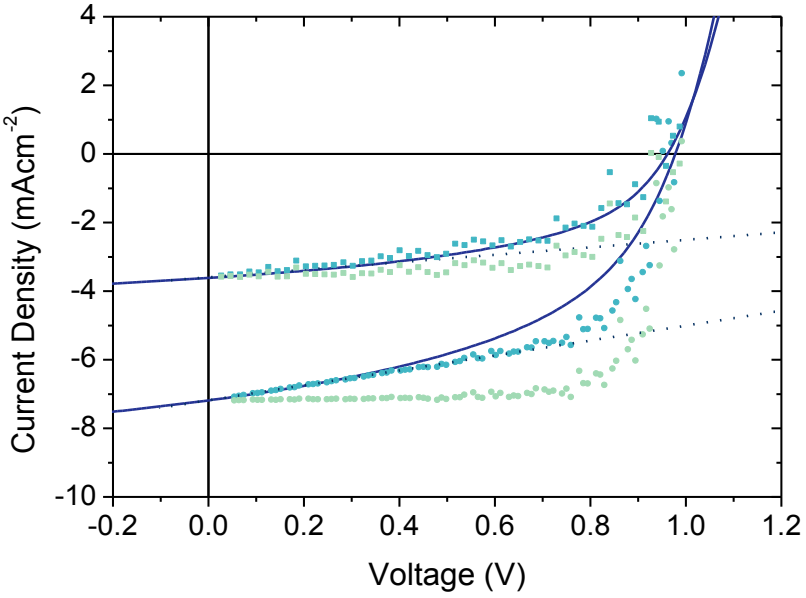

Figure 7.17. J-V curve reconstructions from measurements of non-geminate recombination with and without a voltage-dependent charge generation, compared to experimental J-V curves.

The combination of all this evidence allows us to determine which mechanisms are lowering the *FF* of APFO-3:$PC_{71}BM$ devices. It is clear from the highly linear J_{SC} with light intensity and the extremely low non-geminate recombination fluxes calculated at low voltages that non-geminate recombination cannot be responsible for the current losses in this region of the *J-V* curve. In contrast the population of charges measured on early timescales using transient absorption spectroscopy shows a large voltage dependence of the free charge generation. In the power generating quadrant of the solar cell this voltage dependence matches the voltage dependence measured by subtracting a non-geminate recombination current from the experimental extracted current. This indicates that the generation of free charges is dependent upon the electric field within the device; we conclude that in this device excitons reaching the interface form a charge transfer state that requires a certain degree of electric field to separate into free charges. Thus a reduction in the electric field in the device due to a reduction in voltage across the active layer will result in the separation of fewer charges, the charge transfer states that aren't separated will undergo geminate recombination, and thus this process can also be described as a voltage-dependent geminate recombination process.

We also note that the *J-V* reconstruction accurately predicts the open circuit voltage of the device whether the non-geminate recombination current is subtracted from a voltage-dependent or –independent generation profile. This is not general to cells in which field-dependent geminate recombination impacts the *FF*; recent results with a small molecule:fullerene blend shows in that case that geminate recombination additionally reduces the V_{OC}.[83] This indicates that in APFO-3:$PC_{71}BM$ devices the open circuit is fundamentally still limited by non-geminate recombination even though the *FF* is limited by geminate

recombination. This is due to the extremely steep relationship between charge density and non-geminate recombination rate, as shown in Figure 7.11; as soon as the bias reduces enough such that any charge accumulates in the active layer, the non-geminate recombination rapidly increases, Figure 7.12 shows that whilst between 0.8 and 1V the charge density increases by just under one order of magnitude, the number of charges lost to non-geminate recombination via J_{REC} increases by almost 100 times. In the case of the small molecule:PCBM devices, the geminate and non-geminate losses are of comparable magnitude close to open-circuit, as the non-geminate recombination increases so quickly in these APFO-3:$PC_{71}BM$ devices, the non-geminate dominates around V_{OC}.

To conclude, this shows that the *J-V* behaviour of APFO-3 devices is determined by both a voltage-dependent geminate recombination limiting free charge generation, and by a subsequent non-geminate recombination, yet across the *J-V* curve the ratio of these recombination losses changes. The behaviour around short circuit conditions is primarily determined by the geminate recombination process as the free charge density is so low that almost no geminate recombination is occurring. Whereas under open circuit conditions, the number of free charges being generated is being severely limited by geminate recombination, yet the V_{OC} value is determined by non-geminate recombination losses. We have shown that in these devices the primary cause of the low *FF*s is the voltage dependent geminate recombination process.

7.4 COMPARISON OF RECOMBINATION IN DIFFERENT MATERIAL SYSTEMS

From the results shown above it is quite clear that the *FF* behaviour of P3HT devices and APFO-3 devices is determined by quite different mechanisms, namely non-geminate and geminate recombination respectively. We can additionally compare these devices to those fabricated from a blend of PCPDTBT:$PC_{71}BM$ with the solvent additive ODT. Like the P3HT:PCBM device under high light intensity, these devices have been shown using TAS studies to exhibit voltage-independent charge generation[68] and the short circuit current under 1 sun illumination is limited by non-geminate recombination. However, this has recently been countered by the results of the Neher group which show that cells fabricated with the same blend materials actually have a voltage-dependent charge generation mechanism.[69, 84] We can thus compare the *J-V* behaviour of 4 devices; P3HT:PCBM under 1 and 5 suns illumination, APFO-3:$PC_{71}BM$ and PCPDTBT:$PC_{71}BM$+ODT, to attempt to draw some generalisations about device behaviour. As can be seen in Figure 7.18, the PCPDTBT device is the only one whose JSC becomes sub-linear around 1 sun light intensity, where as the other two devices stay relatively linear.

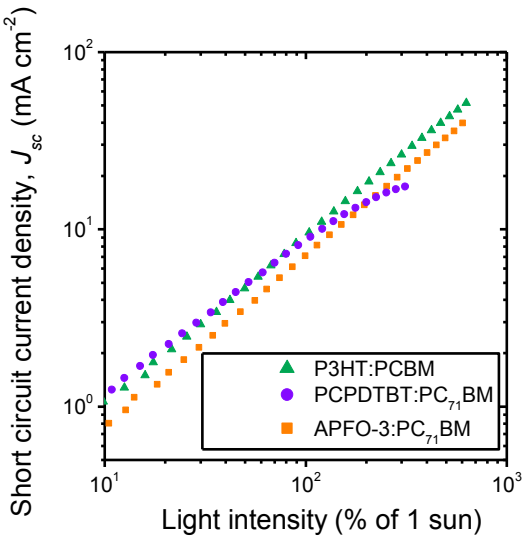

Figure 7.18. A comparison of the behaviour of short circuit current density as a function of light intensity in P3HT, PCPDTBT and APFO-3 devices.

Firstly, we must analyse the general non-geminate recombination dynamics under open circuit and over a wide range of light intensities. Figure 7.19 shows recombination dynamics under open circuit and it is clear that in the different devices there is a wide range of behaviour. Whilst the slope with regards to charge density is most likely related to the density of trap states in the material, it has been shown that the absolute magnitude of the recombination lifetime can be related to the morphology of the blend.[162] It is clear that APFO-3 can support the least charge within the active layer without incurring heavy non-geminate recombination losses and P3HT:PCBM is the better tau vs. n relationship as it can support much higher steady-state charge densities. This may seem counter-intuitive as under 1 sun illumination APFO-3 has very low recombination fluxes whereas P3HT has much higher, however this is due to how much charge is present in the device and how efficiently the charges are collected.

Figure 7.21 shows the non-geminate recombination losses as a function of bias under 1sun intensity for all blends and under 5 suns for P3HT:PCBM. Additionally VOC values are indicated by vertical dashed lines for each device. This shows the huge variation in non-geminate recombination behaviour in the different devices. Where PCPDTBT is evidently heavily limited by non-geminate recombination at all biases, APFO-3 has extremely low non-geminate recombination losses for voltages between short circuit and ~0.6V.

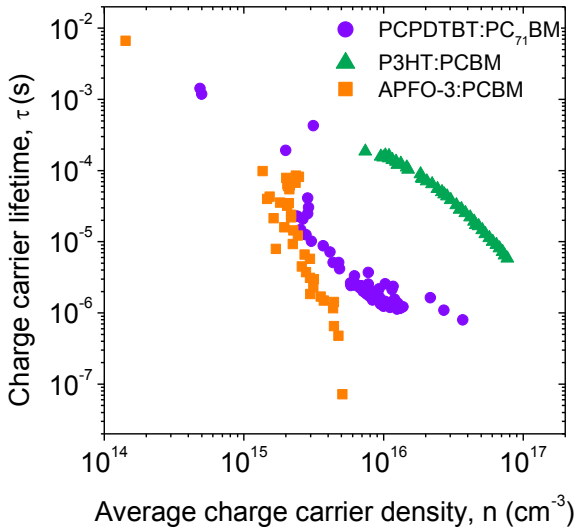

Figure 7.19. A plot of non-geminate recombination lifetime against average charge density for P3HT:, APFO-3: and PCPDTBT:$PC_{71}BM$ devices under open circuit conditions, indicating differences in non-geminate recombination dynamics between different material systems.

Additionally note that from Figure 7.19 PCPDTBT and APFO-3 devices have quite similar recombination dynamics, thus almost the entire difference in recombination loss current is not due to differing relationships between charge density and recombination but to differences in the magnitude of charge density within the device. As the steady state charge density present within the device is an equilibrium between generation, non-geminate recombination and collection, and the generation and non-geminate recombination are similar, the difference in charge density between PCPDTBT and APFO-3 devices implies that the charge collection must be considerably better in APFO-3. Presumably, although there is little in the literature to suggest that PCPDTBT exhibits poor charge mobilities, either the blends ability to transport charge, or some morphological phenomenon, means that PCPDTBT devices have issues with sweep-out of charges. Figure 7.20 shows transient photocurrent transients measured in both the APFO-3 and PCPDTBT devices at short circuit conditions and under 1 sun illumination. The transients show the speed with which a small number of charges photoexcited in the device by a laser pulse are extracted by the built-in field present at short circuit. These normalised transients indicate that the charges are swept out of the device much quicker in the APFO-3 system, supporting the conclusion that slower collection of charges in PCPDTBT results in a higher charge density and therefore a considerably higher non-geminate recombination loss current.

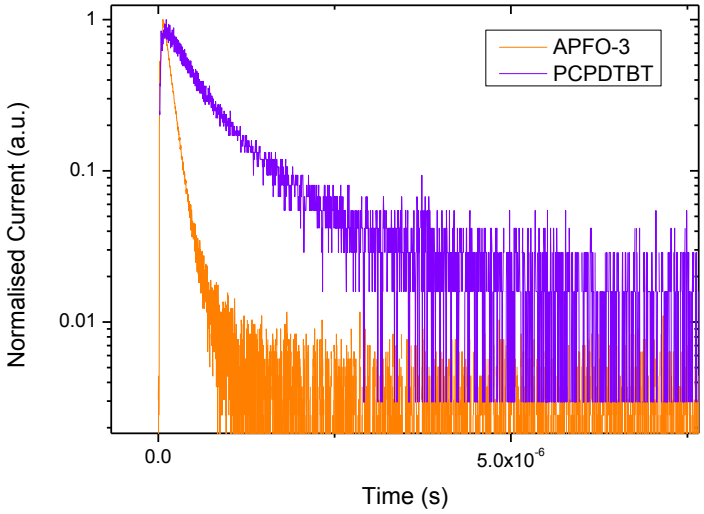

Figure 7.20. A comparison of short circuit TPC current transients for APFO-3 and PCPDTBT devices under 1 sun illumination indicating slower charge extraction in the case of PCPDTBT.

Note in Figure 7.21 the huge changes in the magnitude of non-geminate recombination current between 1 sun and 5 suns in the P3HT:PCBM device. Around open circuit conditions the recombination fluxes are quite similar, differing obviously by a factor of 5 between the respective V_{OC}s. However, as has been shown above, non-geminate recombination around short circuit increases substantially once the device is taken past 1 sun illumination, this is clearly demonstrated by an increase of over 10 times in the loss current.

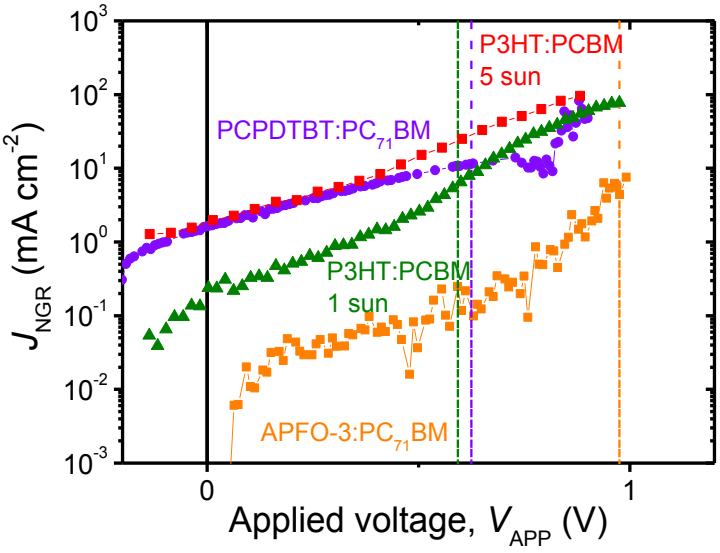

Figure 7.21. A comparison of the non-geminate recombination current densities under 1 sun illumination in P3HT, APFO-3 and PCPDTBT devices and under 5 suns illumination for the P3HT device.

Figure 7.22 shows two different assays of charge generation rates; (a) shows the yield of polarons measured by transient absorption spectroscopy on early time scales, these yields are measured over a range of voltages, from reverse bias to +1V and are normalised to the most negative voltage value. Values for P3HT:PCBM devices is not shown here, however it has been shown to be voltage independent.[70] Whilst charge generation is generally considered to be a fast process, perhaps on the order of picoseconds, non-geminate recombination is expected to occur on a much later timescale. It is not entirely clear how quickly non-geminate recombination acts to reduce charge populations, however the presence of an apparent plateau in the TAS traces shown in Figure 7.15 at 100ns would indicate that at this time non-geminate recombination has not significantly reduced the charge densities and the charge density we measure is still close to that initially photogenerated. The second measurement shown in (b) is generation current measured by subtracting the measured non-geminate recombination current from the experimentally measured *J-V* curves, these are measured through the operating quadrant and are normalised to the value at short circuit conditions. Both of these measurement techniques indicate that whilst charge generation in P3HT:PCBM devices is independent of applied electric field, the charge generation in APFO-3:$PC_{71}BM$ devices certainly is. PCPDTBT appears to be either voltage independent, or to have a very small dependence upon voltage.

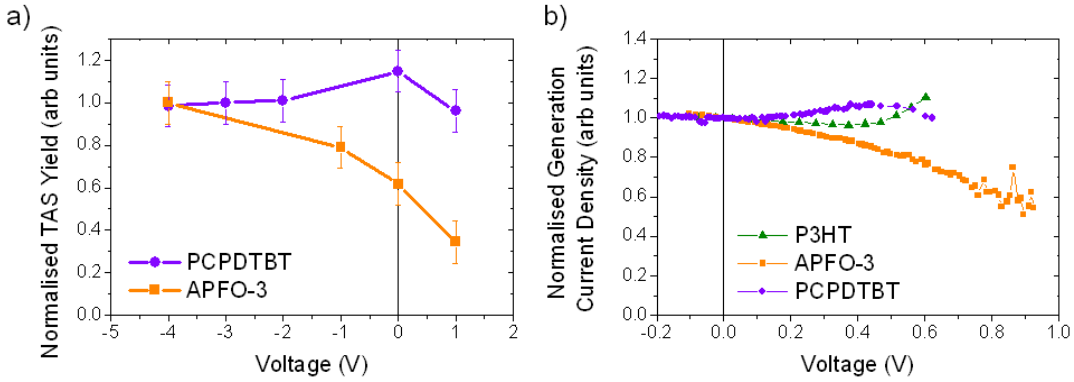

Figure 7.22. A comparison of the voltage dependence of charge generation in PCPDTBT and APFO-3 devices using two experimental techniques. (a) TAS yields and (b) the subtraction of non-geminate currents from experimental J-V curves.

Currently it is unclear why charge generation may be voltage dependent in some material systems and not in others. This is in part due to ongoing discussion of the actually mechanism by which charge generation or exciton splitting occurs, particularly with respect to the charge transfer state. Whilst some authors believe that charge generation occurs via a charge transfer state where a bound charge species exists across the donor:acceptor interface,[163] this is commonly expected to be an energetic trap thus it is unclear how high internal quantum yields are possible.[79] Other authors believe an energetically hot exciton state can separate at an interface without falling into the trap of a charge transfer state.[76, 78] Furthermore there are no techniques that can observe the actual morphology of the materials donor:acceptor interface, meaning there is some uncertainty about whether charge separation occurs in a mixed phase or at a clear interface.

It is known that P3HT:PCBM and PCPDTBT:$PC_{71}BM$+ODT material systems form well defined domains and that both polymers are relatively crystalline compared to other conjugated polymers, whereas APFO-3 is a relatively amorphous polymer. This is shown by Figure 7.23 which compares the x-ray diffraction spectra of P3HT and APFO-3 showing an almost featureless spectrum for APFO-3. Additionally, voltage-dependent geminate recombination losses have been observed in a small molecule:PCBM blend which also exhibited low crystallinity.[83] Both modelling and experimental studies of the effect of crystallinity on charge separation at a polymer:fullerene interface indicate that larger and purer crystalline domains may aid in the formation of more extended charge transfer states. Additionally models of energetic disorder have shown that a crystalline polymer will be more disordered at an interface, forcing it to have a larger band-gap, this would provide an energetic driving force away from the interface for charges, but only in crystalline polymers as this effect wouldn't be present in amorphous materials. Both these phenomena would cause any charge transfer states formed to be more spatially extended and delocalised, thus separation may be efficient without an electric field, but importantly only in crystalline polymers. If at an amorphous polymer:fullerene interface there is no energetic driving force away from the interface and the states are highly localised at the interface these would be strongly bound and may only be separated with the aid of an electric field.

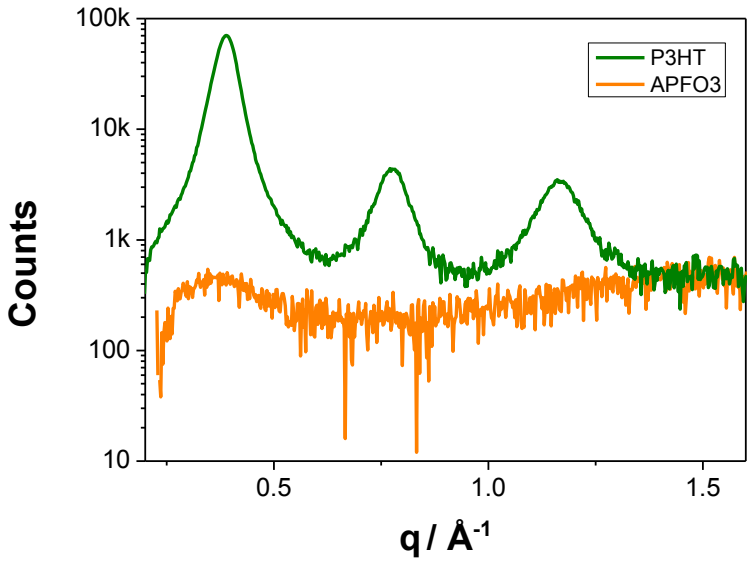

Figure 7.23. X-ray diffraction spectra for P3HT:PCBM and APFO-3:$PC_{71}BM$ films indicating differences in crystallinity between different material systems. This data was collected by, and is shown courtesy of, Yvonne Soon.

7.5 CONCLUSIONS

We have shown that two distinct charge recombination loss mechanisms, geminate and non-geminate recombination, have the potential to reduce the fill-factor of organic solar cells. Additionally we

have shown how these two processes can be experimentally discerned and analysed. Using these methods, results have been presented showing that APFO-3:$PC_{71}BM$ solar cells exhibit a low fill-factor because these devices show an electric field dependent separation of charges, or a voltage-dependent geminate recombination process. This significantly reduces the fill-factor of these devices, although the open-circuit voltage is still determined by non-geminate recombination.

Furthermore we have shown that whilst P3HT:PCBM devices under 1 sun illumination are only affected by non-geminate recombination around the maximum power point, under higher illumination intensities the charge density within the device accumulates, incurring non-geminate losses at lower and lower voltages, reducing the *FF* of the *J-V* curve. In fact, in the devices studied here under sufficiently high illuminations the non-geminate recombination limits the short circuit current density of the device. This is observed as a non-linear J_{SC} at high light intensity, along with a reduction in charge extracted using the TPC method. Whilst the fill-factors in these devices were as low as in the APFO-3 device, there was no evidence of voltage-dependent geminate losses and the device performance under high illumination is still consistent with the device characteristics being dominated by non-geminate recombination.

7.6 EXPERIMENTAL METHODS

APFO-3:$PC_{71}BM$ devices were fabricated by spin-coating blends in the architecture glass/ITO/PEDOT:PSS/APFO-3:$PC_{71}BM$/Ca/Al. P3HT:PCBM devices were fabricated as described previously, in the architecture glass/ITO/PEDOT:PSS/P3HT:PCBM/Al and were annealed at 140°C. PCPDTBT:$PC_{71}BM$ + ODT devices were fabricated by Konarka, as previously reported, by spin-coating the polymer:fullerene active layer in the configuration glass/ITO/ PEDOT:PSS/PCPDTBT:$PC_{71}BM$ + ODT/LiF/Al. The active layer thicknesses for both the PCPDTBT and P3HT devices tested were approximately 150nm, and the active layer thickness of the APFO-3 devices was 95 nm.

For transient photovoltage and charge extraction experiments, white light illumination was provided by 12 LEDs, with the brightness calibrated such that the J_{SC} under LED illumination was the same as that under simulated AM1.5 illumination. In the TPV experiments, pulsed excitation used a nitrogen-dye-pumped laser (PTI), with a fixed wavelength pump source. The excitation wavelength used was 620 nm for the P3HT and APFO-3 cells and 650 nm for the PCPDTBT cells.

Transient absorption spectroscopy experiments upon APFO-3:$PC_{71}BM$ devices was performed employing an excitation at 520 nm with pulse fluence of 3 μJcm^{-2} and probing at 980 nm, shown previously to monitor APFO-3 polaron absorption.

Transient absorption spectroscopy data in on APFO-3 devices was performed in collaboration with Dr. Fiona Jamieson, furthermore data on PCPDTBT:$PC_{71}BM$ devices was collected by Dr. Andrea Maurano. Finally X-ray diffraction data on P3HT and APFO-3 were kindly provided by Yvonne Soon.

CHAPTER VIII

THE INFLUENCE OF SPACE CHARGE AND DOPING ON CHARGE COLLECTION AND RECOMBINATION IN ORGANIC SOLAR CELLS

8.1 INTRODUCTION

8.1.1 Electric Fields In Organic Solar Cells

Charge carrier mobilities in organic solar cells are orders of magnitude lower than those in other inorganic photovoltaic technologies, this impacts the extraction and collection of charges and in some cases limits the photovoltaic performance. It has previously been shown that low charge mobilities can consequently limit both the J_{SC} and *FF* of organic solar cells.[98, 139, 150, 153, 164-166] Low charge mobilities, in addition to low diffusion coefficients, mean that diffusion alone is too slow a mechanism to be relied upon for efficient charge collection and thus drift transport is particularly important in OPV. In fact, as shown in the previous chapters, non-geminate recombination is the limiting process in many organic solar cells,[49] and this is only reduced around short circuit by stronger drift currents driving charges to the electrodes more efficiently. One consequence of this reliance on drift transport is that organic solar cells are typically thin compared to their inorganic counterparts, on the order of hundreds of nanometres compared to micron thick silicon cells. This means that both the electric field driving charges from the device is enhanced, and

additionally it reduces the distance charges must travel to be collected. This is particularly important when non-geminate recombination is strong and charge transport is inefficient.[51]

Whilst organic solar cells are generally not intentionally electronically doped, several studies have shown significant unintentional doping of the active layer in some OPV devices.[40, 102, 150, 167-169] This doping is typically p-doping, or an excess of positive charges. The presence of charged dopants can affect the electric field distribution within the solar cell, and as the spatial distribution of the electric field is particularly important in organic solar cells for drift transport and charge collection, this could affect the performance of the device. Electronic doping has been shown by several groups to detrimentally affect the performance of OPV devices, although sometimes a conduction improvement has been observed.[150, 170-178] Many recent analyses of device performance have neglected the impact of doping upon charge carrier dynamics.[101, 179-180]

The electric field within the active layer of an OPV device is commonly simulated using a metal-insulator-metal model, where charge on the electrodes generates a relatively spatially uniform electric field. However the presence of an imbalance in the number of electrons and holes can create a non-uniform electric field through the formation of a depletion region. This excess of one carrier, or space-charge, can be caused by electronic or chemical doping[150, 170] or unequal charge carrier mobilities.[103] For sufficiently high levels of space charge, in sufficiently thick devices, the active layer thickness exceeds the width of the resulting depletion region leaving a neutral region with low electric field which carriers must diffuse through. The depletion region thickness, w, can be expressed as

$$w = \sqrt{\frac{2\epsilon_r\epsilon_0(V_{BI} - V)}{qN_A}} \qquad (8\text{-}1)$$

where V_{BI} is the built in field between the electrodes, N_A is the doping concentration, q is the elementary charge and ε_r and ε_0 are the dielectric permittivities of the semiconducting medium and the vacuum respectively.

Here we investigate the effects of electronic doping of the active layer of OPV devices, the spatial non-uniformity of the electric field that results and the changes in device performance as a consequence.

8.2 PBDTTBTZT:$PC_{71}BM$ DEVICE PERFORMANCE

In this chapter we compare devices made from a low band gap conjugated polymer poly[2,6[4,8-bis(2-ethyl-hexyl)benzo [1,2-b;4,5-b']dithiophene-co-2,5-thiophene-co-4,7[5,6-bis-octyloxy-benzo [1,2,5]thiadiazole]-co-2,5-thiophene] (PBDTTBTZT), whose structure is shown in Figure 8.1, blended with [6,6]-phenyl-C_{71}-butyric acid methyl ester ($PC_{71}BM$).

8.2.1 Device Architecture

Almost all organic solar cells are constructed by sandwiching a photovoltaic medium (typically an intermixed polymer:fullerene blend) between two electrodes, one transparent to allow light to enter the device, and the other metallic which ideally acts to reflect unabsorbed photons back into the active layer. In the "standard" OPV device architecture the transparent electrode (usually indium tin oxide or ITO) acts as the anode, collecting holes, whilst the metal back-contact acts as the cathode, collecting electrons. In the inverted device architecture the roles of the transparent and metal contacts are reversed, such that the transparent electrode now acts as a cathode collecting electrons.

The devices studied in this chapter are made by blade coating the active layer blend of PBDTTBTZT:$PC_{71}BM$ from solution in the following configurations. The standard architecture devices have the layer structure (ITO/PEDOT:PSS/PBDTTBTZT:$PC_{71}BM$/Ca/Al) and the inverted devices have the structure (ITO/ZnO/PBDTTBTZT:$PC_{71}BM$/PEDOT:PSS/Ag).

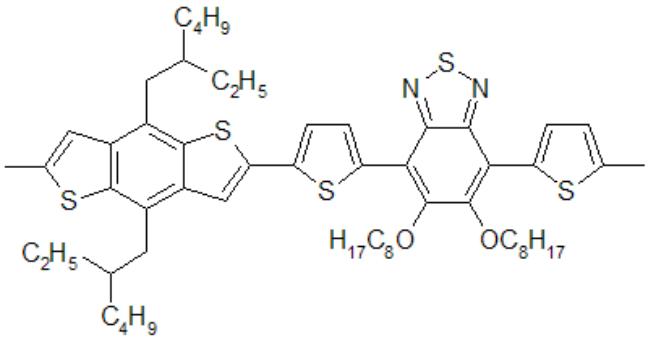

Figure 8.1. The chemical structure of the polymer **PBDTTBTZT.**

Figure 8.2a shows the *J-V* curves of these standard and inverted devices with thin active layers of thickness 100nm. The *J-V* behaviour can be seen to be relatively similar, particularly the current generation appears to be similar as both the devices have very similar J_{SC}s. This is consistent with the active layer being very similar between the devices and the generation and recombination dynamics being insensitive to device architecture. However, Figure 8.2b shows the *J-V* curves of devices with active layers with a thickness of 330nm. The device behaviour in these devices is extremely different; whilst the V_{OC} remains similar, the *FF* and J_{SC} of the standard architecture device are considerably reduced. The inverted device has a *FF* of 35.6% compared to 39.9% in the standard device, and the J_{SC} is reduced from 7.75mAcm^{-2} to 3.38mAcm^{-2}.

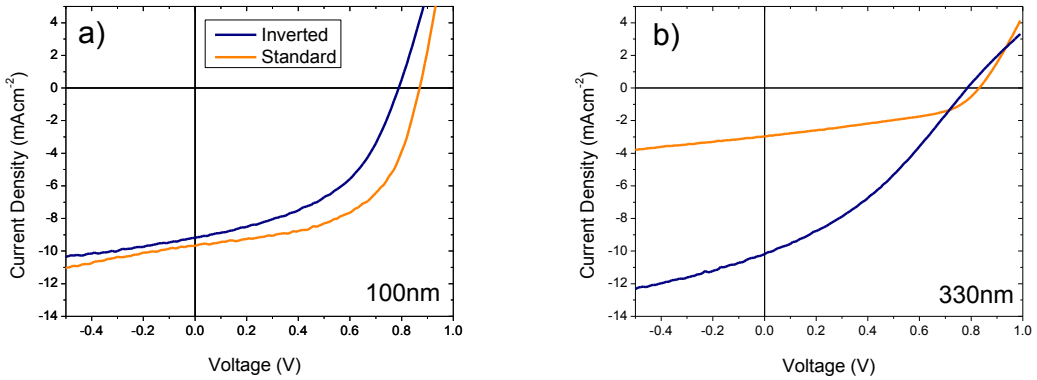

Figure 8.2. Current-voltage curves of PBDTTBTZT:$PC_{71}BM$ solar cells in standard (orange) and inverted (blue) architectures with active layer thicknesses of 100nm (a) and 330nm (b).

Figure 8.3 shows the external quantum efficiencies of the two 330nm thick standard and inverted devices. It can be seen that consistent with the reduced J_{SC} in the standard architecture device, the EQE is significantly reduced in magnitude across the entire wavelength spectrum. Additionally the EQE spectra also peak at a different wavelength than the inverted device, indicating a difference in fundamental device behaviour.

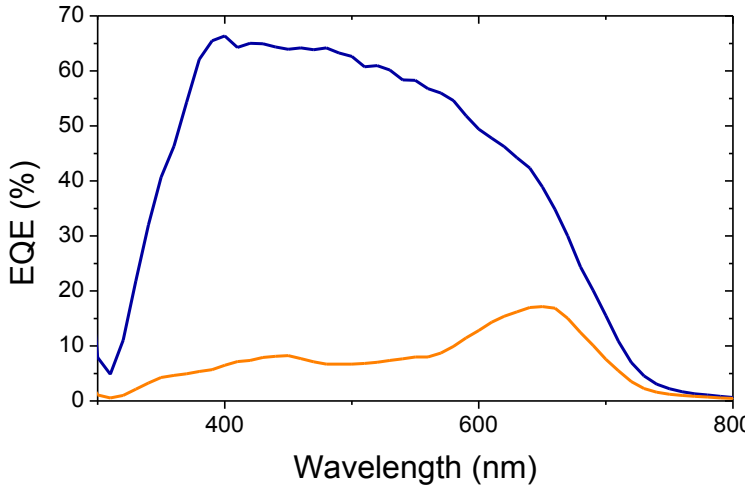

Figure 8.3. a plot of external quantum efficiency of inverted and standard architecture PBDTTBTZT:$PC_{71}BM$ solar cells.

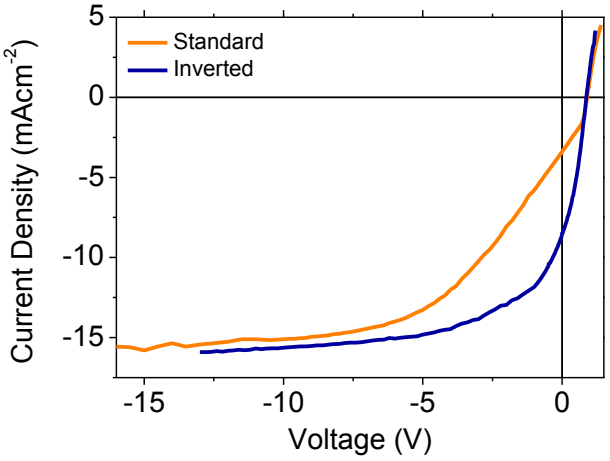

Figure 8.4. A plot of corrected photocurrent of PBDTTBTZT:PC$_{71}$BM solar cells in standard and inverted architectures showing the differences in photocurrent around short circuit conditions.

8.2.2 Corrected Photocurrent

By utilising pulsed illumination it is possible to measure the device *J-V* behaviour in the light and dark almost simultaneously and further into the reverse bias than would otherwise be possible in steady state.[140, 181-182] The corrected photocurrent under 1 sun, calculated by subtracting the dark current from the current under 1 sun illumination, is shown in Figure 8.4 for both the thick 330nm devices. As this allows measurement to far reverse bias it allows accurate comparison of the saturation currents for both devices. It can be seen that contrary to the very different *J-V* curves in Figure 8.2b, the saturation currents under the same light intensity are actually very similar. This would indicate that actually the active layers in the thick devices are actually generating very similar numbers of charges but the charge collection in the standard device is being impaired. Additionally Figure 8.4 shows that there is a linear region in the *J-V* of the standard device that extends from approximately -5V to +0.6V. This linear region extends through short circuit and appears to be limiting both *FF* and the J_{SC} of the standard device.

The evidence described above indicate that the charge collection in the standard architecture device may be being impaired by the presence of space charge in these thick active layer devices. It is therefore essential to determine if the semiconducting material of these devices is electronically doped.

8.3 MEASUREMENTS OF DOPING

8.3.1 Capacitance-Voltage Measurements

To determine whether a depletion region is present in the device, capacitance-voltage experiments were performed. Capacitance-voltage measurements are an established technique used to determine the doping density of a semiconductor.[150, 183-188] The width of the space charge region (if present) is probed by a variation of an applied DC voltage and is detected by measuring the capacitance of the device as a function of the DC voltage.[150, 185] The capacitance is proportional to $1/\sqrt{V - V_{BI}}$, thus, data can be analysed using the Mott-Schottky analysis to calculate the dopant density required to produce such a space-charge region.[184] As these experiments were performed in the dark where the mobility of carriers does not affect the electro-statics of the device, we can establish that if a depletion region is measured it is caused by electronic doping rather than a mobility imbalance.

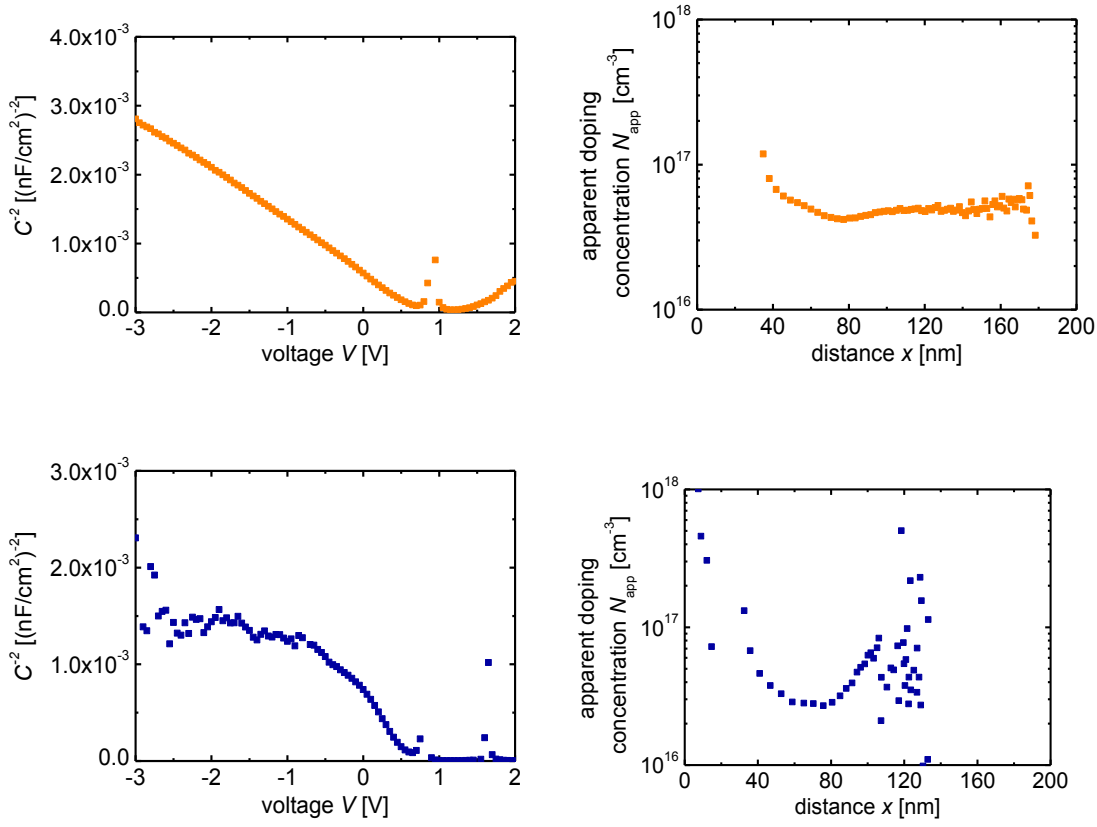

Figure 8.5. Plots showing the Mott-Shottky analysis of inverted and standard architecture devices from capacitance-voltage experiments. Both plots (b) and (d) show apparent doping concentrations of ~4x10^{16}cm^{-3}.

The results of the capacitance-voltage experiments in the dark and the Mott-Schottky analyses are shown in Figure 8.5 for the inverted and standard devices. This indicates that a depletion region is present in the device, and as it is forming under these conditions it must be due to electronic doping of the active layer. Furthermore we can determine that the device was doped with a concentration of $4x10^{16}$ cm^{-3} excess positive charge carriers. This is a relatively high dopant density and it is evidently enough to affect the electrostatics of these devices. Now we know that the electrostatics of these devices are unusual and spatial non-uniform, we can attempt to understand how this affects the transport, collection and recombination of free charges and relate this to device performance.

8.4 MODELLING THE EFFECT OF DOPING

8.4.1 Simple Collection Model

The depletion approximation applies to doped semiconductors and allows the calculation of the thickness of the depletion region, or in the case of photovoltaics, the region in which the largest electric field exists. By substituting into equation 1 the values of ε_r=4 Fm^{-1}, V_{BI}=0.8V and N_A=$4x10^{16}$ cm^{-3} as determined by the capacitance voltage data above, we see that the depletion region will occupy the 100nm closest to the cathode. The remaining 230nm of the device thickness is defined as the neutral region and in this part of the device there is little electric field. Figure 8.6 shows a simulated band diagram of a doped device (from drift-diffusion simulations) with an active layer thickness of 330nm with a doping concentration equal to that described here. Additionally this shows how the collection is modelled in this simple approximation, whereby the device is split into two distinct volumes with uniform electric fields.

We can now model the collection of charges by this electric field distribution using a very simple set of approximations. Firstly we assume that photogeneration and charge mobility imbalances during operation only alter the electric field distribution negligibly, and thus the thickness of the depletion region does not change except with voltage. Secondly, we assume that on the length scales discussed here free charges are generated where the photo-exciting photon is absorbed. We then also made a large assumption by setting charge collection to be a step-function, where all charges generated within the depletion region are collected, and all in the neutral region recombine non-geminately.

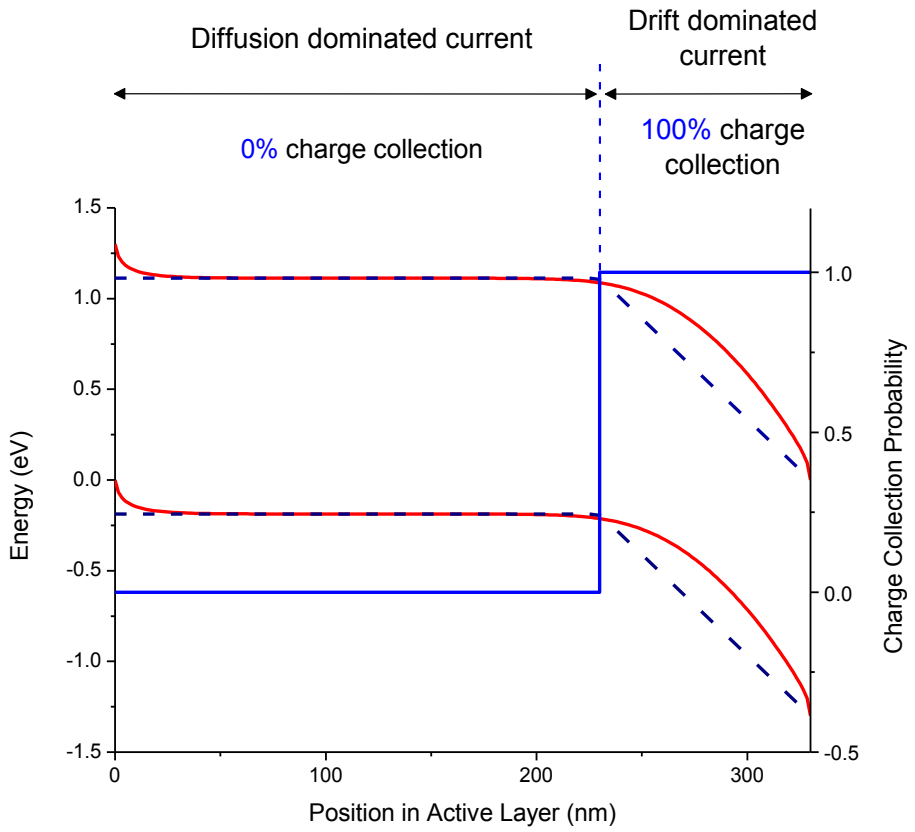

Figure 8.6. A simulated band diagram showing the non-uniform electric field within the active layer of a doped OPV device, with a step-function indicating the simplified collection model used in this chapter.

It is clearly of high importance to now know where within the active layer photons are absorbed and consequently charges are generated. Within a layered medium such as a solar cell light is reflected from any interfaces between materials, this reflected light then interferes with the incoming light creating interference fringes in the photon absorption. We can model this behaviour using the transfer matrix method, which uses the optical properties of each of the layered materials to calculate the photon density throughout the device.[8, 189-190] These optical properties, specifically the real and imaginary parts of the refractive index of the polymer:fullerene blend (*n* & *k* respectively) are measured using spectral ellipsometry measurements. These calculations allow calculation of exactly where in the active layer of the solar cell photons are absorbed, this is shown in Figure 8.7 as the photon absorption rate for the standard and inverted devices as function of wavelength of light. Although the layered materials in each device are different the photon absorption patterns are qualitatively similar, with a broad band of absorption close to the transparent electrode, where the polymer:fullerene blend absorbs strongly (300-600nm). Additionally where the blend absorbs less strongly (around 650nm) and light can travel through to the metallic electrode and be reflected, clear interference fringes are visible in the photon profiles. Using our assumptions we then take these photon absorption profiles to directly represent the free charge generation profiles through the devices.

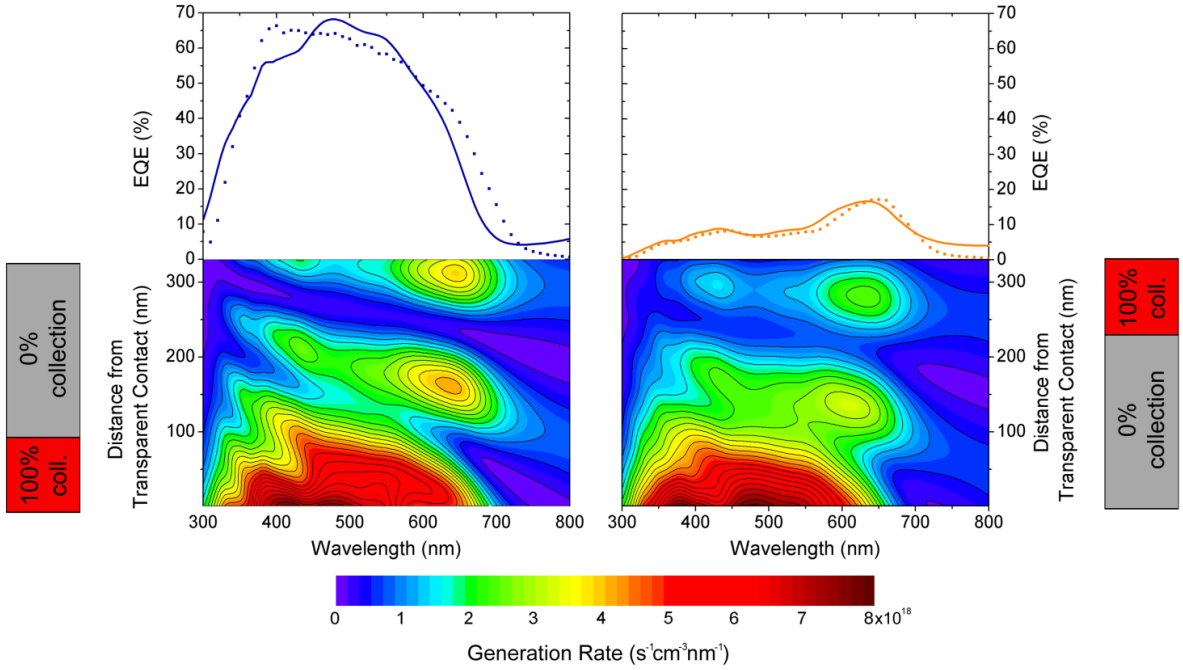

Figure 8.7. Top panels: Comparison of experimentally measured external quantum efficiency spectra (dotted lines) for inverted (left) and standard (right) architecture PBDTTBTZT:$PC_{71}BM$ devices, with simulated EQE spectra (full lines) obtained using the simple model (see text). Bottom panels: spectral charge generation rate as a function of depth calculated using a transfer matrix model of photon absorption . In this figure the light enters the device from the bottom of the figure (0 nm on the y-axis). For each device architecture, the red block indicates the part of the active layer in which generated charges can be collected at short circuit, according to the model used here. Only charges generated within these regions contribute to the simulated EQE.

To these charge generation profiles we can now apply the step-function charge collection profile, noting specifically that as the cathode is on different sides of the device in the standard and inverted architecture device, the depletion region where charges are collected also switches sides. The regions in which charges are collected are indicted on the side of Figure 8.7. When the charge collection is taken into account we gain a measurement of collected current as a function of illumination wavelength, this is equivalent to and can be compared to the experimental measurement of external quantum efficiency (EQE). These are shown in Figure 8.7 where the solid lines represent the calculated EQE spectra and the points are experimental measurements. This clearly shows that the shape and magnitude of the EQE is closely matched by our reconstruction, indicating that our model accurately approximates charge collection in these devices. Importantly these are EQE spectra under short circuit conditions, thus the integrated magnitude of the spectra is analogous to the magnitude of the short circuit current density. As the low EQE spectra is accurately reproduced by the model, this clearly shows that the J_{SC} and therefore performance limitations of the standard device are due to poor charge collection as a result of electronic doping of the device.

The difference between the standard and inverted device can also now be clearly explained. Because of the difference in electrostatics between the devices, in the inverted architecture device the majority of charges are generated where charge collection is efficient. However, in the standard device, the majority of

charges are generated in the neutral region where charge collection is poor. Thus in the standard device only those photons of a wavelength where the blend doesn't strongly absorb, and thus where they can penetrate the device and generate charges close to the cathode, result in current. This is the cause of the unusually shaped EQE of the standard device, which shows a peak where the blend absorption is reducing.

8.4.2 Fill-Factor

Equation *(8-1)* shows how the size of the depletion (or collection) region varies with applied voltage, indicating that as the bias of the device moves away from flat-band conditions the device becomes increasingly depleted and thus the depletion region will extend further into the active layer. This will change the amount of charges collected and thus the photocurrent generated by the device as a function of voltage, or the device fill factor. We can therefore extend the simple collection model to estimate the differences in fill factor, as well as photocurrent, in standard and inverted architectures as the collection region sweeps through the device with changing voltage.

Figure 8.8 shows device *J-V* curves simulated in this manner, using the depletion approximation to calculate the thickness of the collection region at each voltage and subsequently applying this to the photon absorption profiles in Figure 8.7. The qualitative similarity in shape between these simulated *J-V* curves and the corrected photocurrent curves in Figure 8.4 indicates that the changing size of the depletion region contributes significantly to the fill-factor of doped devices.

The corrected photocurrent curves show that under sufficient negative voltage the current extracted from the two devices is almost the same; this is accurately reproduced in the simulated *J-V* curves shown in Figure 8.8. Additionally the results of the transfer matrix model show that the total number of photons absorbed in the entire active layer of the standard architecture device is slightly less than that in the active layer of the inverted device. This is a known phenomenon due to the improved light trapping as a result of not using a layer of PEDOT:PSS on the transparent contact.[42] This results in the photocurrent generation being slightly less in the standard device even under high bias, as shown in Figure 8.8, and the same phenomenon is present in the experimentally measured *J-V* curves.

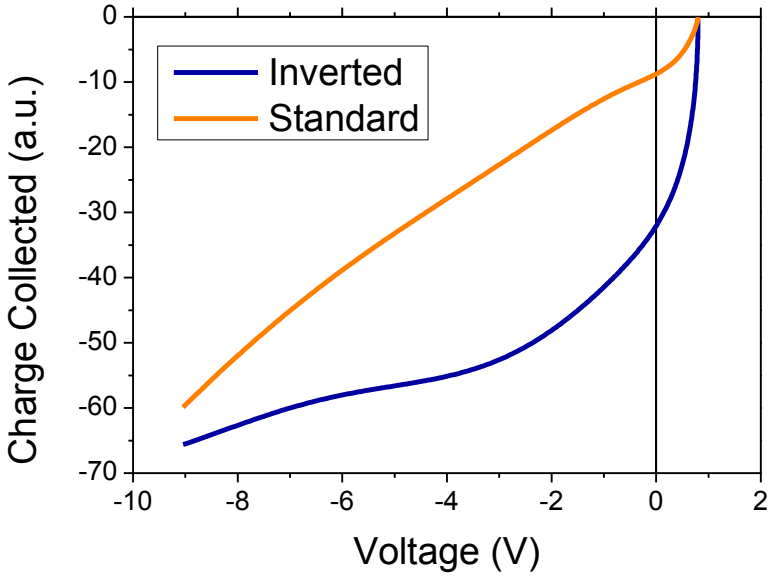

Figure 8.8. A plot of simulated J-V curves from the simple collection model. This can be compared to Figure 8.4 showing that the FF of the actual devices can be recreated by the voltage dependence of a depletion/collection region.

8.4.3 Drift-Diffusion Modelling

In the simple model above we analyse charge collection by using a step-function where the charges are either collected or not, determined by whether they are generated within the depletion region. Of course actual charge collection and device operation is much more complex than this. Not only are the bands "bent" in the real device such that there are a range of different electric fields in the device, but this bending occurs not only in the depletion region but also at the electrode interfaces. In addition to drift transport driven by electric fields, transport via diffusion which is neglected in the simple model above, must be taken account of to fully model the charge transport.[153]

To fully model charge transport through the device in this case, a drift-diffusion model may be used. This is a computational technique which simultaneously solves the electrostatics within the device and the drift and diffusion components of charge transport through the device for all charge carriers. Firstly it accurately represents the detailed electrostatics within the system instead of simply modelling it as two sections with zero and strong field. Secondly it then calculates the drift and diffusion transport, and recombination rates in each case. In addition the model takes into account the complex optical absorption within the active layer of the device that was so important in the section above.

To use the drift-diffusion model there is a large parameter space that must be fit to the particular device parameters which are not experimentally accessible.[61] These parameters are listed in Table 2. Clearly some parameters are known already such as the bang-gap of the system and the doping concentration;

these can be fixed and the remaining variables such as the slopes of energetic disorder, trapping and detrapping rates, and mobilities can be determined through a fitting routine. The fitting routine requires the input of experimental data, in this case the data used to fit the model were the *J-V* curves in the dark and under 1 sun illumination, and the external quantum efficiency. The device parameters for the inverted device were fit first as this has the most "normal" *J-V* curve. This allows us to find a minimum in the fitting of the parameter space and we can then allow the standard architecture device to be fit too. We then assume that the active layer in both the standard and inverted device architectures are identical and thus have all the same parameters, and we then attempt to apply the inverted device parameters to the standard device. Once the two devices are fit with the same parameters to a sufficient accuracy these parameters are fixed. The only parameters which were allowed to differ between the two devices of different architecture were the series and shunt resistances, as these are commonly understood to not originate from the performance of the active layer, but physical properties of the device structure and electrodes, at least in efficient devices. These final fitting parameters are shown in Table 2 and the fits of the experimental light and dark *J-V* curves and EQE data are shown in Figure 8.9.

Table 2. A table of parameters used in the drift-diffusion simulation of inverted and standard architecture devices.

Variable	Units	Inverted	Standard
Electron mobility	$cm^2V^{-1}s^{-1}$	2.46E-08	
Hole mobility	$cm^2V^{-1}s^{-1}$	1.34E-08	
p-type doping density	cm^{-3}	4.00E+16	
Effective density of states of the conduction band	cm^{-3}	1.44E+26	
of the valence band	cm^{-3}	3.99E+25	
Total density of tail states in the conduction band	cm^{-3}	7.93E+23	
in the valence band	cm^{-3}	3.68E+24	
Tail slop of the conduction band	meV	94	
of the valence band	meV	94	
Neutral hole capture coefficient	$cm^3\ s^{-1}$	4.10E-15	
Negative hole capture coefficient	$cm^3\ s^{-1}$	1.90E-18	
Positive electron capture coefficient	$cm^3\ s^{-1}$	2.60E-18	
Neutral electron capture coefficient	$cm^3\ s^{-1}$	4.10E-15	
Band gap	eV	1.30E+00	
Series resistance	Ωcm^2	4.10E-03	2.24E-03
Parallel resistance (light)	Ωcm^2	5.49E-02	1.82E-01
Parallel resistance (dark)	Ωcm^2	6.90E+00	50

8.4.4 Photocurrent

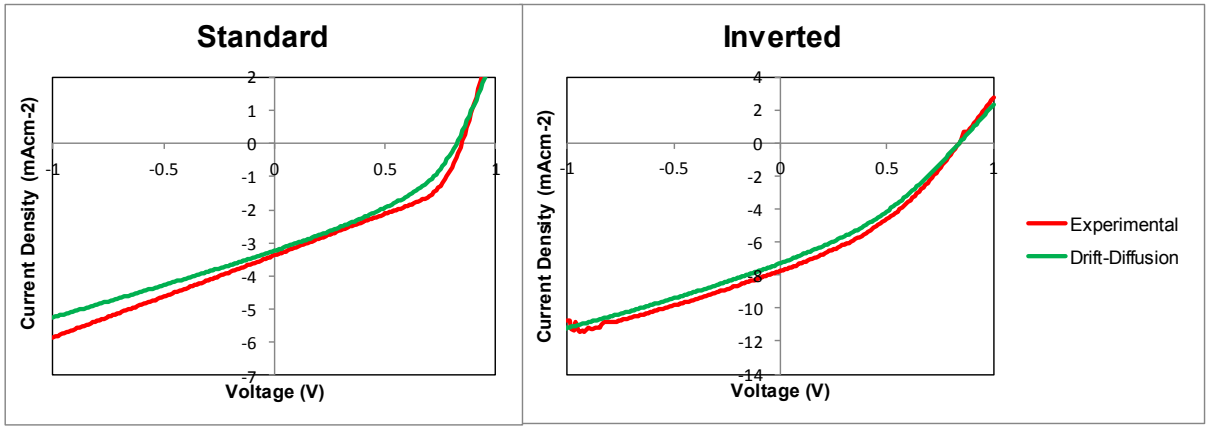

Figure 8.9. A comparison of experimental current-voltage curves (red) and those from the drift diffusion model (green), for PBDTTBTZT:$PC_{71}BM$ devices.

By showing that the device performance and EQE behaviour of both devices can be fit using the same device parameters indicates that our previous supposition that the properties of the active layers are almost identical regardless of them being deposited upon different substrates in different conditions, is in fact accurate. In addition it can be seen that the charge mobilities in the conduction band for electrons and for holes are of the same order of magnitude. This shows that imbalanced charge mobilities is not the only cause of space-charge limitations, and such a device can be consistent with almost identical mobilities for electrons and holes. However in solar cells where all charge transport is in the trap-limited regime, the size and shape of the density of states also determines the effective charge mobility. As parameters electron and hole densities of states show, the distributions of traps states are different for electrons and holes, thus the effective charge mobilities are likely different. This is consistent with our capacitance voltage spectroscopy results in the dark, shown above.

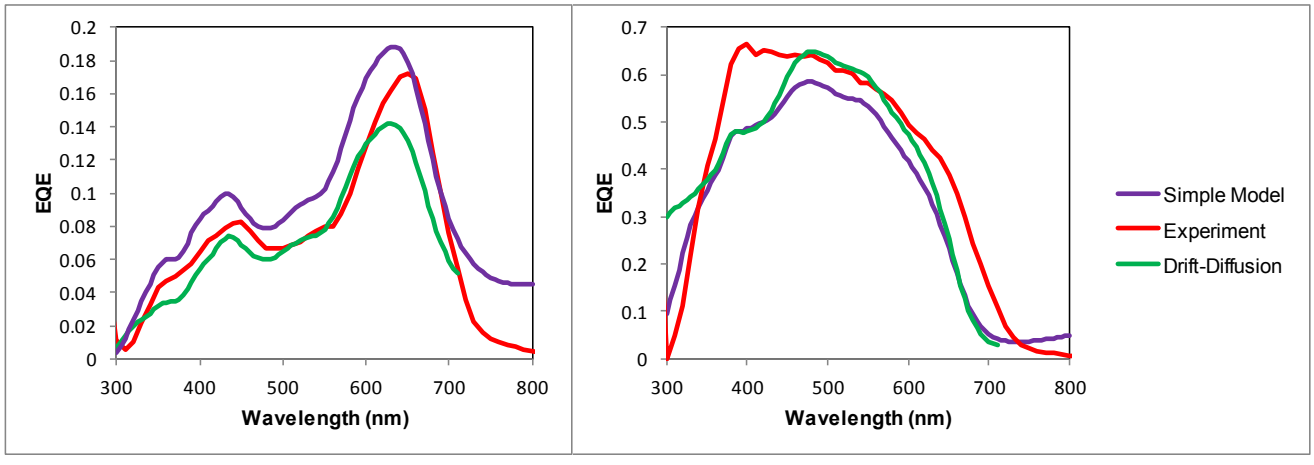

Figure 8.10. A comparison of experimental EQE plots (red) with those resulting from the simple collection model (purple) and the drift-diffusion model (green), for PBDTTBTZT:$PC_{71}BM$ devices.

The EQE spectra that are calculated by the two different models, the simple collection model and the drift-diffusion model, can be compared to each other and the experimental measurements in Figure 8.10. These EQE spectra can be seen to be very similar in shape and magnitude, essentially validating the simplifications made in the simple model as far more complex calculations give comparable results.

8.4.5 Fill Factor

As can be seen in Figure 8.9 the drift-diffusion simulation not only accurately reproduces the experimentally measured photocurrent but also closely matches the experimental fill factor of both devices. The simple collection model described above shows that the *FF*s of both devices are determined by the changes in charge collection due to changes in thickness of the collection region due to varying bias, as determined by the depletion approximation. This can be verified using drift-diffusion modelling. *Figure 8.11* shows the simulated generation and recombination rates of free charges within the active layer of the standard and inverted devices under applied biases between -1V and +0.6V. As can be seen the generation of charges in voltage independent thus the generation rate remains constant, however the recombination rate is strongly correlated to the thickness of the space-charge region. As charges are not collected in the neutral or space-charge region, recombination is high, as shown by the converging plots of recombination rate in the neutral region in *Figure 8.11*. As the voltage increases, the size of the depletion region is reduced, thus the recombination rate is increased and fewer charges are collected. This shows that charge collection and photocurrent is closely related to the size of the depletion region which changes considerably with voltage, and thus the fill factor can also be accounted for by the doping induced space-charge accumulation.

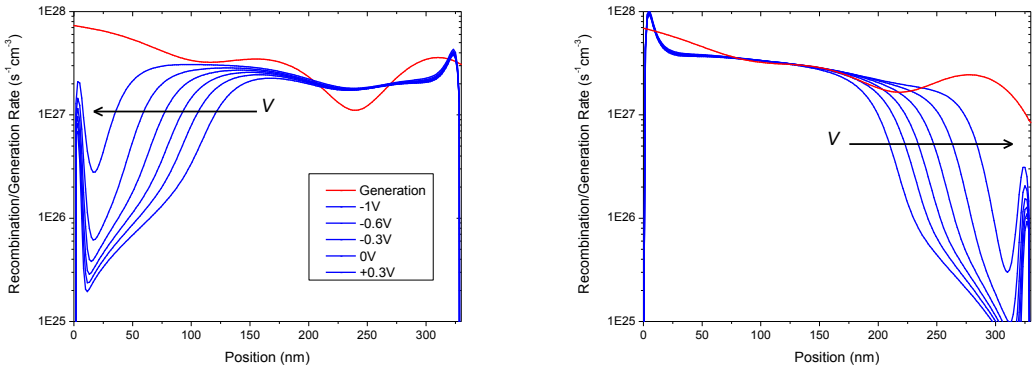

Figure 8.11. A comparison of the voltage-dependence of the simulated recombination and generation rates in inverted (a) and standard (b) architecture devices. These show the changing size of the collection region with changing device bias.

8.5 THICKNESS DEPENDENCE OF DOPED DEVICES

Due to the relatively low charge carrier mobilities exhibited by organic semiconductors, as opposed to other semiconducting materials used in photovoltaic technologies, transport of charge carriers over long distances without recombination losses can be problematic. The poor performance of OPV devices with thick active layers is often attributed to poor charge collection,[191-192] i.e. the photogenerated charges cannot be collected as they must travel over long distances (>100nm) within the device and thus recombination losses become too large.

The results of experiments above on PBDTTBTZT:$PC_{71}BM$ devices show that charge collection is not limited only by the charge mobility but also by the electronic doping of the active layer causing unfavourable electrostatics where an electric field is only present in a specific part of the device. In the depletion approximation the thickness of the depletion region is not dependent upon the thickness of the active layer (see equation 1). For a constant doping concentration the depletion region will be the same thickness regardless of the device thickness. If an active layer is doped to such a level that under short circuit conditions there is a depletion region with a thickness of 100nm; if the device is only 50nm thick then there will be efficient charge collection through the device, whereas if it is 200nm thick only half of the active layer will be able to efficiently extract charges. This provides an alternative explanation for the poor performance of thick OPV devices; the low currents observed are not due to an inability to transport charge over large distances, but a transition from thin devices with uniform electric fields to thick devices where charge collection is limited by the presence of a depletion region.

Figure 8.12a shows the *J-V* curves of a series of PBDTTBTZT:$PC_{71}BM$ devices in standard architecture, fabricated by blade-coating from a solution. These were fabricated to have a range of active layer thicknesses from 80nm to 400nm. It can be seen that whilst the V_{OC} of these devices is consistent with thickness, and the fill factor gradually reduces with thickness, the J_{SC} has a more complex relationship. The red points in Figure 8.12b show the thickness dependence of the J_{SC}.

The thickness dependence of photon absorption and charge collection is already known to be a complex balance between increased absorption in thick devices but enhanced collection in thin device structures. Additionally photon absorption is not a simple exponential relationship (such as in the Beer-Lambert law) due to the interference effects described previously. When photon interference is taken into account this relationship is complex.[193-194] This is shown by the blue line in Figure 8.12b which shows the results of transfer matrix calculations of the thickness dependence of photon absorption in PBDTTBTZT:$PC_{71}BM$ devices. It is clear that the maximum J_{SC} is obtained with a device thickness of 210nm. Furthermore for the thin devices, the short circuit current tracks the photon absorption, however past 210nm the J_{SC} is reduced compared to the photon absorption and clearly not all the absorbed photons contribute to the current.

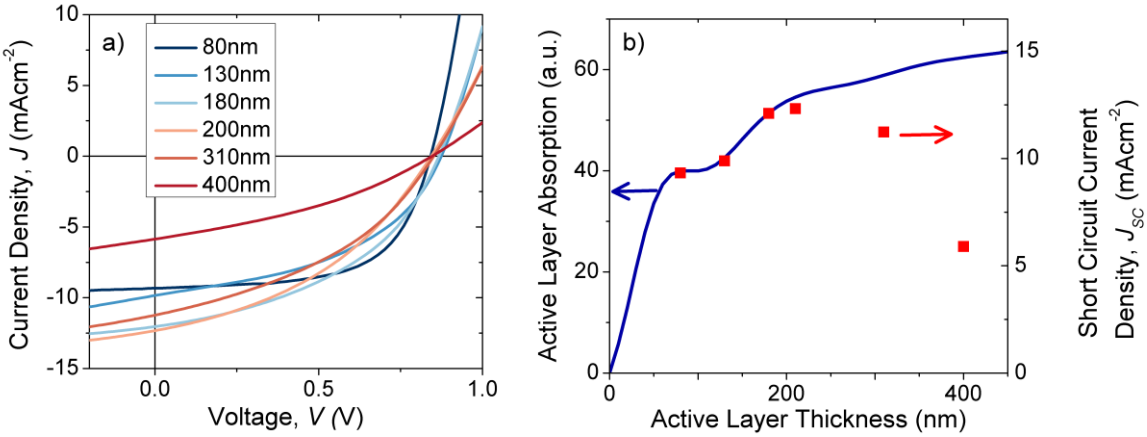

Figure 8.12. (a) J-V curves for six standard architecture PBDTTBTZT:$PC_{71}BM$ devices with different active layer thicknesses, measured under 1 sun illumination and (b) a plot showing the variation with active layer thicknesses of photon absorption from transfer matrix modelling (line) and short circuit current density from experiments (points).

These results would indicate that the J_{SC} of thicker devices is being limited by poor charge collection, of the type seen in the thick standard device above. There are many reasons for non-geminate recombination losses to increase such as changes in charge density or lifetime within a device as shown in other chapters, however in the case of changing thickness the likely reasons are either (i) depletion region limited collection due to electronic doping or (ii) poor charge transport and thus charges cannot travel far enough to be extracted from the device before within the recombination lifetime. These mechanisms can be distinguished using the technique of EQE as shown above. In the case of charge collection being limited by the presence of a depletion region the EQE will accurately be reproduced by only the photon absorption within the depletion region (close to the cathode), whereas in the case of transport limited collection the EQE should be close to the photon absorption of the entire active layer.

Figure 8.13 shows the photon absorption profiles calculated from TMM for each device shown above, with active layer thicknesses between 80-400nm. Considerable changes can be seen as the thickness changes. In the thinnest device the photon absorption is broadly throughout the device and highest in the middle of the device, as the active layers get thicker this changes to two and then three interference fringes.

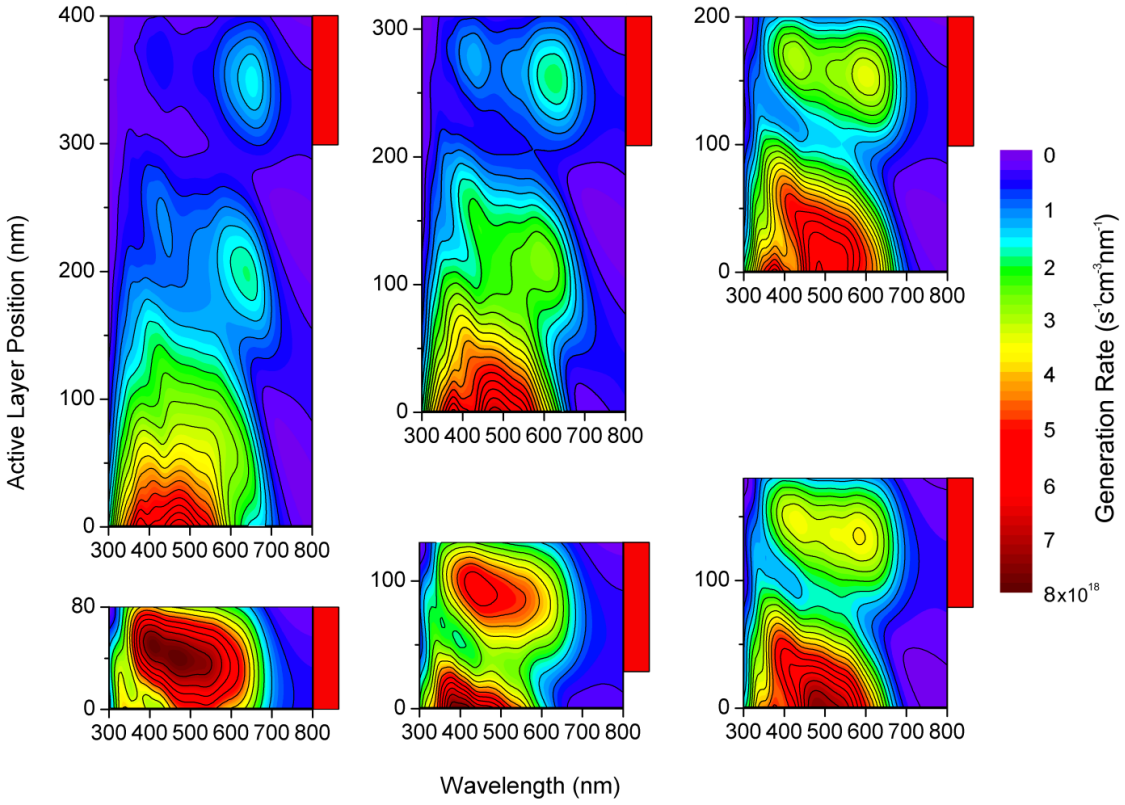

Figure 8.13. Contour plots showing the photon absorption (or charge generation) rates throughout the active layer of the six different standard architecture PBDTTBTZT:$PC_{71}BM$ devices (thicknesses of 80, 130, 180, 200, 310 & 400nm). The red bar alongside each one indicates the width of the depletion region (100nm) from the cathode in which charges can be efficiently collected.

8.5.1 Photocurrent

Although the devices studied here are fabricated from a different solvent to those in the first half of this chapter, both the polymer and fullerene used were the same, thus we assume that the electronic doping level is the same in these devices as in the standard and inverted devices studied above. We now apply the step-function collection model to these devices with different active layer thicknesses with a depletion region of 100nm. Clearly the thinnest device has a thickness thinner than the depletion region, thus the EQE matches the photon absorption, additionally the second thinnest device is only 30nm thicker than the depletion region so will only see very small collection losses. However the thicker devices will suffer much higher losses consistent with the comparison of J_{SC} and photon absorption in Figure 8.12. The experimentally measured EQEs of the devices are shown in Figure 8.14a, and Figure 8.14b shows the reconstructed EQEs from the step-function collection model. It can be seen that the experimental EQEs

change greatly in both magnitude and shape, peaking in entirely different regions of the spectrum for thin and thick devices. The reconstructed EQEs accurately match both the changes in magnitude and shape of the experimental measurements.

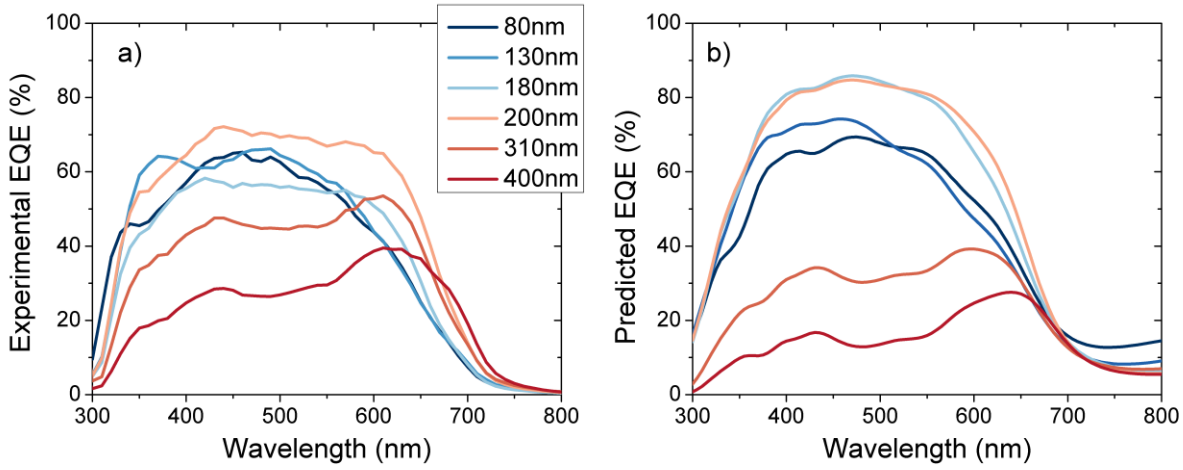

Figure 8.14. plots of external quantum efficiency spectra for standard architecture PBDTTBTZT:$PC_{71}BM$ devices with different active layer thicknesses from experiment (a) and from modelling of charge carrier collection (b).

8.6 DISCUSSION

The effect of electronic doping upon device performance in various device configurations has been demonstrated by the experimental data presented above. The accurate reproduction of the photocurrent and EQE results conclusively demonstrate that in PBDTTBTZT:$PC_{71}BM$ devices the performance of OPV devices is significantly affected by the presence of non-uniform electric fields which are a direct consequence of electronic doping.

As the doping measured in this device was an excess of positive carriers, or p-doping, the depletion region forms closest to the cathode. Thus when a photon is absorbed in the depletion region it generates an exciton that is subsequently split into an electron and a hole, the electron is rapidly driven to the cathode to be collected. However the hole is driven in the opposite direction into the neutral region. This neutral region is populated by a large accumulation of holes, the majority carrier. Thus electrons in the neutral region recombine very quickly with one of the high population of holes therefore having a very short lifetime. Holes however have a relatively long lifetime, as they are statistically unlikely to recombine with an electron due to imbalance in populations. Because of the holes long recombination lifetime in the neutral region once the holes are been driven there by the electric field they diffuse through the region with negligible recombination losses.

As the thickness of the depletion region is dependent upon the voltage applied across the device, and eventually, with a high enough bias, the depletion region will equal the device thickness, regardless of how

thick the active layer is. This transition can be observed in the *J-V* curve of the standard device at approximately -5V in Figure 8.4. At this voltage the two devices give an almost identical current, therefore the depletion region is now thick enough that charges close to the anode and all through the device are collected. This transition point can also be used to estimate the device doping concentration by solving equation *(8-1)* where $d = W$ and V=-5V. This gives a doping concentration of 4x10cm^{-3} which is close to the value measured using capacitance voltage in section 8.3.1.

Figure 8.12b gives an indication of the improvements in device performance that may be possible were the doping concentration in the devices studied here reduced. It can be seen from equation *(8-1)* that were the doping concentration reduced by an order of magnitude, the thickness of the depletion region would more than triple. In the case of the standard device of thickness 400nm, the depletion region would go from being 120nm thick to 380nm. Consequently charge carrier collection would improve significantly and, assuming that other collection losses were negligible, the J_{SC} of the 400nm device would approach the photon absorption. From Figure 8.12 it can be seen that this would correspond to an increase in J_{SC} from about 6mAcm^{-2} to almost 15mAcm^{-2}, an almost tripling of device efficiency. Additionally were this reduction in doping concentration possible then the standard device would perform as well as the inverted one, allowing more flexibility in device structure and electrode choice.

Currently the cause of electronic doping of the active layer is unclear, although several potential candidates have been identified. Incomplete or incorrect synthetic impurities have been shown to significantly reduce device efficiency and to be very difficult to detect,[195] whether these could dope a device depends on the specific molecular properties. Additionally, synthetic routes for conjugated polymers typically involve the use of metallic catalysts which, although removed, could result in low concentrations of metal atoms in the final synthetic product.[196] Finally, the presence of unwanted oxygen, either in its diatomic or radical state, has been shown to form trap states in the semiconductor density of states of the blend,[117, 130, 197] thus altering device performance, it has been suggested that this could additionally electronically dope the blend material.[102, 167-168, 198] Evidently there are uncertainties around the actual cause of the electronic doping, however we have shown here that this is a significant affect that must be considered, and must be the subject of further study.

8.7 CONCLUSIONS

We have shown that unintentional electronic doping of the active layer of an organic solar cell can cause considerable variations in the spatial uniformity of the electric field within the device. Specifically we have demonstrated that if doped with a sufficient concentration of excess charge carriers the electric field changes from being uniformly distributed through the active layer, to forming two distinct regions; one where the field is strong and one where the field is low to negligible due to the accumulation of space charge. As

charge collection in OPVs is dominated by drift currents, these changes in spatial distribution of electric fields result in a large change in the number of charges collected.

We have additionally experimentally demonstrated the effects of doping in an otherwise efficient polymer:fullerene devices. The effect of doping was shown in both changes in device architecture and in active layer thickness. The experimental results were comprehensively understood using two different computational models with comparable levels of accuracy. Both models demonstrated that charge collection was efficient in the region of the device in which the electric field was strong, whilst very few charges are collected from the space-charge region.

The loss of charge and consequent dependence of J_{SC} upon device thickness, at least in this material system, was shown to be almost completely due to doping and electric field changes. Additionally huge differences in device performance, in both photocurrent and fill factor, between inverted and standard device architectures was shown to be accounted for by the electronic doping of the devices. This shows the large potential gains available in device performance were the doping density reduced.

8.8 EXPERIMENTAL METHODS

PBDTTBTZT:$PC_{71}BM$ solar cell devices were fabricated in both standard (ITO/PEDOT:PSS/PBDTTBTZT:$PC_{71}BM$/Ca/Al) and inverted (ITO/ZnO/PBDTTBTZT:$PC_{71}BM$/PEDOT:PSS/Ag) architectures. These were made by blade-coating a PBDTTBTZT:$PC_{71}BM$ solution in CHCl3, this technique allows for greater control of the active layer thickness than spin-coating and these devices were intentionally fabricated with thick active layers of 330nm in both devices. Another series of PBDTTBTZT:$PC_{71}BM$ devices were fabricated, this time blade coated from a dichlorobenzene (oDCB) solution, at six different thicknesses; 80, 130, 180, 210, 310 and 400nm thick active layers. These devices were in the standard architecture thus the layer stack was ITO/PEDOT:PSS/PBDTTBTZT:$PC_{71}BM$/Ca/Al.

The work presented in this chapter resulted from a collaboration with Merck Chemicals Ltd. to whom I am grateful for the supply of polymers samples and data. Additionally some of EQE and *J-V* data presented in this chapter was collected with the assistance of Mathis Muth at Merck. Spectral ellipsometry data used in the optical modelling of devices in this chapter was kindly provided by Dr. Harald Hoppe and Sebastian Engmann of Ilmenau University of Technology. Finally, capacitance-voltage data was collected with assistance of Dr. Thomas Kirchartz.

CHAPTER IX

CONCLUSIONS AND FURTHER WORK

This thesis, through four experimental chapters, addresses the charge generation and recombination processes in polymer:fullerene bulk heterojunction solar cells. Throughout the thesis we utilise various experimental techniques, however the dominant techniques are transient opto-electronic measurements utilising electronic measurement on a fast timescale in response to an optical or electronic stimulus. Here we conclude the main results of these studies and summarise further measurements that could be used to further understand charge processes in organic solar cells.

9.1 NON-GEMINATE RECOMBINATION IN P3HT:PCBM

In chapter 5 an analysis of the non-geminate recombination process in the P3HT:PCBM material system is presented as well as studies of the shape and size of the density of states distribution in these devices. We utilise charge extraction and transient photovoltage experiments to measure non-geminate losses in P3HT devices under various conditions, and the subsequent analysis used to quantify these losses, reproducing the earlier studies performed by Shuttle et. al.. We then extend these experimental techniques to study the temperature dependence of the non-geminate recombination process. Furthermore we rationalise the temperature dependence of recombination in the model P3HT:PCBM system by relating the results to the fundamental charge carrier dynamics within a disordered distribution of density of states whereby the recombination process is significantly reduced at low temperatures as charges are increasingly localised and immobile.

In addition to probes of the non-geminate recombination process we present the results of transient photocurrent experiments used to probe the excitation of charges from the disordered density of states in

P3HT:PCBM devices. This technique is used to demonstrate the change in energetic disorder of devices on thermal annealing, indicating that at least some of the disorder present in such devices must be related to the morphological structure of the semiconductor blend. The TPC data presented indicate that the annealing temperature that corresponds to the optimal device efficiency additionally corresponds to the lowest density of trap states and thus the best density of states. The TPC measurements and temperature-dependent charge extraction/TPV experiments are two complimentary probes of energetic disorder and the analysis of the results from the two experiments largely agree upon the size and slope of the energetic distribution of the DoS in the P3HT:PCBM system.

9.1.1 Further Work

- P3HT:PCBM is a commonly studied material system in which charge separation and device performance are efficient. However there are other material systems in which the non-geminate recombination dynamics affect device performance far more and are thus worthy of further study. Two such systems are studied in chapters 7 and 8.
- The experimental data presented in chapter 5 shows that at least some of the energetic disorder known to be present in polymer:fullerene devices results from morphological disorder of the blend materials. However the shape of the density of states cannot be completely explained by morphological changes to the blend and is of unknown origin. There are several potential sources of energetic disorder in these semiconductors such as disorder in conjugation length, conformation and chemical configuration as well as in molecular packing, influencing the interactions between molecules. To fully understand and optimise device performance some of these sources of disorder could be carefully controlled e.g. via chemical structure, and the effects studied.
- Understanding the degradation of organic solar cells in different environmental conditions is an ongoing challenge and particularly the mechanism of the breakdown of devices in the presence of oxygen is unknown. Recently Street and Davies demonstrated that devices degrade in performance under illumination and linked this to measured changes in the density of states distribution.[130] Clearly the techniques described in chapter 5 can be extended to further investigate the changes in the DoS under various degradation regimes and relate this back to device performance, as performed here.

9.2 LINEARITY OF NON-GEMINATE RECOMBINATION

In chapter 6 we demonstrate, contrary to other reports in the literature, that a device whose performance is determined by a non-geminate recombination process that depends on charge density with

an order greater than two, can simultaneously exhibit a corrected photocurrent that is linear with illumination intensity. In the P3HT:PCBM device studied here, we conclusively show that whilst the *J-V* curve is shaped by non-geminate losses which are super-second order with respect to charge density within the active layer the corrected photocurrent,[140] J_{CORR}, is apparently linear as a function of light intensity. We reconcile these observations with analysis of device behaviour showing that in fact J_{CORR} will always appear linear with light intensity as long as the photogenerated charge density is significantly lower than the charge density already present at the applied voltage. This is significant as other authors have previously used the experimental observation of corrected photocurrent to make conclusions upon the charge recombination process and we show the reasons that such an approach is unfounded.

9.2.1 Further Work

- Recent publications from a research group utilising light induced electron spin resonance to probe recombination kinetics have indicated a new quadrimolecular recombination process in regio-regular P3HT:PCBM devices.[199] In light of the work in chapter 5 and 6 of this thesis, this seems unlikely as we have shown that non-geminate bimolecular processes dominate. It is possible that through a similar analysis of the experimental data as presented in chapter 6, the results would be found to be consistent with non-geminate recombination.

- Whilst this chapter indicated that the use of corrected photocurrents to determine the order of the non-geminate recombination process is flawed, however the question of the what the actual order of the recombination process is and what by what mechanism recombination occurs is still unknown. Understanding how the charges recombine, whether one charge is trapped or if the process involves two free carriers, is still not fully understood. Further investigation into the fundamental recombination process and the way it depends upon charge density is vital in understanding this.

9.3 EFFECTS OF RECOMBINATION UPON FILL FACTOR

The factors controlling FF in bulk heterojunction devices are not well understood. In particular, low FF has been attributed both to electric field dependent charge pair generation (geminate losses) and to super-linear dependence of recombination on charge density (non geminate losses). Here, we present transient optoelectronic techniques to analyse the nature of the recombination processes that control fill factor in a representative set of polymer:PCBM devices. We present analysis of different recombination dynamics, both

geminate and non-geminate, in various material systems, and draw conclusions upon the ways in which they influenced the device fill factor.

The studies presented here indicate that whilst P3HT:PCBM and PCPDBT:$PC_{71}BM$ devices exhibit efficient and voltage-independent charge generation, APFO-3:$PC_{71}BM$ devices suffer voltage-dependent geminate recombination losses and thus the generation of charges is dependent upon device bias limiting the fill factor. Further investigation using charge extraction and transient photovoltage techniques showed that the low fill factors of PCPDTBT and P3HT (under high illumination) based devices were not due to voltage-dependent geminate recombination, but to an inability of the device to extract charge sufficiently and thus high non-geminate losses through the power-generating quadrant of the *J-V* curve. This work as elucidated the ways in which different recombination processes affect alternative material systems in different ways. Additionally potential causes of voltage-dependent charge separation are discussed with reference t the different polymers used and we find that our results support the idea that efficient charge separation can be assisted by the presence of ordered material domains near the donor:acceptor interface providing a driving force for charge separation.

9.3.1 Further Work

- In this chapter we have identified one polymer that does exhibit voltage-dependent charge generation and one that does not. As high efficiency devices are unlikely to result from materials that exhibit voltage-dependent generation understanding what causes this process is vital. Whilst in this chapter we suggest that the relative crystallinities of the donor and acceptor components can aid efficient charge separation through increasing disorder at the interface therefore driving charges to spatially separated and ordered regions away from the interface.[82] This mechanism must be further investigated.
- The question over the causes of voltage-dependent charge generation is additionally complicated by the surrounding debate regarding the fundamental process that enables exciton separation in the first place. This is a topic that is being widely investigated in the field, but for a true understanding of what causes voltage dependent behaviour this must be resolved and fully understood.
- In addition to voltage-dependent geminate recombination losses we identified particularly strong non-geminate losses impacting the *FF* of PCPDTBT:$PC_{71}BM$ devices. Whilst on initial investigation this polymer exhibits mobilities and charge carrier dynamics similar to others, in the devices we measured the material system cannot extract that charge from active layer sufficiently to reduce non-geminate recombination at short circuit. Understanding the cause of this is a potential route to very high fill factors and thus very high device efficiencies, so understanding the voltage dependence of charge transport in various devices must be an area of further study. Additionally the influence of blend microstructure upon a polymer:fullerene blend's charge transport properties must be more fully understood.

9.4 EFFECT OF DOPING UPON CHARGE COLLECTION

In chapter 8 of this thesis we investigate the effect of non-uniform electric fields in the active layer of devices. We study a series of low band gap polymer:fullerene devices we that are moderately doped, using Mott-Schottky capacitance-voltage analyses. Using *J-V* and EQE measurements of devices of different active layer thickness and polarity, together with transfer-matrix optical modelling we investigate the factors that influence charge collection relative to charge. We conclude that inadvertent charge doping of the active semiconducting blend caused the formation of a depletion region with a thickness of approximately 100nm, within this region charge collection was efficient as here the electric field driving collection was strong. However in the rest of the device space-charge accumulation resulted in a very low electric field, thus charge collection was low due to the relatively slow diffusion of charges in organic materials. Using an approximation of 100% charge collection in the depletion region and 0% elsewhere we accurately reproduce the EQE behaviour of inverted and standard architecture devices. Additionally we show that the changes in short circuit current in a series of standard architecture devices with varying active layer thickness, was due mainly to the transition from a regime in which the device thickness was smaller than the depletion region thickness, to one where charge collection was limited by non-uniform fields.

9.4.1 Further Work

- Whilst the effect of doping is clearly demonstrated in this chapter, the root cause of this inadvertent charge doping is uncertain. Several possible routes by which OPV device active layers could become doped are known, such as chemical impurities resulting from polymer synthesis and degradation of the polymer structure in the presence of oxygen. The advantages to reducing and controlling doping are made clear in this chapter, therefore understanding the main route by which the organic semiconductors become doped is evidently important further work in this area.
- Recently some groups have studied the effect of doping on organic semiconductors by doping them with chemical additives in varying quantities.[176, 178] Previously intentionally doping devices has not been an attractive option as the addition of these additives tends to alter other device properties. However, one route to higher device efficiencies could be to compensate the unintentional doping already present in the semiconductor with an equal but opposite intentional dopant, this could possibly reduce the non-uniformities of electric field and consequently improve charge collection. Further investigation of the effect of dopant compensation on devices is required.

LIST OF PUBLICATIONS

1. MacKenzie, R. C. I., Kirchartz, T., Dibb, G. F. A., Nelson, J. Modeling Nongeminate Recombination in P3HT:PCBM Solar Cells *J. Phys. Chem. C* 2011, *115*, 9806-9813.
2. Dibb, G. F. A.; Kirchartz, T.; Credgington, D.; Durrant, J. R.; Nelson, J. Analysis of the Relationship between Linearity of Corrected Photocurrent and the Order of Recombination in Organic Solar Cells *J. Phys. Chem. Lett.* 2011, *2*, 2407-2411.
3. Dibb, G. F. A.; Jamieson, F. C.; Maurano, A.; Nelson, J.; Durrant, J. R. Limits on the Fill Factor in Organic Photovoltaics: Distinguishing Nongeminate and Geminate Recombination Mechanisms *J. Phys. Chem. Lett.* 2013, 803-808.
4. Faist, M. A.; Shoaee, S.; Tuladhar, S.; Dibb, G. F. A.; Foster, S.; Gong, W.; Kirchartz, T.; Bradley, D. D. C.; Durrant, J. R.; Nelson, J. Understanding the Reduced Efficiencies of Organic Solar Cells Employing Fullerene Multiadducts as Acceptors *Advanced Energy Materials* 2013, n/a-n/a.
5. MacKenzie, R. C. I.; Shuttle, C. G.; Dibb, G. F.; Treat, N.; von Hauff, E.; Robb, M. J.; Hawker, C. J.; Chabinyc, M. L.; Nelson, J. Interpreting the Density of States Extracted from Organic Solar Cells Using Transient Photocurrent Measurements *The Journal of Physical Chemistry C* 2013, *117*, 12407-12414.
6. Dibb, G. F. A.; Muth, M-A.; Kirchartz, T.; Engmann, S.; Hoppe, H.; Gobsch, G.; Thelakkat, M.; Blouin, N.; Tierney, S.; Carrasco-Orozco, M.; Durrant, J. R.; Nelson, J. Influence Of Doping On Charge Carrier Collection In Normal And Inverted Geometry Polymer:Fullerene Solar Cells *Scientific Reports* 2013, *3*.

REFERENCES

1. Anderegg, W. R. L.; Prall, J. W.; Harold, J.; Schneider, S. H. Expert credibility in climate change. *Proceedings of the National Academy of Sciences* **2010** *107* (27), 12107-12109.
2. *Fighting Climate Change: Human Solidarity in a Divided World*; United Nations Development Programme: 2007/2008.
3. *International Energy Statistics*; U.S. Energy Information Administration: 2008.
4. Smil, V. *Energy*. 2006.
5. Nelson, J.; Emmott, C. J. M. Can solar power deliver? *Philosophical Transactions of the Royal Society A: Mathematical, Physical and Engineering Sciences* **2013,** *371* (1996).
6. You, J.; Dou, L.; Yoshimura, K.; Kato, T.; Ohya, K.; Moriarty, T.; Emery, K.; Chen, C. C.; Gao, J.; Li, G.; Yang, Y. A polymer tandem solar cell with 10.6% power conversion efficiency. *Nat Commun* **2013,** *4*, 1446.
7. Image reproduced courtesy of the National Centre for Photovoltaics at the National Renewable Energies Laboratory, U. S. o. A., retrieved online on the 15/09/2013 http://www.nrel.gov/ncpv/images/efficiency_chart.jpg.
8. Hoppe, H.; Arnold, N.; Meissner, D.; Sariciftci, N. S. Modeling of optical absorption in conjugated polymer/fullerene bulk-heterojunction plastic solar cells. *Thin Solid Films* **2004,** *451-452*, 589-592.
9. Brabec, C. J.; Gowrisanker, S.; Halls, J. J.; Laird, D.; Jia, S.; Williams, S. P. Polymer-fullerene bulk-heterojunction solar cells. *Adv Mater* **2010,** *22* (34), 3839-56.
10. Shockley, W.; Queisser, H. J. Detailed Balance Limit of Efficiency of p-n Junction Solar Cells. *J. Appl. Phys.* **1961,** *32* (3), 510.
11. Waldauf, C.; Scharber, M. C.; Schilinsky, P.; Hauch, J. A.; Brabec, C. J. Physics of organic bulk heterojunction devices for photovoltaic applications. *J. Appl. Phys.* **2006,** *99* (10), 104503.
12. Baranovskii, S. D.; Wiemer, M.; Nenashev, A. V.; Jansson, F.; Gebhard, F. Calculating the Efficiency of Exciton Dissociation at the Interface between a Conjugated Polymer and an Electron Acceptor. *J. Phys. Chem. Lett.* **2012,** *3* (9), 1214-1221.
13. Blakesley, J. C.; Neher, D. Relationship between energetic disorder and open-circuit voltage in bulk heterojunction organic solar cells. *Phys. Rev. B: Condens. Matter* **2011,** *84* (7), 075210.
14. Nayak, P. K.; Garcia-Belmonte, G.; Kahn, A.; Bisquert, J.; Cahen, D. Photovoltaic efficiency limits and material disorder. *Energy & Environmental Science* **2012,** *5* (3), 6022.
15. Schmechel, R.; von Seggern, H. Electronic traps in organic transport layers. *Phys. Status Solidi A* **2004,** *201* (6), 1215-1235.
16. Gunes, S.; Neugebauer, H.; Sariciftci, N. S. Conjugated Polymer-Based Organic Solar Cells. *Chem. Rev.* **2007,** *107* (4), 1324-1338.
17. Nelson, J. Diffusion-Limited Recombination in Polymer-Fullerene Blends and its Influence on Photocurrent Collection. *Phys. Rev. B: Condens. Matter* **2003,** *67* (15), 155209.
18. Tang, C. W. Two-layer organic photovoltaic cell. *Appl. Phys. Lett.* **1986,** *48* (2), 183-185.
19. Dimitrov, S. D.; Nielsen, C. B.; Shoaee, S.; Shakya Tuladhar, P.; Du, J.; McCulloch, I.; Durrant, J. R. Efficient Charge Photogeneration by the Dissociation of PC70BM Excitons in Polymer/Fullerene Solar Cells. *J. Phys. Chem. Lett.* **2012,** *3* (1), 140-144.
20. Tumbleston, J. R.; Ko, D.-H.; Samulski, E. T.; Lopez, R. Analyzing local exciton generation profiles as a means to extract transport lengths in organic solar cells. *Phys. Rev. B: Condens. Matter* **2010,** *82* (20), 205325.
21. De, S.; Kesti, T.; Maiti, M.; Zhang, F.; Inganäs, O.; Yartsev, A.; Pascher, T.; Sundström, V. Exciton dynamics in alternating polyfluorene/fullerene blends. *Chem. Phys.* **2008,** *350* (1–3), 14-22.
22. Ayzner, A. L.; Tassone, C. J.; Tolbert, S. H.; Schwartz, B. J. Reappraising the Need for Bulk Heterojunctions in Polymerâˆ'Fullerene Photovoltaics: The Role of Carrier Transport in All-Solution-Processed P3HT/PCBM Bilayer Solar Cells. *The Journal of Physical Chemistry C* **2009,** *113* (46), 20050-20060.
23. Halls, J.; Walsh, C.; Greenham, N.; Marseglia, E.; Friend, R.; Moratti, S.; Holmes, A. Efficient photodiodes from interpenetrating polymer networks**1995**.
24. Yu, G.; Gao, J.; Hummelen, J.; Wudl, F.; Heeger, A. Polymer photovoltaic cells: enhanced efficiencies via a network of internal donor-acceptor heterojunctions. *Science-AAAS-Weekly Paper Edition* **1995,** *270* (5243), 1789-1790.
25. Park, H. J.; Lee, J. Y.; Lee, T.; Guo, L. J. Advanced Heterojunction Structure of Polymer Photovoltaic Cell Generating High Photocurrent with Internal Quantum Efficiency Approaching 100%. *Adv. En. Mat.* **2013,** *3* (9), 1135-1142.
26. Bavel, S. S. v.; Sourty, E.; With, G. d.; Loos, J. Three-Dimensional Nanoscale Organization of Bulk Heterojunction Polymer Solar Cells. *Nano Lett.* **2008,** *9* (2), 507-513.
27. Baumann, A.; Savenije, T. J.; Murthy, D. H. K.; Heeney, M.; Dyakonov, V.; Deibel, C. Influence of Phase Segregation on Recombination Dynamics in Organic Bulk-Heterojunction Solar Cells. *Adv. Funct. Mater.* **2011,** *21* (9), 1687-1692.
28. Conings, B.; Baeten, L.; Boyen, H.-G.; D'Haen, J.; Van Bael, M. K.; Manca, J. V. Relation between Morphology and Recombination Kinetics in Nanostructured Hybrid Solar Cells. *The Journal of Physical Chemistry C* **2012,** *116* (27), 14237-14242.
29. Collins, B. A.; Tumbleston, J. R.; Ade, H. Miscibility, Crystallinity, and Phase Development in P3HT/PCBM Solar Cells: Toward an Enlightened Understanding of Device Morphology and Stability. *J. Phys. Chem. Lett.* **2011,** *2* (24), 3135-3145.
30. Stuart, A. C.; Tumbleston, J. R.; Zhou, H.; Li, W.; Liu, S.; Ade, H.; You, W. Fluorine substituents reduce charge recombination and drive structure and morphology development in polymer solar cells. *J. Am. Chem. Soc.* **2013,** *135* (5), 1806-15.
31. Lyons, B. P.; Clarke, N.; Groves, C. The relative importance of domain size, domain purity and domain interfaces to the performance of bulk-heterojunction organic photovoltaics. *Energy & Environmental Science* **2012,** *5* (6), 7657-7663.
32. Jamieson, F. C.; Domingo, E. B.; McCarthy-Ward, T.; Heeney, M.; Stingelin, N.; Durrant, J. R. Fullerene crystallisation as a key driver of charge separation in polymer/fullerene bulk heterojunction solar cells. *Chem. Sci.* **2012,** *3* (2), 485.
33. Tsoi, W. C.; James, D. T.; Domingo, E. B.; Kim, J. S.; Al-Hashimi, M.; Murphy, C. E.; Stingelin, N.; Heeney, M.; Kim, J.-S. Effects of a Heavy Atom on Molecular Order and Morphology in Conjugated Polymer:Fullerene Photovoltaic Blend Thin Films and Devices. *ACS Nano* **2012,** *6* (11), 9646-9656.
34. Groves, C.; Reid, O. G.; Ginger, D. S. Heterogeneity in Polymer Solar Cells: Local Morphology and Performance in Organic Photovoltaics Studied with Scanning Probe Microscopy. *Acc. Chem. Res.* **2010,** *43* (5), 612-620.

35. Howard, I. A.; Mauer, R.; Meister, M.; Laquai, F. d. r. Effect of Morphology on Ultrafast Free Carrier Generation in Polythiophene:Fullerene Organic Solar Cells. *J. Am. Chem. Soc.* **2010,** *132* (42), 14866-14876.
36. Badrou Aïch, R.; Zou, Y.; Leclerc, M.; Tao, Y. Solvent effect and device optimization of diketopyrrolopyrrole and carbazole copolymer based solar cells. *Org. Electron.* **2010,** *11* (6), 1053-1058.
37. Treat, N. D.; Shuttle, C. G.; Toney, M. F.; Hawker, C. J.; Chabinyc, M. L. In situ measurement of power conversion efficiency and molecular ordering during thermal annealing in P3HT:PCBM bulk heterojunction solar cells. *J. Mater. Chem.* **2011,** *21* (39), 15224-15231.
38. Kempe, M. D.; Reese, M. O.; Dameron, A. A. Evaluation of the sensitivity limits of water vapor transmission rate measurements using electrical calcium test. *The Review of scientific instruments* **2013,** *84* (2), 025109.
39. Braun, C. L. Electric Field Assisted Dissociation of Charge Transfer States as a Mechanism of Photocarrier Production. *J. Chem. Phys.* **1984,** *80* (9), 4157-4161.
40. Liu, A.; Zhao, S.; Rim, S. B.; Wu, J.; Könemann, M.; Erk, P.; Peumans, P. Control of Electric Field Strength and Orientation at the Donor–Acceptor Interface in Organic Solar Cells. *Adv. Mater.* **2008,** *20* (5), 1065-1070.
41. Sánchez-Díaz, A.; Burtone, L.; Riede, M.; Palomares, E. Measurements of Efficiency Losses in Blend and Bilayer-Type Zinc Phthalocyanine/C60 High-Vacuum-Processed Organic Solar Cells. *The Journal of Physical Chemistry C* **2012,** *116* (31), 16384-16390.
42. He, Z. C.; Zhong, C. M.; Su, S. J.; Xu, M.; Wu, H. B.; Cao, Y. Enhanced power-conversion efficiency in polymer solar cells using an inverted device structure. *Nat. Photon.* **2012,** *6* (9), 591-595.
43. Servaites, J. D.; Savoie, B. M.; Brink, J. B.; Marks, T. J.; Ratner, M. A. Modeling geminate pair dissociation in organic solar cells: high power conversion efficiencies achieved with moderate optical bandgaps. *Energy & Environmental Science* **2012**.
44. De, S.; Pascher, T.; Maiti, M.; Jespersen, K. G.; Kesti, T.; Zhang, F.; Inganäs, O.; Yartsev, A.; Sundström, V. Geminate Charge Recombination in Alternating Polyfluorene Copolymer/Fullerene Blends. *J. Am. Chem. Soc.* **2007,** *129* (27), 8466-8472.
45. Deibel, C.; Strobel, T.; Dyakonov, V. Role of the Charge Transfer State in Organic Donor–Acceptor Solar Cells. *Adv. Mater.* **2010,** *22* (37), 4097-4111.
46. Nogueira, A. F.; Montanari, I.; Nelson, J.; Durrant, J. R.; Winder, C.; Sariciftci, N. S.; Brabec, C. Charge Recombination in Conjugated Polymer/Fullerene Blended Films Studied by Transient Absorption Spectroscopy. *The Journal of Physical Chemistry B* **2003,** *107* (7), 1567-1573.
47. Koster, L. J. A.; Mihailetchi, V. D.; Blom, P. W. M. Bimolecular Recombination in Polymer/Fullerene Bulk Heterojunction Solar Cells. *Appl. Phys. Lett.* **2006,** *88* (5), 052104-3.
48. Street, R. A.; Schoendorf, M.; Roy, A.; Lee, J. H. Interface State Recombination in Organic Solar Cells. *Phys. Rev. B: Condens. Matter* **2010,** *81* (20), 205307.
49. Shuttle, C. G.; Hamilton, R.; O'Regan, B. C.; Nelson, J.; Durrant, J. R. Charge-Density-Based Analysis of the Current-Voltage Response of Polythiophene/Fullerene Photovoltaic Devices. *Proc. Natl. Acad. Sci. U. S. A.* **2010,** *107* (38), 16448-16452.
50. Credgington, D.; Hamilton, R.; Atienzar, P.; Nelson, J.; Durrant, J. R. Non-Geminate Recombination as the Primary Determinant of Open-Circuit Voltage in Polythiophene:Fullerene Blend Solar Cells: an Analysis of the Influence of Device Processing Conditions. *Adv. Funct. Mater.* **2011,** *21* (14), 2744-2753.
51. Cowan, S. R.; Banerji, N.; Leong, W. L.; Heeger, A. J. Charge Formation, Recombination, and Sweep-Out Dynamics in Organic Solar Cells. *Adv. Funct. Mater.* **2012,** *22* (6), 1116-1128.
52. Rauh, D.; Deibel, C.; Dyakonov, V. Charge Density Dependent Nongeminate Recombination in Organic Bulk Heterojunction Solar Cells. *Adv. Funct. Mater.* **2012,** *22* (16), 3371-3377.
53. Credgington, D.; Kim, Y.; Labram, J.; Anthopoulos, T. D.; Durrant, J. R. Analysis of Recombination Losses in a Pentacene/C60 Organic Bilayer Solar Cell. *J. Phys. Chem. Lett.* **2011,** *2* (21), 2759-2763.
54. Homa, B.; Andersson, M.; Inganas, O. Photogenerated charge carrier transport and recombination in polyfluorene/fullerene bilayer and blend photovoltaic devices. *Org. Electron.* **2009,** *10* (3), 501-505.
55. Nenashev, A. V.; Jansson, F.; Baranovskii, S. D.; Osterbacka, R.; Dvurechenskii, A. V.; Gebhard, F. Role of diffusion in two-dimensional bimolecular recombination. *Appl. Phys. Lett.* **2010,** *96* (21), 3.
56. Gonzalez-Rabade, A.; Morteani, A. C.; Friend, R. H. Correlation of Heterojunction Luminescence Quenching and Photocurrent in Polymer-Blend Photovoltaic Diodes. *Adv. Mater.* **2009,** *21* (38-39), 3924-3927.
57. Keivanidis, P. E.; Kamm, V.; Dyer-Smith, C.; Zhang, W.; Laquai, F.; McCulloch, I.; Bradley, D. D. C.; Nelson, J. Delayed Luminescence Spectroscopy of Organic Photovoltaic Binary Blend Films: Probing the Emissive Non-geminate Charge Recombination. *Adv. Mater.* **2010,** *22* (45), 5183-5187.
58. Marsh, R. A.; Hodgkiss, J. M.; Friend, R. H. Direct Measurement of Electric Field-Assisted Charge Separation in Polymer:Fullerene Photovoltaic Diodes. *Adv. Mater.* **2010,** *22* (33), 3672-3676.
59. Deibel, C.; Wagenpfahl, A. Comment on "Interface state recombination in organic solar cells". *Phys. Rev. B: Condens. Matter* **2010,** *82* (20), 207301.
60. Deibel, C.; Dyakonov, V. Polymer:fullerene bulk heterojunction solar cells. *Rep. Prog. Phys.* **2010,** *73* (9), 096401.
61. MacKenzie, R. C. I.; Kirchartz, T.; Dibb, G. F. A.; Nelson, J. Modeling Nongeminate Recombination in P3HT:PCBM Solar Cells. *J. Phys. Chem. C* **2011,** *115* (19), 9806-9813.
62. Clarke, T. M.; Jamieson, F. C.; Durrant, J. R. Transient Absorption Studies of Bimolecular Recombination Dynamics in Polythiophene/Fullerene Blend Films. *J. Phys. Chem. C* **2009,** *113* (49), 20934-20941.
63. Garcia-Belmonte, G.; Bisquert, J. Open-circuit Voltage Limit Caused by Recombination Through Tail States in Bulk Heterojunction Polymer-Fullerene Solar Cells. *Appl. Phys. Lett.* **2010,** *96* (11), 113301.
64. Inal, S.; Schubert, M.; Sellinger, A.; Neher, D. The Relationship between the Electric Field-Induced Dissociation of Charge Transfer Excitons and the Photocurrent in Small Molecular/Polymeric Solar Cells. *J. Phys. Chem. Lett.* **2010,** *1* (6), 982-986.
65. Tvingstedt, K.; Vandewal, K.; Gadisa, A.; Zhang, F.; Manca, J.; Inganalˆs, O. Electroluminescence from Charge Transfer States in Polymer Solar Cells. *J. Am. Chem. Soc.* **2009,** *131* (33), 11819-11824.
66. Veldman, D.; Ìǂpek, O. z.; Meskers, S. C. J.; Sweelssen, J. r.; Koetse, M. M.; Veenstra, S. C.; Kroon, J. M.; Bavel, S. S. v.; Loos, J.; Janssen, R. A. J. Compositional and Electric Field Dependence of the Dissociation of Charge Transfer Excitons in Alternating Polyfluorene Copolymer/Fullerene Blends. *J. Am. Chem. Soc.* **2008,** *130* (24), 7721-7735.
67. Proctor, C. M.; Kuik, M.; Nguyen, T.-Q. Charge Carrier Recombination in Organic Solar Cells. *Prog. Polym. Sci.* **2013**.
68. Jamieson, F. C.; Agostinelli, T.; Azimi, H.; Nelson, J.; Durrant, J. R. Field-Independent Charge Photogeneration in PCPDTBT/PC70BM Solar Cells. *J. Phys. Chem. Lett.* **2010,** *1* (23), 3306-3310.
69. Albrecht, S.; Schindler, W.; Kurpiers, J.; Kniepert, J.; Blakesley, J. C.; Dumsch, I.; Allard, S.; Fostiropoulos, K.; Scherf, U.; Neher, D. On the Field Dependence of Free Charge Carrier Generation and Recombination in Blends of PCPDTBT/PC70BM: Influence of Solvent Additives. *J. Phys. Chem. Lett.* **2012,** *3* (5), 640-645.
70. Shuttle, C. G.; O'Regan, B.; Ballantyne, A. M.; Nelson, J.; Bradley, D. D. C.; Durrant, J. R. Bimolecular Recombination Losses in Polythiophene: Fullerene Solar Cells. *Phys. Rev. B: Condens. Matter* **2008,** *78* (11), 113201.
71. Grzegorczyk, W. J.; Savenije, T. J.; Dykstra, T. E.; Piris, J.; Schins, J. M.; Siebbeles, L. D. A. Temperature-Independent Charge Carrier Photogeneration in P3HT-PCBM Blends with Different Morphology. *The Journal of Physical Chemistry C* **2010,** *114* (11), 5182-5186.

72. Thakur, A. K.; Wantz, G.; Garcia-Belmonte, G.; Bisquert, J.; Hirsch, L. Temperature dependence of open-circuit voltage and recombination processes in polymer-fullerene based solar cells. *Sol. Energy Mater. Sol. Cells* **2011,** *95* (8), 2131-2135.
73. Dimitrov, S. D.; Durrant, J. R. Materials design considerations for charge generation in organic solar cells. *Chem. Mater.* **2013**, 130909140418004.
74. Dimitrov, S. D.; Bakulin, A. A.; Nielsen, C. B.; Schroeder, B. C.; Du, J.; Bronstein, H.; McCulloch, I.; Friend, R. H.; Durrant, J. R. On the energetic dependence of charge separation in low-band-gap polymer/fullerene blends. *J. Am. Chem. Soc.* **2012,** *134* (44), 18189-92.
75. Grancini, G.; Martino, N.; Antognazza, M. R.; Celebrano, M.; Egelhaaf, H.-J.; Lanzani, G. Influence of Blend Composition on Ultrafast Charge Generation and Recombination Dynamics in Low Band Gap Polymer-Based Organic Photovoltaics. *The Journal of Physical Chemistry C* **2012,** *116* (17), 9838-9844.
76. Grancini, G.; Maiuri, M.; Fazzi, D.; Petrozza, A.; Egelhaaf, H. J.; Brida, D.; Cerullo, G.; Lanzani, G. Hot exciton dissociation in polymer solar cells. *Nat Mater* **2012,** *advance online publication*.
77. Silva, C. Organic photovoltaics: Some like it hot. *Nat Mater* **2012,** *advance online publication*.
78. Jailaubekov, A. E.; Willard, A. P.; Tritsch, J. R.; Chan, W.-L.; Sai, N.; Gearba, R.; Kaake, L. G.; Williams, K. J.; Leung, K.; Rossky, P. J.; Zhu, X. Y. Hot charge-transfer excitons set the time limit for charge separation at donor/acceptor interfaces in organic photovoltaics. *Nat Mater* **2012,** *advance online publication*.
79. Bakulin, A. A.; Rao, A.; Pavelyev, V. G.; van Loosdrecht, P. H.; Pshenichnikov, M. S.; Niedzialek, D.; Cornil, J.; Beljonne, D.; Friend, R. H. The role of driving energy and delocalized States for charge separation in organic semiconductors. *Science* **2012,** *335* (6074), 1340-4.
80. Caruso, D.; Troisi, A. Long-range exciton dissociation in organic solar cells. *Proc. Natl. Acad. Sci. U. S. A.* **2012,** *109* (34), 13498-502.
81. Burkhard, G. F.; Hoke, E. T.; Beiley, Z. M.; McGehee, M. D. Free Carrier Generation in Fullerene Acceptors and Its Effect on Polymer Photovoltaics. *The Journal of Physical Chemistry C* **2012,** *116* (50), 26674-26678.
82. McMahon, D. P.; Cheung, D. L.; Troisi, A. Why Holes and Electrons Separate So Well in Polymer/Fullerene Photovoltaic Cells. *J. Phys. Chem. Lett.* **2011,** *2* (21), 2737-2741.
83. Credgington, D.; Jamieson, F. C.; Walker, B.; Nguyen, T.-Q.; Durrant, J. R. Quantification of Geminate and Non-Geminate Recombination Losses within a Solution-Processed Small-Molecule Bulk Heterojunction Solar Cell. *Adv. Mater.* **2012,** *24* (16), 2135-2141.
84. Albrecht, S.; Janietz, S.; Schindler, W.; Frisch, J.; Kurpiers, J.; Kniepert, J.; Inal, S.; Pingel, P.; Fostiropoulos, K.; Koch, N.; Neher, D. Fluorinated Copolymer PCPDTBT with Enhanced Open-Circuit Voltage and Reduced Recombination for Highly Efficient Polymer Solar Cells. *J. Am. Chem. Soc.* **2012,** *134* (36), 14932-14944.
85. Groves, C.; Blakesley, J. C.; Greenham, N. C. Effect of Charge Trapping on Geminate Recombination and Polymer Solar Cell Performance. *Nano Lett.* **2010,** *10* (3), 1063-1069.
86. van Eersel, H.; Janssen, R. A. J.; Kemerink, M. Mechanism for Efficient Photoinduced Charge Separation at Disordered Organic Heterointerfaces. *Adv. Funct. Mater.* **2012,** *22* (13), 2700-2708.
87. Liu, T.; Cheung, D. L.; Troisi, A. Structural variability and dynamics of the P3HT/PCBM interface and its effects on the electronic structure and the charge-transfer rates in solar cells. *PCCP* **2011,** *13* (48), 21461-21470.
88. Langevin, P. Recombinaison et Mobilités des Ions dans les Gaz. *Ann. Chem. Phys.* **1903,** *28*, 289.
89. Pivrikas, A.; Juscaronka, G.; Ouml; sterbacka, R.; Westerling, M.; Viliumacrnas, M.; Arlauskas, K.; Stubb, H. Langevin recombination and space-charge-perturbed current transients in regiorandom poly(3-hexylthiophene). *Phys. Rev. B: Condens. Matter* **2005,** *71* (12), 125205.
90. Pivrikas, A.; Juska, G.; Mozer, A. J.; Scharber, M.; Arlauskas, K.; Sariciftci, N. S.; Stubb, H.; Osterbacka, R. Bimolecular Recombination Coefficient as a Sensitive Testing Parameter for Low-Mobility Solar-Cell Materials. *Phys. Rev. Lett.* **2005,** *94* (17), 176806.
91. Hamilton, R.; Shuttle, C. G.; Oâ€™Regan, B.; Hammant, T. C.; Nelson, J.; Durrant, J. R. Recombination in Annealed and Nonannealed Polythiophene/Fullerene Solar Cells: Transient Photovoltage Studies versus Numerical Modeling. *J. Phys. Chem. Lett.* **2010,** *1* (9), 1432-1436.
92. Shuttle, C. G.; Hamilton, R.; Nelson, J.; O'Regan, B. C.; Durrant, J. R. Measurement of Charge-Density Dependence of Carrier Mobility in an Organic Semiconductor Blend. *Adv. Funct. Mater.* **2010,** *20* (5), 698-702.
93. Shuttle, C. G.; Regan, B. O.; Ballantyne, A. M.; Nelson, J.; Bradley, D. D. C.; Mello, J. d.; Durrant, J. R. Experimental Determination of the Rate Law for Charge Carrier Decay in a Polythiophene: Fullerene Solar Cell. *Appl. Phys. Lett.* **2008,** *92*, 093311.
94. Shuttle, C. G.; Maurano, A.; Hamilton, R.; O'Regan, B.; de Mello, J. C.; Durrant, J. R. Charge Extraction Analysis of Charge Carrier Densities in a Polythiophene/Fullerene Solar Cell: Analysis of the Origin of the Device Dark Current. *Appl. Phys. Lett.* **2008,** *93* (18), 183501-3.
95. Maurano, A.; Hamilton, R.; Shuttle, C. G.; Ballantyne, A. M.; Nelson, J.; O'Regan, B.; Zhang, W.; McCulloch, I.; Azimi, H.; Morana, M.; Brabec, C. J.; Durrant, J. R. Recombination Dynamics as a Key Determinant of Open Circuit Voltage in Organic Bulk Heterojunction Solar Cells: A Comparison of Four Different Donor Polymers. *Adv. Mater.* **2010,** *22* (44), 4987-4992.
96. Scharber, M. C.; Mühlbacher, D.; Koppe, M.; Denk, P.; Waldauf, C.; Heeger, A. J.; Brabec, C. J. Design Rules for Donors in Bulk-Heterojunction Solar Cells - Towards 10 % Energy-Conversion Efficiency. *Adv. Mater.* **2006,** *18* (6), 789-794.
97. Maurano, A.; Shuttle, C. G.; Hamilton, R.; Ballantyne, A. M.; Nelson, J.; Zhang, W.; Heeney, M.; Durrant, J. R. Transient Optoelectronic Analysis of Charge Carrier Losses in a Selenophene/Fullerene Blend Solar Cell. *The Journal of Physical Chemistry C* **2011,** *115* (13), 5947-5957.
98. Proctor, C. M.; Kim, C.; Neher, D.; Nguyen, T.-Q. Nongeminate Recombination and Charge Transport Limitations in Diketopyrrolopyrrole-Based Solution-Processed Small Molecule Solar Cells. *Adv. Funct. Mater.* **2013,** *23* (28), 3584-3594.
99. Deibel, C.; Rauh, D.; Foertig, A. Order of Decay of Mobile Charge Carriers in P3HT:PCBM Solar Cells. *arXiv* **2013,** *arXiv:1302.0367*.
100. Kirchartz, T.; Deledalle, F.; Tuladhar, P. S.; Durrant, J. R.; Nelson, J. On the Differences between Dark and Light Ideality Factor in Polymer:Fullerene Solar Cells. *J. Phys. Chem. Lett.* **2013**, 2371-2376.
101. Street, R. A.; Krakaris, A.; Cowan, S. R. Recombination Through Different Types of Localized States in Organic Solar Cells. *Adv. Funct. Mater.* **2012,** *22* (21), 4608-4619.
102. Schafferhans, J.; Baumann, A.; Wagenpfahl, A.; Deibel, C.; Dyakonov, V. Oxygen doping of P3HT:PCBM blends: Influence on trap states, charge carrier mobility and solar cell performance. *Org. Electron.* **2010,** *11* (10), 1693-1700.
103. Mihailetchi, V. D.; Wildeman, J.; Blom, P. W. M. Space-Charge Limited Photocurrent. *Phys. Rev. Lett.* **2005,** *94* (12), 126602.
104. Jespersen, K. G.; Zhang, F.; Gadisa, A.; Sundström, V.; Yartsev, A.; Inganäs, O. Charge formation and transport in bulk-heterojunction solar cells based on alternating polyfluorene copolymers blended with fullerenes. *Org. Electron.* **2006,** *7* (4), 235-242.
105. Lenes, M.; Morana, M.; Brabec, C. J.; Blom, P. W. M. Recombination-Limited Photocurrents in Low Bandgap Polymer/Fullerene Solar Cells. *Adv. Funct. Mater.* **2009,** *19* (7), 1106-1111.
106. Mauer, R.; Howard, I. A.; Laquai, F. d. r. Effect of Nongeminate Recombination on Fill Factor in Polythiophene/Methanofullerene Organic Solar Cells. *J. Phys. Chem. Lett.* **2010,** *1* (24), 3500-3505.
107. Shrotriya, V.; Li, G.; Yao, Y.; Moriarty, T.; Emery, K.; Yang, Y. Accurate Measurement and Characterization of Organic Solar Cells. *Adv. Funct. Mater.* **2006,** *16* (15), 2016-2023.
108. Luber, E. J.; Buriak, J. M. Reporting Performance in Organic Photovoltaic Devices. *ACS Nano* **2013,** *7* (6), 4708-4714.

109. Lee, M. M.; Teuscher, J.; Miyasaka, T.; Murakami, T. N.; Snaith, H. J. Efficient hybrid solar cells based on meso-superstructured organometal halide perovskites. *Science* **2012,** *338* (6107), 643-7.
110. Kirchartz, T.; Pieters, B. E.; Kirkpatrick, J.; Rau, U.; Nelson, J. Recombination via Tail States in Polythiophene:Fullerene Solar Cells. *Phys. Rev. B: Condens. Matter* **2011,** *83* (11), 115209.
111. Dagamseh, A. M. K.; Vet, B.; Šutta, P.; Zeman, M. Modelling and optimization of a-Si:H solar cells with ZnO:Al back reflector. *Sol. Energy Mater. Sol. Cells* **2010,** *94* (12), 2119-2123.
112. Ding, K.; Kirchartz, T.; Pieters, B. E.; Ulbrich, C.; Ermes, A. M.; Schicho, S.; Lambertz, A.; Carius, R.; Rau, U. Characterization and simulation of a-Si:H/μc-Si:H tandem solar cells. *Sol. Energy Mater. Sol. Cells* **2011,** *95* (12), 3318-3327.
113. Kirchartz, T.; Pieters, B.; Taretto, K.; Rau, U. Mobility dependent efficiencies of organic bulk heterojunction solar cells: Surface recombination and charge transfer state distribution. *Phys. Rev. B: Condens. Matter* **2009,** *80* (3).
114. Pivrikas, A.; Sariciftci, N. S.; Juška, G.; Österbacka, R. A review of charge transport and recombination in polymer/fullerene organic solar cells. *Progress in Photovoltaics: Research and Applications* **2007,** *15* (8), 677-696.
115. Steiger, J.; Schmechel, R.; von Seggern, H. Energetic trap distributions in organic semiconductors. *Synth. Met.* **2002,** *129* (1), 1-7.
116. Shuttle, C. G.; Treat, N. D.; Douglas, J. D.; Fréchet, J. M. J.; Chabinyc, M. L. Deep Energetic Trap States in Organic Photovoltaic Devices. *Adv. En. Mat.* **2011,** n/a-n/a.
117. Nicolai, H. T.; Kuik, M.; Wetzelaer, G. A. H.; de Boer, B.; Campbell, C.; Risko, C.; Brédas, J. L.; Blom, P. W. M. Unification of trap-limited electron transport in semiconducting polymers. *Nat Mater* **2012,** *11* (10), 882-887.
118. Street, R. A. Localized state distribution and its effect on recombination in organic solar cells. *Phys. Rev. B: Condens. Matter* **2011,** *84* (7), 075208.
119. Westenhoff, S.; Howard, I. A.; Hodgkiss, J. M.; Kirov, K. R.; Bronstein, H. A.; Williams, C. K.; Greenham, N. C.; Friend, R. H. Charge Recombination in Organic Photovoltaic Devices with High Open-Circuit Voltages. *J. Am. Chem. Soc.* **2008,** *130* (41), 13653-13658.
120. Deibel, C.; Baumann, A.; Dyakonov, V. Polaron Recombination in Pristine and Annealed Bulk Heterojunction Solar Cells. *Appl. Phys. Lett.* **2008,** *93* (16), 163303-3.
121. Juska, G.; Arlauskas, K.; Viliunas, M.; Kocka, J. Extraction Current Transients: New Method of Study of Charge Transport in Microcrystalline Silicon. *Phys. Rev. Lett.* **2000,** *84* (21), 4946.
122. Garcia-Belmonte, G.; Boix, P. P.; Bisquert, J.; Sessolo, M.; Bolink, H. J. Simultaneous determination of carrier lifetime and electron density-of-states in P3HT:PCBM organic solar cells under illumination by impedance spectroscopy. *Sol. Energy Mater. Sol. Cells* **2010,** *94* (2), 366-375.
123. Street, R. A.; Cowan, S.; Heeger, A. J. Experimental Test for Geminate Recombination Applied to Organic Solar Cells. *Phys. Rev. B: Condens. Matter* **2010,** *82* (12), 121301.
124. Kniepert, J.; Schubert, M.; Blakesley, J. C.; Neher, D. Photogeneration and Recombination in P3HT/PCBM Solar Cells Probed by Time-Delayed Collection Field Experiments. *J. Phys. Chem. Lett.* **2011,** *2* (7), 700-705.
125. Kirchartz, T.; Nelson, J. Meaning of reaction orders in polymer:fullerene solar cells. *Phys. Rev. B: Condens. Matter* **2012,** *86* (16).
126. Foertig, A.; Baumann, A.; Rauh, D.; Dyakonov, V.; Deibel, C. Charge Carrier Concentration and Temperature Dependen Recombination in Polymer-Fullerene Solar Cells. *Appl. Phys. Lett.* **2009,** *95* (5), 052104-3.
127. Riedel, I.; Parisi, J.; Dyakonov, V.; Lutsen, L.; Vanderzande, D.; Hummelen, J. Effect of Temperature and Illumination on the Electrical Characteristics of Polymer–Fullerene Bulk-Heterojunction Solar Cells. *Adv. Funct. Mater.* **2004,** *14* (1), 38-44.
128. Montanari, I.; Nogueira, A. F.; Nelson, J.; Durrant, J. R.; Winder, C.; Loi, M. A.; Sariciftci, N. S.; Brabec, C. Transient Optical Studies of Charge Recombination Dynamics in a Polymer/Fullerene Composite at Room Temperature. *Appl. Phys. Lett.* **2002,** *81*, 3001-3003.
129. Carr, J. A.; Chaudhary, S. On the identification of deeper defect levels in organic photovoltaic devices. *J. Appl. Phys.* **2013,** *114* (6), 064509.
130. Street, R. A.; Davies, D. M. Kinetics of light induced defect creation in organic solar cells. *Appl. Phys. Lett.* **2013,** *102* (4), 043305.
131. Seynhaeve, G.; Barclay, R.; Adriaenssens, G.; Marshall, J. Post-transit time-of-flight currents as a probe of the density of states in hydrogenated amorphous silicon. *Physical Review B* **1989,** *39* (14), 10196-10205.
132. Vithanage, D. A.; Devizis, A.; Abramavicius, V.; Infahsaeng, Y.; Abramavicius, D.; Mackenzie, R. C.; Keivanidis, P. E.; Yartsev, A.; Hertel, D.; Nelson, J.; Sundstrom, V.; Gulbinas, V. Visualizing charge separation in bulk heterojunction organic solar cells. *Nat Commun* **2013,** *4*, 2334.
133. Kim, Y.; Choulis, S. A.; Nelson, J.; Bradley, D. D. C.; Cook, S.; Durrant, J. R. Device annealing effect in organic solar cells with blends of regioregular poly(3-hexylthiophene) and soluble fullerene. *Appl. Phys. Lett.* **2005,** *86* (6), 063502-3.
134. Carati, C.; Bonoldi, L.; Po, R. Density of trap states in organic photovoltaic materials from LESR studies of carrier recombination kinetics. *Phys. Rev. B: Condens. Matter* **2011,** *84* (24).
135. Cowan, S. R.; Leong, W. L.; Banerji, N.; Dennler, G.; Heeger, A. J. Identifying a Threshold Impurity Level for Organic Solar Cells: Enhanced First-Order Recombination Via Well-Defined PC84BM Traps in Organic Bulk Heterojunction Solar Cells. *Adv. Funct. Mater.* **2011,** *21* (16), 3083-3092.
136. Deibel, C.; Wagenpfahl, A.; Dyakonov, V. Origin of reduced polaron recombination in organic semiconductor devices. *Phys. Rev. B: Condens. Matter* **2009,** *80* (7), 075203.
137. Sanchez-Diaz, A.; Izquierdo, M.; Filippone, S.; Martin, N.; Palomares, E. The Origin of the High Voltage in DPM12/P3HT Solar Cells. *Adv. Funct. Mater.* **2010,** *20* (16), 2695-2700.
138. Liu, L.; Li, G. Investigation of Recombination Loss in Organic Solar Cells by Simulating Intensity-Dependent Current-Voltage Measurements. *Sol. Energy Mater. Sol. Cells* **2011,** *95* (9), 2557-2563.
139. Azimi, H.; Senes, A.; Scharber, M. C.; Hingerl, K.; Brabec, C. J. Charge Transport and Recombination in Low-Bandgap Bulk Heterojunction Solar Cell using Bis-adduct Fullerene. *Adv. En. Mat.* **2011,** *1* (6), 1162-1168.
140. Ooi, Z. E.; Jin, R.; Huang, J.; Loo, Y. F.; Sellinger, A.; deMello, J. C. On the Pseudo-Symmetric Current-Voltage Response of Bulk Heterojunction Solar Cells. *J. Mater. Chem.* **2008,** *18* (14), 1644-1651.
141. Marsh, R. A.; McNeill, C. R.; Abrusci, A.; Campbell, A. R.; Friend, R. H. A Unified Description of Current-Voltage Characteristics in Organic and Hybrid Photovoltaics under Low Light Intensity. *Nano Lett.* **2008,** *8* (5), 1393-1398.
142. Liang, Y.; Feng, D.; Wu, Y.; Tsai, S.-T.; Li, G.; Ray, C.; Yu, L. Highly Efficient Solar Cell Polymers Developed via Fine-Tuning of Structural and Electronic Properties. *J. Am. Chem. Soc.* **2009,** *131* (22), 7792-7799.
143. Bronstein, H.; Frost, J. M.; Hadipour, A.; Kim, Y.; Nielsen, C. B.; Ashraf, R. S.; Rand, B. P.; Watkins, S.; McCulloch, I. Effect of Fluorination on the Properties of a Donor–Acceptor Copolymer for Use in Photovoltaic Cells and Transistors. *Chem. Mater.* **2013,** *25* (3), 277-285.
144. Ishwara, T.; Bradley, D. D. C.; Nelson, J.; Ravirajan, P.; Vanseveren, I.; Cleij, T.; Vanderzande, D.; Lutsen, L.; Tierney, S.; Heeney, M.; McCulloch, I. Influence of polymer ionization potential on the open-circuit voltage of hybrid polymer/TiO[sub 2] solar cells. *Appl. Phys. Lett.* **2008,** *92* (5), 053308-3.
145. Peet, J.; Kim, J. Y.; Coates, N. E.; Ma, W. L.; Moses, D.; Heeger, A. J.; Bazan, G. C. Efficiency enhancement in low-bandgap polymer solar cells by processing with alkane dithiols. *Nat Mater* **2007,** *6* (7), 497-500.

146. Hwang, I. W.; Cho, S.; Kim, J. Y.; Lee, K.; Coates, N. E.; Moses, D.; Heeger, A. J. Carrier generation and transport in bulk heterojunction films processed with 1,8-octanedithiol as a processing additive. *J. Appl. Phys.* **2008,** *104* (3), 033706-9.
147. Svanstrom, C. M. B.; Rysz, J.; Bernasik, A.; Budkowski, A.; Zhang, F.; Inganas, O.; Andersson, M. R.; Magnusson, K. O.; Benson-Smith, J. J.; Nelson, J.; Moons, E. Device Performance of APFO-3/PCBM Solar Cells with Controlled Morphology. *Adv. Mater.* **2009,** *21* (43), 4398-+.
148. Green, M. A.; Emery, K.; Hishikawa, Y.; Warta, W.; Dunlop, E. D. Solar cell efficiency tables (version 39). *Progress in Photovoltaics: Research and Applications* **2012,** *20* (1), 12-20.
149. Koster, L. J. A.; Smits, E. C. P.; Mihailetchi, V. D.; Blom, P. W. M. Device model for the operation of polymer/fullerene bulk heterojunction solar cells. *Phys. Rev. B: Condens. Matter* **2005,** *72* (8), 085205.
150. Kirchartz, T.; Agostinelli, T.; Campoy-Quiles, M.; Gong, W.; Nelson, J. Understanding the Thickness-Dependent Performance of Organic Bulk Heterojunction Solar Cells: The Influence of Mobility, Lifetime, and Space Charge. *J. Phys. Chem. Lett.* **2012,** *3* (23), 3470-3475.
151. Mühlbacher, D.; Scharber, M.; Morana, M.; Zhu, Z.; Waller, D.; Gaudiana, R.; Brabec, C. High Photovoltaic Performance of a Low-Bandgap Polymer. *Adv. Mater.* **2006,** *18* (21), 2884-2889.
152. Schilinsky, P.; Waldauf, C.; Hauch, J.; Brabec, C. J. Simulation of light intensity dependent current characteristics of polymer solar cells. *J. Appl. Phys.* **2004,** *95* (5), 2816-2819.
153. Savoie, B. M.; Movaghar, B.; Marks, T. J.; Ratner, M. A. Simple Analytic Description of Collection Efficiency in Organic Photovoltaics. *J. Phys. Chem. Lett.* **2013,** *4* (5), 704-709.
154. Servaites, J. D.; Savoie, B. M.; Brink, J. B.; Marks, T. J.; Ratner, M. A. Modeling geminate pair dissociation in organic solar cells: high power conversion efficiencies achieved with moderate optical bandgaps. *Energy & Environmental Science* **2012,** *5* (8), 8343-8350.
155. Andersson, L. M.; Muller, C.; Badada, B. H.; Zhang, F. L.; Wurful, U.; Inganas, O. Mobility and fill factor correlation in geminate recombination limited solar cells. *J. Appl. Phys.* **2011,** *110* (2), 024509.
156. Deibel, C.; Baumann, A.; Wagenpfahl, A.; Dyakonov, V. Polaron recombination in pristine and annealed bulk heterojunction solar cells. *Synth. Met.* **2009,** *159* (21-22), 2345-2347.
157. Pal, S. K.; Kesti, T.; Maiti, M.; Zhang, F.; Inganäs, O.; Hellström, S.; Andersson, M. R.; Oswald, F.; Langa, F.; Österman, T.; Pascher, T. r.; Yartsev, A.; Sundström, V. Geminate Charge Recombination in Polymer/Fullerene Bulk Heterojunction Films and Implications for Solar Cell Function. *J. Am. Chem. Soc.* **2010,** *132* (35), 12440-12451.
158. Gadisa, A.; Zhang, F. L.; Sharma, D.; Svensson, M.; Andersson, M. R.; Inganas, O. Improvements of fill factor in solar cells based on blends of polyfluorene copolymers as electron donors. *Thin Solid Films* **2007,** *515* (5), 3126-3131.
159. Wong, H. M. P.; Wang, P.; Abrusci, A.; Svensson, M.; Andersson, M. R.; Greenham, N. C. Donor and acceptor behavior in a polyfluorene for photovoltaics. *J. Phys. Chem. C* **2007,** *111* (13), 5244-5249.
160. Schafferhans, J.; Baumann, A.; Deibel, C.; Dyakonov, V. Trap distribution and the impact of oxygen-induced traps on the charge transport in poly(3-hexylthiophene). *Appl. Phys. Lett.* **2008,** *93* (9), 093303-3.
161. McNeill, C. R. Photocurrent transients in all-polymer solar cells: Trapping and detrapping effects. *J. Appl. Phys.* **2009,** *106* (2), 024507.
162. Credgington, D.; Durrant, J. R. Insights from Transient Optoelectronic Analyses on the Open-Circuit Voltage of Organic Solar Cells. *J. Phys. Chem. Lett.* **2012**, 1465-1478.
163. Lee, J.; Vandewal, K.; Yost, S. R.; Bahlke, M. E.; Goris, L.; Baldo, M. A.; Manca, J. V.; Voorhis, T. V. Charge Transfer State Versus Hot Exciton Dissociation in Polymer-Fullerene Blended Solar Cells. *J. Am. Chem. Soc.* **2010,** *132* (34), 11878-11880.
164. Tress, W.; Merten, A.; Furno, M.; Hein, M.; Leo, K.; Riede, M. Correlation of Absorption Profile and Fill Factor in Organic Solar Cells: The Role of Mobility Imbalance. *Adv. En. Mat.* **2013,** *3* (5), 631-638.
165. Tumbleston, J. R.; Liu, Y. C.; Samulski, E. T.; Lopez, R. Interplay between Bimolecular Recombination and Carrier Transport Distances in Bulk Heterojunction Organic Solar Cells. *Adv. En. Mat.* **2012,** *2* (4), 477-486.
166. Koster, L. J.; Kemerink, M.; Wienk, M. M.; Maturova, K.; Janssen, R. A. Quantifying bimolecular recombination losses in organic bulk heterojunction solar cells. *Adv Mater* **2011,** *23* (14), 1670-4.
167. Luer, L.; Egelhaaf, H. J.; Oelkrug, D.; Cerullo, G.; Lanzani, G.; Huisman, B. H.; de Leeuw, D. Oxygen-induced quenching of photoexcited states in polythiophene films. *Org. Electron.* **2004,** *5* (1-3), 83-89.
168. Hintz, H.; Peisert, H.; Egelhaaf, H. J.; Chassé, T. Reversible and Irreversible Light-Induced p-Doping of P3HT by Oxygen Studied by Photoelectron Spectroscopy (XPS/UPS). *J. Phys. Chem. C* **2011,** *115* (27), 13373-13376.
169. Liang, Z.; Gregg, B. A. Compensating Poly(3-hexylthiophene) Reveals Its Doping Density and Its Strong Exciton Quenching by Free Carriers. *Adv. Mater.* **2012,** *24* (24), 3258-3262.
170. Trukhanov, V. A.; Bruevich, V. V.; Paraschuk, D. Y. Effect of doping on performance of organic solar cells. *Phys. Rev. B: Condens. Matter* **2011,** *84* (20), 205318.
171. Chan, M. Y.; Lai, S. L.; Fung, M. K.; Lee, C. S.; Lee, S. T. Doping-induced efficiency enhancement in organic photovoltaic devices. *Appl. Phys. Lett.* **2007,** *90* (2), 023504.
172. Maennig, B.; Pfeiffer, M.; Nollau, A.; Zhou, X.; Leo, K.; Simon, P. Controlled p-type doping of polycrystalline and amorphous organic layers: Self-consistent description of conductivity and field-effect mobility by a microscopic percolation model. *Phys. Rev. B: Condens. Matter* **2001,** *64* (19), 195208.
173. Chan, C. K.; Zhao, W.; Kahn, A.; Hill, I. G. Influence of chemical doping on the performance of organic photovoltaic cells. *Appl. Phys. Lett.* **2009,** *94* (20), 203306.
174. Kao, P.-C.; Chu, S.-Y.; Huang, H.-H.; Tseng, Z.-L.; Chen, Y.-C. Improved efficiency of organic photovoltaic cells using tris (8-hydroxy-quinoline) aluminum as a doping material. *Thin Solid Films* **2009,** *517* (17), 5301-5304.
175. Kröger, M.; Hamwi, S.; Meyer, J.; Riedl, T.; Kowalsky, W.; Kahn, A. P-type doping of organic wide band gap materials by transition metal oxides: A case-study on Molybdenum trioxide. *Org. Electron.* **2009,** *10* (5), 932-938.
176. Olthof, S.; Mehraeen, S.; Mohapatra, S. K.; Barlow, S.; Coropceanu, V.; Brédas, J.-L.; Marder, S. R.; Kahn, A. Ultralow Doping in Organic Semiconductors: Evidence of Trap Filling. *Phys. Rev. Lett.* **2012,** *109* (17), 176601.
177. Lüssem, B.; Riede, M.; Leo, K. Doping of organic semiconductors. *Phys. Status Solidi A* **2013,** *210* (1), 9-43.
178. Pingel, P.; Neher, D. Comprehensive picture of p-type doping of P3HT with the molecular acceptor F_{4}TCNQ. *Phys. Rev. B: Condens. Matter* **2013,** *87* (11), 115209.
179. Min Nam, Y.; Huh, J.; Ho Jo, W. Optimization of thickness and morphology of active layer for high performance of bulk-heterojunction organic solar cells. *Sol. Energy Mater. Sol. Cells* **2010,** *94* (6), 1118-1124.
180. Pandey, R.; Holmes, R. J. Characterizing the charge collection efficiency in bulk heterojunction organic photovoltaic cells. *Appl. Phys. Lett.* **2012,** *100* (8), 083303.
181. Dibb, G. F. A.; Kirchartz, T.; Credgington, D.; Durrant, J. R.; Nelson, J. Analysis of the Relationship between Linearity of Corrected Photocurrent and the Order of Recombination in Organic Solar Cells. *J. Phys. Chem. Lett.* **2011,** *2* (19), 2407-2411.
182. Faist, M. A.; Shoaee, S.; Tuladhar, S.; Dibb, G. F. A.; Foster, S.; Gong, W.; Kirchartz, T.; Bradley, D. D. C.; Durrant, J. R.; Nelson, J. Understanding the Reduced Efficiencies of Organic Solar Cells Employing Fullerene Multiadducts as Acceptors. *Adv. En. Mat.* **2013**, n/a-n/a.

183. Bisquert, J.; Garcia-Belmonte, G. On Voltage, Photovoltage, and Photocurrent in Bulk Heterojunction Organic Solar Cells. *J. Phys. Chem. Lett.* **2011,** *2* (15), 1950-1964.
184. Kirchartz, T.; Gong, W.; Hawks, S. A.; Agostinelli, T.; MacKenzie, R. C. I.; Yang, Y.; Nelson, J. Sensitivity of the Mott–Schottky Analysis in Organic Solar Cells. *J. Phys. Chem. C* **2012,** *116* (14), 7672-7680.
185. Khelifi, S.; Decock, K.; Lauwaert, J.; Vrielinck, H.; Spoltore, D.; Piersimoni, F.; Manca, J.; Belghachi, A.; Burgelman, M. Investigation of defects by admittance spectroscopy measurements in poly (3-hexylthiophene):(6,6)-phenyl C[sub 61]-butyric acid methyl ester organic solar cells degraded under air exposure. *J. Appl. Phys.* **2011,** *110* (9), 094509.
186. Troshin, P. A.; Susarova, D. K.; Moskvin, Y. L.; Kuznetsov, I. E.; Ponomarenko, S. A.; Myshkovskaya, E. N.; Zakharcheva, K. A.; Balakai, A. A.; Babenko, S. D.; Razumov, V. F. Impedance Measurements as a Simple Tool to Control the Quality of Conjugated Polymers Designed for Photovoltaic Applications. *Adv. Funct. Mater.* **2010,** *20* (24), 4351-4357.
187. Guerrero, A.; Marchesi, L. F.; Boix, P. P.; Ruiz-Raga, S.; Ripolles-Sanchis, T.; Garcia-Belmonte, G.; Bisquert, J. How the Charge-Neutrality Level of Interface States Controls Energy Level Alignment in Cathode Contacts of Organic Bulk-Heterojunction Solar Cells. *ACS Nano* **2012,** *6* (4), 3453-3460.
188. Garcia-Belmonte, G.; Munar, A.; Barea, E. M.; Bisquert, J.; Ugarte, I.; Pacios, R. Charge carrier mobility and lifetime of organic bulk heterojunctions analyzed by impedance spectroscopy. *Org. Electron.* **2008,** *9* (5), 847-851.
189. Katsidis, C. C.; Siapkas, D. I. General Transfer-Matrix Method for Optical Multilayer Systems with Coherent, Partially Coherent, and Incoherent Interference. *Appl. Opt.* **2002,** *41* (19), 3978-3987.
190. Pettersson, L. A. A.; Roman, L. S.; Inganas, O. Modeling photocurrent action spectra of photovoltaic devices based on organic thin films. *J. Appl. Phys.* **1999,** *86* (1), 487-496.
191. Lenes, M.; Koster, L. J. A.; Mihailetchi, V. D.; Blom, P. W. M. Thickness dependence of the efficiency of polymer:fullerene bulk heterojunction solar cells. *Appl. Phys. Lett.* **2006,** *88* (24), 243502.
192. Peet, J.; Wen, L.; Byrne, P.; Rodman, S.; Forberich, K.; Shao, Y.; Drolet, N.; Gaudiana, R.; Dennler, G.; Waller, D. Bulk heterojunction solar cells with thick active layers and high fill factors enabled by a bithiophene-co-thiazolothiazole push-pull copolymer. *Appl. Phys. Lett.* **2011,** *98* (4), 043301.
193. Hoppe, H.; Shokhovets, S.; Gobsch, G. Inverse relation between photocurrent and absorption layer thickness in polymer solar cells. *Phys. Status Solidi RRL* **2007,** *1* (1), R40-R42.
194. Andersson, B. V.; Huang, D. M.; Moule, A. J.; Inganas, O. An optical spacer is no panacea for light collection in organic solar cells. *Appl. Phys. Lett.* **2009,** *94* (4), 043302-3.
195. Leong, W. L.; Welch, G. C.; Kaake, L. G.; Takacs, C. J.; Sun, Y. M.; Bazan, G. C.; Heeger, A. J. Role of trace impurities in the photovoltaic performance of solution processed small-molecule bulk heterojunction solar cells. *Chem. Sci.* **2012,** *3* (6), 2103-2109.
196. Mityashin, A.; Cheyns, D.; Rand, B. P.; Heremans, P. Understanding metal doping for organic electron transport layers. *Appl. Phys. Lett.* **2012,** *100* (5), 053305.
197. Maddalena, F.; Meijer, E. J.; Asadi, K.; de Leeuw, D. M.; Blom, P. W. M. Doping kinetics of organic semiconductors investigated by field-effect transistors. *Appl. Phys. Lett.* **2010,** *97* (4), 043302-043302-3.
198. Kumar, P.; Gaur, A. Model for the J-V characteristics of degraded polymer solar cells. *J. Appl. Phys.* **2013,** *113* (9), 094505.
199. Tanaka, H.; Yokoi, Y.; Hasegawa, N.; Kuroda, S.-i.; Iijima, T.; Sato, T.; Yamamoto, T. Quadrimolecular recombination kinetics of photogenerated charge carriers in the composites of regioregular polythiophene derivatives and soluble fullerene. *J. Appl. Phys.* **2010,** *107* (8), 083708.